

# COUPLED-CLUSTER STUDIES OF QUANTUM DOTS

Magnus Pedersen Lohne



THESIS SUBMITTED FOR THE DEGREE OF  
MASTER OF SCIENCE IN COMPUTATIONAL PHYSICS

Department of Physics  
University of Oslo

June 2010



# Acknowledgements

First of all I would like to thank my supervisor Morten Hjorth-Jensen for support and advice during the last two years. Through many discussions in your office I have learned a lot. Thanks for providing me with such an interesting topic, and for inspiring and enthusiastic guidance all the way.

I would also like to thank my fellow students Håvard Sandsdalen, Lars Eivind Lervåg and Sigurd Wenner for friendship and interesting discussions in our office. Moreover, I would like to thank Dag-Filip Roaldsnes, Knut Olav Skyttemyr and Tom Andreas Kristensen for friendship and support during the last two years. Our bible group is really a blessing, guys. Furthermore, I would like to thank Jarle Frette for his proofreading of this thesis.

Last, but not at all least, I would like to thank my mom and dad, my sister Ragnhild and brother Kristoffer, and Kristin for love and support.

Magnus Pedersen Lohne



# Contents

<b>1</b>	<b>Introduction</b>	<b>1</b>
<b>I</b>	<b>THEORY</b>	<b>5</b>
<b>2</b>	<b>Quantum Mechanics</b>	<b>7</b>
2.1	Postulates of Quantum Mechanics . . . . .	8
2.2	Single-Particle Quantum Mechanics . . . . .	10
2.2.1	Coordinate Representation . . . . .	11
2.2.2	Intrinsic Spin . . . . .	13
2.2.3	Total Wavefunction . . . . .	15
<b>3</b>	<b>Many-Body Theory</b>	<b>17</b>
3.1	The Many-Body Problem . . . . .	17
3.2	The Non-Interacting System . . . . .	19
3.3	Identical Particles . . . . .	20
3.4	The Interacting Many-Body System . . . . .	21
3.4.1	Hilbert Space of Distinguishable Particles . . . . .	22
3.4.2	Hilbert Space of Bosons and Fermions . . . . .	22
3.5	Second Quantization . . . . .	24
3.5.1	Creation and Annihilation Operators . . . . .	24
3.5.2	Operators in Second Quantization . . . . .	25
3.5.3	Wick's Theorem . . . . .	27
3.5.4	Particle-Hole Formalism . . . . .	29
<b>4</b>	<b>Theoretical Description of Quantum Dots</b>	<b>33</b>
4.1	Approximations . . . . .	33
4.2	Schrödinger Equation for Spherically Symmetric Potentials . . . . .	34
4.3	Solutions for the Single-Electron Parabolic Quantum Dot . . . . .	36
4.4	$N$ -Electron Model Hamiltonian . . . . .	42
4.5	Scaling the Model Hamiltonian . . . . .	43
<b>II</b>	<b>MANY-BODY METHODS</b>	<b>45</b>
<b>5</b>	<b>Hartree-Fock Method</b>	<b>47</b>
5.1	Introduction . . . . .	47
5.2	Basic Ideas . . . . .	48
5.3	Derivation of the Hartree-Fock Equations . . . . .	48

<b>6 Coupled-Cluster Method</b>	<b>51</b>
6.1 Introduction and Fundamental Ideas . . . . .	51
6.1.1 Notation . . . . .	54
6.2 Fundamental Concepts . . . . .	55
6.3 Formal Coupled-Cluster Theory . . . . .	59
6.4 Coupled-Cluster Singles and Doubles Equations . . . . .	59
6.4.1 Normal-Ordered Form of the Hamiltonian . . . . .	60
6.4.2 The Campbell-Baker-Hausdorff Expansion . . . . .	61
6.4.3 Energy Equation - An Algebraic Approach . . . . .	62
6.4.4 Coupled-Cluster Diagrams . . . . .	67
6.4.5 Energy Equation on Diagrammatic Form . . . . .	72
6.4.6 Amplitude Equations on Diagrammatic Form . . . . .	74
6.4.7 Amplitude Equations on Algebraic Form . . . . .	79
<b>III IMPLEMENTATIONS AND RESULTS</b>	<b>87</b>
<b>7 Implementation</b>	<b>89</b>
7.1 Implementation of the Hartree-Fock Method . . . . .	89
7.1.1 Overview . . . . .	90
7.1.2 Validation of the Code . . . . .	90
7.1.3 Code Structure and Class Implementation . . . . .	91
7.2 Implementation of the Coupled-Cluster Method . . . . .	94
7.2.1 Overview . . . . .	95
7.2.2 Validation of the Code . . . . .	96
7.2.3 Code Structure and Class Implementation . . . . .	98
7.2.4 Implementation of the CCSD Algorithm . . . . .	100
7.2.5 F-matrix and Interaction Elements . . . . .	103
7.2.6 Implementation of the Amplitude Equations . . . . .	106
<b>8 Numerical Results and Analysis</b>	<b>125</b>
8.1 Standard interaction . . . . .	125
8.1.1 Tables of Numerical Results . . . . .	127
8.1.2 General Analysis and Discussion . . . . .	135
8.1.3 Full Correlation Energy . . . . .	141
8.1.4 Correlation Energy . . . . .	143
8.1.5 CCSD Correlation Energy . . . . .	145
8.1.6 Analysis of the Amplitudes . . . . .	147
8.1.7 Analysis of Basis Size . . . . .	150
8.1.8 Hartree-Fock Basis . . . . .	153
8.2 Effective Interaction . . . . .	155
8.2.1 Basic Ideas . . . . .	155
8.2.2 Energy Cut Model Space . . . . .	157
8.2.3 Direct Product Model Space . . . . .	165
8.2.4 Hartree-Fock Basis . . . . .	166
8.3 Comparison with other CCSD Calculations . . . . .	166
8.4 Comparison with other Many-Body Methods . . . . .	167
<b>9 Conclusions</b>	<b>169</b>
<b>A Solution of the Single-Electron Schrödinger Equation</b>	<b>173</b>

# Chapter 1

## Introduction

This thesis deals with electronic structure calculations of quantum dots using the Coupled-Cluster Singles and Doubles method (CCSD). The first thing that pops into ones head might be: “What is a quantum dot?” In fact, it is not an easy task to give a precise definition. “Quantum” and “dot” reveal some of the answer. The last word reflects its spatial structure which is much like a small dot. The word “quantum” indicates the physical size of the system (microscopic scale) and the laws that govern the physical behavior: quantum mechanics. Put simply, a quantum dot is a semiconductor device with electrons spatially confined. These structures are designed and fabricated in the laboratory, which is the reason why quantum dots are dubbed “designer atoms” or “artificial atoms” in the literature. Semiconductor quantum dots are structures where charge carriers are confined in all three spatial dimensions. The size of the dot is on the order of the Fermi wavelength in the host material, which is typically between 10 nm and 1  $\mu\text{m}$ . The confinement of charge carriers are usually obtained by electrical gating of a 2-dimensional electron gas, possibly combined by etching techniques. Scientists have been able to obtain precise control of the number of electrons in the conduction band of a quantum dot in GaAs heterostructures. For a general introduction to the topic we refer to [1, 2].

Quantum dots have provided the basis for a whole new research area in condensed-matter physics during the last 20 years [2]. They are fabricated and designed artificially in the laboratory using essentially macroscopic techniques. However, the fabricated structures are small enough to observe quantum mechanical behavior such as energy shell structure [3] and entanglement [4]. Coulomb blockade effects [5], tunneling [6] and magnetization [7] can be observed in coupled quantum dots. Moreover, quantum dots have exceptional electrical and optical properties. They are therefore attractive components for integration into electronic devices. One advantage over traditional optoelectronic materials is that quantum dots exist in the solid state. Moreover, quantum dots can interconvert light and electricity in a tuneable manner. They offer a wide absorption spectrum while maintaining a distinct and static emission spectrum. We refer to [8] for further reading. Scientists have experimented and used quantum dots in LEDs (Light-Emitting Diode) [9], lasers [10], new generation of transistors [11, 12], and so forth. They can also be used as qubits in quantum computing [13]. Furthermore, quantum dots can be used for biological applications [14]. For example, they can be used as tools for monitoring cancer cells and providing a means to better understand its evolution [15]. Another exciting application is towards solar cells [16]. Traditional solar cell materials have a theoretical efficiency limit of approximately 30% for conversion of energy from light to electricity. Utilizing quantum dots may allow realization of third generation solar cells with a theoretical efficiency close to 70% [16].

Besides all the possible technological applications, quantum dots are fundamentally interesting because of their strong analogies in nature (such as atoms, nuclei and metallic clusters) and their definition of paradigms in many-body physics [2]. The fact that their properties can be controlled and designed by electrostatic gates, changes in the spatial geometry, or magnetic fields, offers exciting possibilities to study quantum mechanical behavior both experimentally and theoretically. Quantum dots have probably most clear similarities with natural atoms. However,

there are also significant differences. First of all, quantum dots are designed and fabricated in the laboratory, with typical length scale of about 1 – 1000 nm. The size of atoms range from approximately 53 pm (Hydrogen, Bohr radius) to 0.26 nm (empirical radius of Caesium) [17], making them much smaller than a typical quantum dot. Secondly, the potentials that confine the electrons are quite different. In atoms, the potential is set up by the nucleus. In quantum dots we typically have an applied electromagnetic field that sets up the potential. The geometric form of this potential can be tuned as wanted by varying the applied field. However, it can often be approximated with a harmonic oscillator potential leading to the so-called parabolic (circular) quantum dot. Despite the differences between atoms and quantum dots, they share many features such as shell structure [2].

Electronic structure calculations, i.e. numerical solutions of the time-independent Schrödinger equation for an electronic system, have become extremely important in the field of material science in order to describe and predict properties of materials. In order to numerically investigate the properties of a solid, one needs to model a *large* number of particles. An approach starting from the degrees of freedom from quantum many-body theory and *ab initio* methods is impossible without substantial simplifications and approximations. The most popular many-body method for numerical studies of materials is the Density Functional Theory (DFT). However, the major problem in DFT is that the exact functionals for exchange and correlation are not known (except for the free electron gas), see [18]. A commonly used approximation is the so-called local density approximation (LDA). It is clear that such an approximation is a source of error in the calculations. *Ab initio* many-body methods, however, are methods starting from first principles, i.e. the Schrödinger equation without any approximations. This is a mature field ranging from advanced perturbation theoretical approaches to the various Monte Carlo techniques, via Coupled-Cluster (CC) theory and Full Configuration Interaction (FCI) theory. Many of these methods are extremely powerful and have provided electronic structure calculations that are in excellent agreement with experimental results. The major disadvantage with *ab initio* methods is that they are computationally demanding, especially when the number of particles in the system increases. The so-called adiabatic-connection method (see for example [19]) can be used to link *ab initio* methods, such as the Coupled-Cluster and Configure Interaction method, with DFT in order to construct a more accurate density functional than the standard approximations. Thus by doing *ab initio* calculations on small fragments, such as *one* quantum dot, a more accurate density functional can be obtained in order to model a material containing a large number of quantum dots more precisely. However, in the case of a quantum dot, an accurate electronic structure calculation must be done. We require an accurate and reliable *ab initio* many-body method.

The aim of this thesis is to study quantum dots numerically using the Coupled-Cluster Singles and Double (CCSD) *ab initio* method [20]. The Coupled-Cluster (CC) method has been extremely successful in providing almost exact *ab initio* results in quantum chemistry, atomic physics, molecular physics, and nuclear physics. We will consider the so-called parabolic quantum dot in two dimensions, see Section 4 for details. On the surface, this thesis is about quantum dots. However, the goal of the analysis, and thus this thesis, is to study the CCSD method itself, and investigate the reliability and accuracy of the calculations. The study of the accuracy of the CCSD method with respect to the size of the model space will constitute an important part of this thesis. The main drawback with wavefunction based methods such as FCI and CC is that the problem scales almost exponentially with the numbers of particles in the system. This is called the curse of dimensionality. A common way to circumvent the dimensionality problem is to introduce a renormalized interaction, called effective interaction. This technique is widely applied in the nuclear many-body problem, see for example [21, 22]. In addition to the standard Coulomb interaction, we will therefore also employ an effective interaction and investigate the accuracy of the CCSD results. This analysis will contain important elements such as Hartree-Fock calculations, correlation energies, choice of basis, discussion of the CC amplitudes, size of the model space, and the *type* of the model space. Where possible, the accuracy of our results will be compared with results obtained by other *ab initio* methods.

---

In order to achieve this we have developed a Restricted Hartree-Fock (HF) program and a Coupled Cluster Singles and Doubles (CCSD) program for studies of quantum dots. The ground state energies for parabolic quantum dots containing 2, 6, 12 and 20 electron have been calculated with different strengths of the confinement potential. These numbers are so-called *magic numbers* (discussed in Chapter 4) meaning that the quantum dots are closed-shell systems.

## Overview

The thesis is structured into three main parts:

- Part I : Theory
- Part II : Many-Body Methods
- Part III : Implementations and Results

Part I gives a presentation of the theoretical foundation of this thesis. We have organized the theory into three chapters. Chapter 1 gives a review of non-relativistic quantum mechanics and the fundamental postulates that form the basis of the theory. We focus on the single-particle system and emphasize important notions such as coordinate representation, intrinsic spin and total wavefunction. In Chapter 2 we move over to non-relativistic many-body theory, i.e. quantum mechanics of systems containing more than one particle. First we present the apparently everlasting many-body problem. Then we move over to the non-interacting system and present important aspects such as identical particles and implications on the many-body wavefunction. We will also give a review of the formalism of second quantization including definitions of creation and annihilation operators, operators in second quantization, Wick's theorem and the particle-hole formalism. Chapter 3 gives a presentation of the theoretical description of quantum dots. First we discuss the approximations of the Hamiltonian leading to the so-called parabolic quantum dot system. Then we solve the Schrödinger equation for the single-electron quantum dot in 2 dimensions. This is needed in the the many-body treatment. Finally we establish the  $N$ -electron Hamiltonian and scale it into a dimensionless form.

Part II is devoted to a presentation of the Restricted Hartree-Fock (RHF) method and the Coupled-Cluster Singles and Doubles (CCSD) method. Chapter 5 gives a review of the RHF method. We present the basic ideas and derive the HF equations that are implemented in our program. In Chapter 6 we present the Coupled-Cluster (CC) method. The first sections are devoted to a general presentation of the method including a motivation for CC wavefunction, fundamental concepts, and the formal CC theory. Then we move over to the CCSD scheme and derive the energy equation in detail using both an analytical (Wick's theorem) and diagrammatic approach. We will also derive the programmable form of the amplitude equations using diagrams.

Part III gives a presentation of the implementations and the results. In Chapter 7 we present the implementation of the Restricted Hartree-Fock method and the Coupled-Cluster Singles and Doubles method. We will focus on the CCSD implementation. We present the structure of the code, derivation of the implemented amplitude equations (leading to definitions of intermediates), and code examples. Furthermore, Chapter 8 presents our numerical results. The results are discussed and analyzed. We also compare with results obtained by other CCSD calculations as well as other many-body methods. Finally at the end of the thesis we summarize and draw our conclusions.



# Part I

# THEORY



# Chapter 2

## Quantum Mechanics

Mechanics is the field of physics concerned with the behavior of physical bodies when subjected to forces, and the effect of the bodies on the environment. We have two major sub-fields in the science of mechanics. *Classical mechanics* is used for describing the dynamics of macroscopic objects, while *quantum mechanics* is used for describing the dynamics of microscopic objects. Quantum mechanics is a theoretical description of Nature that was developed by many physicists during the first decades of the last century. The theory contained elements that were completely unknown in classical mechanics:

- Quantization: Many physical quantities can only have certain discrete values.
- Wave-particle duality: Both particles and fields (for example electromagnetic fields) have wave properties and particle properties.
- Probability interpretation: The quantum mechanical description can only give the probability to find a particle at a certain location.
- Uncertainty principle: Nature puts fundamental limits on the precision that some physical variables can be measured by.
- Annihilation and creation: Any particle can be created and/or destroyed.

Quantum mechanics was created because many experimental results were totally inconsistent with classical physics. Already in 1752, Thomas Melville observed the characteristic sodium line. Fraunhofer's measurements of the spectrum of the sunlight in 1814 served as a basis for many spectroscopic experiments. Johann Balmer discovered in 1885 an empirical formula for the wavelength of the emitted light from a hydrogen gas. It is given as

$$\lambda_n = 3.6456 \cdot 10^{-7} \frac{n^2}{n^2 - 4} \text{m}, \quad (2.1)$$

where  $n = 3, 4, 5, 6$ , and so forth. None of these experiments could be understood with classical physics. However, the *real* crisis in physics came with the photoelectric effect, the Compton effect, and diffraction experiments with electrons. We refer to [23] for details.

Put simply, quantum mechanics is the theoretical framework within which it has been found possible to describe, correlate and predict the behavior of a vast range of physical systems: from systems containing elementary particles, through nuclei and atoms, to molecules and solids. This chapter aims to give a short review of quantum mechanics. It is assumed that the reader is well acquainted with the fundamental theory. The focus in the presentation will be on parts that are directly relevant for this thesis. The first section is devoted to the general postulates of quantum mechanics. In the second section we present basic concepts of single-particle quantum mechanics, with an emphasize on the time-independent Schrödinger equation, coordinate representation, intrinsic spin, and the total wavefunction of a particle. We refer to [24] and [25] for an introduction to the field. For a more profound presentation, we refer to [26].

## 2.1 Postulates of Quantum Mechanics

Every fundamental physical theory is based on postulates. We will in the following present the postulates of quantum mechanics.

- [1] A quantum state of an isolated system is described by a vector in a complex (finite/infinite) and linear vector space, called Hilbert space.

*Comments:* In the bra-ket formalism, for every quantum state  $|\Psi\rangle$  in the Hilbert space (called “ket”), there exists a dual state  $\langle\Psi|$  in a dual vector space (called “bra”). The Hilbert space  $\mathcal{H}$  is a complex inner product space meaning that  $\mathcal{H}$  is a complex vector space on which there exists an inner product. An inner product is a function that to each pair of vectors  $|\alpha\rangle$  and  $|\beta\rangle$  in  $\mathcal{H}$  associates a complex number

$$\langle\alpha|\beta\rangle. \quad (2.2)$$

It satisfies

$$\langle\alpha|\beta\rangle = \langle\beta|\alpha\rangle^* \quad (2.3)$$

$$\langle c_1\alpha_1 + c_2\alpha_2|\beta\rangle = c_1\langle\alpha_1|\beta\rangle + c_2\langle\alpha_2|\beta\rangle \quad (2.4)$$

$$\langle c\alpha|\beta\rangle = c\langle\alpha|\beta\rangle \quad (2.5)$$

$$\langle\alpha|\alpha\rangle \geq 0, \quad (2.6)$$

where  $*$  is the complex conjugate, and  $c$ ,  $c_1$  and  $c_2$  are complex numbers. We refer to [27] for more details. Assume we have a discrete basis,

$$\mathcal{B} = \{|i\rangle\}_{i=1}^d, \quad (2.7)$$

where  $d = \dim(\mathcal{H})$ . The orthonormality relation reads

$$\langle i|j\rangle = \delta_{ij}, \quad (2.8)$$

and completeness relation is given as

$$\hat{I} = \sum_i^d |i\rangle\langle i|, \quad (2.9)$$

where  $\delta_{ij}$  is the Kronecker delta,  $\hat{I}$  is the identity operator, and  $d$  is the dimension of the space. The quantum state can then be written as a linear combination of these basis functions, viz.

$$|\Psi\rangle = \sum_i |i\rangle\langle i|\Psi\rangle = \sum_i c_i|i\rangle, \quad (2.10)$$

where  $c_i \equiv \langle i|\Psi\rangle$ . When the basis is continuous, the orthonormality relation is given as

$$\langle x|x'\rangle = \delta(x - x'), \quad (2.11)$$

and the completeness relation as

$$\hat{I} = \int dx|x\rangle\langle x|, \quad (2.12)$$

where  $\delta(x - x')$  is the Dirac delta function. The quantum state then reads

$$|\Psi\rangle = \int dx|x\rangle\langle x|\Psi\rangle = \int dx c(x)|x\rangle, \quad (2.13)$$

where  $c(x) \equiv \langle x|\Psi\rangle$ .

- [2] To every physical observable of a quantum system corresponds a linear, hermitian operator acting on vectors in the Hilbert space. Operators representing the generalized coordinate  $q_n$  and the corresponding generalized momentum  $p_n$  satisfy the commutation relation

$$[\hat{q}_n, \hat{p}_n] = i\hbar, \quad (2.14)$$

where  $i$  is the imaginary unit, and  $\hbar$  is the (reduced) Planck constant.

*Comments:* A hermitian operator is defined as

$$\hat{A} = \hat{A}^\dagger, \quad (2.15)$$

where  $\hat{A}^\dagger$  is the hermitian conjugate of  $\hat{A}$ . The eigenvalue equation of  $\hat{A}$  reads

$$\hat{A}|a_i\rangle = a_i|a_i\rangle, \quad (2.16)$$

where  $|a_i\rangle$  is an eigenfunction with corresponding eigenvalue  $a_i$ . The set of eigenfunctions  $\{|a_i\rangle\}_{i=1}^d$ , where  $d$  is the dimension of the Hilbert space, forms a complete set of vectors, i.e.

$$\hat{I} = \sum_i^d |a_i\rangle\langle a_i|. \quad (2.17)$$

The spectral decomposition of any hermitian operator is given as

$$\hat{A} = \sum_i^d a_i |a_i\rangle\langle a_i|. \quad (2.18)$$

- [3] The time evolution of the quantum state is (in the Schrödinger picture) represented by a time-dependent state vector  $|\Psi(t)\rangle$  that satisfies the fundamental Schrödinger equation

$$i\hbar \frac{d}{dt} |\Psi(t)\rangle = \hat{H} |\Psi(t)\rangle, \quad (2.19)$$

with  $\hat{H}$  as the Hamiltonian of the system.

*Comments:* Since the Schrödinger equation is a linear differential equation with a first order time derivative, the quantum state  $|\Psi(t)\rangle$  is uniquely determined by  $|\Psi(t_0)\rangle$  for  $t_0 \neq t$ . Thus

$$|\Psi(t)\rangle = \hat{\mathcal{U}}(t, t_0) |\Psi(t_0)\rangle, \quad (2.20)$$

where  $\hat{\mathcal{U}}(t, t_0)$  is the time evolution operator determined by  $\hat{H}$ . We have that  $\hat{\mathcal{U}}(t, t_0)$  must be linear and unitary, i.e.

$$\hat{\mathcal{U}}\hat{\mathcal{U}}^\dagger = \hat{\mathcal{U}}^\dagger\hat{\mathcal{U}} = \hat{I}, \quad (2.21)$$

where  $\hat{I}$  is the identity operator. Inserting Eq. (2.20) into Eq. (2.19) yields the following equation for the time evolution operator,

$$i\hbar \frac{\partial}{\partial t} \hat{\mathcal{U}}(t, t_0) = \hat{H}(t) \hat{\mathcal{U}}(t, t_0). \quad (2.22)$$

When the Hamiltonian is time-independent, we obtain

$$\hat{\mathcal{U}}(t, t_0) = e^{-i\hat{H}(t-t_0)/\hbar}. \quad (2.23)$$

Given an initial quantum state  $|\Psi(t_0)\rangle$ , the quantum state (for an isolated system) at  $t > t_0$  reads

$$|\Psi(t)\rangle = e^{-i\hat{H}(t-t_0)/\hbar} |\Psi(t_0)\rangle. \quad (2.24)$$

- [4] In any measurement of the observable associated with the operator  $\hat{A}$ , the measured value will *always* be an eigenvalue of  $\hat{A}$ . The eigenvalue equation is given as

$$\hat{A}|a_i\rangle = a_i|a_i\rangle, \quad (2.25)$$

where  $a_i$  is the eigenvalue and  $|a_i\rangle$  is the corresponding eigenvector.

*Comments:* Assume the system is in quantum state  $|\Psi\rangle$ . The measured eigenvalue  $a_i$  will appear with probability

$$p_i = \sum_{n=1}^l |\langle a_{in}|\Psi\rangle|^2, \quad (2.26)$$

where  $l = 1, 2, 3, \dots$ , and

$$\hat{A}|a_{in}\rangle = a_i|a_{in}\rangle, \quad (2.27)$$

where  $\{|a_{in}\rangle\}_{n=1}^l$  are possible degenerate eigenfunctions. When the energy level is degenerate, i.e. several eigenfunctions have the same energy, we have that  $l > 1$ . In the non-degenerate case we have that  $l = 1$ . When the eigenvalue  $x$  of an operator  $\hat{x}$  is a continuous variable,  $p_i$  in Eq. (2.26) is a probability density.

- [5] In an ideal measurement, when the measured value of an observable  $\hat{A}$  is  $a_i$ , the quantum state immediately changes to the corresponding eigenstate, i.e.

$$|\Psi\rangle \rightarrow |a_i\rangle. \quad (2.28)$$

*Comments:* This is called the collapse of the wavefunction. When a measurement of  $\hat{A}$  yields  $a_i$ , measurements at all later times will with certainty yield  $a_i$ .

## 2.2 Single-Particle Quantum Mechanics

Consider a single-particle system with Hamiltonian

$$\hat{H} = \hat{T} + \hat{U}, \quad (2.29)$$

where  $\hat{T}$  is the kinetic energy operator, and  $\hat{U}$  is the potential energy operator. The dynamics of the system is provided by the time-dependent Schrödinger equation, which in bra-ket notation reads

$$i\hbar \frac{d}{dt} |\Psi(t)\rangle = \hat{H} |\Psi(t)\rangle, \quad (2.30)$$

where  $|\Psi(t)\rangle$  is the quantum state of the system at time  $t$ ,  $i$  is the standard imaginary unit with the property  $i^2 = -1$ , and  $\hbar$  is the (reduced) Planck constant. When the Hamiltonian is time-independent, the time evolution of the state vector reads (see Postulate 3 in Sec. 2.1)

$$\hat{U}(t, t_0) = e^{i\hat{H}(t-t_0)/\hbar}, \quad (2.31)$$

where  $|\Psi(t_0)\rangle$  is the initial state vector. Since the time evolution of the state vector is totally determined by the Hamiltonian, the solutions of the energy eigenvalue equation,

$$\hat{H}|\phi_j\rangle = \varepsilon_j|\phi_j\rangle, \quad (2.32)$$

can be used to obtain an analytical expression of  $|\Psi(t)\rangle$ . This equation is called the time-independent Schrödinger equation. When the eigenvalues  $\varepsilon_j$  and eigenvectors  $|\phi_j\rangle$  are determined, the initial state vector can be written as

$$|\Psi(t_0)\rangle = \sum_{j=1}^d \langle \phi_j | \Psi(t_0) \rangle |\phi_j\rangle, \quad (2.33)$$

since

$$\hat{I} = \sum_{j=1}^d |\phi_j\rangle\langle\phi_j|, \quad (2.34)$$

where  $d$  is the dimension of the Hilbert space, see Postulate 1 in Section 2.1. The quantum state at time  $t > t_0$  then reads

$$|\Psi(t)\rangle = e^{i\hat{H}(t-t_0)/\hbar} \sum_{j=1}^d \langle \phi_j | \Psi(t_0) \rangle |\phi_j\rangle = \sum_{j=1}^d \langle \phi_j | \Psi(t_0) \rangle e^{i\varepsilon_j(t-t_0)/\hbar} |\phi_j\rangle. \quad (2.35)$$

Provided an initial state vector and a time-independent Hamiltonian, the state vector at time  $t > t_0$  can in principle always be determined by solving the time-independent Schrödinger equation in (2.32). In addition, the energy spectrum is often the main interest in quantum mechanical calculations. We will therefore in the following consider the time-independent Schrödinger equation.

### 2.2.1 Coordinate Representation

The time-independent Schrödinger equation in (2.32) is written in the bra-ket formalism. This formalism offers a general and concise notation. When we want to do explicit calculations, we often transform the time-independent Schrödinger equation to the coordinate representation. In the 1-dimensional case, the eigenvalue equation of the position operator  $\hat{x}$  reads

$$\hat{x}|x\rangle = x|x\rangle, \quad (2.36)$$

where  $|x\rangle$  is the eigenvector and  $x$  is the corresponding eigenvalue. The completeness relation reads

$$\hat{I} = \int_{-\infty}^{\infty} dx |x\rangle\langle x|. \quad (2.37)$$

The energy eigenfunctions in Eq. (2.32) can then be written as (suppressing the  $j$ -index)

$$|\phi\rangle = \int_{-\infty}^{\infty} dx \phi(x) |x\rangle, \quad (2.38)$$

where we have defined

$$\phi(x) \equiv \langle x | \phi \rangle. \quad (2.39)$$

We multiply Eq. (2.32) with  $\langle x |$  from the left, yielding

$$\langle x | \hat{H} | \phi \rangle = \varepsilon \langle x | \phi \rangle. \quad (2.40)$$

Using the completeness relation in Eq. (2.37) we obtain

$$\int_{-\infty}^{\infty} dx' \langle x | \hat{H} | x' \rangle \langle x' | \phi \rangle = \varepsilon \langle x | \phi \rangle, \quad (2.41)$$

leading to

$$\int_{-\infty}^{\infty} dx' \langle x | \hat{H} | x' \rangle \phi(x') = \varepsilon \phi(x), \quad (2.42)$$

where we have used the definition in Eq. (2.39). In the 1-dimensional case, the momentum operator is given as [24]

$$\hat{p} = -i\hbar \frac{\partial}{\partial x}. \quad (2.43)$$

When  $\hat{H} = \hat{H}(\hat{x}, \hat{p})$  we obtain that

$$\langle x | \hat{H}(\hat{x}, \hat{p}) | x' \rangle = \hat{H}(x, -i\hbar \frac{\partial}{\partial x}) \delta(x - x'), \quad (2.44)$$

where  $\delta(x - x')$  is the Dirac delta function. See [24] for a derivation. Inserting this expression into Eq. (2.42) yields

$$\hat{H}(x, -i\hbar \frac{\partial}{\partial x}) \phi(x) = \varepsilon \phi(x), \quad (2.45)$$

which is nothing but the time-independent Schrödinger equation in the coordinate representation. Suppressing the parenthesis in the Hamiltonian, the 3-dimensional time-independent Schrödinger equation reads

$$\hat{H} \phi(x, y, z) = \varepsilon \phi(x, y, z), \quad (2.46)$$

where  $x, y$  and  $z$  are cartesian coordinates. In classical mechanics, the kinetic energy of a particle is given as

$$T = \frac{p^2}{2m}, \quad (2.47)$$

where  $p = mv$  is the momentum, and  $m$  is the mass of the particle. The quantum mechanical kinetic energy thus reads

$$\hat{T} = \frac{\hat{p}^2}{2m}, \quad (2.48)$$

where  $T$  and  $p$  are changed to  $\hat{T}$  and  $\hat{p}$ , respectively. The momentum operator is given as

$$\hat{p} = -i\hbar \nabla, \quad (2.49)$$

where  $\nabla$  is the gradient. The Hamiltonian thus reads

$$\hat{H} = \frac{\hat{p}^2}{2m} + u(x, y, z) = -\frac{\hbar^2}{2m} \nabla^2 + u(x, y, z), \quad (2.50)$$

leading to the most common form of the time-independent Schrödinger equation,

$$\left( -\frac{\hbar^2}{2m} \nabla^2 + u(x, y, z) \right) \phi(x, y, z) = \varepsilon \phi(x, y, z), \quad (2.51)$$

where  $\phi(x, y, z)$  is the eigenfunction with corresponding eigenvalue  $\varepsilon$ ,  $m$  is the mass of the particle, and  $u = u(x, y, z)$  is the potential.

### 2.2.2 Intrinsic Spin

In classical mechanics, an object admits two kinds of angular momentum. The first is the orbital momentum defined as

$$\mathbf{L} = \mathbf{r} \times \mathbf{p}, \quad (2.52)$$

where  $\mathbf{r}$  is the position vector and  $\mathbf{p}$  is the momentum vector. The second is the spin momentum

$$\mathbf{S} = I\omega, \quad (2.53)$$

where  $I$  is the moment of inertia, and  $\omega$  is the angular velocity. While the orbital momentum is associated with the motion of the center of mass, the spin momentum is associated with motion about the center of mass. In quantum mechanics, orbital momentum is also associated with the motion of particles in space. Particles also carry another form of angular momentum, called *intrinsic spin*. This spin has nothing to do with motion in space. The algebraic theory of spin ( $\hat{S}$ ) is identical to the theory of orbital momentum ( $\hat{L}$ ), see [24]. The fundamental commutation relations reads

$$[\hat{S}_x, \hat{S}_y] = i\hbar\hat{S}_z \quad [\hat{S}_y, \hat{S}_z] = i\hbar\hat{S}_x \quad [\hat{S}_z, \hat{S}_x] = i\hbar\hat{S}_y, \quad (2.54)$$

where  $\hat{S}_x$ ,  $\hat{S}_y$  and  $\hat{S}_z$  are the components of  $\hat{S}$ . The eigenvectors of  $\hat{S}^2$  and  $\hat{S}_z$  satisfy [24]

$$\hat{S}^2|s m_s\rangle = \hbar s(s+1)|s m_s\rangle \quad (2.55)$$

$$\hat{S}_z|s m_s\rangle = \hbar m_s|s m_s\rangle, \quad (2.56)$$

where  $s$  is the principal spin quantum number, and  $m_s$  is the quantum number associated with the  $z$ -projection of the spin. Since the components of the spin do not have a common set of eigenfunctions, they are incompatible observables. This means that we cannot determine two components, say  $\hat{S}_z$  and  $\hat{S}_x$ , at the same time. However, we can determine *one* of the components and  $\hat{S}^2$  simultaneously. Standard textbooks in quantum mechanics often choose the  $z$ -component of the spin (see for example [24], [25] and [28]), and we therefore also do so. Since the intrinsic spin cannot be associated with motion in space, the eigenfunctions of  $\hat{S}_z$  and  $\hat{S}^2$  cannot be written down as analytical functions. The spin quantum numbers are given as [25]

$$s = 0, \frac{1}{2}, 1, \frac{3}{2}, 2, \frac{5}{2}, \dots \quad (2.57)$$

$$m_s = -s, -s+1, \dots, s-1, s. \quad (2.58)$$

Each elementary particle has a fixed value of  $s$ . Often we call  $s$  the *spin* of the particle. Electrons have spin  $1/2$ , photons have spin  $1$ , gravitons have spin  $2$ , and so forth. The measured value of  $\hat{S}^2$  for a certain elementary particle will therefore *always* be  $\hbar s(s+1)$ .

We will now consider the spin  $1/2$  case, i.e.

$$s = \frac{1}{2}, \quad (2.59)$$

which is by far the most important case. This is the spin of electrons (and other leptons), protons, neutrons (and other baryons), and quarks. The measured value of  $\hat{S}^2$  will in this case be  $3\hbar^2/4$ . Since  $s = 1/2$ , the quantum number associated with the  $z$ -projection of the spin can have two values,

$$m_s = \pm \frac{1}{2}. \quad (2.60)$$

The measured value of  $\hat{S}_z$  (or another component of the spin) will therefore be either  $\hbar/2$  or  $-\hbar/2$ . The eigenfunctions of  $\hat{S}^2$  and  $\hat{S}_z$  are given as

$$\left| \frac{1}{2}, \frac{1}{2} \right\rangle \equiv |+\rangle \quad (2.61)$$

$$\left| \frac{1}{2}, -\frac{1}{2} \right\rangle \equiv |-\rangle \quad (2.62)$$

which are often referred to as *spin up* and *spin down*, respectively. Thus, when  $s = 1/2$ , the Hilbert space of the spin is 2-dimensional. Using the eigenstates of  $\hat{S}^2$  and  $\hat{S}_z$  in Eqs. (2.61) and (2.62) as basis vectors, the general state of a spin 1/2 particle reads

$$|\chi\rangle = a|+\rangle + b|-\rangle, \quad (2.63)$$

where  $a$  and  $b$  are the weights. We often call  $|\chi\rangle$  a spinor. The spinor must be normalized, i.e.  $\sqrt{a^2 + b^2} = 1$ . The measured value of the z-component of the spin for a particle in state  $|\chi\rangle$  will be  $\hbar/2$  with probability  $|a|^2$ , and  $-\hbar/2$  with probability  $|b|^2$ . Since the Hilbert space is 2-dimensional, we can represent spinors by [24]

$$|\chi\rangle = \begin{pmatrix} a \\ b \end{pmatrix}, \quad (2.64)$$

and operators by

$$\hat{A} = \begin{pmatrix} c & d \\ e & f \end{pmatrix}. \quad (2.65)$$

The basis is thus given as

$$|+\rangle = \begin{pmatrix} 1 \\ 0 \end{pmatrix} \quad |-\rangle = \begin{pmatrix} 0 \\ 1 \end{pmatrix}. \quad (2.66)$$

The matrix representation of  $\hat{S}^2$  and  $\hat{S}_z$  are determined by considering the eigenvalue equation for  $|+\rangle$  and  $|-\rangle$ , yielding

$$\hat{S}^2 = \frac{3}{4}\hbar^2 \begin{pmatrix} 1 & 0 \\ 0 & 1 \end{pmatrix}, \quad (2.67)$$

and

$$\hat{S}_z = \frac{\hbar}{2} \begin{pmatrix} 1 & 0 \\ 0 & -1 \end{pmatrix}. \quad (2.68)$$

In the basis of  $|+\rangle$  and  $|-\rangle$ , we have the following matrix representation of  $\hat{S}_x$  and  $\hat{S}_y$ ,

$$\hat{S}_x = \frac{\hbar}{2} \begin{pmatrix} 0 & 1 \\ 1 & 0 \end{pmatrix} \quad \hat{S}_y = \frac{\hbar}{2} \begin{pmatrix} 0 & -i \\ i & 0 \end{pmatrix}, \quad (2.69)$$

where  $i$  is the imaginary unit. Defining the so-called *Pauli spin matrices* [24]

$$\hat{\sigma}_x \equiv \begin{pmatrix} 0 & 1 \\ 1 & 0 \end{pmatrix} \quad \hat{\sigma}_y \equiv \begin{pmatrix} 0 & -i \\ i & 0 \end{pmatrix} \quad \hat{\sigma}_z \equiv \begin{pmatrix} 1 & 0 \\ 0 & -1 \end{pmatrix}, \quad (2.70)$$

we obtain

$$\hat{S}_x = \frac{\hbar}{2}\hat{\sigma}_x \quad \hat{S}_y = \frac{\hbar}{2}\hat{\sigma}_x \quad \hat{S}_z = \frac{\hbar}{2}\hat{\sigma}_z. \quad (2.71)$$

### 2.2.3 Total Wavefunction

Consider the time-independent Schrödinger equation in (2.51). Since the intrinsic spin of a particle has nothing to do with motion in space, the spin degree of freedom cannot be included directly in the energy eigenfunctions  $\phi(x, y, z)$ . However, the spin degree of freedom must be included in some way. First we note that the Hilbert space of the spin, and the Hilbert space spanned by the energy eigenfunctions, are two distinct spaces. The solution to include the spin is to divide the wavefunction into two parts that exist in different spaces. Operators must also be modified in order to reflect which space they act in. Mathematically, this is obtained by the so-called tensor product [29]. We now define the *total* energy eigenfunctions of the time-independent Schrödinger equation as

$$\psi(\mathbf{r}) \equiv \phi(x, y, z) \otimes |\chi\rangle, \quad (2.72)$$

where  $\mathbf{r}$  include the spin degree of freedom,  $\phi(x, y, z)$  is the spatial part, and  $|\chi\rangle = |\pm\rangle$  (see Eqs. 2.61 and 2.62) is the spin part. An operator  $\hat{A}$  acting in the “spatial” Hilbert space is given as

$$\hat{A} \otimes \hat{I}, \quad (2.73)$$

where  $\hat{I}$  is the identity matrix. An operator  $\hat{B}$  that acts in the spin space is given as

$$\hat{I} \otimes \hat{B}. \quad (2.74)$$

For example, given an operator  $\hat{A} \otimes \hat{B}$  acting on the total wavefunction  $\psi(\mathbf{r})$  yields

$$(\hat{A} \otimes \hat{B}) \psi(\mathbf{r}) = \hat{A}\phi(x, y, z) \otimes \hat{B}|\chi\rangle. \quad (2.75)$$

We will in the following drop the tensor product sign when expressing operators. It will be obvious in which space the operators act. We finally obtain the time-independent Schrödinger equation for a single-particle system with Hamiltonian given by Eq. (2.50),

$$\left( -\frac{\hbar^2}{2m} \nabla^2 + u(x, y, z) \right) \psi(\mathbf{r}) = \varepsilon \psi(\mathbf{r}), \quad (2.76)$$

where  $\psi(\mathbf{r})$  is the total wavefunction in Eq. (2.72). Our aim is to solve the time-independent Schrödinger equation and determine the eigenvectors  $\psi(\mathbf{r})$  and eigenvalues  $\varepsilon$ . However, this is as far as we can go before a specific potential  $u$  is provided.



# Chapter 3

## Many-Body Theory

Single-particle quantum mechanics deals with systems consisting of only *one* particle. This is of course a natural and necessary starting point for all quantum mechanical considerations, where fundamental postulates, formalism, quantization effects, and so forth, can be introduced and discussed in peace and quiet without considering the implications of interacting particles. However, *real* systems contain more than one particle. These systems are often called many-body or many-particle systems in the literature, and provide a breeding ground for many-body theory and many approximation schemes and methods.

In this chapter we present the basic quantum mechanics of many-body systems. We will focus on the parts that are directly relevant for this thesis. In the first section we present the "many-body problem", which refers to the  $N$ -particle Schrödinger equation. We will then consider the non-interacting system and the implications of identical particles on the solutions. Then we turn to the interacting system and discuss important properties of the solutions. In the last section we present the formalism of second quantization, including definitions of creation and annihilation operators, Wick's theorem and a presentation of the particle-hole formalism.

### 3.1 The Many-Body Problem

Consider an isolated system consisting of  $N$  particles that can be treated non-relativistic. The properties of the system are given by the Schrödinger equation. In bra-ket notation, the equation reads (see Section 2.1, Postulate 3)

$$i\hbar \frac{\partial}{\partial t} |\Psi(t)\rangle = \hat{H} |\Psi(t)\rangle, \quad (3.1)$$

where  $|\Psi(t)\rangle$  is the  $N$ -particle wavefunction at time  $t$ , and  $\hat{H}$  is the Hamiltonian of the system. The Hamiltonian is defined as

$$\hat{H} = \hat{T} + \hat{V}, \quad (3.2)$$

where  $\hat{T}$  is the total kinetic energy operator, and  $\hat{V}$  is the total potential energy operator. The kinetic energy operator reads

$$\hat{T} = \sum_{k=1}^N \hat{t}_k, \quad (3.3)$$

where  $\hat{t}_k$  is the kinetic energy of electron  $k$ . Since  $\hat{T}$  is the sum of  $\hat{t}_k$ , it is a one-body operator. Furthermore, in the general case, the potential energy operator is given as

$$\hat{V} = \hat{V}_1 + \hat{V}_2 + \hat{V}_3 + \dots + \hat{V}_N \quad (3.4)$$

$$= \sum_{k=1}^N \hat{v}_k^{(1)} + \frac{1}{2!} \sum_{kl}^N \hat{v}_{kl}^{(2)} + \frac{1}{3!} \sum_{klm}^N \hat{v}_{klm}^{(3)} + \dots + \frac{1}{N!} \sum_{klm..q}^N \hat{v}_{klm..q}^{(N)} \quad (3.5)$$

where

$$\hat{V}_n = \frac{1}{n!} \sum_{klm..p}^N \hat{v}_{klm..p}^{(n)} \quad (3.6)$$

is an  $n$ -body potential operator. In electronic systems like atoms and quantum dots, the Hamiltonian is a two-body operator. However, in nuclear physics, the fundamental strong interaction seems to exhibit three-body behavior. This is due to the fact that the exchange particles (gluons) can couple to themselves.

The quantum state at time  $t$  is given as (see Section 2.1)

$$|\Psi(t)\rangle = \hat{\mathcal{U}}(t, t_0)|\Psi(t_0)\rangle, \quad (3.7)$$

where  $t > t_0$ ,  $\mathcal{U}(t, t_0)$  is the time evolution operator, and  $|\Psi(t_0)\rangle$  is the quantum state at time  $t_0$ . When the Hamiltonian is time-independent, the time evolution operator reads

$$\hat{\mathcal{U}}(t, t_0) = e^{-i\hat{H}(t-t_0)/\hbar}. \quad (3.8)$$

If we were to prepare a system in quantum state  $|\Psi(t_0)\rangle$  at time  $t_0$ , the quantum state  $|\Psi(t)\rangle$  at time  $t > t_0$  is determined by simply letting the time evolution operator act on the initial state. Thus the Hamiltonian determines the time evolution of the system. The solution of the energy eigenvalue equation (time-independent Schrödinger equation)

$$\hat{H}|\Psi_\lambda\rangle = E_\lambda|\Psi_\lambda\rangle, \quad (3.9)$$

where  $|\Psi_\lambda\rangle$  is the eigenfunction, and  $E_\lambda$  is the energy eigenvalue, can be used to obtain an algebraic expression of the time evolution. Since the set of eigenfunctions spans the  $N$ -particle Hilbert space, the initial state vector can be written as a linear combinations of eigenfunctions, viz.

$$|\Psi(t_0)\rangle = \sum_\lambda^d C_\lambda |\Psi_\lambda\rangle, \quad (3.10)$$

where  $d$  is the dimension of the Hilbert space, yielding the following analytical expression of the time evolution,

$$|\Psi(t)\rangle = e^{-i\hat{H}(t-t_0)/\hbar}|\Psi_0\rangle = \sum_\lambda^d C_\lambda |\Psi_\lambda\rangle e^{-iE_\lambda(t-t_0)/\hbar}. \quad (3.11)$$

Moreover, the energy eigenvalues and eigenfunctions are often the main target in many-body calculations. The time-independent Schrödinger equation in (3.9) is usually called the quantum mechanical many-body problem. This is a nontrivial problem due to the interaction between the particles. In Nature, particles interact with each other, and realistic Hamiltonians are at least two-body operators. Even for the simplest case when the Hamiltonian is a two-body operator, the many-body problem can in general not be solved exactly. For example, the Hamiltonian for the helium atom reads (in atomic units)

$$\hat{H} = -\frac{1}{2}\nabla_1^2 - \frac{1}{2}\nabla_2^2 - \frac{2}{r_1} - \frac{2}{r_2} + \frac{1}{r_{12}}, \quad (3.12)$$

where  $\nabla_1$  and  $\nabla_2$  are the gradients of electron 1 and 2, respectively,  $r_1$  is the distance between electron 1 and the nucleus,  $r_2$  is the distance between electron 2 and the nucleus, and  $r_{12}$  is the distance between the electrons. This two-body problem cannot be solved exactly. In a quantum mechanical treatment of many-body systems we are therefore forced to utilize approximation schemes and complex techniques. In Part 2, we will present two important many-body methods: the Hartree-Fock [18] and the Coupled-Cluster method [20].

We will in the following consider the non-interacting many-body system. This system serves as a starting point for most many-body methods such as the Hartree-Fock method and the Coupled-Cluster method [30].

## 3.2 The Non-Interacting System

The non-interacting system consists of  $N$  non-interacting particles. This system is also called the unperturbed system. The Hamiltonian reads

$$\hat{H}_0 = \hat{T} + \hat{U}, \quad (3.13)$$

where  $\hat{T}$  is the total kinetic energy operator (given in Eq. 3.3), and  $\hat{U}$  is a possible external one-body potential given as

$$\hat{U} = \sum_{k=1}^N \hat{u}_k, \quad (3.14)$$

where  $\hat{u}_k$  is the potential energy of particle  $k$ . Defining

$$\hat{h} = \hat{T} + \hat{u}, \quad (3.15)$$

we obtain that

$$\hat{H}_0 = \sum_{k=1}^N \hat{h}_k. \quad (3.16)$$

The time-independent Schrödinger equation reads (in bra-ket notation)

$$\hat{H}_0 |\Phi_a\rangle = E_a |\Phi_a\rangle, \quad (3.17)$$

where  $|\Phi_a\rangle$  is the energy eigenvector, and  $E_a$  is the energy eigenvalue. We now assume the particles are distinguishable. Since the Hamiltonian is a one-body operator, Eq. (3.17) is separable. The energy eigenfunctions are given as

$$|\Phi_a\rangle = |\psi_\alpha\rangle \otimes |\psi_\beta\rangle \otimes |\psi_\gamma\rangle \otimes \dots \otimes |\psi_\delta\rangle, \quad (3.18)$$

where  $a$  denotes the set of quantum numbers  $(\alpha, \beta, \gamma, \dots, \delta)$ . The single-particle energy eigenfunctions are determined by

$$\hat{h} |\psi_\alpha\rangle = \varepsilon_\alpha |\psi_\alpha\rangle, \quad (3.19)$$

where  $\varepsilon_\alpha$  is the energy eigenvalue. We note that  $|\psi_\alpha\rangle$  is the total single-particle wavefunction, i.e. it includes the spin, see Sections 2.2.2 and 2.2.3. The energy eigenvalues of the non-interacting system are thus given as

$$E_a = \sum_{\alpha \in a} \varepsilon_\alpha, \quad (3.20)$$

where the sum runs over all occupied single-particle states  $\alpha$  in the Slater determinant  $|\Phi_a\rangle$ . The simple product form in Eq. (3.18) assumes that we can tell the particles apart. It would otherwise make no sense to claim that particle 1 is in state  $\psi_\alpha$ , particle 2 is in state  $\psi_\beta$ , and so forth. On the macroscopic scale, we can in principle always distinguish particles from each other. However, on a microscopic scale, the situation is fundamentally different. Considering for example a system of electrons, we will never be able to tell them apart. Moreover, it is not just that we do not happen to know. There is no such thing as “this” or “that” electron. Electrons are *identical* in a way classical objects will never be. The solution in Eq. (3.18) can therefore not be used for systems consisting of identical particles.

### 3.3 Identical Particles

Consider a non-interacting system consisting of  $N$  identical particles. We will now utilize the coordinate representation. The single-electron energy eigenfunctions (see Eq. 3.19) reads

$$\psi_\alpha(\mathbf{r}) = \langle \mathbf{r} | \psi_\alpha \rangle, \quad (3.21)$$

where  $\mathbf{r}$  includes the spin. We start our discussion by investigating the permutation operator  $\hat{P}$ . It is defined through its action on the  $N$ -particle product state,

$$\hat{P}_{ij}\psi_\alpha(\mathbf{r}_1)\dots\psi_\beta(\mathbf{r}_i)\dots\psi_\gamma(\mathbf{r}_j)\dots\psi_\delta(\mathbf{r}_N) = \psi_\alpha(\mathbf{r}_1)\dots\psi_\beta(\mathbf{r}_i)\dots\psi_\gamma(\mathbf{r}_j)\dots\psi_\delta(\mathbf{r}_N), \quad (3.22)$$

i.e. it interchanges the coordinates of particle  $i$  and  $j$ . When the particles are identical, this should not affect their probability distribution. We define

$$\Phi_a(\mathbf{r}_1, \mathbf{r}_2, \dots, \mathbf{r}_N) = \langle \mathbf{r}_1 \mathbf{r}_2 \dots, \mathbf{r}_N | \Phi_a \rangle \quad (3.23)$$

as the eigenfunction of  $N$  non-interacting and identical particles. Thus we obtain that

$$|\Phi_a(\mathbf{r}_1, \dots, \mathbf{r}_i, \dots, \mathbf{r}_j, \dots, \mathbf{r}_N)|^2 = |\Phi_a(\mathbf{r}_1, \dots, \mathbf{r}_j, \dots, \mathbf{r}_i, \dots, \mathbf{r}_N)|^2, \quad (3.24)$$

leading to

$$\Phi_a(\mathbf{r}_1, \dots, \mathbf{r}_i, \dots, \mathbf{r}_j, \dots, \mathbf{r}_N) = \pm \Phi_a(\mathbf{r}_1, \dots, \mathbf{r}_j, \dots, \mathbf{r}_i, \dots, \mathbf{r}_N). \quad (3.25)$$

The wavefunction is therefore either antisymmetric or symmetric with respect to the interchange of two particles. The non-interacting Hamiltonian is invariant under the interchange of particles. It follows that

$$[\hat{H}_0, \hat{P}_{ik}] = 0, \quad (3.26)$$

i.e.  $\hat{H}_0$  and  $\hat{P}$  are compatible observables. Thus there exist eigenfunctions  $\hat{H}_0$  that are also eigenfunctions of  $\hat{P}_{ij}$  (see [31]). The eigenvalue equation of the permutation operator reads

$$\hat{P}_{ij}\Phi_a(\mathbf{r}_1, \dots, \mathbf{r}_i, \dots, \mathbf{r}_j, \dots, \mathbf{r}_N) = \beta\Phi_a(\mathbf{r}_1, \dots, \mathbf{r}_i, \dots, \mathbf{r}_j, \dots, \mathbf{r}_N). \quad (3.27)$$

Since

$$\hat{P}_{ij}^2 = 1, \quad (3.28)$$

it follows that

$$\beta = \pm 1, \quad (3.29)$$

leading to Eq. (3.25). Particles with a symmetric wavefunction ( $\beta = +1$ ) are called bosons, while particles with an antisymmetric wavefunction ( $\beta = -1$ ) are called fermions. Depending on whether the system consists of identical bosons or fermions, the eigenfunctions of Eq. (3.17) are either symmetric or antisymmetric. Consider now a two-particle system. We can construct the following normalized symmetric (S) and antisymmetric (AS) wavefunctions

$$\Phi_S(\mathbf{r}_1, \mathbf{r}_2) = \frac{1}{\sqrt{2}} [\phi_\alpha(\mathbf{r}_1)\phi_\beta(\mathbf{r}_2) + \phi_\alpha(\mathbf{r}_2)\phi_\beta(\mathbf{r}_1)], \quad (3.30)$$

$$\Phi_{AS}(\mathbf{r}_1, \mathbf{r}_2) = \frac{1}{\sqrt{2}} [\phi_\alpha(\mathbf{r}_1)\phi_\beta(\mathbf{r}_2) - \phi_\alpha(\mathbf{r}_2)\phi_\beta(\mathbf{r}_1)], \quad (3.31)$$

where the single-particle orbitals are given in Eq. (3.19). Both  $\Phi_S$  and  $\Phi_{AS}$  are eigenstates of the permutation operator with eigenvalue  $+1$  and  $-1$ , respectively. Moreover, they are also eigenstates of the non-interacting Hamiltonian  $\hat{H}_0$  with energy eigenvalue

$$E_a = \varepsilon_\alpha + \varepsilon_\beta. \quad (3.32)$$

In the general  $N$ -particle case, symmetric and antisymmetric wavefunctions are constructed by the so-called symmetrizer and antisymmetrizer operators acting on product states, respectively. The symmetrizer is defined as

$$\hat{\mathcal{S}} = \frac{1}{N!} \sum_p \hat{P}, \quad (3.33)$$

and the antisymmetrizer as

$$\hat{\mathcal{A}} = \frac{1}{N!} \sum_p (-1)^p \hat{P}, \quad (3.34)$$

where  $p$  is the permutation number. Normalized symmetric and antisymmetric states are then given by

$$\Phi_S(\mathbf{r}_1, \mathbf{r}_2, \dots, \mathbf{r}_N) = \sqrt{\frac{N!}{n_\alpha! n_\beta! \dots n_\gamma!}} \hat{\mathcal{S}} \psi_\alpha(\mathbf{r}_1) \psi_\beta(\mathbf{r}_2) \dots \psi_\delta(\mathbf{r}_N) \quad (3.35)$$

and

$$\Phi_{AS}(\mathbf{r}_1, \mathbf{r}_2, \dots, \mathbf{r}_N) = \sqrt{N!} \hat{\mathcal{A}} \psi_\alpha(\mathbf{r}_1) \psi_\beta(\mathbf{r}_2) \dots \psi_\delta(\mathbf{r}_N), \quad (3.36)$$

respectively. The antisymmetric wavefunction can be written as a determinant, viz.

$$\Phi_{\alpha\beta\dots\delta}(\mathbf{r}_1, \mathbf{r}_2, \dots, \mathbf{r}_N) = \frac{1}{\sqrt{N!}} \begin{vmatrix} \psi_\alpha(\mathbf{r}_1) & \psi_\beta(\mathbf{r}_1) & \dots & \psi_\delta(\mathbf{r}_1) \\ \psi_\alpha(\mathbf{r}_2) & \psi_\beta(\mathbf{r}_2) & \dots & \psi_\delta(\mathbf{r}_2) \\ \vdots & \vdots & \vdots & \vdots \\ \psi_\alpha(\mathbf{r}_N) & \psi_\beta(\mathbf{r}_N) & \dots & \psi_\delta(\mathbf{r}_N) \end{vmatrix}, \quad (3.37)$$

called a Slater determinant. We observe that a single-particle state can only be occupied by *one* fermion. If we were to put two fermions in the same state, the antisymmetric wavefunction would be equal to zero. This is completely nonsense. In 1925, Wolfgang Pauli formulated the so-called Pauli exclusion principle: Two identical fermions cannot occupy the same single-particle state simultaneously. However, bosons may occupy the same single-particle state. In Nature, bosons have integer spin, and fermions have half integer spin.

## 3.4 The Interacting Many-Body System

In this section we consider the interacting many-body system. We limit the discussion to systems consisting of  $N$  fermions. In the coordinate representation, the Schrödinger equation reads

$$\hat{H} \Psi_\lambda(\mathbf{r}_1, \mathbf{r}_2, \dots, \mathbf{r}_N) = E_\lambda \Psi_\lambda(\mathbf{r}_1, \mathbf{r}_2, \dots, \mathbf{r}_N), \quad (3.38)$$

where  $E_\lambda$  is the energy eigenvalue, and

$$\Psi_\lambda(\mathbf{r}_1, \mathbf{r}_2, \dots, \mathbf{r}_N) = \Upsilon_\eta(\vec{r}_1, \vec{r}_2, \dots, \vec{r}_N) \otimes |\chi_\zeta\rangle \quad (3.39)$$

is the total wavefunction (see Section 2.2.3), where  $\lambda$  denote the set of quantum numbers  $(\eta, \zeta)$ ,  $\Upsilon_\eta(\vec{r}_1, \vec{r}_2, \dots, \vec{r}_N)$  is the spatial part,  $\vec{r}$  is the position vector, and  $|\chi_\zeta\rangle$  is the spin part. As pointed out before, the Schrödinger equation cannot in general be solved exactly. However, the symmetry properties of the Hamiltonian can be used in order to obtain important information about the eigenfunctions. The permutation symmetry is an obvious symmetry for systems consisting of identical fermions. We obtain that

$$[\hat{H}, \hat{P}] = 0, \quad (3.40)$$

where the permutation operator is defined in Eq. (3.22). Thus we can construct a set of functions that are simultaneously eigenfunctions of  $\hat{H}$  and  $\hat{P}$ . The eigenvalue equation for the permutation operator reads

$$\hat{P}_{ij}\Psi_\lambda(\mathbf{r}_1, \dots, \mathbf{r}_i, \dots, \mathbf{r}_j, \dots, \mathbf{r}_N) = \beta\Psi_\lambda(\mathbf{r}_1, \dots, \mathbf{r}_i, \dots, \mathbf{r}_j, \dots, \mathbf{r}_N), \quad (3.41)$$

where  $\hat{P}^2 = 1$  leads to  $\beta = \pm 1$  (symmetric/antisymmetric wavefunction). Thus the *total* wavefunction is antisymmetric with respect to the interchange of two particles. We have two possibilities,

$$\Psi(\mathbf{r}_1, \mathbf{r}_2, \dots, \mathbf{r}_N)_{\text{AS}} = \Upsilon_{\text{AS}}(\vec{r}_1, \vec{r}_2, \dots, \vec{r}_N) \otimes |\chi\rangle_S \quad (3.42)$$

$$\Psi(\mathbf{r}_1, \mathbf{r}_2, \dots, \mathbf{r}_N)_{\text{S}} = \Upsilon_{\text{S}}(\vec{r}_1, \vec{r}_2, \dots, \vec{r}_N) \otimes |\chi\rangle_{\text{AS}}, \quad (3.43)$$

where ‘‘AS’’ denotes antisymmetric and ‘‘S’’ denotes symmetric.

### 3.4.1 Hilbert Space of Distinguishable Particles

Consider a system of  $N$  distinguishable particles. The energy eigenfunctions live in the  $N$ -particle Hilbert space  $\mathcal{H}_N$  with dimension  $d$  (possibly infinite). Assume we have an orthonormal set of single-particle functions

$$\mathcal{B}_1 = \{|\alpha\rangle\}_{\alpha=1}^d \quad (3.44)$$

that spans the 1-particle Hilbert space  $\mathcal{H}_1$ . The  $N$ -particle Hilbert space can mathematically be constructed by combining  $N$  single-particle spaces with tensor products,

$$\mathcal{H}_N = \mathcal{H}_{1 \otimes 1 \otimes \dots \otimes 1} \equiv \mathcal{H}_1^{(1)} \otimes \mathcal{H}_1^{(2)} \otimes \dots \otimes \mathcal{H}_1^{(N)}. \quad (3.45)$$

This is called the direct product space. We denote  $\hat{H}_1^{(n)}$  as the 1-particle Hilbert space for particle  $n$ . The basis set of the  $N$ -particle product space can be constructed in a similar fashion through a tensor product,

$$|\alpha\beta\dots\delta\rangle \equiv |\alpha\rangle \otimes |\beta\rangle \otimes \dots \otimes |\delta\rangle, \quad (3.46)$$

where  $|\alpha\beta\dots\delta\rangle$  is called a product state. See [26] for details. The energy eigenfunctions can be written as a linear combination of product states, viz.

$$|\Psi_D\rangle = \sum_{\{\alpha\beta\dots\gamma\}} c_{\alpha\beta\dots\gamma} |\alpha\beta\dots\gamma\rangle, \quad (3.47)$$

where ‘‘D’’ denotes distinguishable. In the coordinate representation, the expression above reads

$$\Psi_D(\mathbf{r}_1, \mathbf{r}_2, \dots, \mathbf{r}_N) = \langle \mathbf{r}_1 \mathbf{r}_2 \dots \mathbf{r}_N | \Psi_D \rangle = \sum_{\alpha\beta\dots\delta} c_{\alpha\beta\dots\delta} \xi_\alpha(\mathbf{r}_1) \xi_\beta(\mathbf{r}_2) \dots \xi_\delta(\mathbf{r}_N), \quad (3.48)$$

where  $\mathbf{r}$  includes the spin, and  $c_{\alpha\beta\dots\delta}$  is the expansion coefficient. Eq. (3.48) is always valid provided that the set of functions  $\{\xi(\mathbf{r})\}$  are orthogonal and complete.

### 3.4.2 Hilbert Space of Bosons and Fermions

Consider a system of  $N$  bosons or fermions. As pointed out before, the total  $N$ -particle quantum state must either be symmetric or antisymmetric. We denote the  $N$ -particle Hilbert space of symmetric states as  $\mathcal{H}_N^S$ , and the Hilbert space of antisymmetric states as  $\mathcal{H}_N^{\text{AS}}$ . In the two-particle system, to each pair of product states  $|\alpha\beta\rangle$  and  $|\beta\alpha\rangle$ , there exist one symmetric state and one antisymmetric state. When  $\alpha = \beta$ , the product state is already symmetric, and an antisymmetric state does not exist due to the Pauli exclusion principle. The two-particle Hilbert

space (of distinguishable particles) has thus enough product states to form one symmetric space and one antisymmetric space, viz.

$$\mathcal{H}_2 = \mathcal{H}_2^S \otimes \mathcal{H}_2^{AS}, \quad (3.49)$$

In the general  $N$ -particle case we have that (see [26])

$$\mathcal{H}_N = \mathcal{H}_N^S \otimes \mathcal{H}_N^{AS}, \quad (3.50)$$

where  $\mathcal{H}_N$  is the Hilbert space of distinguishable particles,  $\mathcal{H}_N^S$  is the Hilbert space of bosons (symmetric states), and  $\mathcal{H}_N^{AS}$  is the Hilbert space of fermions (antisymmetric states). Defining

$$\mathcal{B}_N^S = \{|\sigma\rangle\}_{\sigma=1}^d \quad (3.51)$$

as the basis of  $\mathcal{H}_N^S$  with dimension  $d$ , and

$$\mathcal{B}_N^{AS} = \{|\varsigma\rangle\}_{\varsigma=1}^{d'} \quad (3.52)$$

as the basis of  $\mathcal{H}_N^{AS}$  with dimension  $d'$ , a symmetric and antisymmetric  $N$ -particle state can be written as

$$|\Psi_S\rangle = \sum_{\sigma}^d f_{\sigma} |\sigma\rangle \quad (3.53)$$

$$|\Psi_{AS}\rangle = \sum_{\varsigma}^{d'} g_{\varsigma} |\varsigma\rangle, \quad (3.54)$$

where  $f_{\sigma}$  and  $g_{\varsigma}$  are expansion coefficients. The basis functions in  $\mathcal{B}_N^S$  and  $\mathcal{B}_N^{AS}$  must be symmetric and antisymmetric, respectively. The direct product states in Eq. (3.46) are neither symmetric nor antisymmetric. Thus they cannot constitute a basis for  $\mathcal{H}_N^S$  or  $\mathcal{H}_N^{AS}$ . In section 3.3, symmetric and antisymmetric states were constructed from product states (see Eqs. 3.35 and 3.36). These states have correct symmetry. Moreover, they are orthogonal and complete [26]. Thus,

$$|\sigma\rangle = \sqrt{\frac{N!}{n_{\alpha}! n_{\beta}! \dots n_{\delta}!}} \hat{S} |\alpha\beta..\delta\rangle \quad (3.55)$$

$$|\varsigma\rangle = \sqrt{N!} \hat{A} |\alpha\beta..\delta\rangle, \quad (3.56)$$

where  $\sigma$  and  $\varsigma$  denote a set of quantum numbers  $(\alpha, \beta, \dots, \delta)$ ,  $|\alpha\beta..\delta\rangle$  is the product state,  $\hat{S}$  is the symmetrizer defined in Eq. (3.33), and  $\hat{A}$  is the antisymmetrizer defined in Eq. (3.34). This is *one* possible choice of basis functions. We emphasize that any set

$$\{|\alpha\rangle\}_{\alpha=1}^d \quad (3.57)$$

that spans the single-particle Hilbert space  $\mathcal{H}_1$  with dimension  $d$ , can be used. A general symmetric and antisymmetric  $N$ -particle function can then be written as

$$\Psi_S(\mathbf{r}_1, \mathbf{r}_2, \dots, \mathbf{r}_N) = \sum_{\alpha\beta..\delta} f_{\alpha\beta..\delta} \sqrt{\frac{N!}{n_{\alpha}! n_{\beta}! \dots n_{\gamma}!}} \hat{S} \xi_{\alpha}(\mathbf{r}_1) \xi_{\beta}(\mathbf{r}_2) \dots \xi_{\delta}(\mathbf{r}_N) \quad (3.58)$$

$$\Psi_{AS}(\mathbf{r}_1, \mathbf{r}_2, \dots, \mathbf{r}_N) = \sum_{\alpha\beta..\delta} g_{\alpha\beta..\delta} \sqrt{N!} \hat{A} \xi_{\alpha}(\mathbf{r}_1) \xi_{\beta}(\mathbf{r}_2) \dots \xi_{\delta}(\mathbf{r}_N), \quad (3.59)$$

where

$$\xi_{\alpha}(\mathbf{r}) = \langle \mathbf{r} | \alpha \rangle. \quad (3.60)$$

The energy eigenfunctions of the interacting  $N$ -fermion system in Eq. (3.38) can therefore be written as a linear combination of the eigenfunctions of the non-interacting system in Eq. (3.17), viz.

$$\Psi_\lambda(\mathbf{r}_a, \mathbf{r}_2, \dots, \mathbf{r}_N) = \sum_{\alpha\beta..\delta} C_{\alpha\beta..\delta}^\lambda \Phi_{\alpha\beta..\delta}(\mathbf{r}_1, \mathbf{r}_2, \dots, \mathbf{r}_N), \quad (3.61)$$

where  $C_{\alpha\beta..\delta}^\lambda$  is the expansion coefficient, and  $\Phi_{\alpha\beta..\delta}(\mathbf{r}_1, \mathbf{r}_2, \dots, \mathbf{r}_N)$  is the Slater determinant given in Eq. (3.37).

## 3.5 Second Quantization

We have seen that the energy eigenstates of a non-interacting many-fermion system are given as Slater determinants (see Eq. 3.37). This is a consequence of the Pauli principle and the fact that the particles are identical. Moreover, a single-particle orbital can only be occupied by *one* electron. It is therefore appropriate to utilize the occupancy notation for Slater determinants. We define

$$\Phi_{\alpha_1\alpha_2..\alpha_N} \equiv |\alpha_1\alpha_2..\alpha_N\rangle. \quad (3.62)$$

Note that in Eq. (3.46) we defined  $|\alpha\beta..\delta\rangle$  as a product state. In the rest of the thesis, the context will clearly show which definition that is used. The notation in Eq. (3.62) is called the occupancy representation. This form of the Slater determinant does not explicitly reflect the antisymmetry in the particle coordinates. Nevertheless, the Slater determinant changes sign in the permutation of two columns, yielding

$$|\alpha_1..\alpha_i..\alpha_j..\alpha_N\rangle = -|\alpha_1..\alpha_i..\alpha_j..\alpha_N\rangle. \quad (3.63)$$

The full potential of this notation appears when creation and annihilation operators are introduced. A creation operator creates a fermion in single-particle state, while an annihilation operator removes a fermion from single-particle state. This formalism is called second quantization [31].

### 3.5.1 Creation and Annihilation Operators

In this section, we will define creation and annihilation operators. These operators are mappings between the many-particle Hilbert spaces of different particle numbers, viz.

$$a_\alpha^\dagger : \mathcal{H}_N^{\text{AS}} \rightarrow \mathcal{H}_{N+1}^{\text{AS}} \quad (3.64)$$

$$a_\alpha : \mathcal{H}_N^{\text{AS}} \rightarrow \mathcal{H}_{N-1}^{\text{AS}}, \quad (3.65)$$

where

$$\alpha \in \mathcal{H}_1. \quad (3.66)$$

Creation and annihilation operators are operators that create and annihilate fermions. We define the fermionic creation operator by

$$a_\alpha^\dagger |\alpha_1\alpha_2..\alpha_N\rangle \equiv |\alpha\alpha_1\alpha_2..\alpha_N\rangle, \quad (3.67)$$

i.e. it adds a fermion with quantum number  $\alpha$  to an antisymmetric state (Slater determinant) in which  $N$  fermions occupy single-particle orbitals ( $\alpha_1, \alpha_2, \dots, \alpha_N$ ). An antisymmetric ( $N+1$ )-fermion state is the result. Note that if  $\alpha$  is already occupied, the result is zero. We can now write a Slater determinant as a product of creation operators, viz.

$$|\alpha_1\alpha_2..\alpha_N\rangle = a_{\alpha_1}^\dagger a_{\alpha_2}^\dagger .. a_{\alpha_N}^\dagger |0\rangle = \prod_{i=1}^N a_{\alpha_i}^\dagger |0\rangle, \quad (3.68)$$

where  $|0\rangle$  is the vacuum state. Combining Eqs. (3.63) and (3.68) yields

$$a_{\alpha_1}^\dagger \dots a_{\alpha_i}^\dagger \dots a_{\alpha_j}^\dagger \dots a_{\alpha_N}^\dagger |0\rangle = -a_{\alpha_1}^\dagger \dots a_{\alpha_j}^\dagger \dots a_{\alpha_i}^\dagger \dots a_{\alpha_N}^\dagger |0\rangle, \quad (3.69)$$

leading to the following anticommutation relation

$$\{a_\alpha^\dagger, a_\beta^\dagger\} = a_\alpha^\dagger a_\beta^\dagger + a_\beta^\dagger a_\alpha^\dagger = 0. \quad (3.70)$$

The adjoint of  $a_\alpha^\dagger$  is called an annihilation operator,

$$a_\alpha = (a_\alpha^\dagger)^\dagger. \quad (3.71)$$

It can be shown that its action on a Slater determinant (see [31, 32]) is given by

$$a_\alpha |\alpha_1 \alpha_2 \dots \alpha_{i-1} \alpha_i \alpha_{i+1} \dots \alpha_{N-1} \alpha_N\rangle = (-1)^{i-1} |\alpha_1 \alpha_2 \dots \alpha_{i-1} \alpha_{i+1} \dots \alpha_{N-1} \alpha_N\rangle \quad (3.72)$$

when  $\alpha = \alpha_i$  is occupied by a fermion, and

$$a_\alpha |\alpha_1 \alpha_2 \dots \alpha_N\rangle = 0, \quad (3.73)$$

when  $\alpha$  is unoccupied, i.e.  $\alpha \neq \alpha_i$  for  $i = 1, 2, \dots, N$ . The annihilation operator  $a_\alpha$  has therefore the property that its action upon an antisymmetric  $N$ -fermion state (Slater determinant) produces an antisymmetric  $(N-1)$ -fermion state, provided that  $\alpha$  is occupied. The anticommutation relation reads

$$\{a_\alpha, a_\beta\} = a_\alpha a_\beta + a_\beta a_\alpha = 0. \quad (3.74)$$

Furthermore, the anticommutation relation between the creation and annihilation operator (see [31]) reads

$$\{a_\alpha^\dagger, a_\beta\} = \delta_{\alpha\beta}. \quad (3.75)$$

### 3.5.2 Operators in Second Quantization

We are now in a position where we can express many-fermion states by creation and annihilation operators. In many-body theory in general, we often need to calculate matrix elements or expectation values of operators. Consider for example the matrix element

$$\langle \alpha_1 \alpha_2 | \hat{O} | \alpha_3 \alpha_4 \rangle, \quad (3.76)$$

where  $|\alpha_1 \alpha_2\rangle$  and  $|\alpha_3 \alpha_4\rangle$  are Slater determinants. In second quantization, this element reads

$$\langle 0 | a_{\alpha_1} a_{\alpha_2} \hat{O} a_{\alpha_3}^\dagger a_{\alpha_4}^\dagger | 0 \rangle. \quad (3.77)$$

Is it possible to write  $\hat{O}$  in terms of creation and annihilation operators? The answer is yes, provided that the operators conserve the particle number. Thus we can solve the matrix element by using the anticommutation relations in Eqs. (3.70), (3.74) and (3.75). Operators expressed in second quantization have the convenient property that they do not depend on the numbers of particles in the system. They work in the so-called Fock space (see [31]), which is the vector space constructed by the direct sum of the vacuum space, the single-particle Hilbert space, the two-particle Hilbert space, and so forth, viz.

$$\mathcal{F} \equiv \bigoplus_{n=0}^{\infty} \mathcal{H}_n^{\text{AS}}, \quad (3.78)$$

where  $\mathcal{H}_n^{\text{AS}}$  is the  $n$ -fermion Hilbert space. We will in the following only consider the second quantized form of one-body and two-body operators.

Consider a one-body operator  $\hat{F}$ . It is given as

$$\hat{F} = \sum_{i=1}^N \hat{f}_i, \quad (3.79)$$

where  $\hat{f}_i$  acts on particle  $i$ , and  $N$  is the number of fermions. Given an *arbitrary* single-particle basis

$$\mathcal{B}_1 = \{|\alpha\rangle\}_{i=1}^d \quad (3.80)$$

that spans the one-fermion Hilbert space  $\mathcal{H}_1$  with dimension  $d$  (often infinity), the second quantized form of  $\hat{F}$  reads

$$\hat{F} = \sum_{\alpha\beta} \langle\alpha|f|\beta\rangle a_\alpha^\dagger a_\beta. \quad (3.81)$$

See [31] for details. Thus for every set of quantum numbers  $(\alpha, \beta)$ , the operator  $\hat{F}$  annihilates a fermion in state  $\beta$  and creates a fermion in state  $\alpha$  with probability amplitude  $\langle\alpha|f|\beta\rangle$ . Furthermore, consider a two-body operator  $\hat{V}$ . It is given as

$$\hat{V}_N = \sum_{i=1 < j}^N \hat{v}_{ij}, \quad (3.82)$$

where  $\hat{v}_{ij}$  acts on particle  $i$  and  $j$ , and  $N$  is the number of fermions in the system. Given an *arbitrary* single-particle basis (see Eq. 3.80), the second quantized form of  $\hat{V}$  reads

$$\hat{V} = \frac{1}{2} \sum_{\alpha\beta\gamma\delta} \langle\alpha\beta|v|\gamma\delta\rangle a_\alpha^\dagger a_\beta^\dagger a_\delta a_\gamma \quad (3.83)$$

$$= \frac{1}{4} \sum_{\alpha\beta\gamma\delta} \langle\alpha\beta|v|\gamma\delta\rangle_{\text{AS}} a_\alpha^\dagger a_\beta^\dagger a_\delta a_\gamma, \quad (3.84)$$

where the antisymmetrized matrix element is defined as

$$\langle\alpha\beta|v|\gamma\delta\rangle_{\text{AS}} = \langle\alpha\beta|v|\gamma\delta\rangle - \langle\alpha\beta|v|\delta\gamma\rangle. \quad (3.85)$$

See [31] for details. For every set of quantum numbers  $(\alpha, \beta, \gamma, \delta)$ , the operator  $\hat{V}$  annihilates a fermion from states  $\gamma$  and  $\delta$ , and creates a fermion in states  $\alpha$  and  $\gamma$ , with probability amplitude  $\frac{1}{4}\langle\alpha\beta|v|\gamma\delta\rangle_{\text{AS}}$ .

We are now in a position where we can write antisymmetric wavefunctions (Slater determinants), one-body operators and two-body operators in second quantization. As pointed out before, in a quantum mechanical treatment of many-body systems, we often end up with evaluating matrix elements. As an example, consider

$$\langle\alpha_1\alpha_2|\hat{V}|\alpha_3\alpha_4\rangle, \quad (3.86)$$

where  $|\alpha_1\alpha_2\rangle$  and  $|\alpha_3\alpha_4\rangle$  denote Slater determinants, and  $\hat{V}$  a two-body operator. Since

$$\langle\alpha_1\alpha_2| = \langle 0|a_{\alpha_1}a_{\alpha_2} \quad (3.87)$$

$$|\alpha_3\alpha_4\rangle = a_{\alpha_3}^\dagger a_{\alpha_4}^\dagger |0\rangle, \quad (3.88)$$

we obtain that

$$\langle\alpha_1\alpha_2|\hat{V}|\alpha_3\alpha_4\rangle = \frac{1}{4} \sum_{\alpha\beta\gamma\delta} \langle\alpha\beta|v|\gamma\delta\rangle_{\text{AS}} \langle 0|a_{\alpha_1}a_{\alpha_2}a_\alpha^\dagger a_\beta^\dagger a_\delta a_\gamma a_{\alpha_3}^\dagger a_{\alpha_4}^\dagger |0\rangle, \quad (3.89)$$

where the second quantized form of  $\hat{V}$  is given in Eq. (3.83). Thus we end up with evaluating the vacuum expectation value of products of creation and annihilation operators. These elements can be determined by using the anticommutation relations in Eqs. (3.70), (3.74) and (3.75). However, this approach can be quite tedious and time-consuming. Wick's theorem provides an easy, yet sophisticated, method for writing a string of creation and annihilation operators as a sum of *normal ordered* terms with all possible combinations of *contractions*. This will allow us to easily point out which terms that contribute to the expression. We will in the next section define Wick's theorem, and the concepts of normal-ordering and contractions.

### 3.5.3 Wick's Theorem

As pointed out in the previous section, a quantum mechanical treatment of many-body systems often entails calculating matrix elements of operators between state vectors. Thus, in the formalism of second quantization, we often end up with vacuum expectation values of creation and annihilation operators. We can use the anticommutation relations in Eqs. (3.70), (3.74) and (3.75) to rearrange the product into an operator string where the annihilation operators are placed to the right of the creation operators. All terms with a rightmost annihilation operator are zero, by construction. Thus, according to Eq. (3.75), every vacuum expectation value of creation and annihilation operators can be written as a sum of delta functions. Although the procedure is straightforward in itself, it becomes tedious and time-consuming even for simple cases. The so-called Wick's theorem allow us to determine these matrix elements in a simple and convenient way.

Wick's theorem is based on two fundamental concepts, viz. normal-ordering and contractions. Consider a product of creation and annihilation operators,

$$\hat{A}\hat{B}..\hat{X}\hat{Y}. \quad (3.90)$$

Its normal-ordered form is defined as

$$\left\{ \hat{A}\hat{B}..\hat{X}\hat{Y} \right\} \equiv (-1)^p [\text{creation operators}] \cdot [\text{annihilation operators}], \quad (3.91)$$

where  $p$  denotes the number of permutations that is needed to transform the original string into the normal-ordered form. The contraction between two operators  $\hat{X}$  and  $\hat{Y}$  is defined as

$$\overline{\hat{A}\hat{B}} \equiv \langle 0 | \hat{A}\hat{B} | 0 \rangle. \quad (3.92)$$

Furthermore, we define the contraction between two operators within a normal-ordered product as

$$\left\{ \overline{\hat{A}\hat{B}..\hat{X}\hat{Y}} \right\} = (-1)^p \left\{ \overline{\hat{A}\hat{X}..\hat{R}\hat{Y}} \right\}, \quad (3.93)$$

where  $p$  is the number of permutations needed to bring both operators to the left. In the general case when we have  $m$  contractions within a normal-ordered product, the prefactor reads

$$(-1)^{p_1+p_2+..+p_m}. \quad (3.94)$$

Wick's theorem states that every string of creation and annihilation operators can be written as a sum of normal-ordered products with all possible combinations of contractions. The theorem

reads

$$\begin{aligned}
 \hat{A}\hat{B}\hat{C}\hat{D}..\hat{R}\hat{X}\hat{Y}\hat{Z} = & \left\{ \hat{A}\hat{B}\hat{C}\hat{D}..\hat{R}\hat{X}\hat{Y}\hat{Z} \right\} \\
 & + \sum_{(1)} \left\{ \overline{\hat{A}\hat{B}\hat{C}\hat{D}..\hat{R}\hat{X}\hat{Y}\hat{Z}} \right\} \\
 & + \sum_{(2)} \left\{ \overline{\overline{\hat{A}\hat{B}\hat{C}\hat{D}..\hat{R}\hat{X}\hat{Y}\hat{Z}}} \right\} \\
 & + \dots \\
 & + \sum_{(n/2)} \left\{ \overline{\overline{\overline{\hat{A}\hat{B}\hat{C}\hat{D}..\hat{R}\hat{X}\hat{Y}\hat{Z}}}} \right\}, 
 \end{aligned} \tag{3.95}$$

where  $(m)$  denotes the number of contractions, and  $(n/2)$  denotes the largest integer that do not exceed  $n/2$  ( $n$  being the number of operators). When  $n$  is even, we obtain fully contracted terms. However, when  $n$  is odd, none of the terms in Eq. (3.95) are fully contracted. See [31] for a proof of Wick's theorem. An important extension of Wick's theorem is the so-called generalized Wick's theorem. This theorem reads

$$\begin{aligned}
 \left\{ \hat{A}\hat{B}\hat{C}\hat{D}..\right\} \left\{ \hat{R}\hat{X}\hat{Y}\hat{Z}..\right\} = & \left\{ \hat{A}\hat{B}\hat{C}\hat{D}..\hat{R}\hat{X}\hat{Y}\hat{Z} \right\} \\
 & + \sum_{(1)} \left\{ \overline{\hat{A}\hat{B}\hat{C}\hat{D}..\hat{R}\hat{X}\hat{Y}\hat{Z}} \right\} \\
 & + \sum_{(2)} \left\{ \overline{\overline{\hat{A}\hat{B}\hat{C}\hat{D}..\hat{R}\hat{X}\hat{Y}\hat{Z}}} \right\} \\
 & + \dots 
 \end{aligned} \tag{3.96}$$

The vacuum expectation value of creation and annihilation operators can now be written as

$$\begin{aligned}
 \langle 0 | \hat{A}\hat{B}\hat{C}\hat{D}..\hat{R}\hat{X}\hat{Y}\hat{Z} | 0 \rangle = & \langle 0 | \left\{ \hat{A}\hat{B}\hat{C}\hat{D}..\hat{R}\hat{X}\hat{Y}\hat{Z} \right\} | 0 \rangle \\
 & + \sum_{(1)} \langle 0 | \left\{ \overline{\hat{A}\hat{B}\hat{C}\hat{D}..\hat{R}\hat{X}\hat{Y}\hat{Z}} \right\} | 0 \rangle \\
 & + \sum_{(2)} \langle 0 | \left\{ \overline{\overline{\hat{A}\hat{B}\hat{C}\hat{D}..\hat{R}\hat{X}\hat{Y}\hat{Z}}} \right\} | 0 \rangle \\
 & + \dots \\
 & + \sum_{(N/2)} \langle 0 | \left\{ \overline{\overline{\overline{\hat{A}\hat{B}\hat{C}\hat{D}..\hat{R}\hat{X}\hat{Y}\hat{Z}}}} \right\} | 0 \rangle. 
 \end{aligned} \tag{3.97}$$

Since

$$\langle 0 | \left\{ \overline{\hat{A}\hat{B}..\hat{X}\hat{Y}} \right\} | 0 \rangle = 0, \tag{3.98}$$

by construction (see Eq. 3.93), obtain that

$$\begin{aligned}
 \langle 0 | \hat{A}\hat{B}\hat{C}\hat{D}..\hat{R}\hat{X}\hat{Y}\hat{Z} | 0 \rangle = & \sum_{(\text{fc})} \langle 0 | \left\{ \overline{\overline{\hat{A}\hat{B}\hat{C}\hat{D}..\hat{R}\hat{X}\hat{Y}\hat{Z}}} \right\} | 0 \rangle \\
 = & \sum_{(\text{fc})} \overline{\overline{\overline{\hat{A}\hat{B}\hat{C}\hat{D}..\hat{R}\hat{X}\hat{Y}\hat{Z}}}}, 
 \end{aligned} \tag{3.99}$$

where “fc” denotes full contractions meaning that all operators are contracted. When the number of creation and annihilation operators is odd, the vacuum expectation value is zero. However, when the number is even, the expectation value is simply the sum of fully contracted terms. We observe from the definition in Eq. (3.91) the following relations,

$$a_\alpha^\dagger a_\beta^\dagger = \delta_{\alpha\beta} \quad (3.100)$$

$$a_\alpha^\dagger a_\beta = 0 \quad (3.101)$$

$$a_\alpha a_\beta^\dagger = 0 \quad (3.102)$$

$$a_\alpha a_\beta = 0. \quad (3.103)$$

Wick’s theorem can thus be used to calculate matrix elements of operators between Slater determinants.

### 3.5.4 Particle-Hole Formalism

We have seen that the formalism of second quantization is a convenient formalism for constructing antisymmetric wavefunctions and operators that conserves the particle-number. However, the real power of second quantization emerges when the particle-hole formalism is introduced. This is a so-called quasi-particle formalism.

In Sec. 3.5.1, we saw that antisymmetric wavefunctions can be written as

$$|\alpha_1 \alpha_2 .. \alpha_N\rangle = a_{\alpha_1}^\dagger a_{\alpha_2}^\dagger .. a_{\alpha_N}^\dagger |0\rangle, \quad (3.104)$$

where  $|0\rangle$  is the vacuum state. The vacuum state is often called the reference state. In many-body theory we often deal with Slater determinants that have a few fermions excited relative to another determinant. For example, the first excited energy eigenstate of the non-interacting  $N$ -fermion system (provided by the Schrödinger equation in Eq. 3.17) has one particle excited relative to the ground state. Another excited state may have two particles excited relative to the ground state, and so forth. It is therefore in many cases appropriate to introduce a new reference state. In the previous example, when we are dealing with energy eigenstates of the non-interacting system, the reference state could be the ground state. The transition from the ordinary particle representation to the particle-hole representation is shown schematically in Fig. (3.5.4). We have in the figure illustrated three antisymmetric states (Slater determinants),

$$|a\rangle = |\alpha_1 \alpha_2 .. \alpha_{N-1} \alpha_N\rangle \in \mathcal{H}_N^{\text{AS}} \quad (3.105)$$

$$|b\rangle = |\alpha_1 \alpha_2 .. \alpha_{N-1} \alpha_N \alpha_{N+1}\rangle \in \mathcal{H}_{N+1}^{\text{AS}} \quad (3.106)$$

$$|c\rangle = |\alpha_1 \alpha_2 .. \alpha_{N-1}\rangle \in \mathcal{H}_{N-1}^{\text{AS}}, \quad (3.107)$$

in both the particle representation (left), and the particle-hole representation (right). Here we denote the single-particle state by quantum numbers  $\alpha_1 \alpha_2 .. \alpha_{N+1}$ . In the particle representation, the determinants are written as a product of creation operators acting on the vacuum state, viz.

$$|a\rangle_0 = |\alpha_1 \alpha_2 .. \alpha_{N-1} \alpha_N\rangle = a_{\alpha_1}^\dagger a_{\alpha_2}^\dagger .. a_{\alpha_{N-1}}^\dagger a_{\alpha_N}^\dagger |0\rangle \quad (3.108)$$

$$|b\rangle_0 = |\alpha_1 \alpha_2 .. \alpha_{N-1} \alpha_N \alpha_{N+1}\rangle = a_{\alpha_1}^\dagger a_{\alpha_2}^\dagger .. a_{\alpha_{N-1}}^\dagger a_{\alpha_N}^\dagger a_{\alpha_{N+1}}^\dagger |0\rangle \quad (3.109)$$

$$|c\rangle_0 = |\alpha_1 \alpha_2 .. \alpha_{N-1}\rangle = a_{\alpha_1}^\dagger a_{\alpha_2}^\dagger .. a_{\alpha_{N-1}}^\dagger |0\rangle, \quad (3.110)$$

where the 0-subscript denotes that the vacuum state is the reference state. By defining a new reference state

$$|r\rangle \equiv |a\rangle = a_{\alpha_1}^\dagger a_{\alpha_2}^\dagger .. a_{\alpha_{N-1}}^\dagger a_{\alpha_N}^\dagger |0\rangle, \quad (3.111)$$

the two other determinants can be expressed as

$$|b\rangle_r = (-1)^N a_{\alpha_{N+1}}^\dagger |r\rangle \equiv (-1)^N |\alpha_{N+1}\rangle_r \quad (3.112)$$

$$|c\rangle_r = (-1)^{N-1} a_{\alpha_N} |r\rangle \equiv (-1)^{N-1} |\alpha_N^{-1}\rangle_r. \quad (3.113)$$

The difference between  $|b\rangle$  and the reference state is the particle occupying single-state  $\alpha_{N+1}$ . Thus in the new representation,  $|b\rangle$  is called a particle-state. Furthermore, relative to the reference state,  $|c\rangle$  has a particle removed from single-particle state  $\alpha_N$ , and is therefore called a hole-state.

The new representation is known as the particle-hole representation, and the new reference state  $|r\rangle$  is the so-called particle-hole vacuum. This is a quasi-particle representation. The idea is that both holes (unoccupied single-particle states below the Fermi level) and particles (occupied single-particle states above the Fermi level) are treated as quasi-particles, where the Fermi level denotes the single-particle state  $\alpha_N$ . Creation of a quasi-particle means *either* creating a particle in state  $\alpha > \alpha_N$ , *or* creating a hole (i.e. removing a particle) in state  $\alpha \leq \alpha_N$ . Annihilation of a quasi-particle means *either* removing a particle from state  $\alpha > \alpha_N$ , *or* removing a hole (create a particle) in state  $\alpha \leq \alpha_N$ . The choice of reference state is in principle arbitrary, but the particle-hole formalism is only appropriate when the reference state corresponds to a system which is physically steady.

When defining a new reference state, the ordinary creation and annihilation operators for particles must be replaced with corresponding operators for quasi-particles. We will denote the single-particle states that are part of the occupied space ( $\alpha \leq \alpha_N$ ) with  $ijk\dots$ , and the states that are part of the unoccupied space ( $\alpha > \alpha_N$ ) with  $abc\dots$ . We will refer to  $i$  as a hole state, and  $a$  as a particle state. The quasi-particle creation operator is defined as

$$b_\alpha^\dagger \equiv \begin{cases} a_\alpha^\dagger & \text{if } \alpha = a, b, c, \dots \\ a_\alpha & \text{if } \alpha = i, j, k, \dots \end{cases}, \quad (3.114)$$

and the annihilation operator

$$b_\alpha \equiv \begin{cases} a_\alpha^\dagger & \text{if } \alpha = i, j, k, \dots \\ a_\alpha & \text{if } \alpha = a, b, c, \dots \end{cases}. \quad (3.115)$$

The definitions above yield the following anticommutation relations,

$$\{b_\alpha, b_\beta\} = 0 \quad (3.116)$$

$$\{b_\alpha^\dagger, b_\beta^\dagger\} = 0 \quad (3.117)$$

$$\{b_\alpha^\dagger, b_\beta\} = \delta_{\alpha\beta}, \quad (3.118)$$

which are identical to Eqs. (3.70), (3.74) and (3.75), as expected. We can now express quasi-particle states as

$$|ijkl..abcd..\rangle_r \equiv b_i^\dagger b_j^\dagger b_k^\dagger b_l^\dagger .. b_a^\dagger b_b^\dagger b_c^\dagger b_d^\dagger .. |r\rangle, \quad (3.119)$$

where  $ijkl..$  are occupied by holes, and  $abcd..$  are occupied by particles. Operators can also be expressed by quasi-particle creation and annihilation operators. This is for example necessary in order to utilize the particle-hole formalism when evaluating matrix elements of operators between quasi-particle states. Moreover, Wick's theorem in Eq. (3.95) is valid for products of quasi-particle creation and annihilation operators, provided that the contractions are defined relative to the reference state. The only nonzero contraction is

$$\overline{b_\alpha b_\beta^\dagger} = \langle r | b_\alpha b_\beta^\dagger | r \rangle = \delta_{\alpha\beta}. \quad (3.120)$$

We will omit the discussion of operators in quasi-particle representation, and evaluation of matrix elements of such operators between quasi-particle states. This is not directly relevant for this thesis.

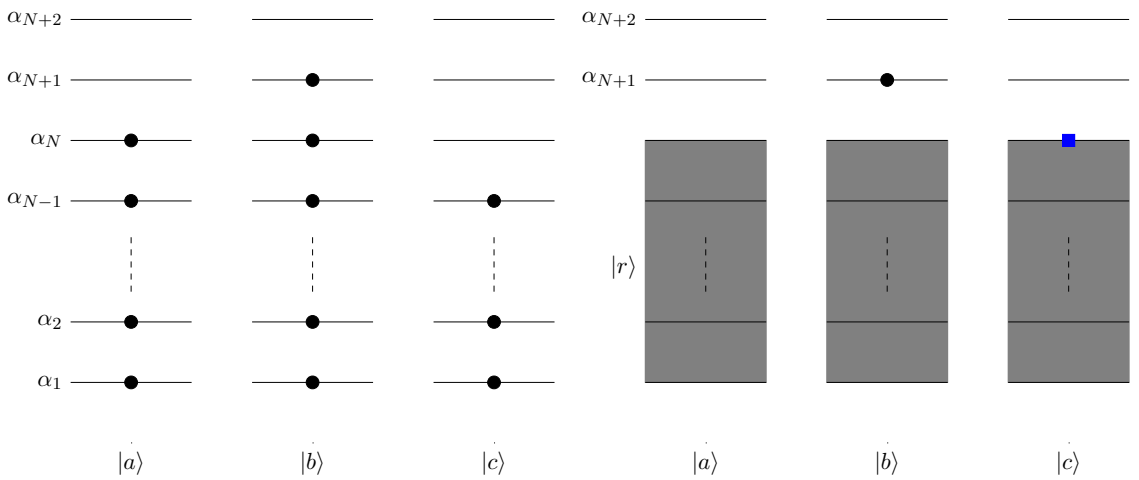


**Figure 3.1:** Illustration of the particle-hole representation. We have three Slater determinants:  $|a\rangle \in \mathcal{H}_N^{\text{AS}}$ ,  $|b\rangle \in \mathcal{H}_{N+1}^{\text{AS}}$  and  $|c\rangle \in \mathcal{H}_{N-1}^{\text{AS}}$ . To the left we have the ordinary particle representation where each occupied single-particle state is specified. The corresponding expressions are given in Eqs. (3.108), (3.109) and (3.110). To the right we have the particle-hole representation where each occupied state (by a particle or hole), that is not occupied in the reference determinant, is specified. The expressions are given in Eqs. (3.111), (3.112) and (3.113). Note that  $\bullet$  represents a particle, and  $\square$  represents a hole.



## Chapter 4

# Theoretical Description of Quantum Dots

In this chapter we aim at developing a theoretical framework for the 2-dimensional quantum dot. Put simply, we want to establish a quantum mechanical description of the single-electron system, i.e. solve the time-independent Schrödinger equation in 2 dimensions. In order to achieve our goal, a model of the system must be determined. The results from this chapter will be used in the many-body treatment of quantum dots.

The first section is devoted to the theoretical model of quantum dots and the approximations that are done. We will see that the confinement potential can be approximated by the harmonic oscillator potential, which belongs to the class of spherically symmetric potentials. Therefore, the second section consider the time-independent Schrödinger equation for a general spherically symmetric potential in 2 dimensions. For these potentials, the Schrödinger equation simplifies to two independent equations: one angular equation, and one radial equation. The angular equation can be solved without specifying the potential. Then, in the third section, we will specify the potential to the harmonic oscillator potential and solve the time-independent Schrödinger equation. Finally, we will in the last two sections develop our final model Hamiltonian and scale this into dimensionless form.

### 4.1 Approximations

As pointed out before, quantum dots are fabricated systems of trapped electrons. They are created in a semiconductor, typically gallium arsenide (GaAs). The electrons in a quantum dot are confined by either a physical barrier, typically an insulator like aluminum gallium arsenide (AlGaAs), or/and an electromagnetic field [2]. In order to calculate properties of real life quantum dots, we obviously need a model Hamiltonian which is as close to the exact one as possible. However, quantum dots are complex devices. It is impossible to give a simple, yet totally complete, theoretical model. For example, we should determine an exact analytical expression of the confinement potential, account for edge effects, and so forth. In addition, all interactions that are present in the system should be included in our model. However, the complexity of such a model would quickly reach the limit of computational resources. Approximations are therefore necessary. In this thesis we disregard edge effects. Moreover, we only include the electron-electron interaction, which is given by the Coulomb interaction

$$v(r_{ij}) = \frac{e^2}{4\pi\epsilon_0\epsilon_r} \frac{1}{r_{ij}}, \quad (4.1)$$

where  $e$  is the electron charge,  $\epsilon_0$  is the vacuum permittivity,  $\epsilon_r$  is the relative permittivity, and  $r_{ij}$  is the distance between the electrons. Numerical [33, 34, 35, 36] and experimental [37, 38, 39] studies show that the confinement potential can be approximated by the harmonic oscillator

potential

$$u(r) = \frac{1}{2}m^*\omega^2r^2, \quad (4.2)$$

where  $m^*$  is the effective mass of the electron,  $\omega$  is the oscillator frequency, and  $r$  is the distance between the electron and the point in space where  $u(r) = 0$ . For example, the effective mass of the electron in Gallium Arsenide (GaAs) is approximately  $0.067m_e$ , where  $m_e$  is the electron mass. See [40] for a discussion of effective masses. Furthermore, theoretical simulations with this potential have predicted strong absorption of far-infrared light at the frequency corresponding to the oscillator frequency. See for example [41, 42]. This prediction is consistent with experimental results, such as [43]. Furthermore, another common approximation of quantum dots is to reduce the spatial dimensions from three to two. The third dimension is usually fixed by a manufacture technique, which force the electrons to occupy a planar region. We will in this thesis consider the 2-dimensional quantum dot. The confinement potential will be given by the harmonic oscillator potential, and the electron-electron interaction will be modeled with the Coulomb interaction. This is what we call the *parabolic* quantum dot. We will also include the effect of an electromagnetic field, where the magnetic field is constant and uniform in the  $z$ -direction, i.e. the direction that is perpendicular to the 2-dimensional electron plane.

## 4.2 Schrödinger Equation for Spherically Symmetric Potentials

In Nature we observe many important potentials that are spherically symmetric, i.e. they only depend on the distance from a certain point in space,

$$V = V(r). \quad (4.3)$$

The single-particle Schrödinger equation can in these cases be simplified to a set of independent equations by first introducing spherical coordinates  $(r, \varphi, \theta)$ , and then separate the equation in these new variables. We will in the following present how we can rewrite the time-independent Schrödinger equation as a set of independent equations in 2 dimensions. The total wavefunction is given as (see Sec. 2.2.3) a tensor product between a spatial part and a spin part. Since the potential is independent of the spin of the particle, the spin part can be omitted in the calculation. We here assume that the magnetic field is zero. In the case of an electron, the eigenstates of  $\hat{S}_z$  and  $\hat{S}^2$  is given by Eqs. (2.61) and (2.62). We will therefore in the following only consider the spatial part of the total wavefunction.

In the cartesian coordinate representation, the time-independent Schrödinger equation for a single-particle system reads

$$-\frac{\hbar^2}{2m^*} \left( \frac{\partial^2}{\partial x^2} + \frac{\partial^2}{\partial y^2} \right) \phi(x, y) + u(\sqrt{x^2 + y^2})\phi(x, y) = \varepsilon\phi(x, y), \quad (4.4)$$

where  $m$  is the mass of the particle,  $u = u(\sqrt{x^2 + y^2})$  is a spherically symmetric potential, and  $\phi(x, y)$  is the eigenfunction with corresponding eigenvalue  $\varepsilon$ . We now introduce spherical coordinates  $(r, \theta)$  defined as

$$r \equiv \sqrt{x^2 + y^2} \quad (4.5)$$

$$\theta \equiv \arccos\left(\frac{x}{r}\right) = \arcsin\left(\frac{y}{r}\right). \quad (4.6)$$

In this representation, the time-independent Schrödinger equation reads

$$-\frac{\hbar^2}{2m^*} \left( \frac{\partial^2}{\partial r^2} + \frac{1}{r} \frac{\partial}{\partial r} + \frac{1}{r^2} \frac{\partial^2}{\partial \theta^2} \right) \phi(r, \theta) + u(r)\phi(r, \theta) = \varepsilon\phi(r, \theta). \quad (4.7)$$

We are seeking the solutions that are separable in  $r$  and  $\theta$ , viz.

$$\phi(r, \theta) = R(r)Y(\theta), \quad (4.8)$$

and substitute this expression into Eq. (4.7), yielding

$$-\frac{\hbar^2}{2m^*} \left( Y(\theta) \frac{\partial^2 R(r)}{\partial r^2} + \frac{Y(\theta)}{r} \frac{\partial R(r)}{\partial r} + \frac{R(r)}{r^2} \frac{\partial^2 Y(\theta)}{\partial \theta^2} \right) + u(r)R(r)Y(\theta) = \varepsilon R(r)Y(\theta). \quad (4.9)$$

We multiply  $-2m^*r^2/\hbar^2 R(r)Y(\theta)$  on both sides and collect the terms containing  $r$  and  $\theta$  for themselves,

$$\left[ \frac{r^2}{R(r)} \frac{\partial^2 R(r)}{\partial r^2} + \frac{r}{R(r)} \frac{\partial R(r)}{\partial r} - \frac{2m^*r^2}{\hbar^2} (u(r) - \varepsilon) \right] + \left[ \frac{1}{Y(\theta)} \frac{\partial^2 Y(\theta)}{\partial \theta^2} \right] = 0. \quad (4.10)$$

The term in the first square bracket depends only on  $r$ , whereas the second term in square bracket depends only on  $\theta$ . Each term is therefore equal to a constant,

$$\frac{r^2}{R(r)} \frac{\partial^2 R(r)}{\partial r^2} + \frac{r}{R(r)} \frac{\partial R(r)}{\partial r} - \frac{2m^*r^2}{\hbar^2} (u(r) - \varepsilon) = k_r \quad (4.11)$$

$$\frac{1}{Y(\theta)} \frac{\partial^2 Y(\theta)}{\partial \theta^2} = k_\theta, \quad (4.12)$$

where

$$k_r = -k_\theta. \quad (4.13)$$

We choose  $k_r = m^2$ . Do not confuse  $m$  with the mass of the particle  $m^*$ . Eq. (4.10) can now be written as two independent differential equations,

$$r^2 \frac{d^2 R(r)}{dr^2} + r \frac{dR(r)}{dr} - \frac{2m^*r^2 R(r)}{\hbar^2} (V(r) - \varepsilon) = m^2 R(r) \quad (4.14)$$

$$\frac{d^2 Y(\theta)}{d\theta^2} = -m^2 Y(\theta). \quad (4.15)$$

The solution of the *angular equation* in (4.15) is

$$Y(\theta) = C e^{im\theta}, \quad (4.16)$$

where  $C$  is a constant, and  $i$  is the imaginary unit. Actually, there is also another solution:  $e^{-im\theta}$ . This is covered by allowing  $m$  to run negative. Since the spatial wavefunction must be normalized, i.e.

$$\int_0^\infty \int_0^{2\pi} |R(r)Y(\theta)|^2 r dr d\theta = 1, \quad (4.17)$$

the angular solution must satisfy

$$\int_0^{2\pi} |Y(\theta)|^2 d\theta = 1, \quad (4.18)$$

yielding  $C^2 = 1/2\pi$ . The normalized solution of the angular equation thus reads

$$Y(\theta) = \frac{1}{\sqrt{2\pi}} e^{im\theta}. \quad (4.19)$$

At this point, there are no mathematical restrictions on  $m$ . Since the system is invariant under  $2\pi$ -rotation, we demand that

$$Y(\theta + 2\pi) = Y(\theta). \quad (4.20)$$

This imply that

$$e^{im\theta} = 1, \quad (4.21)$$

leading to the following allowed values of  $m$ ,

$$m = 0, \pm 1, \pm 2, \pm 3, \dots \quad (4.22)$$

We now turn to Eq. (4.14). In order to simplify the equation, we define

$$\rho(r) \equiv \sqrt{r}R(r) \quad \Rightarrow \quad R(r) = \frac{\rho(r)}{\sqrt{r}}, \quad (4.23)$$

and substitute this expression into Eq. (4.14), yielding

$$-\frac{\hbar^2}{2m^*} \frac{d^2\rho(r)}{dr^2} + \left[ u(r) + \frac{\hbar^2}{2m^*} \frac{m^2 - \frac{1}{4}}{r^2} \right] \rho(r) = \varepsilon \rho(r). \quad (4.24)$$

This is called the *radial equation*. It is identical to the 1-dimensional Schrödinger equation with an effective potential

$$u_{\text{eff}}(r) = u(r) + \frac{\hbar^2}{2m^*} \frac{m^2 - \frac{1}{4}}{r^2}. \quad (4.25)$$

Just like the centrifugal pseudo-force in classical mechanics, the second term in the above expression can be characterized as a centrifugal term which tends to push the particle outwards. The radial part of the wavefunction must satisfy the normalization condition

$$\int_0^\infty |R(r)|^2 r dr = \int_0^\infty |\rho(r)|^2 dr = 1 \quad (4.26)$$

This is as far as we can go before we specify the potential. Given a spherically symmetric potential  $u(r)$ , the solution of the single-particle Schrödinger equation is found by solving the radial equation in (4.24), yielding  $R(r)$  (through Eq. 4.23) and the eigenvalues  $\varepsilon$ . The normalized form of  $R(r)$  is found by Eq. (4.26). The final spatial solution reads

$$\phi_m(r, \theta) = \frac{1}{\sqrt{2\pi}} R(r) e^{im\theta}, \quad (4.27)$$

with  $m$  given in Eq. (4.22).

### 4.3 Solutions for the Single-Electron Parabolic Quantum Dot

We will in this section solve the Schrödinger equation for the single-electron parabolic quantum dot in 2 dimensions. The potential is given by Eq. (4.2). In the absence of an electromagnetic field, the Hamiltonian of the single-electron system reads

$$\hat{H} = -\frac{\hat{p}^2}{2m^*} + \frac{1}{2} m^* \omega^2 r^2, \quad (4.28)$$

where

$$\hat{p} = -i\hbar\nabla = -i\hbar \left( \frac{\partial}{\partial x} \mathbf{i} + \frac{\partial}{\partial y} \mathbf{j} \right) \quad (4.29)$$

is the momentum operator,  $m^*$  is the effective mass of the electron,  $\omega$  is the oscillator frequency,  $r$  is the distance between the electron and the point where  $1/2m^*\omega^2r^2 = 0$ , and  $\mathbf{i}$  and  $\mathbf{j}$  are the

cartesian unit vectors. We now introduce an electromagnetic field. The classical Hamiltonian of a charged electron in an electromagnetic field reads [44]

$$H = \frac{1}{2m}(\mathbf{p} - e\mathbf{A})^2 + e\Omega, \quad (4.30)$$

with  $\Omega$  and  $\mathbf{A}$  as the electromagnetic potentials,  $m$  as the mass,  $e$  as the charge, and  $\mathbf{p} = m\mathbf{v}$  is the classical momentum vector. The electromagnetic potentials are related to electromagnetic field by the equations

$$\mathbf{E} = -\frac{\partial \mathbf{A}}{\partial t} - \nabla\Omega \quad (4.31)$$

$$\mathbf{B} = \nabla \times \mathbf{A}, \quad (4.32)$$

where  $t$  is the time. In quantum mechanics, electrons carry intrinsic spin (see Sec. 2.2.2). This leads to an additional energy contribution,  $-\hat{\mu} \cdot \mathbf{B}$ , where  $\hat{\mu}$  is the magnetic moment of the electron. The Hamiltonian of a single-electron parabolic quantum dot subjected to an electromagnetic field then reads

$$\hat{H} = \frac{1}{2m^*}(\hat{p} - e\mathbf{A})^2 + e\Omega - \hat{\mu} \cdot \mathbf{B} + \frac{1}{2}m^*\omega_0^2r^2, \quad (4.33)$$

where  $\hat{p}$  is given by Eq. (4.29). For reasons that will appear later, the oscillator frequency is changed from  $\omega$  to  $\omega_0$ . We are seeking the solution of the time-independent Schrödinger equation,

$$\left( \frac{1}{2m^*}(\hat{p} - e\mathbf{A})^2 + e\Omega - \hat{\mu} \cdot \mathbf{B} + \frac{1}{2}m^*\omega_0^2r^2 \right) \psi(\mathbf{r}) = \varepsilon\psi(\mathbf{r}), \quad (4.34)$$

where  $\varepsilon$  is the energy eigenvalue, and  $\mathbf{r}$  includes the spin degree of freedom. The total wavefunction (energy eigenfunction)  $\psi(\mathbf{r})$  (see Sec. 2.2.3) is defined as

$$\psi(\mathbf{r}) = \phi(x, y) \otimes |\chi\rangle, \quad (4.35)$$

where  $\phi(x, y)$  is the spatial part, and  $|\chi\rangle$  is the spin part. We observe that the Hamiltonian contains a spin dependent part and two parts that depend on the position of the electron, i.e. parts that act in different spaces (see Sec. 2.2.3). Inserting the total wavefunction in Eq. (4.35) into the Schrödinger equation (4.34), we obtain

$$\left( \frac{1}{2m^*}[\hat{p} - e\mathbf{A}]^2 + \frac{1}{2}m^*\omega_o^2(x^2 + y^2) \right) \phi(x, y) = \varepsilon_r \phi(x, y) \quad (4.36)$$

$$- (\mu \cdot \mathbf{B}) |\chi\rangle = \varepsilon_s |\chi\rangle. \quad (4.37)$$

The total energy is given as

$$\varepsilon = \varepsilon_r + \varepsilon_s + e\Omega. \quad (4.38)$$

We first consider the spatial equation in (4.36). This equation can be simplified by writing out the first term on the left hand side,

$$\frac{1}{2m^*}(\hat{p} - e\mathbf{A})^2 = \frac{1}{2m^*}(\hat{p}^2 + e^2\mathbf{A}^2 - e\mathbf{B} \cdot \hat{L}), \quad (4.39)$$

where  $\hat{L}$  is the angular momentum operator [24] defined as

$$\hat{L} = (x\mathbf{i} + y\mathbf{j}) \times \hat{p}, \quad (4.40)$$

where  $\hat{p}$  is given in Eq. (4.29). Furthermore, we are working in the Coulomb gauge [44], i.e.

$$\nabla \cdot \mathbf{A} = 0. \quad (4.41)$$

One possible solution is [44]

$$\mathbf{A} = \frac{1}{2}\mathbf{B} \times (x\mathbf{i} + y\mathbf{j}). \quad (4.42)$$

The Hamiltonian can then be written in the following form,

$$\hat{H} = \frac{1}{2m^*} \left[ \hat{p}^2 + \frac{e^2}{4} \left( \mathbf{B} \times (x\mathbf{i} + y\mathbf{j}) \right)^2 - e\mathbf{B} \cdot \hat{\mathbf{L}} \right] + \frac{1}{2}m^*\omega_o^2(x^2 + y^2). \quad (4.43)$$

We now consider the special case of a constant and uniform magnetic field in the z-direction, i.e.

$$\mathbf{B} = B_0\mathbf{k}, \quad (4.44)$$

where  $\mathbf{k}$  is the unit vector in the  $z$ -direction, and  $B_0$  is a constant. The Hamiltonian then reads

$$\hat{H} = \frac{1}{2m^*} \left[ \hat{p}^2 + \frac{e^2B_0^2}{4} (x^2 + y^2) - eB_0(x\hat{p}_y - y\hat{p}_x) \right] + \frac{1}{2}m^*\omega_o^2(x^2 + y^2). \quad (4.45)$$

Defining

$$\omega_B \equiv \frac{eB_0}{2m^*}, \quad (4.46)$$

and

$$\omega^2 \equiv \omega_0^2 + \omega_B^2, \quad (4.47)$$

the Hamiltonian can be written as

$$\hat{H} = \frac{1}{2m^*} \left[ \hat{p}^2 - eB_0(x\hat{p}_y - y\hat{p}_x) \right] + \frac{1}{2}m^*\omega^2(x^2 + y^2). \quad (4.48)$$

We identify

$$x\hat{p}_y - y\hat{p}_x = \hat{L}_z, \quad (4.49)$$

i.e. the  $z$ -projection of the angular momentum  $\hat{\mathbf{L}}$ . Thus we obtain

$$\hat{H} = \frac{1}{2m^*} \left( \hat{p}^2 - eB_0\hat{L}_z \right) + \frac{1}{2}m^*\omega^2(x^2 + y^2). \quad (4.50)$$

We now introduce spherical coordinates, see Eqs. (4.5) and (4.6). In this representation, the  $z$ -projection of the angular momentum reads

$$\hat{L}_z = -i\hbar \frac{\partial}{\partial\theta}. \quad (4.51)$$

The Hamiltonian is now given as

$$\hat{H} = -\frac{\hbar^2}{2m^*} \left( \frac{\partial^2}{\partial r^2} + \frac{1}{r} \frac{\partial}{\partial r} + \frac{1}{r^2} \frac{\partial^2}{\partial\theta^2} - \frac{ieB_0}{\hbar} \frac{\partial}{\partial\theta} \right) + \frac{1}{2}m^*\omega^2r^2. \quad (4.52)$$

We are seeking the solution of the time-independent Schrödinger equation,

$$\left[ -\frac{\hbar^2}{2m^*} \left( \frac{\partial^2}{\partial r^2} + \frac{1}{r} \frac{\partial}{\partial r} + \frac{1}{r^2} \frac{\partial^2}{\partial\theta^2} - \frac{ieB_0}{\hbar} \frac{\partial}{\partial\theta} \right) + \frac{1}{2}m^*\omega^2r^2 \right] \phi(r, \theta) = \varepsilon_r \phi(r, \theta). \quad (4.53)$$

We observe that the time-independent Schrödinger equation for a general spherically symmetric potential (4.7) is almost identical to the equation above. The magnetic field provides an additional term,

$$-\frac{ieB_0}{\hbar} \frac{\partial}{\partial\theta}. \quad (4.54)$$

Since it only depends on the angle  $\phi$ , the solution of Eq. (4.53) is separable. In the previous section we found that the solution of the angular equation in (4.15) is given as  $\exp(im\theta)/\sqrt{2\pi}$ . We therefore make the following ansatz

$$\phi(r, \theta) = R(r)e^{im\theta}, \quad (4.55)$$

where  $m$  is given by Eq. (4.22) since we demand  $e^{im\theta} = 1$ . Substituting the ansatz into Eq. (4.53), yields

$$\left[ -\frac{\hbar^2}{2m^*} \left( \frac{d^2}{dr^2} + \frac{1}{r} \frac{d}{dr} - \frac{m^2}{r^2} + \frac{emB_0}{\hbar} \right) + \frac{1}{2} m^* \omega^2 r^2 \right] R(r) = \varepsilon_r R(r). \quad (4.56)$$

The normalized energy eigenfunctions are given as

$$\psi_{nm}(r, \theta) = \sqrt{\frac{n!}{\pi(n+|m|)!}} \beta^{\frac{1}{2}(1+|m|)} r^{|m|} e^{-\frac{1}{2}\beta r^2} L_n^{|m|}(\beta r^2) e^{im\theta}, \quad (4.57)$$

where  $L(\beta r^2)_n^{|m|}$  is the associated Laguerre polynomials, and  $\beta$  is defined as

$$\beta \equiv \frac{m^* \omega}{\hbar}. \quad (4.58)$$

The eigenvalues are given as

$$\varepsilon_{r,nm} = (1 + |m| + 2n) \hbar\omega + m\hbar\omega_B, \quad (4.59)$$

where  $\omega_B$  is defined in Eq. (4.46), and  $n = 0, 1, 2, 3, \dots$ . See App. (A) for the full derivation of Eq. (4.57) and Eq. (4.59).

We now consider the spin equation in (4.37). The magnetic moment is given as

$$\hat{\mu} = \frac{eg}{2m^*} \hat{S}, \quad (4.60)$$

where  $g$  is the  $g$ -factor of the electron,  $e$  is the charge,  $m^*$  is the effective mass, and  $\hat{S}$  is the spin operator. Since  $\mathbf{B} = B_0 \mathbf{k}$ , where  $\mathbf{k}$  is the cartesian unit vector in the  $z$ -direction, the spin equation reads

$$-\frac{egB_0}{2m^*} S_z |\chi\rangle = \varepsilon_s |\chi\rangle, \quad (4.61)$$

where  $\hat{S}_z$  is the  $z$ -projection of the spin. The eigenvectors are given by Eqs. (2.61) and (2.62). The eigenvalues are (see Sec 2.2.2)

$$\varepsilon_{s,m_s} = -\frac{eg\hbar B_0}{2m^*} m_s = g m_s \hbar \omega_B. \quad (4.62)$$

Collecting all terms that contribute to the *total* energy  $\varepsilon$  in Eq. (4.38), yields

$$\varepsilon_{nmm_s} = (1 + |m| + 2n) \hbar\omega + m\hbar\omega_B + g m_s \hbar\omega_B + e\Omega. \quad (4.63)$$

The *total* energy eigenfunctions are given as

$$\psi_{nmm_s}(r, \theta) = \sqrt{\frac{n!}{\pi(n+|m|)!}} \beta^{\frac{1}{2}(1+|m|)} r^{|m|} e^{-\frac{1}{2}\beta r^2} L_n^{|m|}(\beta r^2) e^{im\phi} \otimes |\chi_{m_s}\rangle, \quad (4.64)$$

where  $|\chi_{m_s}\rangle$  is given in Eqs. (2.61) and (2.62).

When the electromagnetic field vanishes, i.e.  $\omega_B = 0$  and  $\Omega = 0$ , the energy is given as

$$\varepsilon_{nm}^0 = (1 + |m| + 2n) \hbar\omega_0, \quad (4.65)$$

where the superscript denotes the absence of an electromagnetic field. This is the energy spectrum we would have obtained by directly solving the radial equation in (4.24) with the harmonic oscillator potential. Since

$$n = 0, 1, 2, 3, \dots \quad (4.66)$$

$$m = 0, \pm 1, \pm 2, \pm 3, \dots \quad (4.67)$$

$$m_s = -\frac{1}{2}, \frac{1}{2}, \quad (4.68)$$

the total degeneracy of energy level  $\varepsilon_{nm}^0$  is given as

$$D = 2d = 2(1 + |m| + 2n), \quad (4.69)$$

where the factor of 2 comes from the spin degree of freedom (spin up/down). This is what we call a *shell structure*. In Nature, we often observe this feature. The most well-known case is perhaps the Hydrogen atom. The energy eigenvalues are given as (Bohr formula)

$$E_n = -\frac{1}{2\hbar^2} \left( \frac{e^2}{4\pi\epsilon_0} \right)^2 \frac{1}{n^2}, \quad (4.70)$$

where  $n$  is the so-called principal quantum number. The quantum state is characterized by four quantum numbers  $n, l, m_l$  and  $m_s$ , where  $l$  is the orbital quantum numbers,  $m_l$  is the magnetic quantum number, and  $m_s$  is the quantum number associated with the  $z$ -projection of the spin. Since the energy only depends on  $n$ , each energy level has degeneracy. Turning back to the quantum dot system, we define the shell number as

$$R \equiv (1 + |m| + 2n). \quad (4.71)$$

The shell structure is shown in Table 4.1 and illustrated in Figure 4.1. For each shell number

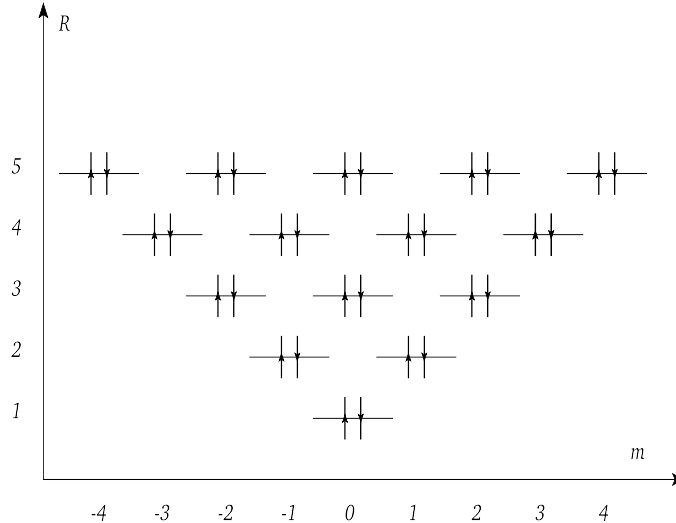


**Figure 4.1:** Shell structure of a single-electron parabolic quantum dot, where  $R$  is the shell number defined in Eq. (4.71),  $m$  is the angular quantum number, and  $\uparrow\downarrow$  denote  $m_s = \pm 1/2$  (spin quantum number).

$R$ , we associate  $D$  orbitals. Also, for a given shell  $R$ , there are

$$D + (D - 2) + (D - 4) + \dots + 2 \quad (4.72)$$

orbitals associated with shells  $R' \leq R$ . We have in Table 4.1 tabulated this value for each  $R$  (Shell-filling). These are the so-called *magic numbers*, which represent the number of non-interacting electrons that are needed to obtain a closed-shell ground state. These numbers are important for many-body calculations of interacting systems. We will come back to this later.

$R$	$D = 2d$	Shell-filling
1	2	2
2	4	6
3	6	12
4	8	20
5	10	30
6	12	42
7	14	56

**Table 4.1:** Shell structure of the single-electron parabolic quantum dot, where  $R$  is the shell number (energy level) defined in Eq. (4.71),  $D$  is the degeneracy for each level, and “shell-filling” is the number of orbitals from shell 1 up to shell  $R$ .

Consider Eqs. (4.65) and (4.64). We see that the presence of the magnetic field makes the energy depend on  $m_s$  and the sign of  $m$ . When the strength of the magnetic field increases, the degenerate states for  $\mathbf{B} = 0$  will separate more and more. In order to illustrate this feature, we set  $\Omega = 0$  (this is just a constant) and remove the spin contribution  $gm_s\hbar\omega_B$ . By substituting Eq. (4.47) into Eq. (4.59) and divide by  $\hbar\omega_0$ , we obtain

$$\frac{\varepsilon_{nm}}{\hbar\omega_0} = (1 + |m| + 2n) \sqrt{1 + \frac{\omega_B^2}{\omega_0^2} + m \frac{\omega_B}{\omega_0}}. \quad (4.73)$$

This leads to the so-called Fock-Darwin energy spectrum [8] shown in Figure (4.2). Including the

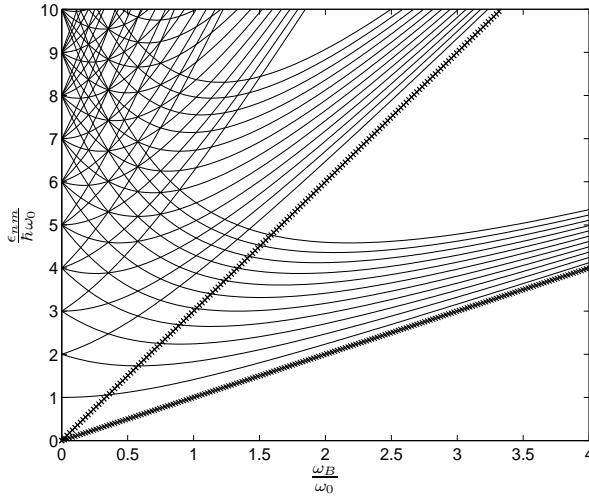


**Figure 4.2:** The 2-dimensional Fock-Darwin energy spectrum for a single-electron quantum dot. For  $\omega_B = 0$ , the energy levels are degenerate. When  $\omega_B$  increases, the energy levels split due to the contribution from  $m\hbar\omega_B$ . Sudden degeneracy occur, with subsequent splitting. If we were to follow the “energy history” of an electron when  $\omega_B$  increases, we would observe a zig-zag line since it chooses the state with the most favorable energy (after a sudden degeneracy). We clearly observe that the energy levels converge to the high field limits in Eq. (4.78), forming the so-called Landau bands [45]. The straight (bold) lines indicate the Landau bands for  $N_L = 0$  and  $1$ , see Eq. (4.78).

spin part would split up each energy line and result in an even more complicated Fock-Darwin diagram. When  $\omega_B = 0$ , the energy levels are degenerate, as discussed above. When the magnetic field is turned on, the degenerate states separate due to the  $m\hbar\omega_B$  term. Further increment of the magnetic field leads to sudden degeneracies with other states, i.e. states belonging to different shells. When the magnetic field increases even more (after a sudden degeneracy), an electron in a degenerate state will choose the state (if available) with the most favorable energy. Further increment leads to more sudden degeneracies. In Figure (4.2) we clearly observe that the energy

lines congregate into bands when the magnetic field increases. These bands are often called Landau bands [45, 46]. In the limit when  $\omega_B \rightarrow \infty$ , the energy eigenvalues (4.73) reads

$$\lim_{\omega_B \rightarrow \infty} \varepsilon_{nm} = (1 + |m| + m + 2n) \hbar \omega_B. \quad (4.74)$$

When  $m \geq 0$  we obtain

$$\lim_{\omega_B \rightarrow \infty} \varepsilon_{nm} = (1 + 2(m + n)) \hbar \omega_B. \quad (4.75)$$

In the other case, when  $m < 0$ , the expression reads

$$\lim_{\omega_B \rightarrow \infty} \varepsilon_{nm} = (1 + 2n) \hbar \omega_B. \quad (4.76)$$

It is natural to define the Landau number

$$N_L \equiv 0, 1, 2, 3, \dots \quad (4.77)$$

Therefore, for a sufficient strong magnetic field, the energy eigenvalues are approximately given as

$$\varepsilon_L \approx (1 + 2N_L) \hbar \omega_B. \quad (4.78)$$

In Figure (4.2), the Landau bands for  $N_L = 0$  and  $N_L = 1$  are shown by the straight (bold) lines. We clearly observe that when the magnetic field increases, the energy spectrum form Landau bands which converges to the Landau energies in Eq. (4.78).

## 4.4 N-Electron Model Hamiltonian

When the quantum dot contains more than one electron, the time-independent Schrödinger equation must be solved numerically. In order to do numerical simulations, a Hamiltonian must be provided. The Hamiltonian of an  $N$ -electron parabolic quantum dot in an electromagnetic field with  $\mathbf{B} = B_0 \mathbf{k}$  reads (see Sections 4.2 and 4.3)

$$\begin{aligned} \hat{H} = & \sum_{i=1}^N \left( -\frac{\hbar^2}{2m^*} \nabla_i^2 + \frac{1}{2} m^* \omega_0^2 r_i^2 \right) + \frac{e^2}{4\pi\epsilon_0\epsilon_r} \sum_{i=1 < j}^N \frac{1}{r_{ij}} \\ & + \sum_{i=1}^N \left( \frac{1}{2} m^* \omega_B^2 r_i^2 - \omega_B \hat{L}_z^{(i)} - g\omega_B \hat{S}_z^{(i)} \right), \end{aligned} \quad (4.79)$$

where  $\hbar$  is the Planck constant,  $m^*$  is the effective mass of the electron,  $-\hbar \nabla_i^2 / 2m^*$  is the kinetic energy of electron  $i$ ,  $\omega_0$  is the oscillator frequency,  $r_i$  is the distance between electron  $i$  and the point where the harmonic oscillator potential is zero,  $e$  is the electron charge,  $\epsilon_0$  is the vacuum permittivity,  $\epsilon_r$  is the relative permittivity,  $r_{ij}$  is the distance between electron  $i$  and  $j$ ,  $\omega_B$  is the cyclotron frequency defined in Eq. (4.46),  $g$  is the  $g$ -factor of the electron,  $\hat{L}_z^{(i)}$  is the z-component of the angular momentum, and  $\hat{S}_z^{(i)}$  is the z-component of the spin. The Hamiltonian can be simplified to the following form by defining the total frequency  $\omega$  in Eq. (4.47),

$$\begin{aligned} \hat{H} = & \sum_{i=1}^N \left( -\frac{\hbar^2}{2m^*} \nabla_i^2 + \frac{1}{2} m^* \omega^2 r_i^2 \right) + \frac{e^2}{4\pi\epsilon_0\epsilon_r} \sum_{i=1 < j}^N \frac{1}{r_{ij}} \\ & - \sum_{i=1}^N \left( \omega_B \hat{L}_z^{(i)} + g\omega_B \hat{S}_z^{(i)} \right). \end{aligned} \quad (4.80)$$

Since both  $\hat{L}_z$  and  $\hat{S}_z$  commute with the Hamiltonian, we can perform the calculations separately in subspaces of given  $m$  and  $m_s$  [47]. We can therefore rewrite the Hamiltonian,

$$\begin{aligned}\hat{H} = & \sum_{i=1}^N \left( -\frac{\hbar^2}{2m^*} \nabla_i^2 + \frac{1}{2} m^* \omega^2 r_i^2 \right) + \frac{e^2}{4\pi\epsilon_0\epsilon_r} \sum_{i=1<j}^N \frac{1}{r_{ij}} \\ & - \sum_{i=1}^N \left( \omega_B m^{(i)} + g\omega_B m_s^{(i)} \right).\end{aligned}\quad (4.81)$$

Since the angular-part and the spin-part of the Hamiltonian only involve the good quantum numbers and not the operators themselves, one merely needs to solve the problem without the magnetic field [47], but with  $\omega_0 \rightarrow \omega$ . The contributions from these terms can be added after the simulation. Our final model Hamiltonian thus reads

$$\hat{H} = \sum_{i=1}^N \left( -\frac{\hbar^2}{2m^*} \nabla_i^2 + \frac{1}{2} m^* \omega^2 r_i^2 \right) + \frac{e^2}{4\pi\epsilon_0\epsilon_r} \sum_{i=1<j}^N \frac{1}{r_{ij}}.\quad (4.82)$$

## 4.5 Scaling the Model Hamiltonian

In order to simplify the computations, the Hamiltonian in Eq. (4.82) can be scaled into a dimensionless form. We will in the following present the scaling used by for example [48, 49, 50]. First we define

$$\begin{aligned}\omega &\equiv \omega_k \omega' \\ \mathbf{r} &\equiv l_0 \mathbf{r}' = l_0 (x' \mathbf{i} + y' \mathbf{j} + z' \mathbf{k}) \\ \nabla'^2 &\equiv \frac{\partial^2}{\partial x'^2} + \frac{\partial^2}{\partial y'^2} + \frac{\partial^2}{\partial z'^2},\end{aligned}\quad (4.83)$$

where  $\omega_k$  and  $l_0$  are constants. We then obtain

$$\begin{aligned}\nabla_i^2 &= \frac{1}{l_0^2} \nabla'_i^2 \\ r_i^2 &= l_0^2 r_i'^2 \\ r_{ij} &= l_0 r_{ij}'\end{aligned}\quad (4.84)$$

Inserting these expression into Eq. (4.82), yields

$$\hat{H} = -\frac{\hbar^2}{2m^* l_0^2} \sum_{i=1}^N \nabla_i'^2 + \frac{1}{2} m^* \omega_k^2 \omega'^2 l_0^2 \sum_{i=1}^N r_i'^2 + \frac{\hbar}{\kappa l_0} \sum_{i<j}^N \frac{1}{r_{ij}'},\quad (4.85)$$

where

$$\kappa \equiv \frac{4\pi\epsilon_0\epsilon_r\hbar}{e^2}.\quad (4.86)$$

Since  $e^2/4\pi\epsilon_0\epsilon_r$  has dimension length,  $\kappa$  has dimension time per length. Furthermore, we define

$$l_0 \equiv \sqrt{\frac{\hbar}{m^* \omega}} = \sqrt{\frac{\hbar}{m^* \omega_k \omega'}},\quad (4.87)$$

where  $l_0$  has dimension length. We now substitute this expression into Eq. (4.85), yielding

$$\hat{H} = -\frac{\omega_k \omega' \hbar}{2} \sum_{i=1}^N \nabla_i'^2 + \frac{\hbar}{2} \omega_k \omega' \sum_{i=1}^N r_i'^2 + \frac{\hbar}{\kappa} \sqrt{\frac{m^* \omega_k \omega'}{\hbar}} \sum_{i<j}^N \frac{1}{r_{ij}'}. \quad (4.88)$$

We want to express the energy in units of effective Hartrees,

$$\begin{aligned} E_H^* &\equiv m^* \left( \frac{e^2}{4\pi\epsilon_0\epsilon_r\hbar} \right)^2 \\ &= \frac{m^*}{\kappa^2}. \end{aligned} \quad (4.89)$$

We observe that  $E_H^*$  has dimension energy, as wanted. This follows from the definition of  $\kappa$  in Eq. (4.86). We divide Eq. (4.88) by  $E_H^*$ , i.e. multiply with  $\kappa^2\hbar/m^*$ , yielding

$$\hat{H}' = -\frac{\omega_k\omega'\hbar\kappa^2}{2m^*} \sum_{i=1}^N \nabla_i'^2 + \frac{\hbar\kappa^2}{2m^*}\omega_k\omega' \sum_{i=1}^N r_i'^2 + \frac{\kappa\hbar}{m^*} \sqrt{\frac{m^*\omega_k\omega'}{\hbar}} \sum_{i<j}^N \frac{1}{r_{ij}'}, \quad (4.90)$$

where  $\hat{H}' \equiv \hat{H}/E_H^*$ . We now define

$$\omega_k \equiv \frac{m^*}{\hbar\kappa^2},$$

and observe that  $\omega_k$  has dimension inverse time. Inserting this expression into the above equation finally yields

$$\hat{H}' = -\frac{\omega'}{2} \sum_{i=1}^N \nabla_i'^2 + \frac{1}{2}\omega' \sum_{i=1}^N r_i'^2 + \sqrt{\omega'} \sum_{i<j}^N \frac{1}{r_{ij}'}. \quad (4.91)$$

This is the dimensionless model Hamiltonian for which we have performed all of our numerical calculations. Energies are measured in units of effective Hartrees  $E_H^*$ , lengths in units of  $l_0$  and oscillator frequencies in units of  $\omega_k$ .

We now define the one-body and two-body part of the Hamiltonian as

$$\hat{h}_i' \equiv -\frac{\omega'}{2}\nabla_i'^2 + \frac{1}{2}\omega'r_i'^2 \quad (4.92)$$

$$\hat{v}_i' \equiv \sqrt{\omega'} \sum_{i<j}^N \frac{1}{r_{ij}'}, \quad (4.93)$$

leading to the following simplified form,

$$\hat{H}' = \sum_{i=1}^N \hat{h}_i' + \sum_{i<j}^N \hat{v}_{ij}'. \quad (4.94)$$

Part II

## MANY-BODY METHODS



# Chapter 5

## Hartree-Fock Method

In this chapter we present the Hartree-Fock (HF) method for a closed-shell system [18], called the Restricted Hartree-Fock method (RHF). The aim of the chapter is to give a brief overview of the theory and a derivation of the HF equations that is implemented in this thesis. In the first section we give an introduction to the method. Then we present the basic ideas of HF and the variational principle. Thereafter, we derive the Hartree-Fock equations.

### 5.1 Introduction

The Hartree-Fock (HF) method is an approximate method to determine the ground state energy and wavefunction of a many-fermion system. Its origin dates back to the end of 1920s, just after the Schrödinger equation was introduced in 1926 [51]. One year later, in 1927, D.R. Hartree introduced the self-consistent field method, which we today know as the Hartree method. This was a method to calculate approximate ground state energies and wavefunctions for atoms and ions. One of Hartree's main objectives behind the development of the Hartree method was to solve the many-body Schrödinger equation from fundamental physical principles alone. Such methods are today called *ab initio* methods. Many of Hartree's competitors did not understand the physical reasoning behind the Hartree equations and the self-consistent procedure. Furthermore, the connection to the time-independent Schrödinger equation was unclear to many people. In 1928, J. C. Slater showed that the Hartree equations can be derived by applying the quantum mechanical variational principle on a trial wavefunction (ansatz) which consists of products of single-particle functions. A few years earlier, in 1925, W. Pauli formulated the important Pauli exclusion principle stating that fermions cannot occupy identical single-particle states. In 1929, J. C. Slater published that determinants ensure the antisymmetry requirement of fermionic wavefunction and the Pauli exclusion principle [52]. V. A. Fock and J. C. Slater pointed out that the Hartree method did not respect the antisymmetry requirement of the wavefunction. Thus a more correct ansatz would be the Slater determinants. Applying the variational principle on a Slater determinant ansatz leads to the so-called Hartree-Fock method. The Hartree method can be regarded as an approximation to the Hartree-Fock method, where the exchange term is removed. Despite the physical and intuitive picture of the Hartree-Fock method, it was infrequently used until the 1950s with the advent of modern computers.

The HF method is often called a mean-field approximation [31]. The main idea of HF is that the interactions in the system are replaced by an effective (averaged) interaction. The result is essentially that the many-body Schrödinger equation reduces to a one-body problem. Such a description means that we potentially loose important information in the system. We can only *hope* that most of the correlations in the system are well-described in this approximation. However, it turns out that HF calculations often give important information of the system.

## 5.2 Basic Ideas

The basic idea of HF is the following. First we approximate the ground state wavefunction by a Slater determinant. Then we vary the single-particle orbitals in order to determine the best estimate of the ground state energy. The foundation of HF is the variational principle of Rayleigh and Ritz (RR) (see for example [53]). This is one of the oldest and most powerful tools in quantum mechanical theory. The Rayleigh Ritz principle forms the basis of other important many-body methods such as Density Functional Theory (DFT) [32, 54]. It states that given an (in principle arbitrary) ansatz  $\psi_T$  for the ground state wavefunction, the expectation value of  $\hat{H}$  in state  $\psi_T$  is certain to overestimate the exact ground state energy. This can be verified by the following proof,

$$\begin{aligned}\langle \hat{H} \rangle &\equiv \langle \psi_{\text{HF}} | \hat{H} | \psi_{\text{HF}} \rangle \\ &= \left\langle \sum_n c_n \psi_n | \hat{H} | \sum_m c_m \psi_m \right\rangle \\ &= \left\langle \sum_n c_n \psi_n | \sum_m c_m E_m \psi_n \right\rangle \\ &= \sum_{n,m} c_n^* E_m c_m \langle \psi_n | \psi_m \rangle \\ &= \sum_{n,m} c_n c_m E_m \delta_{mn} \\ &= \sum_n |c_n|^2 E_n \\ &\leq E_0,\end{aligned}$$

where  $E_0$  is the exact ground state energy. Our goal is to minimize  $\langle \hat{H} \rangle$  in order to obtain an approximation to the ground state energy.

## 5.3 Derivation of the Hartree-Fock Equations

The HF ansatz reads

$$\Psi_{\text{HF}}(\mathbf{r}_1, \mathbf{r}_2, \dots, \mathbf{r}_N) = \frac{1}{\sqrt{N!}} \sum_p (-1)^p \hat{P} \varphi_a(\mathbf{r}_1) \varphi_b(\mathbf{r}_2) \dots \varphi_d(\mathbf{r}_N), \quad (5.1)$$

where  $\varphi_a(\mathbf{r})$  is a so-called HF orbital. In order to minimize the energy expectation value, we have two possibilities. The first is to vary the HF orbitals directly, leading to the so-called Roothaan-Hartree-Fock [55] method. Another opportunity, which we have chosen in this thesis, is to expand the orbitals in well known single-particle functions and vary the expansion coefficients. We define the HF orbital as

$$\varphi_a(\mathbf{r}) = \sum_{\alpha}^{d_b} C_{a\alpha} \psi_{\alpha}(\mathbf{r}), \quad (5.2)$$

where  $C_{a\alpha}$  is an expansion coefficient, and

$$\mathcal{B}_{\text{HF}} = \{\psi(\mathbf{r})\}_{\alpha=1}^{d_b} \quad (5.3)$$

is an orthonormal set of single-particle functions spanning our model space with dimension  $d_b$ . The basis set can in principle be chosen arbitrarily. We now limit the discussion to two-body Hamiltonians. Consider the Hamiltonian

$$\hat{H} = \hat{H}_0 + \hat{V}$$

where

$$\hat{H}_0 = \sum_{i=1}^N \hat{h}_i$$

is the Hamiltonian of the non-interacting system, and

$$\hat{V} = \sum_{i=1 < j}^N \hat{v}_{ij}$$

is the interaction potential between the particles. In the formalism of second quantization (see Section 3.5), the Hamiltonian reads

$$\hat{H} = \sum_{ab} \langle a|h|b\rangle a_a^\dagger a_b + \frac{1}{2} \sum_{abcd} \langle ab|v|cd\rangle a_a^\dagger a_b^\dagger a_d a_c,$$

where  $a_b^\dagger$  is the creation operator and  $a_b$  is the annihilation operator. We have here chosen the Hartree-Fock orbitals in Eq. (5.2) as basis functions. Using Wick's theorem (see Sec. 3.5.3), the energy expectation value reads

$$\begin{aligned} E[\Psi_{\text{HF}}] &\equiv \langle \Psi_{\text{HF}} | \hat{H} | \Psi_{\text{HF}} \rangle \\ &= \langle \Psi_{\text{HF}} | \hat{H}_0 | \Psi_{\text{HF}} \rangle + \langle \Psi_{\text{HF}} | \hat{V} | \Psi_{\text{HF}} \rangle \\ &= \sum_{ab} \langle a|h|b\rangle \langle \Psi_{\text{HF}} | a_a^\dagger a_b | \Psi_{\text{HF}} \rangle + \frac{1}{2} \sum_{abde} \langle ab|v|de\rangle \langle \Psi_{\text{HF}} | a_a^\dagger a_b^\dagger a_d a_c | \Psi_{\text{HF}} \rangle. \\ &= \sum_a^N \langle a|h|a\rangle + \frac{1}{2} \sum_{ab}^N \left[ \langle ab|v|ab\rangle - \langle ab|v|ba\rangle \right]. \end{aligned} \quad (5.4)$$

Inserting Eq. (5.2) into this expression yields

$$E[\Psi_{\text{HF}}] = \sum_a^N \sum_{\alpha\beta}^{d_b} C_{a\alpha}^* C_{a\beta} \langle \alpha|h|\beta\rangle + \frac{1}{2} \sum_{ab}^N \sum_{\alpha\beta\gamma\delta}^{d_b} C_{a\alpha}^* C_{b\beta}^* C_{a\gamma} C_{b\delta} \left[ \langle \alpha\beta|v|\gamma\delta\rangle - \langle \alpha\beta|v|\delta\gamma\rangle \right], \quad (5.5)$$

where  $N$  is the number of particles, the Latin letters denote the new basis (Hartree-Fock orbitals), and the Greek letters denote the old basis in Eq. (5.3). We now want to minimize  $E[\Psi_{\text{HF}}]$  with the constraint that the Hartree-Fock orbitals are orthonormal, viz.

$$\langle a|b\rangle = \sum_\lambda C_{a\lambda}^* C_{b\lambda} = \delta_{ab}.$$

Thus we have to introduce Lagrangian multipliers [29]. In general, in order to find the minimum or maximum of a function  $f(x, y, z, \dots, w)$  subjected to the constraints

$$g_1(x, y, z, \dots, w) = k_1 \quad (5.6)$$

$$g_2(x, y, z, \dots, w) = k_2 \quad (5.7)$$

⋮

$$g_N(x, y, z, \dots, w) = k_N, \quad (5.8)$$

we define

$$F \equiv f + \vartheta_1 g_1 + \dots + \vartheta_n g_n, \quad (5.9)$$

and set each partial derivative  $\partial F / \partial x_i = 0$ . The minimum or maximum is found by solving the differential equations and the constraint equations for  $x, y, z, \dots, w$  and the Lagrangian multipliers  $\vartheta_1, \vartheta_2, \dots, \vartheta_N$ .

We define

$$\begin{aligned} F &\equiv E[\Psi_{\text{HF}}] - \sum_{a=1}^N \vartheta_a g_a \\ &= E[\Psi_{\text{HF}}] - \sum_{a=1}^N \vartheta_a \sum_{\alpha} C_{a\alpha}^* C_{a\alpha}. \end{aligned}$$

Then we take the partial derivative of  $F$  with respect to  $C_{k\alpha}^*$ , yielding

$$\begin{aligned} 0 &= \frac{\partial}{\partial C_{k\alpha}^*} \left( E[\Psi_{\text{HF}}] - \sum_{a=1}^N \vartheta_a \sum_{\alpha} C_{a\alpha}^* C_{a\alpha} \right) \\ &= \frac{\partial}{\partial C_{k\alpha}^*} \left( \sum_a^N \sum_{\alpha\beta} C_{a\alpha}^* C_{a\beta} \langle \alpha | h | \beta \rangle + \frac{1}{2} \sum_{ab}^N \sum_{\alpha\beta\gamma\delta} C_{a\alpha}^* C_{b\beta}^* C_{a\gamma} C_{b\delta} [\langle \alpha\beta | v | \gamma\delta \rangle - \langle \alpha\beta | v | \delta\gamma \rangle] \right. \\ &\quad \left. - \sum_{a=1}^N \vartheta_a \sum_{\alpha} C_{a\alpha}^* C_{a\alpha} \right) \\ &= \sum_{\alpha\beta} C_{k\beta} \langle \alpha | h | \beta \rangle + \sum_a^N \sum_{\alpha\beta\gamma\delta} C_{a\beta}^* C_{k\gamma} C_{a\delta} [\langle \alpha\beta | v | \gamma\delta \rangle - \langle \alpha\beta | v | \delta\gamma \rangle] - \vartheta_k \sum_{\alpha} C_{k\alpha}. \end{aligned}$$

The factor of 1/2 disappears since  $C_{a\alpha}$  and  $C_{a\alpha}^*$  are independent. We simplify the expression into

$$\sum_{\alpha\beta} C_{k\beta} \langle \alpha | h | \beta \rangle + \sum_a^N \sum_{\alpha\beta\gamma\delta} C_{a\beta}^* C_{k\gamma} C_{a\delta} [\langle \alpha\beta | v | \gamma\delta \rangle - \langle \alpha\beta | v | \delta\gamma \rangle] = \vartheta_k \sum_{\alpha} C_{k\alpha}, \quad (5.10)$$

leading to

$$\sum_{\gamma} C_{k\gamma} \langle \alpha | h | \gamma \rangle + \sum_a^N \sum_{\beta\gamma\delta} C_{a\beta}^* C_{k\gamma} C_{a\delta} [\langle \alpha\beta | v | \gamma\delta \rangle - \langle \alpha\beta | v | \delta\gamma \rangle] = \vartheta_k C_{k\alpha}, \quad (5.11)$$

where we have changed the dummy index  $\beta$  to  $\gamma$ . Thus we obtain

$$\sum_{\gamma} \left( \langle \alpha | h | \gamma \rangle + \sum_a^N \sum_{\beta\delta} C_{a\beta}^* C_{a\delta} [\langle \alpha\beta | v | \gamma\delta \rangle - \langle \alpha\beta | v | \delta\gamma \rangle] \right) C_{k\gamma} = \vartheta_k C_{k\alpha}. \quad (5.12)$$

By defining the Hartree-Fock Hamiltonian as

$$h_{\alpha\gamma}^{HF} \equiv \langle \alpha | h | \gamma \rangle + \sum_a^N \sum_{\beta\delta} C_{a\beta}^* C_{a\delta} [\langle \alpha\beta | v | \gamma\delta \rangle - \langle \alpha\beta | v | \delta\gamma \rangle], \quad (5.13)$$

we finally obtain the Hartree-Fock equations,

$$\sum_{\gamma} h_{\alpha\gamma}^{HF} C_{k\gamma} = \vartheta_k C_{k\alpha}. \quad (5.14)$$

The Hartree-Fock equations are non-linear eigenvalue equations. They must be solved iteratively. Equation (5.14) determines the expansion coefficients in Eq. (5.2) that minimize the energy expectation value in Eq. (5.4).

# Chapter 6

## Coupled-Cluster Method

We will in this chapter give a presentation of the Coupled-Cluster (CC) method [56]. The first chapter is devoted to some introductory and historical aspects of the method and motivation for what we call the Coupled-Cluster wavefunction. In the following sections we present fundamental concepts and the formal theory. The focus will be on the formal Coupled-Cluster equations, and how programmable equations are obtained. We will derive the programmable equations in detail using both an analytical and diagrammatic method. Both methods will be thoroughly presented.

### 6.1 Introduction and Fundamental Ideas

The CC method was introduced in the context of nuclear physics by Coester and Kümmel around 1960. In the later 1960s, the method was introduced in quantum chemistry by Čížek [57, 58] and Paldus. The community was however slow to accept the theory. The reason for this was probably that the earliest researches used elegant but unfamiliar theoretical tools such as the formalism of second quantization and Feynman-like diagrams to derive equations. Almost ten years after the important contributions from Čížek and Paldus, in 1970s, Hurley presented a re-derivation of the Coupled-Cluster Doubles (CCD) equations [59] in a framework that was more familiar to quantum chemists. Thereafter, Monkhorst [60] developed a CC response theory for calculating properties of molecular systems. In the later 1970s, computer implementations for realistic systems began to appear, with important contributions from the groups of Pople and Bartlett. Then, in 1982, Purvis and Bartlett derived the Coupled-Cluster Singles and Doubles (CCSD) equations, and implemented them in a computer program [61]. After this work, CC methods became very popular in quantum chemistry. However, in the nuclear physics community, the method gained little attention before the 1990s. Tremendous efforts have been made to construct efficient CC codes, inclusion of higher excitations (for example CCSDT), and develop methods to treat excited states (Equation of Motion Coupled-Cluster).

The CC method is a numerical method used for quantum mechanical treatment of many-body systems. It is today probably the most powerful *ab initio* method to obtain the ground state energy of many-body systems. Other important many-body methods are Configuration Interaction (CI) [56], Many-Body Perturbation Theory (MBPT) [56], Variational Monte Carlo (VMC) [62], and Diffusion Monte Carlo (DMC) [62]. The fundamental idea of the method is that the exact many-body wavefunction can be written as a linear combination of Slater determinants. The set of determinants must therefore span the whole  $N$ -electron Hilbert space. Let us now prove this. Consider a complete and orthonormal set of one-electron functions  $\{\psi_\alpha(\mathbf{r})\}_{\alpha=1}^n$ , where  $\mathbf{r}$  includes spin. The orthonormality is expressed as

$$\int \psi_\alpha^*(\mathbf{r}) \psi_\beta(\mathbf{r}) d\mathbf{r} = \delta_{\alpha\beta}, \quad (6.1)$$

and the completeness relation as

$$\sum_{\alpha}^n \psi_{\alpha}^{*}(\mathbf{r}') \psi_{\alpha}(\mathbf{r}) = \delta(\mathbf{r} - \mathbf{r}'). \quad (6.2)$$

We now construct an  $N$ -electron Slater determinant  $\Phi_a$  from the set of single-electron functions,

$$\Phi_a(\mathbf{r}_1, \mathbf{r}_2, \dots, \mathbf{r}_N) = \frac{1}{\sqrt{N!}} \sum_p (-1)^p \widehat{P} \psi_{\alpha_1}(\mathbf{r}_1) \psi_{\alpha_2}(\mathbf{r}_2) \dots \psi_{\alpha_N}(\mathbf{r}_N). \quad (6.3)$$

The many-body quantum number  $a$  denotes the set of single-particle quantum numbers  $(\alpha_1, \alpha_2, \dots, \alpha_N)$ . Similarly, we construct another determinant

$$\Phi_b(\mathbf{r}_1, \mathbf{r}_2, \dots, \mathbf{r}_N) = \frac{1}{\sqrt{N!}} \sum_p (-1)^p \widehat{P} \psi_{\beta_1}(\mathbf{r}_1) \psi_{\beta_2}(\mathbf{r}_2) \dots \psi_{\beta_N}(\mathbf{r}_N), \quad (6.4)$$

where at least one function  $\psi_{\beta_j} \neq \psi_{\alpha_i}$ . The Slater determinants  $\Phi_a$  and  $\Phi_b$  are orthonormal since the set of single-electron functions are orthonormal. This is proved by

$$\begin{aligned} \int \Phi_a^{*}(\mathbf{R}) \Phi_a(\mathbf{R}) d\mathbf{R} &= \sqrt{N!} \int \Phi_a^{*}(\mathbf{R}) \psi_{\alpha_1}(\mathbf{r}_1) \dots \psi_{\alpha_N}(\mathbf{r}_N) d\mathbf{R} \\ &= \int \left[ \sum_p (-1)^p \widehat{P} \psi_{\alpha_1}^{*}(\mathbf{r}_1) \dots \psi_{\alpha_N}^{*}(\mathbf{r}_N) \right] \psi_{\alpha_1}(\mathbf{r}_1) \dots \psi_{\alpha_N}(\mathbf{r}_N) d\mathbf{R} \\ &= \int |\psi_{\alpha_1}(\mathbf{r}_1)|^2 d\mathbf{r}_1 \int |\psi_{\alpha_2}(\mathbf{r}_2)|^2 d\mathbf{r}_2 \dots \int |\psi_{\alpha_N}(\mathbf{r}_N)|^2 d\mathbf{r}_N, \\ &= 1, \end{aligned} \quad (6.5)$$

and

$$\begin{aligned} \int \Phi_a^{*}(\mathbf{R}) \Phi_b(\mathbf{R}) d\mathbf{R} &= \sqrt{N!} \int \Phi_a^{*}(\mathbf{R}) \psi_{\beta_1}(\mathbf{r}_1) \dots \psi_{\beta_N}(\mathbf{r}_N) d\mathbf{R} \\ &= \int \left[ \sum_p (-1)^p \widehat{P} \psi_{\alpha_1}^{*}(\mathbf{r}_1) \dots \psi_{\alpha_N}^{*}(\mathbf{r}_N) \right] \psi_{\beta_1}(\mathbf{r}_1) \dots \psi_{\beta_N}(\mathbf{r}_N) d\mathbf{R} \\ &= \int |\psi_{\alpha_1}(\mathbf{r}_1)|^2 d\mathbf{r}_1 \dots \int \psi_{\alpha_i}^{*}(\mathbf{r}_i) \psi_{\beta_i}(\mathbf{r}_i) d\mathbf{r}_i \dots \int |\psi_{\alpha_N}(\mathbf{r}_N)|^2 d\mathbf{r}_N \\ &= 0. \end{aligned} \quad (6.6)$$

The first equality in Eqs. (6.5) and (6.6) follows from the fact that given a symmetric operator  $\widehat{F}$ ,

$$\int \Phi_a^{*}(\mathbf{R}) \widehat{F} \Phi_b(\mathbf{R}) d\mathbf{R} = \sqrt{N!} \int \Phi_a^{*}(\mathbf{R}) \widehat{F} \psi_{\beta_1}(\mathbf{r}_1) \dots \psi_{\beta_N}(\mathbf{r}_N) d\mathbf{R}. \quad (6.7)$$

See [63] for a proof. We conclude that Slater determinants constructed from an orthonormal set of single-electron functions, form an orthonormal set as well. We will assume that the set of Slater determinants constructed from all possible combinations of single-electron functions is a complete set, i.e. it spans the whole antisymmetric  $N$ -electron Hilbert space, provided that the single-electron functions form a complete set as well. In the bra-ket notation, the completeness relation reads

$$\sum_a |\Phi_a\rangle \langle \Phi_a| = 1. \quad (6.8)$$

Any  $N$ -electron wavefunction  $|\Psi\rangle$  can thus be written as a linear combination of  $N$ -electron Slater determinants,

$$|\Psi\rangle = \sum_a C_a |\Phi_a\rangle, \quad (6.9)$$

where  $\{C_a\}$  are the expansion coefficients. This sum goes in most cases to infinity. The expansion coefficient  $C_b$  is determined by projecting  $|\Psi\rangle$  down on  $|\Phi_b\rangle$ ,

$$\langle \Phi_b | \Psi \rangle = \sum_a C_a \langle \Phi_b | \Phi_a \rangle = \sum_a C_a \delta_{ba} = C_b. \quad (6.10)$$

The set of single-electron basis functions can in principle be chosen arbitrary. However, for a given many-electron system, the most appropriate functions (as a first step) are the solutions of the single-electron system. By “most appropriate” we mean the basis functions that allow us to truncate Eq. (6.9) without losing important information about the system, i.e. without losing the important correlations that are present. Assume we have solved the single-electron system and obtained a complete set of orthonormal energy eigenfunctions. As pointed out in Chapter 3, Slater determinants constructed from such a basis set are energy eigenfunctions of the non-interacting many-body system. Thus in this basis, the exact wavefunction of the interacting system, see Eq. (6.9), is the infinite sum of excited states in the non-interacting system. We have in Figure 6.1 illustrated this. The horizontal lines represent the single-electron functions

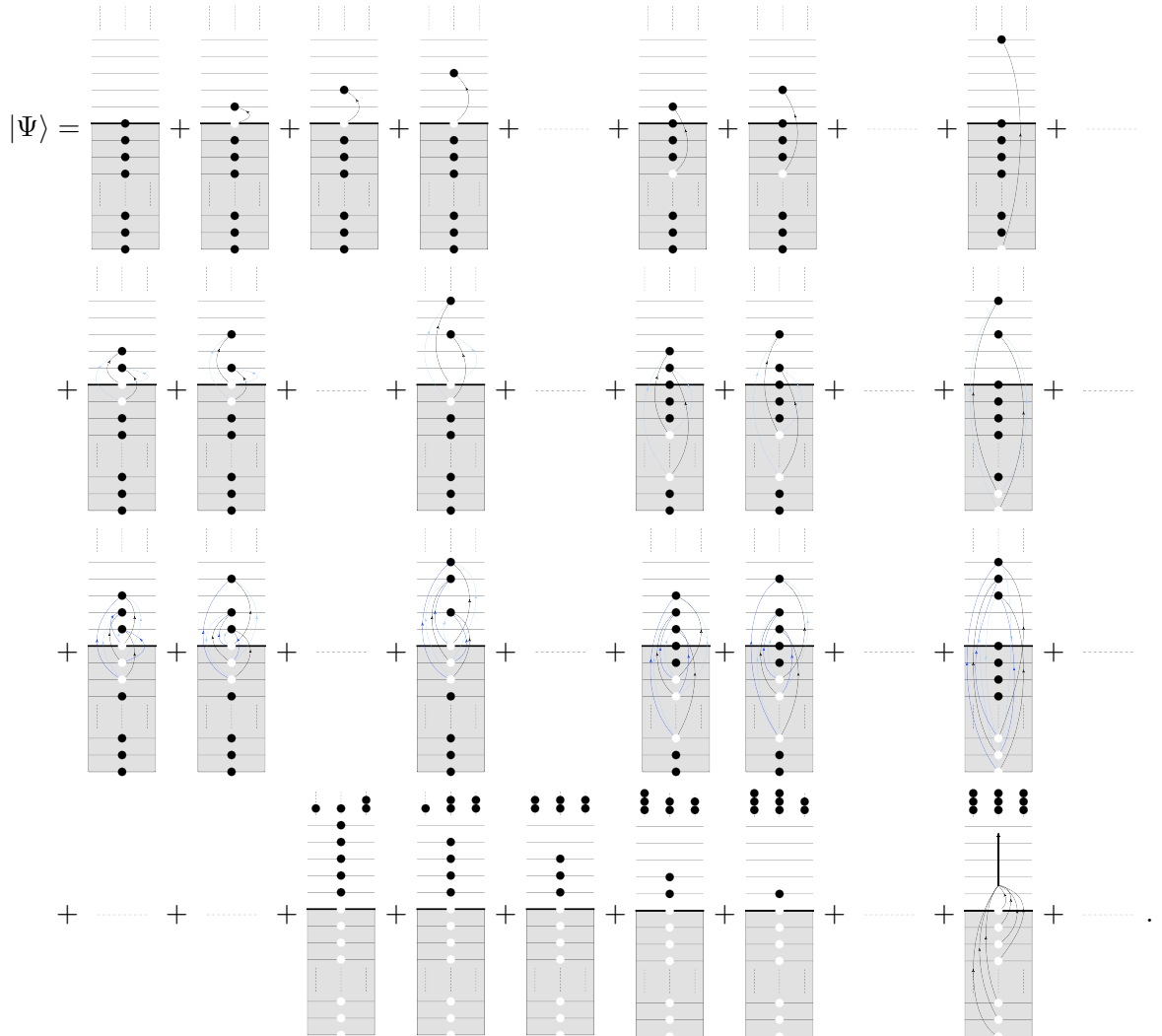


**Figure 6.1:** Illustration of the exact wavefunction  $|\Psi\rangle$  in Eq. (6.9), written as a linear combination of eigenfunctions of the non-interacting system. The expansion coefficients are suppressed in the drawing.

(spin included). Each orbital can therefore only be occupied by one electron at most. The non-interacting ground state is represented by the shadowed area with a bold horizontal line denoting the Fermi level of the system. The black circles represent electrons, and the white ones

represent holes. We define an  $n$ -particle  $n$ -hole excited state as an excited eigenfunction of the non-interacting system where  $n$  electrons are excited from below the Fermi level, to orbitals above the Fermi level, leaving  $n$  holes. We will in the following denote  $n$ -particle  $n$ -hole excitations by the shorthand notation  $npnh$ . The 1p1h excitations are unique in the sense that given a 1p1h excited determinant, we can only obtain this state in one way. In the the 2p2h case, each excited state can be reached in two ways, indicated by the excitation lines in the figure. In the general case, one can produce each  $npnh$  excited state in  $n!$  different ways. Physically, however, this is irrelevant. The physical information lies in which single-electron states that are occupied by an electron. Each diagram in Figure 6.1 therefore represents *one* Slater determinant, with its corresponding expansion coefficient suppressed.

Given the exact wavefunction  $|\Psi\rangle$  and a complete set of Slater determinants, the linear combination in Eq. (6.9) is uniquely determined. However, the exact many-body wavefunction is *not* known, simply because this is the main objective in our calculation. In addition, the many-body problem can in most cases not be solved exactly. At first sight, this does not look promising. The fact is, however, that Eq. (6.9) serves as a fundamental basis for several powerful and accurate *ab initio* methods such as CC and CI. The basic idea is that the exact wavefunction is approximated with a (necessarily) truncated expansion of Slater determinants, and that the coefficients are determined by solving Schrödinger's equation. When the  $N$ -electron basis is the set of eigenfunctions of the non-interacting system, the expansion coefficient  $C_b$  tells us "how much" of the correlations in the system that are represented by  $|\Phi_b\rangle$ . The "correct" formulation is:  $|C_b|^2$  is the probability to measure the non-interacting energy eigenvalue  $E_b$  corresponding to  $|\Phi_b\rangle$ . Given the exact wavefunction, the coefficients are determined by Eq. (6.10). However, since the exact wavefunction is unknown, physical considerations must be build into these coefficients right from the beginning. Different approximations schemes serve as the basis for different many-body methods. Before turning to this point, we present basic notation.

### 6.1.1 Notation

We will in the following use the particle-hole formalism presented in Sec. 3.5.4. The reference state is defined as

$$|r\rangle = |\Phi_0\rangle, \quad (6.11)$$

where  $|\Phi_0\rangle$  is the ground state of the non-interacting system,

$$|\Phi_0\rangle = a_{\alpha_1}^\dagger a_{\alpha_2}^\dagger \dots a_{\alpha_N}^\dagger |0\rangle. \quad (6.12)$$

We will denote hole states as  $ijk\dots$ , and particle states as  $abc\dots$ . Hole states are single-electron orbitals that are occupied in the reference state, while particle states are all states beyond the Fermi level. These subspaces are called the occupied space and the virtual space, respectively. States that are in either of the subspaces are denoted  $pqr\dots$ . We will not use the standard quasi-particle creation and annihilation operators  $b_\alpha^\dagger$  and  $b_\alpha$  explicitly, but in an implicit way by using vacuum creation and annihilation operators with quantum numbers  $ij..ab..pq\dots$ . This notation tells us in which subspace the operators act.

$$a_i^\dagger = b_\alpha \quad \alpha \leq \alpha_F \quad (6.13)$$

$$a_a^\dagger = b_\alpha^\dagger \quad \alpha > \alpha_F \quad (6.14)$$

$$a_i = b_\alpha \quad \alpha \leq \alpha_F \quad (6.15)$$

$$a_a = b_\alpha \quad \alpha > \alpha_F \quad (6.16)$$

We can now construct particle states, hole states and particle-hole (excited determinants) states, by acting with strings of creation and annihilation operators on the reference state:

$$\begin{aligned}
 a_a^\dagger a_b^\dagger a_c^\dagger \dots |\Phi_0\rangle &= \begin{array}{c} \text{Diagram showing three virtual orbitals (dotted lines) with particles (black dots) at positions } a, b, c. \\ \text{Below it: } \equiv |\Phi^{abc..}\rangle \end{array} \\
 a_i a_j a_k \dots |\Phi_0\rangle &= \begin{array}{c} \text{Diagram showing three occupied orbitals (solid lines) with particles (black dots) at positions } i, j, k. \\ \text{Below it: } \equiv |\Phi_{ijk..}\rangle \end{array} \\
 a_a^\dagger a_b^\dagger a_c^\dagger \dots a_k a_j a_i |\Phi_0\rangle &= \begin{array}{c} \text{Diagram showing a mix of virtual (dotted lines) and occupied (solid lines) orbitals with particles at various positions.} \\ \text{Below it: } \equiv |\Phi_{ijk..}^{abc}\rangle \end{array}
 \end{aligned}$$

Particle states will be denoted with virtual orbitals on the top right position of the ket, hole states with occupied orbitals in the lower right position, and particle-hole states with both virtual states and occupied states at their respective positions. The number of particles in a system that are represented by

$$|\Phi_{n_o}^{n_v}\rangle, \quad (6.17)$$

are given as

$$N = N' + n_v - n_o \quad (6.18)$$

where  $N'$  is the number of particles in the reference state. When  $n_v = n_o \neq 0$ , the state represents an excitation of the reference state.

## 6.2 Fundamental Concepts

We are seeking the solution of the Schrödinger equation

$$\hat{H}|\Psi\rangle = E|\Psi\rangle \quad (6.19)$$

for a system containing  $N$  interacting electrons. The Hamiltonian reads

$$\hat{H} = \hat{T} + \hat{U} + \hat{V}, \quad (6.20)$$

where

$$\hat{T} = \sum_{i=1}^N \hat{t}_i \quad (6.21)$$

$$\hat{U} = \sum_{i=1}^N \hat{u}_i \quad (6.22)$$

$$\hat{V} = \sum_{i=1}^N \hat{v}_{ij}, \quad (6.23)$$

where  $\hat{T}$  is the total kinetic energy,  $\hat{U}$  is the total potential energy,  $\hat{V}$  is the total interaction energy,  $\hat{t}_i$  is the kinetic energy of electron  $i$ ,  $\hat{u}_i$  is the potential energy of electron  $i$ , and finally,  $\hat{v}_{ij}$  is the interaction energy (Coulomb interaction) between electron  $i$  and  $j$ . We define

$$\hat{h}_i \equiv \hat{t}_i + \hat{u}_i, \quad (6.24)$$

leading to

$$\hat{H}_0 \equiv \sum_{i=1}^N \hat{h}_i = \hat{T} + \hat{U}, \quad (6.25)$$

which is the Hamiltonian of the non-interacting system. In second quantization (see See 3.5), the Hamiltonian reads

$$\hat{H} = \sum_{pq} \langle p|h|q \rangle a_p^\dagger a_q + \frac{1}{4} \sum_{pqrs} \langle pq|v|rs \rangle a_p^\dagger a_q^\dagger a_s a_r, \quad (6.26)$$

where the interaction elements  $\langle pq|v|rs \rangle$  are antisymmetrized.

The many-electron problem in Eq. (6.19) can in general not be solved exactly. However, as pointed out previously, given an arbitrary orthonormal and complete set of single-electron functions, the exact energy eigenfunctions of Eq. (6.19) can be written as linear combinations (see 6.9) of Slater determinants constructed from these. We now choose the single-electron basis to be the solutions of the single-electron Schrödinger equation

$$\hat{h}|\psi_\alpha\rangle = \epsilon_\alpha |\psi_\alpha\rangle, \quad (6.27)$$

with  $\hat{h}$  defined in Eq. (6.24). By using the set of Slater determinants

$$\mathcal{B}_N = \{|\Phi_a\rangle\}_{a=1}^\infty, \quad (6.28)$$

where

$$\langle \mathbf{r}_1 \mathbf{r}_2 .. \mathbf{r}_N | \Phi_a \rangle = \frac{1}{\sqrt{N!}} \sum_p (-1)^p \hat{P} \psi_{\alpha_1}(\mathbf{r}_1) \psi_{\alpha_2}(\mathbf{r}_2) .. \psi_{\alpha_N}(\mathbf{r}_N), \quad (6.29)$$

as basis functions ( $a$  running over all possible combinations of  $\alpha_1 \alpha_2 .. \alpha_N$ ), the exact wavefunction is a linear combination of the energy eigenstates of the non-interacting system. The exact wavefunction thus reads

$$|\Psi\rangle = C_0 |\Phi\rangle + \sum_{ia} C_i^a |\Phi_i^a\rangle + \sum_{ijab} C_{ij}^{ab} |\Phi_{ij..}^{ab}\rangle + ... + \sum_{ijk..abc..} C_{ijk..}^{abc..} |\Phi_{ijk..}^{abc..}\rangle, \quad (6.30)$$

where all the electrons are excited in the last term. The first sum gives the contributions from all 1p1h excitations, the second gives the contributions from all 2p2h excitations, and so forth up to  $NpNh$  excitations. Even though the sum naturally truncates after  $NpNh$  excitations, it is still an infinite sum since the subspace containing the virtual orbitals are infinite. If the summations over single-particle orbitals are not truncated, the exact wavefunction is given by Eq. (6.30). In practice this is not possible. However, Eq. (6.30) tells us an important thing: given the exact wavefunction, there exists a set of expansion coefficients  $\{C\}$  so that the linear combination in Eq. (6.30) is equal to the exact state. The wavefunction is *not* known, meaning that the expansion coefficients are the unknowns to be determined by the Schrödinger equation. Before this can be done, we must specify the contributions to each expansion coefficient  $C_{ij..}^{ab..}$ . For a given excited Slater determinant  $|\Phi_{ij..}^{ab..}\rangle$ , the corresponding expansion coefficients  $C_{ij..}^{ab..}$  gets contributions from *excitation amplitudes* with all possible couplings. As an example, consider the 3p3h-excited determinant  $|\Phi_{ijk}^{abc}\rangle$ . The corresponding coefficient  $C_{ijk}^{abc}$  gets contributions from excitation amplitudes with all possible couplings ,

$$C_{ijk}^{abc} = t_i^a t_j^b t_k^c + t_{ij}^{ab} t_k^c + t_i^a t_{jk}^{bc} + t_j^b t_{ik}^{ac} + t_{ijk}^{abc} \quad (6.31)$$

We thus obtain

$$C_{ijk}^{abc} |\Phi_{ijk}^{abc}\rangle = \left( t_i^a t_j^b t_k^c + t_{ij}^{ab} t_k^c + t_i^a t_{jk}^{bc} + t_j^b t_{ik}^{ac} + t_{ijk}^{abc} \right) |\Phi_{ijk}^{abc}\rangle \quad (6.32)$$

$$= \begin{array}{c} \text{Diagram 1} \\ \vdots \end{array} + \begin{array}{c} \text{Diagram 2} \\ \vdots \end{array} + \begin{array}{c} \text{Diagram 3} \\ \vdots \end{array} + \begin{array}{c} \text{Diagram 4} \\ \vdots \end{array} + \begin{array}{c} \text{Diagram 5} \\ \vdots \end{array} \quad (6.33)$$

where we have illustrated the coupling in the figures by wavy lines. Each figure in Eq. (6.33) represents the contribution from one specific coupling to the total expansion coefficient  $C_{ijk}^{abc}$ . The first figure in Eq. (6.33) represents the 3p3h determinants with three 1p1h excitations that do not couple any of the electrons. This is a crucial contribution when we consider a system consisting of two subsystems that do not interact with each other. In addition, a weakly interacting system gets important contributions from this term. The second, third and fourth term in Eq. (6.33) denote 3p3h determinants where electrons in two orbitals are coupled. The fifth term denotes the contribution from the 3p3h determinant where all three electrons are coupled. This example illustrates that for a certain determinant  $|\Phi_{ijk..}^{abc..}\rangle$ , one may divide its corresponding expansion coefficient into a sum of all possible couplings.

We now define the single-orbital excitation operator (cluster operator) as

$$\hat{t}_i \equiv \sum_a t_i^a a_a^\dagger a_i. \quad (6.34)$$

Acting with this operator on the reference state, yields

$$\hat{t}_i |\Phi\rangle = \sum_a t_i^a |\Phi_i^a\rangle. \quad (6.35)$$

Similarly, we define the two-orbital excitation operator as

$$\hat{t}_{ij}^{ab} \equiv \frac{1}{2} \sum_{ab} t_{ij}^{ab} a_a^\dagger a_b^\dagger a_j a_i. \quad (6.36)$$

Acting with this operator on the reference states, yields

$$\hat{t}_{ij}^{ab} |\Phi\rangle = \frac{1}{2} \sum_{ab} t_{ij}^{ab} |\Phi_{ij}^{ab}\rangle, \quad (6.37)$$

where the factor of 1/2 is due to two independent summations, viz.  $a = c_1$  and  $b = c_2$  yields the same excited state as  $a = c_2$  and  $b = c_1$ . In general, the  $n$ -orbital excitation operator is defined as

$$\hat{t}_{ijk..}^{abc..} \equiv \frac{1}{n!} \sum_{abc..} t_{ijk..}^{abc..} a_a^\dagger a_b^\dagger a_c^\dagger \dots a_k a_j a_i. \quad (6.38)$$

When we act with this operator on the reference state, we obtain

$$\hat{t}_{ijk..}^{abc..} |\Phi\rangle = \frac{1}{n!} \sum_{abc..} t_{ijk..}^{abc..} |\Phi_{ijk..}^{abc..}\rangle. \quad (6.39)$$

These definitions allow us to produce excited determinants with all possible couplings between electrons. For example,

$$\left( \frac{1}{2} \hat{t}_i \hat{t}_j + \hat{t}_{ij} \right) |\Phi_0\rangle = \frac{1}{2} \sum_{ab} \left( t_i^a t_j^b + t_{ij}^{ab} \right) |\Phi_{ij}^{ab}\rangle, \quad (6.40)$$

produces all 2p2h excited determinants with a hole in  $i$  and  $j$ . By summing over the hole states, we obtain *all* 2p2h states

$$\frac{1}{4} \sum_{ijab} \left( t_i^a t_j^b + t_{ij}^{ab} \right) |\Phi_{ij}^{ab}\rangle, \quad (6.41)$$

with all possible couplings. We now define *total* excitation amplitudes,

$$\hat{T}_1 \equiv \sum_i \hat{t}_i = \sum_{ia} t_i^a a_a^\dagger a_i \quad (6.42)$$

$$\hat{T}_2 \equiv \frac{1}{2} \sum_{ij} \hat{t}_{ij}^{ab} = \frac{1}{4} \sum_{ijab} t_{ij}^{ab} a_a^\dagger a_b^\dagger a_j a_i \quad (6.43)$$

$$\vdots \quad \vdots$$

$$\hat{T}_N \equiv \frac{1}{N!} \sum \hat{t}_{ijk..}^{abc..} a_a^\dagger a_b^\dagger a_c^\dagger \dots a_k a_j a_i = \left( \frac{1}{N!} \right)^2 \sum_{ijk..abc..} t_{ijk..}^{abc..} a_a^\dagger a_b^\dagger a_c^\dagger \dots a_k a_j a_i, \quad (6.44)$$

where  $N$  is the number of particles in the system. The total excitation amplitudes can be used to obtain all excitations with all possible couplings between the electrons. For example, all 3p3h determinants are obtained by using combinations of  $\hat{T}_1$ ,  $\hat{T}_2$  and  $\hat{T}_3$ , yielding

$$|3p3h\rangle = \left( \frac{1}{6} \hat{T}_1^3 + \hat{T}_1 \hat{T}_2 + \hat{T}_3 \right) |\Phi_0\rangle. \quad (6.45)$$

In the general case,  $n$ pnh determinants ( $1 \leq n \leq N$ ) are obtained by using combinations of  $\hat{T}_1$ ,  $\hat{T}_2$ , ...,  $\hat{T}_n$ . We thus obtain the following expression for the exact wavefunction in Eq. (6.30),

$$|\Psi\rangle = \left( 1 + \hat{T}_1 + \left[ \frac{1}{2!} \hat{T}_1^2 + \hat{T}_2 \right] + \left[ \frac{1}{3!} \hat{T}_1^3 + \hat{T}_1 \hat{T}_2 + \hat{T}_3 \right] + \left[ \frac{1}{4!} \hat{T}_1^4 + \frac{1}{2!} \hat{T}_1^2 \hat{T}_2 + \hat{T}_1 \hat{T}_3 + \frac{1}{2!} \hat{T}_2^2 + \hat{T}_4 \right] + \dots + [\dots + \hat{T}_N] \right) |\Phi_0\rangle. \quad (6.46)$$

Higher-order terms (like  $\hat{T}_{N+1}$ ) do not appear since  $N$  is the number of electrons in the system. Because all excitation operators commute, i.e.

$$[\hat{T}_i, \hat{T}_j] = 0, \quad (6.47)$$

all terms in Eq. (6.46) match those from the power series expansion of an exponential function. We define the *Coupled-Cluster wavefunction* as

$$|\Psi_{CC}\rangle \equiv e^{\hat{T}} |\Phi_0\rangle, \quad (6.48)$$

where the total excitation operator reads

$$\hat{T} \equiv \sum_{n=1}^{n_{\max}} \hat{T}_n, \quad (6.49)$$

and  $1 \leq n_{\max} \leq N$ . When the total excitation operator is not truncated, i.e.  $n_{\max} = N$ , and the single-particle basis is not truncated, the Coupled-Cluster wavefunction in Eq. (6.48) is *exact*, viz. the exact solution of the Schrödinger equation. However, in actual calculations we are often forced to truncate the single-particle basis. Moreover, when the system consists of many particles, the total excitation operator must be truncated, i.e.  $n_{\max} < N$ . These truncations constitute the sources of errors in CC calculations. Truncation at specific excitation levels leads to a hierarchy of CC schemes,

$$\hat{T} = \hat{T}_1 + \hat{T}_2 \rightarrow \text{CCSD} \quad (6.50)$$

$$\hat{T} = \hat{T}_1 + \hat{T}_2 + \hat{T}_3 \rightarrow \text{CCSDT} \quad (6.51)$$

$$\hat{T} = \hat{T}_1 + \hat{T}_2 + \hat{T}_3 + \hat{T}_4 \rightarrow \text{CCSDTQ} \quad (6.52)$$

$$\hat{T} = \hat{T}_1 + \hat{T}_2 + \hat{T}_3 + \hat{T}_4 + \dots + \hat{T}_N \rightarrow \text{CCSDTQ..N}$$

where S, D, T and Q denote single-, double-, triple- and quadruple-excitations, respectively. We emphasize that, provided that the single-particle basis is not truncated, a CCSD calculation yields an exact result for the 2-particle system, a CCSDT calculation yields an exact result for the 3-particle system, and so forth. In the next section, the formal CC theory is presented.

## 6.3 Formal Coupled-Cluster Theory

The CC wavefunction in Eq. (6.48) is the starting point for all CC calculations. We are seeking the ground state wavefunction and energy of a system. As pointed out in the previous section, when the total excitation operator and single-particle basis is truncated, the CC wavefunction is exact. However, in actual calculations, truncations are often necessary. The CC wavefunction is then hopefully, but not *a priori*, a good approximation to the exact solution. Inserting the CC wavefunction into the Schrödinger equation, yields

$$\hat{H}e^{\hat{T}}|\Phi_0\rangle = E_0 e^{\hat{T}}|\Phi_0\rangle, \quad (6.53)$$

where  $E_0$  is the ground state energy. The unknowns are the excitation amplitudes ( $t_i^a, t_{ij}^{ab}, \dots, t_{ijk..}^{abc..}$ ) and the energy  $E_0$ , which are determined by Eq. (6.53). The basic CC equations are the so-called energy equation and the amplitude equations. These equations constitute the basic CC machinery. The formal form of these equations are found by using a “projective” technique. The energy equation is found by multiplying the equation with the dual reference state from the left, yielding

$$\langle\Phi_0|\hat{H}e^{\hat{T}}|\Phi_0\rangle = E_0 \langle\Phi_0|e^{\hat{T}}|\Phi_0\rangle = E_0. \quad (6.54)$$

The last equality follows from the fact that  $\langle\Phi_0|\Psi\rangle_{\text{CC}} = 1$ , by construction. Expressions for the excitation amplitudes are obtained by left-multiplying the Schrödinger equation with excited determinants. For example, in order to obtain the  $\hat{T}_2$  equation,  $|\Phi_{ij}^{ab}\rangle$  must be used. The general amplitude equation reads

$$\langle\Phi_{ijk..}^{abc..}|\hat{H}e^{\hat{T}}|\Phi_0\rangle = E_0 \langle\Phi_{ijk..}^{abc..}|e^{\hat{T}}|\Phi_0\rangle = E_0 t_{ijk..}^{abc..}. \quad (6.55)$$

Due to the presence of  $e^{\hat{T}}$ , all amplitude equations are coupled, meaning that for example  $t_i^a$  depends on all other amplitudes. The CC equations must therefore be solved iteratively.

Eqs. (6.54) and (6.55) serve only as a way to get formal insight into the CC method. In practical computer implementation, however, they are not useful [20]. In order to obtain programmable equations, the first step is to multiply Eq. (6.53) with  $e^{-\hat{T}}$  from the left, and then use the “projective” technique. The modified equations are given as

$$\langle\Phi_0|e^{-\hat{T}}\hat{H}e^{\hat{T}}|\Phi_0\rangle = E_0 \quad (6.56)$$

$$\langle\Phi_{ijk..}^{abc..}|e^{-\hat{T}}\hat{H}e^{\hat{T}}|\Phi_0\rangle = 0. \quad (6.57)$$

These equations define the conventional CC method. Furthermore, they are equivalent to the formal equations in (6.54) and (6.55), but have two important advantages. First, the amplitude equations are decoupled from the energy equation. Secondly, the similarity transformed Hamiltonian,

$$e^{-\hat{T}}\hat{H}e^{\hat{T}}, \quad (6.58)$$

can be written as a sum of nested commutators by the so-called Campbell-Baker-Hausdorff (CBH) expansion [56]. This sum is in principle infinite, but as we will see, it truncates naturally in our case, yielding simplified CC equations.

## 6.4 Coupled-Cluster Singles and Doubles Equations

We will in this section derive programmable Coupled-Cluster Singles and Doubles (CCSD) equations using both an algebraic approach, and a diagrammatic approach. In the first two subsections, we present the notion of normal-ordered form of the Hamiltonian and the Campbell-Baker-Hausdorff expansion. Thereafter, we will derive the programmable energy equation

using the algebraic approach. Then we will give an introduction to CC diagrams, forming the diagrammatic approach. Both the energy and amplitude equations will be written on diagrammatic form, and then transformed to algebraic expressions using the so-called diagram rules.

In CCSD we define the total excitation operator as

$$\hat{T} \equiv \hat{T}_1 + \hat{T}_2, \quad (6.59)$$

where

$$\hat{T}_1 = \sum_{ia} t_i^a a_a^\dagger a_i \quad (6.60)$$

$$\hat{T}_2 = \frac{1}{4} \sum_{ijab} t_{ij}^{ab} a_a^\dagger a_b^\dagger a_j a_i. \quad (6.61)$$

#### 6.4.1 Normal-Ordered Form of the Hamiltonian

The Hamiltonian is given as

$$\hat{H} = \sum_{pq} \langle p|h|q \rangle + \frac{1}{4} \sum_{pqrs} \langle pq|v|rs \rangle a_p^\dagger a_q^\dagger a_s a_r. \quad (6.62)$$

According to Wick's theorem, the two operator strings in Eq. (6.62) can be written as

$$\begin{aligned} a_p^\dagger a_q &= \left\{ a_p^\dagger a_q \right\} + \left\{ a_p^\dagger \overline{a_q} \right\} \\ &= \left\{ a_p^\dagger a_q \right\} + \delta_{pq \in i} \\ a_p^\dagger a_q^\dagger a_s a_r &= \left\{ a_p^\dagger a_q^\dagger a_s a_r \right\} + \left\{ a_p^\dagger \overline{a_q^\dagger a_s a_r} \right\} + \left\{ a_p^\dagger a_q^\dagger \overline{a_s a_r} \right\} + \left\{ a_p^\dagger \overline{a_q^\dagger a_s a_r} \right\} \\ &\quad + \left\{ a_p^\dagger \overline{a_q^\dagger a_s a_r} \right\} + \left\{ a_p^\dagger \overline{a_q^\dagger a_s} \overline{a_r} \right\} + \left\{ a_p^\dagger \overline{a_q^\dagger a_s} \overline{a_r} \right\} \\ &= \left\{ a_p^\dagger a_q^\dagger a_s a_r \right\} - \left\{ a_q^\dagger a_r \right\} \delta_{ps \in i} + \left\{ a_q^\dagger a_s \right\} \delta_{pr \in i} \\ &\quad + \left\{ a_p^\dagger a_r \right\} \delta_{qs \in i} - \left\{ a_p^\dagger a_s \right\} \delta_{qr \in i} + \delta_{pr \in i} \delta_{qs \in j} - \delta_{ps \in i} \delta_{qr \in j}, \end{aligned}$$

where the contraction is defined relative to the non-interacting ground state  $|\Phi_0\rangle$ , and  $p \in i$  means that  $p$  must be contained in the set of occupied orbitals and must be equal to  $i$ . Substitute these expressions into Eq. (6.62), yields

$$\begin{aligned} \hat{H} &= \sum_{pq} \langle p|h|q \rangle \left\{ a_p^\dagger a_q \right\} + \sum_i \langle i|h|i \rangle \\ &\quad + \frac{1}{4} \sum_{pqrs} \langle pq|v|rs \rangle \left\{ a_p^\dagger a_q^\dagger a_s a_r \right\} - \frac{1}{4} \sum_{qri} \langle iq|v|ri \rangle \left\{ a_q^\dagger a_r \right\} + \frac{1}{4} \sum_{qsi} \langle iq|v|is \rangle \left\{ a_q^\dagger a_s \right\} \\ &\quad + \frac{1}{4} \sum_{pri} \langle pi|v|ri \rangle \left\{ a_p^\dagger a_r \right\} - \frac{1}{4} \sum_{psi} \langle pi|v|is \rangle \left\{ a_p^\dagger a_s \right\} + \frac{1}{4} \sum_{ij} \langle ij|v|ij \rangle - \frac{1}{4} \sum_{ij} \langle ij|v|ji \rangle. \end{aligned}$$

Furthermore, since the two-particle matrix element  $\langle pq|v|rs \rangle$  is antisymmetrized, it satisfies the following relation,

$$\langle pq|v|rs \rangle = -\langle pr|v|sr \rangle = -\langle rp|v|rs \rangle = \langle rp|v|sr \rangle. \quad (6.63)$$

Using this relation, the Hamiltonian can then be written as

$$\hat{H} = \sum_{pq} \langle p|h|q \rangle \left\{ a_p^\dagger a_q \right\} + \sum_{pqi} \langle pi|v|qi \rangle \left\{ a_p^\dagger a_q \right\} \quad (6.64)$$

$$+ \sum_{pqrs} \langle pq|v|rs \rangle \left\{ a_p^\dagger a_q^\dagger a_s a_r \right\} + \sum_i \langle i|h|i \rangle + \frac{1}{2} \sum_{ij} \langle ij|v|ij \rangle. \quad (6.65)$$

We now define

$$f_q^p \equiv \langle p|h|q \rangle + \sum_i \langle pi|v|qi \rangle \quad (6.66)$$

$$\hat{F}_N \equiv \sum_{pq} f_q^p \left\{ a_p^\dagger a_q \right\} \quad (6.67)$$

$$\hat{V}_N \equiv \sum_{pqrs} \langle pq|v|rs \rangle \left\{ a_p^\dagger a_q^\dagger a_s a_r \right\}. \quad (6.68)$$

By identifying

$$\langle \Phi_0 | \hat{H} | \Phi_0 \rangle = \sum_i \langle i|h|i \rangle + \frac{1}{2} \sum_{ij} \langle ij|v|ij \rangle, \quad (6.69)$$

the Hamiltonian reads

$$\hat{H} = \hat{F}_N + \hat{V}_N + \langle \Phi_0 | \hat{H} | \Phi_0 \rangle \quad (6.70)$$

$$= \hat{H}_N + \langle \Phi_0 | \hat{H} | \Phi_0 \rangle, \quad (6.71)$$

where the normal-ordered Hamiltonian is defined as

$$\hat{H}_N \equiv \hat{F}_N + \hat{V}_N. \quad (6.72)$$

The  $N$ -subscript must not be confused with the number of particles in the system. We observe that

$$\hat{H}_N = \hat{H} - \langle \Phi_0 | \hat{H} | \Phi_0 \rangle. \quad (6.73)$$

The normal-ordered form of the Hamiltonian is thus equal to the Hamiltonian itself minus its reference expectation value. It is therefore natural to consider  $\hat{H}_N$  as a correlation operator. Actually, the normal-ordered form of *any* operator is equal to the operator itself minus its reference expectation value.

At this point, the benefit of introducing the normal-ordered form of the Hamiltonian may be unclear. We will shortly see that it forms the basis needed to derive programmable equations with the algebraic method.

#### 6.4.2 The Campbell-Baker-Hausdorff Expansion

The conventional energy and amplitude equations in (6.56) and (6.57) contain the similarity transformed Hamiltonian

$$\underline{\hat{H}} \equiv e^{-\hat{T}} \hat{H} e^{\hat{T}}. \quad (6.74)$$

Inserting Eq. (6.71) into Eq. (6.74) yields

$$\underline{\hat{H}} = e^{-\hat{T}} \hat{H}_N e^{\hat{T}} + \langle \Phi_0 | \hat{H} | \Phi_0 \rangle. \quad (6.75)$$

We now insert this expression into the Eqs. (6.56) and (6.57), leading to

$$E_0 = \langle \Phi_0 | e^{-\hat{T}} \hat{H}_N e^{\hat{T}} | \Phi_0 \rangle + \langle \Phi_0 | \hat{H} | \Phi_0 \rangle \quad (6.76)$$

$$0 = \langle \Phi_i^a | e^{-\hat{T}} \hat{H}_N e^{\hat{T}} | \Phi_0 \rangle \quad (6.77)$$

$$0 = \langle \Phi_{ij}^{ab} | e^{-\hat{T}} \hat{H}_N e^{\hat{T}} | \Phi_0 \rangle. \quad (6.78)$$

Since the reference expectation value of the Hamiltonian is known, the CC problem is reduced to calculating matrix elements of the similarity transformed normal-ordered Hamiltonian. We now define the CC energy as

$$E_{CC} \equiv \langle \Phi_0 | e^{-\hat{T}} \hat{H}_N e^{\hat{T}} | \Phi_0 \rangle = E_0 - \langle \Phi_0 | \hat{H} | \Phi_0 \rangle. \quad (6.79)$$

The CCSD equations are usually written as

$$\langle \Phi_0 | e^{-\hat{T}} \hat{H}_N e^{\hat{T}} | \Phi_0 \rangle = E_{CC} \quad (6.80)$$

$$\langle \Phi_i^a | e^{-\hat{T}} \hat{H}_N e^{\hat{T}} | \Phi \rangle = 0 \quad (6.81)$$

$$\langle \Phi_{ij}^{ab} | e^{-\hat{T}} \hat{H}_N e^{\hat{T}} | \Phi \rangle = 0. \quad (6.82)$$

The next step is to find an expression for  $e^{-\hat{T}} \hat{H}_N e^{\hat{T}}$ . Using the well-known Campbell-Baker-Hausdorff formula [56], we obtain

$$e^{-\hat{T}} \hat{H}_N e^{\hat{T}} = \hat{H}_N + [\hat{H}_N, \hat{T}] + \frac{1}{2!} [[\hat{H}_N, \hat{T}], \hat{T}] + \frac{1}{3!} [[[[\hat{H}_N, \hat{T}], \hat{T}], \hat{T}] + \dots \quad (6.83)$$

The CC problem is therefore reduced to evaluating matrix elements of nested commutators. Fortunately, the sum truncates naturally.

### 6.4.3 Energy Equation - An Algebraic Approach

We will in this section derive the programmable form of the CCSD energy equation using the so-called algebraic approach. This equation is actually valid for all CC schemes (CCSD, CCSDT, CCSDTQ, and so forth), provided that the Hamiltonian is a two-body operator. In the CCSD scheme (see Eq. 6.59), the Hausdorff expansion in Eq. (6.83) reads

$$\begin{aligned} e^{-\hat{T}} \hat{H}_N e^{\hat{T}} &= \hat{H}_N + [\hat{H}_N, \hat{T}_1] + [\hat{H}_N, \hat{T}_2] + \frac{1}{2!} [[\hat{H}_N, \hat{T}_1], \hat{T}_1] + [\hat{H}_N, \hat{T}_2] + \frac{1}{2!} [[[\hat{H}_N, \hat{T}_2], \hat{T}_1], \hat{T}_1] \\ &\quad + \frac{1}{2!} [[[\hat{H}_N, \hat{T}_2], \hat{T}_1], \hat{T}_1] + \frac{1}{2!} [[[\hat{H}_N, \hat{T}_2], \hat{T}_2], \hat{T}_2] + \frac{1}{3!} [[[[\hat{H}_N, \hat{T}_1], \hat{T}_1], \hat{T}_1], \hat{T}_1] + \dots \end{aligned} \quad (6.84)$$

We will in the following determine the contribution to the CC energy from each of the terms above. The contribution from  $\langle \Phi_0 | \hat{X} | \Phi_0 \rangle$  will be denoted as

$$E_{CC} \leftarrow \langle \Phi_0 | \hat{X} | \Phi_0 \rangle, \quad (6.85)$$

where  $E_{CC}$  is the CC energy. We emphasize that the excitation operators are already on normal-ordered form, viz.

$$\langle \Phi_0 | \hat{T}_k | \Phi_0 \rangle = 0. \quad (6.86)$$

#### Term 1

The first contribution is

$$E_{CC} \leftarrow \langle \Phi_0 | \hat{H}_N | \Phi_0 \rangle = 0. \quad (6.87)$$

## Term 2

The second contribution reads

$$E_{CC} \leftarrow \langle \Phi_0 | [\hat{H}_N, \hat{T}_1] | \Phi_0 \rangle = \langle \Phi_0 | [\hat{F}_N, \hat{T}_1] | \Phi_0 \rangle + \langle \Phi_0 | [\hat{V}_N, \hat{T}_1] | \Phi_0 \rangle. \quad (6.88)$$

Using Eqs. (6.67) and (6.60), we obtain the following expressions for  $\hat{F}_N \hat{T}_1$  and  $\hat{T}_1 \hat{F}_N$ ,

$$\hat{F}_1 \hat{T}_1 = \sum_{pqia} f_q^p t_i^a \left\{ a_p^\dagger a_q \right\} \left\{ a_a^\dagger a_i \right\}, \quad (6.89)$$

$$\hat{T}_1 \hat{F}_1 = \sum_{pqia} f_a^p t_i^a \left\{ a_a^\dagger a_i \right\} \left\{ a_p^\dagger a_q \right\}. \quad (6.90)$$

The generalized Wick's theorem allow us to rewrite the product of normal-ordered strings of operators into

$$\begin{aligned} \left\{ a_p^\dagger a_q \right\} \left\{ a_a^\dagger a_i \right\} &= \left\{ a_p^\dagger a_q a_a^\dagger a_i \right\} + \left\{ a_p^\dagger a_q \overline{a_a^\dagger a_i} \right\} + \left\{ a_p^\dagger a_q a_a^\dagger a_i \right\} + \left\{ a_p^\dagger a_q \overline{a_a^\dagger a_i} \right\}, \\ &= \left\{ a_p^\dagger a_q a_a^\dagger a_i \right\} + \left\{ a_q a_a^\dagger \right\} \delta_{pi} + \left\{ a_p^\dagger a_i \right\} \delta_{qa} + \delta_{pi} \delta_{qa} \\ \left\{ a_a^\dagger a_i \right\} \left\{ a_p^\dagger a_q \right\} &= \left\{ a_a^\dagger a_i a_p^\dagger a_q \right\}. \end{aligned}$$

Inserting these expressions into Eqs. (6.89) and (6.90), yields

$$[\hat{F}_N, T_1] = \sum_{qia} f_q^i t_i^a \left\{ a_q a_a^\dagger \right\} + \sum_{pia} f_p^i t_i^a \left\{ a_p^\dagger a_i \right\} + \sum_{ia} f_a^i t_i^a. \quad (6.91)$$

Remembering that the reference expectation value of a normal-ordered string of creation and annihilation operators is zero, i.e.

$$\langle \Phi_0 | \{ \dots \} | \Phi_0 \rangle = 0, \quad (6.92)$$

yields the first non-zero contribution to the CC energy,

$$E_{CC} \leftarrow \langle \Phi_0 | [\hat{F}_N, \hat{T}_1] | \Phi_0 \rangle = \sum_{ia} f_a^i t_i^a. \quad (6.93)$$

Furthermore, using Eqs. (6.68) and (6.60), we obtain the following expression for  $\hat{V}_N \hat{T}_1$  and  $\hat{T}_1 \hat{V}_N$ ,

$$\hat{V}_N \hat{T}_1 = \frac{1}{4} \sum_{pqrsia} \langle pq | v | rs \rangle t_i^a \left\{ a_p^\dagger a_q^\dagger a_s a_r \right\} \left\{ a_a^\dagger a_i \right\}, \quad (6.94)$$

$$\hat{T}_1 \hat{V}_N = \frac{1}{4} \sum_{pqrsia} \langle pq | v | rs \rangle t_i^a \left\{ a_a^\dagger a_i \right\} \left\{ a_p^\dagger a_q^\dagger a_s a_r \right\}. \quad (6.95)$$

We observe that we cannot obtain fully contracted terms, and thus the second term does not contribute to the energy, i.e.

$$E_{CC} \leftarrow \langle \Phi_0 | [\hat{V}_N, \hat{T}_1] | \Phi_0 \rangle = 0. \quad (6.96)$$

## Term 3

We will now determine the contribution from

$$E_{CC} \leftarrow \langle \Phi_0 | [\hat{H}_N, \hat{T}_2] | \Phi_0 \rangle = \langle \Phi_0 | [\hat{F}_N, \hat{T}_2] | \Phi_0 \rangle + \langle \Phi_0 | [\hat{V}_N, \hat{T}_2] | \Phi_0 \rangle. \quad (6.97)$$

Eqs. (6.67) and (6.61) yield the following expressions for  $\hat{F}_N \hat{T}_2$  and  $\hat{T}_2 \hat{F}_N$ ,

$$\hat{F}_N \hat{T}_2 = \frac{1}{4} \sum_{pqijab} f_q^p t_{ij}^{ab} \left\{ a_p^\dagger a_q \right\} \left\{ a_a^\dagger a_b^\dagger a_j a_i \right\}, \quad (6.98)$$

$$\hat{T}_2 \hat{F}_N = \frac{1}{4} \sum_{pqijab} f_q^p t_{ij}^{ab} \left\{ a_a^\dagger a_b^\dagger a_j a_i \right\} \left\{ a_p^\dagger a_q \right\}. \quad (6.99)$$

Using Wick's generalized theorem we observe that that  $[\hat{F}_N, \hat{T}_2]$  does not include any fully contracted terms. Therefore,

$$E_{CC} \leftarrow \langle \Phi_0 | [\hat{F}_N, \hat{T}_2] | \Phi_0 \rangle = 0.$$

Furthermore, Eqs. (6.68) and (6.61) give the following expressions for  $\hat{V}_N \hat{T}_2$  and  $\hat{T}_2 \hat{V}_N$ ,

$$\hat{V}_N \hat{T}_2 = \frac{1}{16} \sum_{pqrsijab} t_{ij}^{ab} \langle pq | v | rs \rangle \left\{ a_p^\dagger a_q^\dagger a_s a_r \right\} \left\{ a_a^\dagger a_b^\dagger a_j a_i \right\}, \quad (6.100)$$

$$\hat{T}_2 \hat{V}_N = \frac{1}{16} \sum_{pqrsijab} t_{ij}^{ab} \langle pq | v | rs \rangle \left\{ a_a^\dagger a_b^\dagger a_i a_j \right\} \left\{ a_p^\dagger a_q^\dagger a_s a_r \right\}. \quad (6.101)$$

Using Wick's generalized theorem, we rewrite the products of normal-ordered strings into

$$\begin{aligned} \left\{ a_p^\dagger a_q^\dagger a_s a_r \right\} \left\{ a_a^\dagger a_b^\dagger a_j a_i \right\} &= \left\{ a_p^\dagger a_q^\dagger a_s a_r a_a^\dagger a_b^\dagger a_j a_i \right\} + \left\{ a_p^\dagger a_q^\dagger a_s a_r a_a^\dagger a_b^\dagger a_j a_i \right\} \\ &\quad + \left\{ a_p^\dagger a_q^\dagger a_s a_r a_a^\dagger a_b^\dagger a_j a_i \right\} + \left\{ a_p^\dagger a_q^\dagger a_s a_r a_a^\dagger a_b^\dagger a_j a_i \right\} \\ &\quad + \left\{ a_p^\dagger a_q^\dagger a_s a_r a_a^\dagger a_b^\dagger a_j a_i \right\} + \dots \\ &= \delta_{pi} \delta_{qj} \delta_{sb} \delta_{ra} - \delta_{pi} \delta_{qj} \delta_{sa} \delta_{rb} - \delta_{pj} \delta_{qi} \delta_{sb} \delta_{ra} + \delta_{pj} \delta_{qi} \delta_{sa} \delta_{rb} \\ &\quad + \left\{ a_p^\dagger a_q^\dagger a_s a_r a_a^\dagger a_b^\dagger a_j a_i \right\} + \dots, \\ \left\{ a_a^\dagger a_b^\dagger a_j a_i \right\} \left\{ a_p^\dagger a_q^\dagger a_s a_r \right\} &= \left\{ a_a^\dagger a_b^\dagger a_j a_i a_p^\dagger a_q^\dagger a_s a_r \right\}, \end{aligned}$$

where we include only fully contracted terms, and the two non-contracted terms. Inserting these expressions into Eqs. (6.101) and (6.100), yields

$$\begin{aligned} [\hat{V}_N, \hat{T}_2] &= \frac{1}{16} \sum_{ijab} [\langle ij | v | ab \rangle - \langle ij | v | ba \rangle - \langle ji | v | ab \rangle + \langle ji | v | ba \rangle] t_{ij}^{ab} + \dots \\ &= \frac{1}{4} \sum_{ijab} \langle ij | v | ab \rangle t_{ij}^{ab} + \dots \end{aligned} \quad (6.102)$$

We note that since

$$\left\{ a_p^\dagger a_q^\dagger a_s a_r a_a^\dagger a_b^\dagger a_j a_i \right\} = \left\{ a_a^\dagger a_b^\dagger a_j a_i a_p^\dagger a_q^\dagger a_s a_r \right\}, \quad (6.103)$$

the two non-contracted terms cancel each other in the commutator. Since only fully contracted terms give contribution to the CC energy, we finally obtain

$$E_{CC} \leftarrow \frac{1}{4} \sum_{ijab} \langle ij | v | ab \rangle t_{ij}^{ab}. \quad (6.104)$$

## Term 4

The fourth contribution to the CC energy reads

$$E_{\text{CC}} \leftarrow \frac{1}{2} \langle \Phi_0 | [[\hat{H}_N, \hat{T}_1], \hat{T}_1] | \Phi_0 \rangle = \frac{1}{2} \langle \Phi_0 | [[\hat{F}_N, \hat{T}_1], \hat{T}_1] | \Phi_0 \rangle + \frac{1}{2} \langle \Phi_0 | [[\hat{V}_N, \hat{T}_1], \hat{T}_1] | \Phi_0 \rangle.$$

Consider the first term in the above expression. Using Eqs. (6.60) and (6.91), we obtain the following expressions,

$$[\hat{F}_N, \hat{T}_1] \hat{T}_1 = \sum_{qijab} f_q^i t_i^a t_j^b \left\{ a_q a_a^\dagger \right\} \left\{ a_b^\dagger a_j \right\} + \sum_{pijab} f_p^p t_i^a t_j^b \left\{ a_p^\dagger a_i \right\} \left\{ a_b^\dagger a_j \right\} + \sum_{ijab} f_a^i t_i^a t_j^b \left\{ a_b^\dagger a_j \right\}, \quad (6.105)$$

$$\hat{T}_1 [\hat{F}_N, \hat{T}_1] = \sum_{qijab} f_q^i t_i^a t_j^b \left\{ a_b^\dagger a_j \right\} \left\{ a_q a_a^\dagger \right\} + \sum_{pijab} f_p^p t_i^a t_j^b \left\{ a_b^\dagger a_j \right\} \left\{ a_p^\dagger a_i \right\} + \sum_{ijab} f_a^i t_i^a t_j^b \left\{ a_b^\dagger a_j \right\}. \quad (6.106)$$

As always, the only terms that give non-zero contribution to the CC energy are those in which all creation and annihilation operators are fully contracted. First we note that the constant terms on the right hand side of Eqs. (6.105) and (6.106) cancel each other in the full commutator expression. Moreover, all non-zero contractions are between a creation (annihilation) operator with quantum number  $a$  ( $i$ ) and an annihilation (creation) operator with quantum number  $p$ , or the other way around. Thus we cannot obtain non-zero fully contracted terms in Eqs. (6.105) and (6.106). Therefore,

$$E_{\text{CC}} \leftarrow \frac{1}{2} \langle \Phi_0 | [[\hat{F}_N, \hat{T}_1], \hat{T}_1] | \Phi_0 \rangle = 0.$$

Furthermore, by using Eqs. (6.60), (6.94) and (6.95), we obtain the following terms in  $[[\hat{V}_N, \hat{T}_1], \hat{T}_1]/2$ ,

$$\begin{aligned} [\hat{V}_N, \hat{T}_1] \hat{T}_1 &= \frac{1}{4} \sum_{pqrsijab} \langle pq|v|rs \rangle t_i^a t_j^b \left\{ a_p^\dagger a_q^\dagger a_s a_r \right\} \left\{ a_a^\dagger a_i \right\} \left\{ a_b^\dagger a_j \right\} \\ &\quad + \frac{1}{4} \sum_{pqrsijab} \langle pq|v|rs \rangle t_i^a t_j^b \left\{ a_a^\dagger a_i \right\} \left\{ a_p^\dagger a_q^\dagger a_s a_r \right\} \left\{ a_b^\dagger a_j \right\}, \\ \hat{T}_1 [\hat{V}_N, \hat{T}_1] &= \frac{1}{4} \sum_{pqrsijab} \langle pq|v|rs \rangle t_i^a t_j^b \left\{ a_b^\dagger a_j \right\} \left\{ a_p^\dagger a_q^\dagger a_s a_r \right\} \left\{ a_a^\dagger a_i \right\} \\ &\quad + \frac{1}{4} \sum_{pqrsijab} \langle pq|v|rs \rangle t_i^a t_j^b \left\{ a_b^\dagger a_j \right\} \left\{ a_a^\dagger a_i \right\} \left\{ a_p^\dagger a_q^\dagger a_s a_r \right\}. \end{aligned}$$

We utilize Wick's generalized theorem in order to obtain

$$\begin{aligned} \frac{1}{2} \langle \Phi_0 | [[\hat{V}_N, \hat{T}_1], \hat{T}_1] | \Phi_0 \rangle &= \frac{1}{8} \sum_{pqrsijab} \langle pq|v|rs \rangle t_i^a t_j^b \\ &\quad \times (\delta_{pi}\delta_{qj}\delta_{sa}\delta_{rb} - \delta_{pi}\delta_{qj}\delta_{sb}\delta_{ra} - \delta_{pj}\delta_{qi}\delta_{sa}\delta_{rb} + \delta_{pj}\delta_{qi}\delta_{sb}\delta_{ra}) + \dots \\ &= \frac{1}{8} \sum_{ijab} (\langle ij|v|ba \rangle - \langle ij|v|ab \rangle - \langle ji|v|ba \rangle + \langle ji|v|ab \rangle) t_i^a t_j^b + \dots \\ &= \frac{1}{2} \sum_{ijab} \langle ij|v|ab \rangle t_i^a t_j^b + \dots, \end{aligned}$$

where only fully contracted terms are included. We finally obtain

$$E_{\text{CC}} \leftarrow \frac{1}{2} \langle \Phi_0 | [[\hat{V}_N, \hat{T}_1], \hat{T}_1] | \Phi_0 \rangle = \frac{1}{2} \sum_{ijab} \langle ij|v|ab \rangle t_i^a t_j^b. \quad (6.107)$$

We have now evaluated the first four contributions to the CC energy in Eq. (6.84). The Hausdorff expansion is in principle infinite. Fortunately, it truncates naturally. First, the examples above allow us to make an important generalization when Wick's generalized theorem is applied to the commutators: the only nonzero terms in the Hausdorff expansion are those in which the Hamiltonian has at least one contraction with every excitation operator  $\hat{T}_i$  on its right side. Thus the Hausdorff expansion reads

$$e^{-\hat{T}} \hat{H}_N e^{\hat{T}} = \left( \hat{H}_N + \hat{H}_N \hat{T} + \frac{1}{2!} \hat{H}_N \hat{T}^2 + \frac{1}{3!} \hat{H}_N \hat{T}^3 + \frac{1}{4!} \hat{H}_N \hat{T}^4 + \dots \right)_c, \quad (6.108)$$

where  $\hat{T} = \hat{T}_1 + \hat{T}_2$ , and the  $c$ -subscript denotes that the Hamiltonian must have *at least* one contraction with every excitation operator. Furthermore, since we are dealing with an electronic system, the Hamiltonian is a two-body operator. The Hausdorff expansion thus simplifies to

$$e^{-\hat{T}} \hat{H}_N e^{\hat{T}} = \left( \hat{H}_N + \hat{H}_N \hat{T} + \frac{1}{2} \hat{H}_N \hat{T}^2 + \frac{1}{6} \hat{H}_N \hat{T}^3 + \frac{1}{24} \hat{H}_N \hat{T}^4 \right)_c, \quad (6.109)$$

i.e. it naturally truncates. The expansion truncates when a specific Hamiltonian is determined. For example, if the Hamiltonian is a three-body operator, the sum truncates after  $\hat{H}_N \hat{T}^6/6!$  for CCSD.

Eq. (6.109) yields the following expression for the CC energy,

$$E_{\text{CC}} = \langle \Phi_0 | (\hat{H}_N + \hat{H}_N \hat{T} + \frac{1}{2} \hat{H}_N \hat{T}^2 + \frac{1}{6} \hat{H}_N \hat{T}^3 + \frac{1}{24} \hat{H}_N \hat{T}^4)_c | \Phi_0 \rangle. \quad (6.110)$$

As pointed out before, only fully contracted terms give nonzero contribution. By inserting Eq. (6.59), we obtain

$$E_{\text{CC}} = \langle \Phi_0 | (\hat{H}_N \hat{T}_1 + \hat{H}_N \hat{T}_2 + \frac{1}{2} \hat{H}_N \hat{T}_1^2)_{\text{fc}} | \Phi_0 \rangle, \quad (6.111)$$

where the fc-subscript denotes that only the fully contracted terms are included. This expression is not limited to the CCSD scheme. It is valid for *all* CC schemes (CCSD, CCSDT, CCSDTQ, and so forth), provided that the Hamiltonian is a two-body operator. It is interesting that the energy only depends explicitly on the  $t_i^a$  and  $t_{ij}^{ab}$  amplitudes. However, in for example CCSDT, all amplitudes are coupled together yielding an implicit dependence of  $t_{ijk}^{abc}$ .

Using Eq. (6.72), we obtain the following expression for the CC energy

$$\begin{aligned} E_{\text{CC}} &= \langle \Phi_0 | (\hat{F}_N \hat{T}_1 + \hat{V}_N \hat{T}_2 + \frac{1}{2} \hat{V}_N \hat{T}_1^2)_{\text{fc}} | \Phi_0 \rangle \\ &= \langle \Phi_0 | (\hat{F}_N \hat{T}_1)_{\text{fc}} | \Phi_0 \rangle + \langle \Phi_0 | (\hat{V}_N \hat{T}_2)_{\text{fc}} | \Phi_0 \rangle + \frac{1}{2} \langle \Phi_0 | (\hat{V}_N \hat{T}_1^2)_{\text{fc}} | \Phi_0 \rangle. \end{aligned}$$

where  $\hat{V}_N \hat{T}_1$  and  $\hat{F}_N \hat{T}_1^2$  are removed since fully contractions are impossible. We obtain the following three contributions:

$$\langle \Phi_0 | (\hat{F}_N \hat{T}_1)_{\text{fc}} | \Phi_0 \rangle = \sum_{pqia} f_q^p t_i^a \left\{ \overbrace{a_p^\dagger a_q a_a^\dagger a_i}^{\square} \right\} = \sum_{pqia} f_q^p t_i^a \delta_{pi} \delta_{qa} = \sum_{ia} f_a^i t_i^a, \quad (6.112)$$

$$\begin{aligned} \frac{1}{2} \langle \Phi_0 | (\hat{V}_N \hat{T}_1^2)_{\text{fc}} | \Phi_0 \rangle &= \frac{1}{8} \sum_{pqrsijab} \langle pq|v|rs\rangle t_i^a t_j^b (\delta_{pi}\delta_{qj}\delta_{sa}\delta_{rb} - \delta_{pi}\delta_{qj}\delta_{sb}\delta_{ra} - \delta_{pj}\delta_{qi}\delta_{sa}\delta_{rb} + \delta_{pj}\delta_{qi}\delta_{sb}\delta_{ra}) \\ &= \frac{1}{2} \sum_{ijab} \langle ij|v|ab\rangle t_i^a t_j^b, \end{aligned} \quad (6.113)$$

$$\begin{aligned}
 \langle \Phi_0 | (\widehat{V}_N \widehat{T}_2)_{\text{fc}} | \Phi_0 \rangle &= \frac{1}{16} \sum_{pqrsijab} \langle pq|v|rs \rangle t_{ij}^{ab} \left\{ \overbrace{\overbrace{a_p^\dagger a_q^\dagger a_s a_r a_a^\dagger a_b^\dagger a_j a_i}^{\text{outer}}}^{\text{inner}} \right\} \\
 &\quad + \frac{1}{16} \sum_{pqrsijab} \langle pq|v|rs \rangle t_{ij}^{ab} \left\{ \overbrace{\overbrace{a_p^\dagger a_q^\dagger a_s a_r a_a^\dagger a_b^\dagger a_j a_i}^{\text{inner}}}^{\text{outer}} \right\} \\
 &\quad + \frac{1}{16} \sum_{pqrsijab} \langle pq|v|rs \rangle t_{ij}^{ab} \left\{ \overbrace{\overbrace{a_p^\dagger a_q^\dagger a_s a_r a_a^\dagger a_b^\dagger a_j a_i}^{\text{outer}}}^{\text{inner}} \right\} \\
 &\quad + \frac{1}{16} \sum_{pqrsijab} \langle pq|v|rs \rangle t_{ij}^{ab} \left\{ \overbrace{\overbrace{a_p^\dagger a_q^\dagger a_s a_r a_a^\dagger a_b^\dagger a_j a_i}^{\text{inner}}}^{\text{outer}} \right\} \\
 &= \frac{1}{16} \sum_{pqrsijab} \langle pq|v|rs \rangle t_{ij}^{ab} (\delta_{pi}\delta_{qj}\delta_{sb}\delta_{ra} - \delta_{pi}\delta_{qj}\delta_{sa}\delta_{rb} - \delta_{pj}\delta_{qi}\delta_{sb}\delta_{ra} + \delta_{pj}\delta_{qi}\delta_{sa}\delta_{rb}) \\
 &= \frac{1}{4} \sum_{ijab} \langle ij|v|ab \rangle t_{ij}^{ab}. \tag{6.114}
 \end{aligned}$$

These expressions are equal to Eqs. (6.93), (6.104) and (6.107), respectively. We finally arrive at the following expression for the CC energy,

$$E_{\text{CC}} = \sum_{ia} f_a^i t_i^a + \frac{1}{4} \sum_{ijab} \langle ij|v|ab \rangle t_{ij}^{ab} + \frac{1}{2} \sum_{ijab} \langle ij|v|ab \rangle t_i^a t_j^b. \tag{6.115}$$

We have now presented the algebraic approach through solving

$$E_{\text{CC}} = \langle \Phi_0 | e^{-\widehat{T}} \widehat{H}_N e^{\widehat{T}} | \Phi_0 \rangle.$$

Programmable amplitude equations can be determined in the same way by using Wick's generalized theorem and evaluate the resulting matrix elements. An important difference to the energy equation is that

$$\langle \Phi_{ijk..}^{abc..} | \widehat{X} | \Phi_0 \rangle,$$

where we have an excited determinant on the left. This means that the nonzero contributions to the amplitudes are *not* the fully contracted ones, but instead those terms with an excitation level that is equal to the excited determinant. The algebraic procedure is simple and straightforward. However, it is tedious and time-consuming even for the  $\widehat{T}_1$  amplitude equation. The so-called diagrammatic method offers a far more convenient and practical approach to construct the programmable CC equations. We will in the next section introduce a diagrammatic approach which is particularly convenient for these equations.

#### 6.4.4 Coupled-Cluster Diagrams

Throughout the history of many-body theory, many varieties of diagrams have been used. Depending on the mathematical context, diagrams represent wavefunctions, operators or matrix elements. Diagrams are most frequently used to represent matrix elements. For example,

$$\begin{aligned}
 \langle \alpha_1 \alpha_2 | \widehat{O} | \alpha_1 \alpha_2 \rangle &= \frac{1}{4} \sum_{pqrs} \langle pq|o|rs \rangle \langle 0| a_{\alpha_1} a_{\alpha_2} a_p^\dagger a_q^\dagger a_s a_r a_{\alpha_1}^\dagger a_{\alpha_2}^\dagger | 0 \rangle \\
 &= \text{Diagram 1} + \text{Diagram 2} + \text{Diagram 3} + \text{Diagram 4}, \tag{6.116}
 \end{aligned}$$

where  $\hat{O}$  is a two-body operator. The standard problem is that we want to evaluate a certain matrix element, and we are seeking an algebraic expression in terms of (in our example) the matrix elements  $\langle pq|v|rs\rangle$ . This can obviously be done by using Wick's theorem. However, this is often a quite tedious and time-consuming procedure. Alternatively, the matrix element can be transformed into a diagrammatic expression (as we have done above), and then use so-called diagram rules in order to obtain an algebraic expression. Many varieties of diagrammatic techniques have been developed in order to give a convenient and practical approach for obtaining algebraic expressions of matrix elements. It is important to note that diagrammatic techniques are constructed and tuned to give the same results as the more “fundamental” algebraic approach using Wick’s theorem.

We will in this section present the diagrammatic technique popularized by Kucharski and Bartlett [64]. This formalism allows us to construct programmable CC equations in a practical and straightforward way. We first present the diagrammatic representation of Slater determinants (particle-hole formalism) and normal-ordered operators. Then we focus on how diagrams of operators may be connected (analogous to contractions) forming operator products. This leads to a simple procedure that determines which terms contribute to the energy and amplitude equations.

### Diagrams Representing Slater Determinants

Arrows constitute an important part of diagrams. They point either upwards or downwards, but will often have a tilt in the diagram. In general, arrows are used to represent Slater determinants. The particle-hole formalism, with reference determinant defined as

$$|r\rangle \equiv |\Phi_0\rangle,$$

where  $|\Phi_0\rangle$  is the ground state of the non-interacting system, allow us to represent Slater determinants in a simple way. Upward and downward directed lines identify those single-particle orbitals that differ from those that are occupied in the reference determinant. We use the convention that downward directed lines represent hole states, while upward directed lines represent particle states. Thus we can represent all excited states of the non-interacting system (Slater determinants) with combinations of hole and particle lines. Figure 6.2 shows some examples.

### Diagrams Representing Dynamical Operators

Diagrams can also represent dynamical operators. They are depicted by horizontal lines, called interaction lines, with vertical directed lines attached to it. These lines are attached to “vertices” on the interacting line. Each vertex represents the action of the operator on individual electrons. Therefore, diagrams associated with an  $n$ -body operator have  $n$  vertices. Each vertex has one incoming line and one outgoing line attached to it, which represents the annihilation and creation operators of the dynamical operators normal-ordered string. Since an  $n$ -body operator contains  $2n$  annihilation and creation operators, diagrams representing an  $n$ -body operator contain  $2n$  directed lines. Operators acting in the occupied space yield downward directed lines, while operators acting in the unoccupied space yield upward directed lines. Since the orbitals in the occupied and unoccupied space are called hole states and particle states, respectively, a downward directed line is called a hole line, while an upward directed line is called a particle line. Furthermore, a directed line is placed beneath or above the interaction line depending on whether its corresponding operator is a quasi-annihilation operator or a quasi-creation operator (see Eqs. 3.115 and 3.114).

We are seeking the diagrammatic representation of  $\hat{F}_N$ ,  $\hat{V}_N$ ,  $\hat{T}_1$  and  $\hat{T}_2$ . Consider first  $\hat{F}_N$ . The second quantized form is given as

$$\hat{F}_N = \sum_{pq} f_q^p \left\{ a_p^\dagger a_q \right\}. \quad (6.117)$$

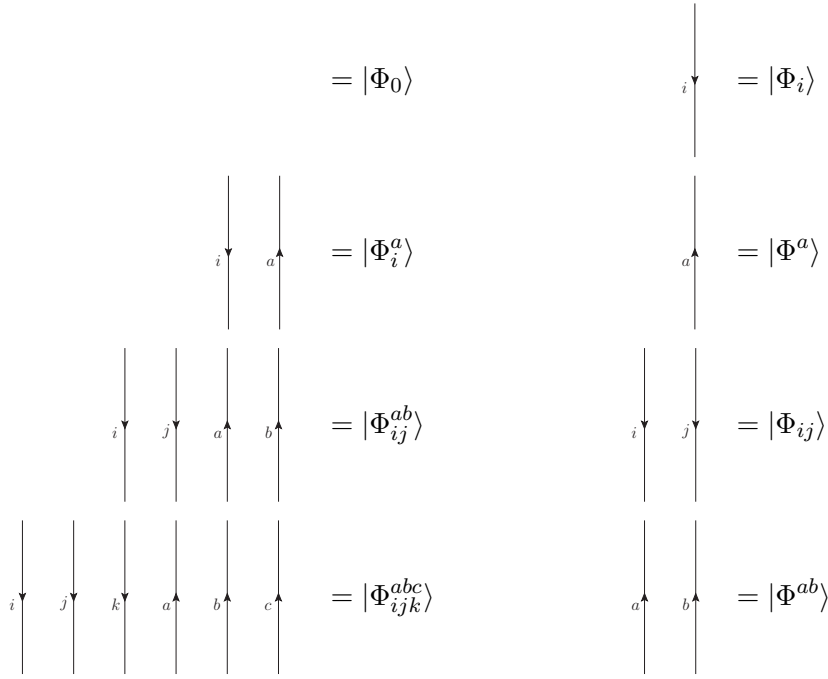


**Figure 6.2:** Diagrammatic representation of Slater determinants. The non-interacting ground state is the reference state, viz.  $|r\rangle = |\Phi_0\rangle$ , represented by empty space. The states in the left column are excited states of the non-interacting system. They are represented with particle and hole lines (equal number) indicating which orbitals that are occupied by a particle-hole pair. In the right column are states with particles added or removed from the system.

Separating the different combinations of orbitals spaces, i.e. terms with  $a_i^\dagger a_j$ ,  $a_i^\dagger a_a$ ,  $a_a^\dagger a_i$  and  $a_a^\dagger a_b$ , we obtain

$$\widehat{F}_N = \sum_{ab} f_b^a \left\{ a_a^\dagger a_b \right\} + \sum_{ij} f_j^i \left\{ a_i^\dagger a_j \right\} + \sum_{ia} f_a^i \left\{ a_i^\dagger a_a \right\} + \sum_{ai} f_i^a \left\{ a_a^\dagger a_i \right\}$$

$$\widehat{F}_N = \begin{array}{c} \text{Diagram 1: } \text{---} \bullet \\ \text{Diagram 2: } \bullet \text{---} \\ \text{Diagram 3: } \text{---} \bullet \text{---} \bullet \\ \text{Diagram 4: } \bullet \text{---} \text{---} \end{array} + \begin{array}{c} \text{Diagram 1: } \bullet \text{---} \\ \text{Diagram 2: } \text{---} \bullet \\ \text{Diagram 3: } \text{---} \bullet \text{---} \bullet \\ \text{Diagram 4: } \bullet \text{---} \text{---} \end{array} + \begin{array}{c} \text{Diagram 1: } \text{---} \bullet \\ \text{Diagram 2: } \bullet \text{---} \\ \text{Diagram 3: } \text{---} \bullet \text{---} \bullet \\ \text{Diagram 4: } \bullet \text{---} \text{---} \end{array} + \begin{array}{c} \text{Diagram 1: } \bullet \text{---} \\ \text{Diagram 2: } \text{---} \bullet \\ \text{Diagram 3: } \text{---} \bullet \text{---} \bullet \\ \text{Diagram 4: } \bullet \text{---} \text{---} \end{array} . \quad (6.118)$$

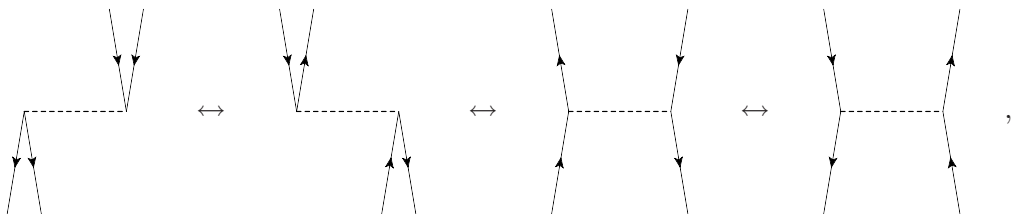
The first diagram contains one quasi-particle annihilation line (particle line) beneath the interaction line corresponding to  $a_i^\dagger$ , and one quasi-particle creation line (particle line) above corresponding to  $a_b$ . In the second diagram, we have one quasi-particle annihilation line corresponding to  $a_i^\dagger$ , and one quasi-particle creation line corresponding to  $a_j$ . In the third and fourth diagram, we have two quasi-particle annihilation lines corresponding to  $a_i^\dagger$  and  $a_a$ , and two quasi-particle creation lines corresponding to  $a_a^\dagger$  and  $a_i$ , respectively.

We now turn to  $\hat{V}_N$  and partition in a similar manner as for  $\hat{F}_N$ , yielding

$$\begin{aligned}
 \hat{V}_N = & \frac{1}{4} \sum_{abcd} \langle ab|v|cd \rangle \left\{ a_a^\dagger a_b^\dagger a_d a_c \right\} + \frac{1}{4} \sum_{ijkl} \langle ij|v|kl \rangle \left\{ a_i^\dagger a_j^\dagger a_l a_k \right\} + \sum_{iabj} \langle ia|v|bj \rangle \left\{ a_i^\dagger a_a^\dagger a_j a_b \right\} \\
 & + \frac{1}{2} \sum_{aibc} \langle ai|v|bc \rangle \left\{ a_a^\dagger a_i^\dagger a_c a_b \right\} + \frac{1}{2} \sum_{ijk a} \langle ij|v|ka \rangle \left\{ a_i^\dagger a_j^\dagger a_a a_k \right\} + \frac{1}{2} \sum_{abci} \langle ab|v|ci \rangle \left\{ a_a^\dagger a_b^\dagger a_i a_c \right\} \\
 & + \frac{1}{2} \sum_{iajk} \langle ia|v|jk \rangle \left\{ a_i^\dagger a_a^\dagger a_k a_j \right\} + \frac{1}{4} \sum_{abij} \langle ab|v|ij \rangle \left\{ a_a^\dagger a_b^\dagger a_j a_i \right\} + \frac{1}{4} \sum_{ijab} \langle ij|v|ab \rangle \left\{ a_i^\dagger a_j^\dagger a_b a_a \right\}
 \end{aligned}$$

(6.119)

Here we have implicit antisymmetry with respect to permutations of the lines leaving or entering the vertices. For example, the sum over  $\langle ia|v|bj \rangle a_i^\dagger a_a^\dagger a_j a_b$  can be transformed into the following four equivalent diagrams,



differing by a sign. Furthermore, the diagrammatic representations of  $\hat{T}_1$  and  $\hat{T}_2$  read

$$\hat{T}_1 = \quad \text{Diagram showing a single vertical line with an arrow pointing down, ending in a V-shape with two arrows pointing up.} \quad (6.120)$$

$$\hat{T}_2 = \quad \text{Diagram showing two vertical lines with arrows pointing down, ending in a V-shape with two arrows pointing up.} \quad (6.121)$$

Since the second quantized form of the excitation operators in Eqs. (6.60) and (6.61) contain only quasi-particle creation operators, their diagrammatic representation do not have any directed lines beneath the interaction line.

### Diagrams Representing Matrix Elements

We will now consider the third representation where diagrams are interpreted as matrix elements of operators between Slater determinants. We present this representation by showing some examples.

#### Example 1

$$\begin{array}{c} \diagdown \quad \diagup \\ \text{---} \end{array} = \langle \Phi_i^a | \hat{T}_1 | \Phi_0 \rangle \quad (6.122)$$

Consider the diagrammatic form of  $\hat{T}_1$ . Since  $|\Phi_0\rangle$  and  $|\Phi_i^a\rangle$  are represented by empty space and a pair particle-hole lines, respectively, the diagram in Eq. (6.122) may be interpreted from bottom to top as the matrix element of  $\hat{T}_1$  between the reference determinant  $|\Phi_0\rangle$  (on its right) and the one-particle one-hole (1p1h) excited determinant  $\langle \Phi_i^a |$  (on its left).

#### Example 2

$$\begin{array}{c} \diagdown \quad \diagup \\ \text{---} \quad \text{---} \end{array} = \langle \Phi_{ij}^{ab} | \hat{T}_2 | \Phi_0 \rangle \quad (6.123)$$

Consider the diagrammatic form of  $\hat{T}_2$ . Since  $|\Phi_0\rangle$  and  $|\Phi_{ij}^{ab}\rangle$  are represented by empty space and two pairs of particle-hole lines, respectively, the diagram in Eq. (6.123) may be interpreted from bottom to top as the matrix element of  $\hat{T}_2$  between the reference determinant  $|\Phi_0\rangle$  (on its right) and the two-particle two-hole (2p2h) excited determinant  $\langle \Phi_{ij}^{ab} |$  (on its left).

#### Example 3

$$\begin{array}{c} \text{---} \quad \text{---} \quad \bullet \\ \diagdown \quad \diagup \end{array} = \langle \Phi_0 | \hat{F}_N | \Phi_i^a \rangle \quad (6.124)$$

Consider the fourth diagram of  $\hat{F}_N$  in Eq. (6.118). Since  $|\Phi_0\rangle$  and  $|\Phi_i^a\rangle$  are represented by empty space and a pair of particle-hole lines, respectively, the diagram in Eq. (6.124) may be interpreted from bottom to top as the matrix element of  $\hat{F}_N$  between the reference determinant  $|\Phi_0\rangle$  (on its right) and the one-particle one-hole (1p1h) excited determinant  $\langle \Phi_i^a |$  (on its left).

#### Example 4

$$\begin{array}{c} \text{---} \quad \text{---} \\ \diagup \quad \diagdown \quad \bullet \\ \text{---} \end{array} = \langle \Phi^c | \hat{V}_N | \Phi_i^{ab} \rangle \quad (6.125)$$

Consider the fourth diagram of  $\hat{V}_N$  in Eq. (6.119). Since  $|\Phi_i^{ab}\rangle$  is represented by two particle lines and one hole line, and  $|\Phi^c\rangle$  is represented by one particle line, the diagram in Eq. (6.125) may be interpreted from bottom to top as the matrix element of  $\hat{V}_N$  between the determinant  $|\Phi_i^{ab}\rangle$  (on its right) and the determinant  $\langle \Phi^c |$  (on its left).

We have now considered four examples that illustrate the matrix element representation of diagrams. This representation able us to find the diagrams that contribute to the CC equations

in a very practical and convenient way. Before we present how this is done in practice, the concept of excitation level must be introduced. The excitation level  $\xi$  of a diagram is defined as

$$\xi = \frac{n_c - n_a}{2}, \quad (6.126)$$

where  $n_c$  is the number of quasi-particle creation lines, and  $n_a$  is the number of quasi-particle annihilation lines. Denoting  $\xi_{X,i}$  as the excitation level of the  $i$ -th diagram of  $\hat{X}$ , we obtain the following excitation levels of  $\hat{F}_N$ ,  $\hat{V}_N$ ,  $\hat{T}_1$  and  $\hat{T}_2$ :

$$\begin{array}{ll} \xi_{F_N,1} = 0 & \xi_{V_N,1} = 0 \\ \xi_{F_N,2} = 0 & \xi_{V_N,2} = 0 \\ \xi_{F_N,3} = -1 & \xi_{V_N,3} = 0 \\ \xi_{F_N,4} = +1 & \xi_{V_N,4} = -1 \\ \xi_{T_1} = +1 & \xi_{V_N,5} = -1 \\ \xi_{T_2} = +2 & \xi_{V_N,6} = +1 \\ & \xi_{V_N,7} = +1 \\ & \xi_{V_N,8} = +2 \\ & \xi_{V_N,9} = -2 \end{array}$$

For example, in the third diagram of  $\hat{V}_N$  (see Eq. 6.119), we have one “incoming” 1p1h excited determinant and one “outgoing” 1p1h excited determinant. Thus no additional excitations are produced, leading to  $\xi_{V_N,3} = 0$ . In the eighth diagram of  $\hat{V}_N$ , however, we have one “incoming” reference determinant and one “outgoing” 2p2h excited determinant, leading to  $\xi_{V_N,8} = +2$ .

#### 6.4.5 Energy Equation on Diagrammatic Form

We will in this section present how the matrix representation of diagrams can be used in order to determine the nonzero contributions to the energy equation. Our task is to translate the equation into diagrammatic form by considering each term in

$$E_{CC} = \langle \Phi_0 | (\hat{H}_N + \hat{H}_N \hat{T} + \frac{1}{2!} \hat{H}_N \hat{T}^2 + \frac{1}{3!} \hat{H}_N \hat{T}^3 + \frac{1}{4!} \hat{H}_N \hat{T}^4 + \dots)_c | \Phi_0 \rangle, \quad (6.127)$$

where  $\hat{T} = \hat{T}_1 + \hat{T}_2$ , and the  $c$ -subscript denotes that  $\hat{H}_N$  must have at least one contraction with every excitation operator. The normal-ordered form of the two-body Hamiltonian is given in Eq. (6.70). The diagrammatic representations of  $\hat{F}_N$ ,  $\hat{V}_N$ ,  $\hat{T}_1$  and  $\hat{T}_2$  are given in Eqs. (6.118), (6.119), (6.120) and (6.121), respectively. We first observe that each matrix element in Eq. (6.127) has one incoming reference determinant (on its right) and one outgoing reference determinant (on its left). Thus, diagrams associated with the energy equation cannot contain directed lines (external lines) that extend above or below the diagram. A diagram contributing to the equation must therefore have *total* excitation level zero, and contain the reference determinant both at the bottom and top of the diagram. Furthermore, Eq. (6.127) contain nested commutators of  $\hat{H}_N$ ,  $\hat{T}_1$  and  $\hat{T}_2$ , producing operator products. In the diagrammatic representation of an operator product, the rightmost operator has its interaction line at the bottom of the diagram, and the leftmost operator has its interaction line at the top. First we observe that the diagrams representing  $\hat{T}_1$  and  $\hat{T}_2$  have no external lines. In Eq. (6.127),  $\hat{H}_N$  must have at least one contraction with every excitation operator. When a quasi-particle creation line from one diagram is merged with a quasi-particle annihilation line from another diagram, the diagrams are said to be connected. This is analogous to contractions in Wick’s theorem. Since the total excitation level of diagrams associated with the energy equation must be zero, and the lowest excitation level of  $\hat{H}_N$  is  $-2$ ,  $\hat{H}_N$  cannot produce a total excitation level of zero. If we were to include  $\hat{T}_3 \dots \hat{T}_N$ , diagrams including terms with these excitations operators would not contribute to the

energy. Furthermore, all terms with  $\hat{T}^n$  ( $n \geq 3$ ) produce excitation level  $\xi \geq 3$ , meaning that  $\hat{H}_N$  (with minimum excitation level  $-2$ ) cannot produce a total excitation level of zero. Moreover, when  $n = 2$ ,  $\hat{T}_2^2$  produces the excitation level  $+4$ . Thus Eq. (6.127) simplifies to

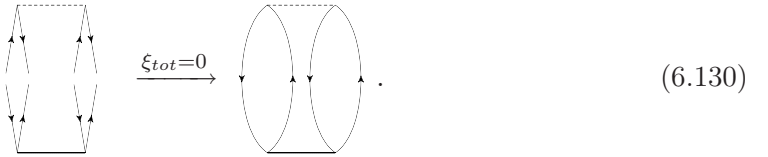
$$E_{CC} = \langle \Phi_0 | (\hat{H}_N \hat{T}_1 + \hat{H}_N \hat{T}_2 + \frac{1}{2} \hat{H}_N \hat{T}_1)_c | \Phi_0 \rangle, \quad (6.128)$$

where we have only included those terms with total excitation level of zero. This is the same expression as we obtained by using Wick's theorem. We will in the following transform each term in Eq. (6.127) to a diagrammatic form.

1. Consider  $\langle \Phi_0 | (\hat{H}_N \hat{T}_1)_c | \Phi_0 \rangle$ . The diagrammatic representation of  $\hat{T}_1$  is given in Eq. (6.120) with excitation level  $+1$ . We require the diagrams of  $\hat{F}_N$  in Eq. (6.118) and  $\hat{V}_N$  in Eq. (6.119) with excitation level  $-1$  and the reference determinant at the top of the diagram. The third diagram of  $\hat{F}_N$  is the only diagram that satisfies these criteria. In order to obtain a total excitation level of zero,  $\hat{F}_N$  and  $\hat{T}_1$  must be fully connected, viz.



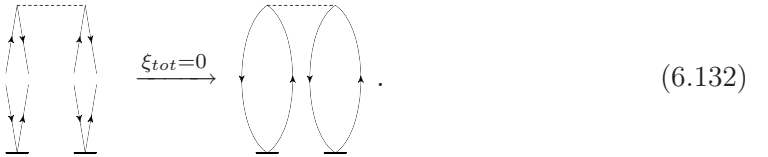
2. Consider  $\langle \Phi_0 | (\hat{H}_N \hat{T}_2)_c | \Phi_0 \rangle$ . The diagrammatic representation of  $\hat{T}_2$  is given in Eq. (6.121) with excitation level  $+2$ . We require the diagrams of  $\hat{H}_N$  with excitation level  $-2$  and the reference determinant at top of the diagram. Obviously,  $\hat{F}_N$  cannot connect to  $\hat{T}_2$  producing a total excitation level of zero. The ninth diagram of  $\hat{V}_N$  in Eq. (6.119) satisfies the criteria. We then fully connect the diagrams, viz.



3. Consider  $\langle \Phi_0 | (\hat{H}_N \hat{T}_1^2)_c | \Phi_0 \rangle$ . Since  $\hat{T}_1$  commute with itself, their vertical ordering in the diagram is not important. The diagrammatic form of the operator product  $\hat{T}_1^2$  is given as

$$\hat{T}_1^2 = \begin{array}{c} \text{V-shaped diagram with a dot at the top} \\ \text{V-shaped diagram with a dot at the top} \end{array}, \quad (6.131)$$

with excitation level  $+2$ . The only diagram of  $\hat{H}_N$  with excitation level  $-2$  and no external lines at the top, is the ninth fragment of  $\hat{V}_N$  in Eq. (6.119). We then fully connect the diagrams, yielding



The diagrammatic form of the energy equation finally reads

$$E_{CC} = \begin{array}{c} \text{dashed oval with a dot at the top} \\ + \end{array} \begin{array}{c} \text{solid oval with two dots at the top} \\ + \end{array} \begin{array}{c} \text{solid oval with two dots at the top} \end{array}. \quad (6.133)$$

These diagrams can be transformed to algebraic expression by using the so-called diagram rules. Before we present these, we transform the amplitude equations to diagrammatic form.

### 6.4.6 Amplitude Equations on Diagrammatic Form

We will in this section transform the amplitude equations into diagrammatic forms. The amplitude equations are given as

$$\langle \Phi_i^a | e^{-\hat{T}} \hat{H}_N e^{\hat{T}} | \Phi_0 \rangle = 0 \quad (6.134)$$

$$\langle \Phi_{ij}^{ab} | e^{-\hat{T}} \hat{H}_N e^{\hat{T}} | \Phi_0 \rangle = 0. \quad (6.135)$$

#### $\hat{T}_1$ Amplitude Equation

We will now transform the  $\hat{T}_1$  equation into a diagrammatic form. Inserting Eq. (6.108) into Eq. (6.134), yields

$$\langle \Phi_i^a | (\hat{H}_N + \hat{H}_N \hat{T} + \frac{1}{2!} \hat{H}_N \hat{T}^2 + \frac{1}{3!} \hat{H}_N \hat{T}^3 + \frac{1}{4!} \hat{H}_N \hat{T}^4 + \dots)_c | \Phi_0 \rangle = 0, \quad (6.136)$$

where  $\hat{T} = \hat{T}_1 + \hat{T}_2$ , and the  $c$ -subscript denote that  $\hat{H}_N$  must connect with every excitation operator. Each matrix element has the reference determinant on its right and the one-particle one-hole (1p1h) excited determinant on its left. Diagrams that contribute to the equation must therefore satisfy the following three criterion:

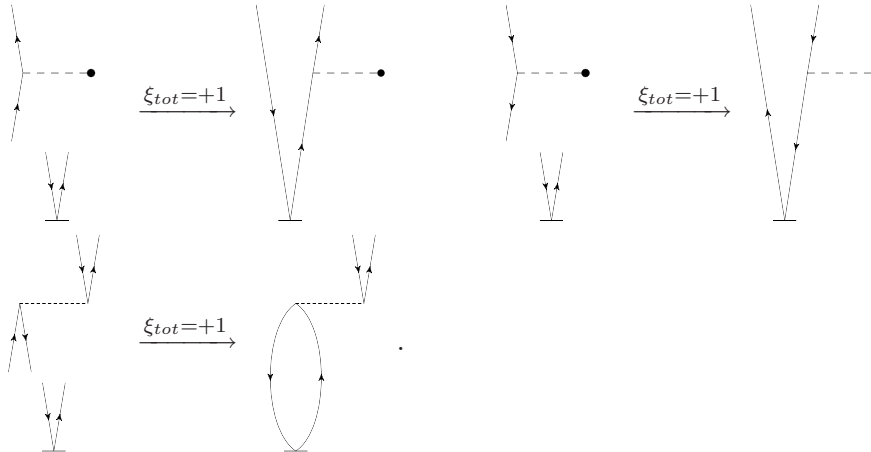
1. Total excitation level +1.
2. The reference determinant at the bottom of the diagram.
3. The 1p1h excited determinant at the top of the diagram.

Since  $\hat{H}_N$  has minimum excitation level of  $-2$ , and  $\hat{T}^n$  ( $n \geq 4$ ) have excitation level  $\xi \geq 4$ , none of the diagrams representing  $(\hat{H}_N \hat{T}^n)_c$  ( $n \geq 4$ ) fulfill these criteria. Moreover, since  $\hat{T}_2^2$  and  $\hat{T}_2^3$  have excitation level +4 and +6, respectively, none of the diagrams representing  $\hat{H}_N \hat{T}_2^2$  and  $\hat{H}_N \hat{T}_2^3$  contribute. The  $\hat{T}_1$  amplitude equation thus reads

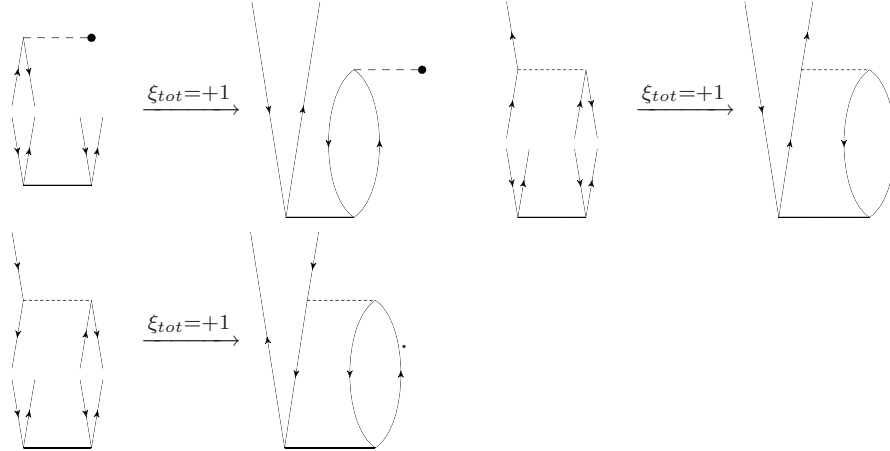
$$\langle \Phi_i^a | (\hat{H}_N + \hat{H}_N \hat{T}_1 + \hat{H}_N \hat{T}_2 + \frac{1}{2} \hat{H}_N \hat{T}_1^2 + \hat{H}_N \hat{T}_1 \hat{T}_2 + \frac{1}{6} \hat{H}_N \hat{T}_1^3)_c | \Phi_0 \rangle = 0. \quad (6.137)$$

We will in the following consider the diagrams of  $\hat{F}_N$ ,  $\hat{V}_N$ ,  $\hat{T}_1$  and  $\hat{T}_2$  in Eq. (6.118), (6.119), (6.120) and (6.121), respectively, and transform each term into a diagrammatic form.

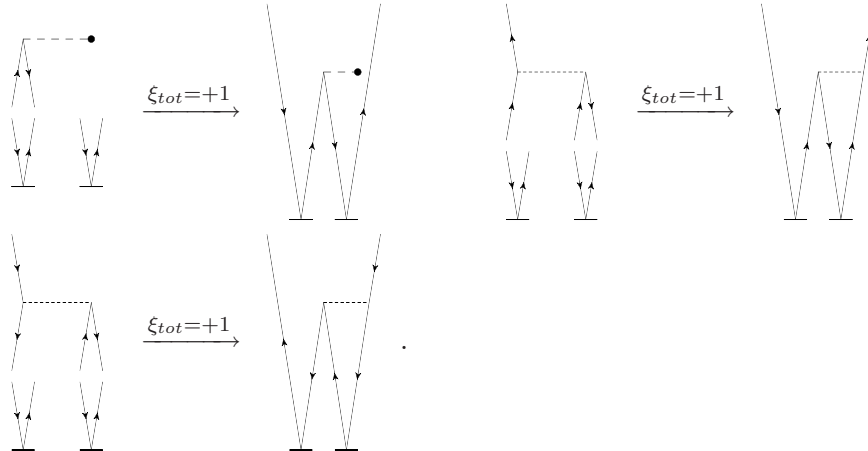
1. Consider  $\langle \Phi_i^a | \hat{H}_N | \Phi_0 \rangle$ . The diagrams of  $\hat{V}_N$  do not contribute to the equation since none of them satisfy our criteria. This is a consequence of the fact that  $\hat{V}_N$  is a two-body operator. The fourth fragment of  $\hat{F}_N$ , however, contribute.
2. Consider  $\langle \Phi_i^a | (\hat{H}_N \hat{T}_1)_c | \Phi_0 \rangle$ . Obviously,  $\hat{T}_1$  has excitation level +1. Thus we require the diagrams of  $\hat{H}_N$  with an excitation level of zero that can connect to  $\hat{T}_1$  satisfying the criteria above. We observe that the first and second diagram of  $\hat{F}_N$ , and the third fragment of  $\hat{V}_N$ , can connect to  $\hat{T}_1$  in this way. We obtain the following three contributions:



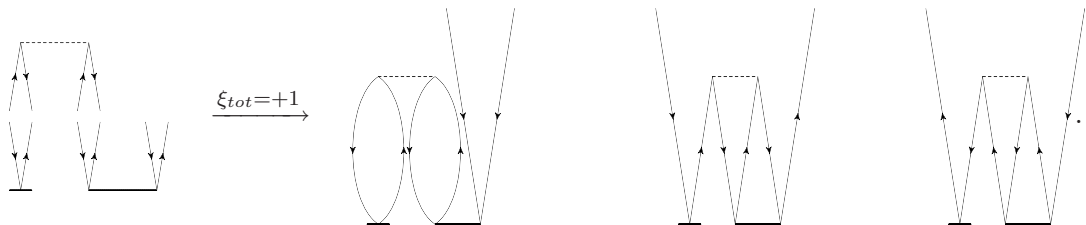
3. Consider  $\langle \Phi_i^a | (\widehat{H}_N \widehat{T}_2)_c | \Phi_0 \rangle$ . Obviously,  $\widehat{T}_2$  has excitation level +2. Thus we require the diagrams of  $\widehat{H}_N$  with excitation level -1 that can connect to  $\widehat{T}_2$  satisfying our criteria. The third fragment of  $\widehat{F}_N$ , and the fourth and fifth fragment of  $\widehat{V}_N$ , give contributions to the equation. By connecting the diagrams, we obtain the following contributions:



4. Consider  $\langle \Phi_i^a | (\frac{1}{2} \widehat{H}_N \widehat{T}_1^2)_c | \Phi_0 \rangle$ . Obviously,  $\widehat{T}_1^2$  has excitation level +2. As for the previous term, we require the third diagram of  $\widehat{F}_N$ , and the fourth and fifth diagram of  $\widehat{V}_N$ . These diagrams have excitation level +1 and can connect to  $\widehat{T}_1^2$  satisfying our criteria. We obtain the following contributions:

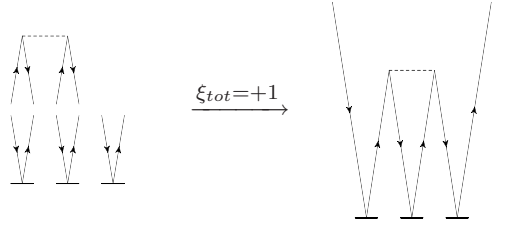


5. Consider  $\langle \Phi_i^a | (\widehat{H}_N \widehat{T}_1 \widehat{T}_2)_c | \Phi_0 \rangle$ . We first observe that  $\widehat{T}_1 \widehat{T}_2$  has excitation level +3. In order to obtain at total excitation level of +1,  $\widehat{T}_1 \widehat{T}_2$  must connect to a diagram with excitation level -2, i.e. the ninth diagram of  $\widehat{V}_N$ . This diagram may be connected to  $\widehat{T}_1 \widehat{T}_2$  in three different ways. We obtain the following contributions to the equation:



6. Consider  $\langle \Phi_i^a | (\frac{1}{6} \widehat{H}_N \widehat{T}_1^3)_c | \Phi_0 \rangle$ . Since  $\widehat{T}_1^3$  has excitation level +3, we require the ninth

diagram fragment of  $\widehat{V}_N$  with excitation level  $-2$ , yielding the following contribution



We finally obtain the diagrammatic representation of the  $\widehat{T}_1$  amplitude equation,

$$\begin{aligned}
 0 = & \quad \text{Diagram 1} + \text{Diagram 2} + \text{Diagram 3} + \text{Diagram 4} \\
 & + \text{Diagram 5} + \text{Diagram 6} + \text{Diagram 7} + \text{Diagram 8} \\
 & + \text{Diagram 9} + \text{Diagram 10} + \text{Diagram 11} + \text{Diagram 12} \\
 & + \text{Diagram 13} + \text{Diagram 14} + \text{Diagram 15} + \text{Diagram 16} \\
 & + \text{Diagram 17} + \text{Diagram 18} . \tag{6.138}
 \end{aligned}$$

## $\widehat{T}_2$ Amplitude Equation

We will now transform the  $\widehat{T}_2$  equation into a diagrammatic form. Inserting Eq. (6.108) into Eq. (6.135), yields

$$\langle \Phi_{ij}^{ab} | (\widehat{H}_N + \widehat{H}_N \widehat{T} + \frac{1}{2!} \widehat{H}_N \widehat{T}^2 + \frac{1}{3!} \widehat{H}_N \widehat{T}^3 + \frac{1}{4!} \widehat{H}_N \widehat{T}^4 + \dots)_c | \Phi_0 \rangle = 0, \tag{6.139}$$

where  $\widehat{T} = \widehat{T}_1 + \widehat{T}_2$ , and the  $c$ -subscript denotes that  $\widehat{H}_N$  must have at least one contraction with every excitation operator. Each matrix element in the equation has the reference determinant on its right and the two-particle two-hole (2p2h) excited determinant on its left. Diagrams that contribute to the equation must therefore satisfy the following three criterion:

1. Total excitation level  $+2$ .
2. The reference determinant at the bottom of the diagram.
3. The 2p2h excited determinant at the top of the diagram.

Since  $\hat{H}_N$  has minimum excitation level  $-2$ , and  $\hat{T}^n$  ( $n \geq 5$ ) have excitation level  $\xi \geq 5$ , diagrams representing  $(\hat{H}_N \hat{T}^n)_c$  ( $n \geq 5$ ) do not satisfy our criteria. Moreover, since  $\hat{T}_2^3$  and  $\hat{T}_2^4$  have excitation level  $+6$  and  $+8$ , respectively,  $(\hat{H}_N \hat{T}_2^3)_c$  and  $(\hat{H}_N \hat{T}_2^4)_c$  do not contribute to the equation. Thus the  $\hat{T}_2$  equation reduces to

$$0 = \langle \Phi_{ij}^{ab} | (\hat{H}_N + \hat{H}_N \hat{T}_1 + \hat{H}_N \hat{T}_2 + \frac{1}{2} \hat{H}_N \hat{T}_1^2 + \frac{1}{2} \hat{H}_N \hat{T}_2^2 + \hat{H}_N \hat{T}_1 \hat{T}_2 + \frac{1}{6} \hat{H}_N \hat{T}_1^3 + \frac{1}{2} \hat{T}_1^2 \hat{T}_2)_c | \Phi_0 \rangle.$$

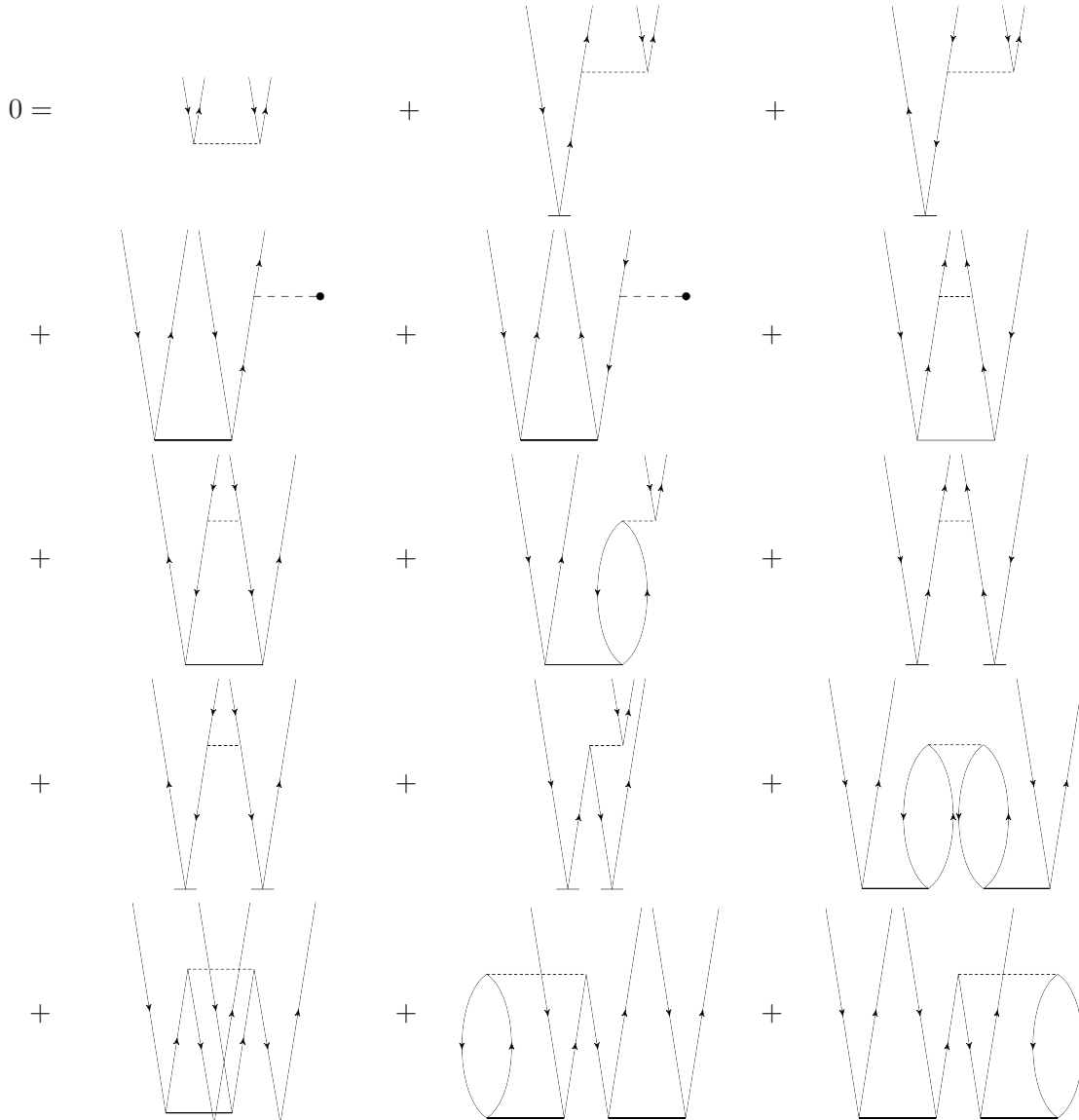
In order to transform each term into a diagrammatic expression, we use the same procedure as we did for the  $\hat{T}_1$  equation. For each term  $\langle \Phi_{ij}^{ab} | \hat{H}_N \hat{X} | \Phi_0 \rangle$ , where  $\hat{X}$  has excitation level  $\xi_X$ , the following procedure is used to obtain the diagrammatic expression:

1. Identify the diagrams of  $\hat{H}_N$  with the 2p2h excited determinant of the top of the diagram, and excitation level  $\xi$  that satisfies

$$\xi + \xi_X = 2. \quad (6.140)$$

2. For each diagram that satisfies 1., connect this diagram to  $\hat{X}$  in accordance with the three criteria listed above.

We will not show the derivation of the diagrammatic forms as we did for the  $\hat{T}_1$ . The final form of  $\hat{T}_2$  reads:



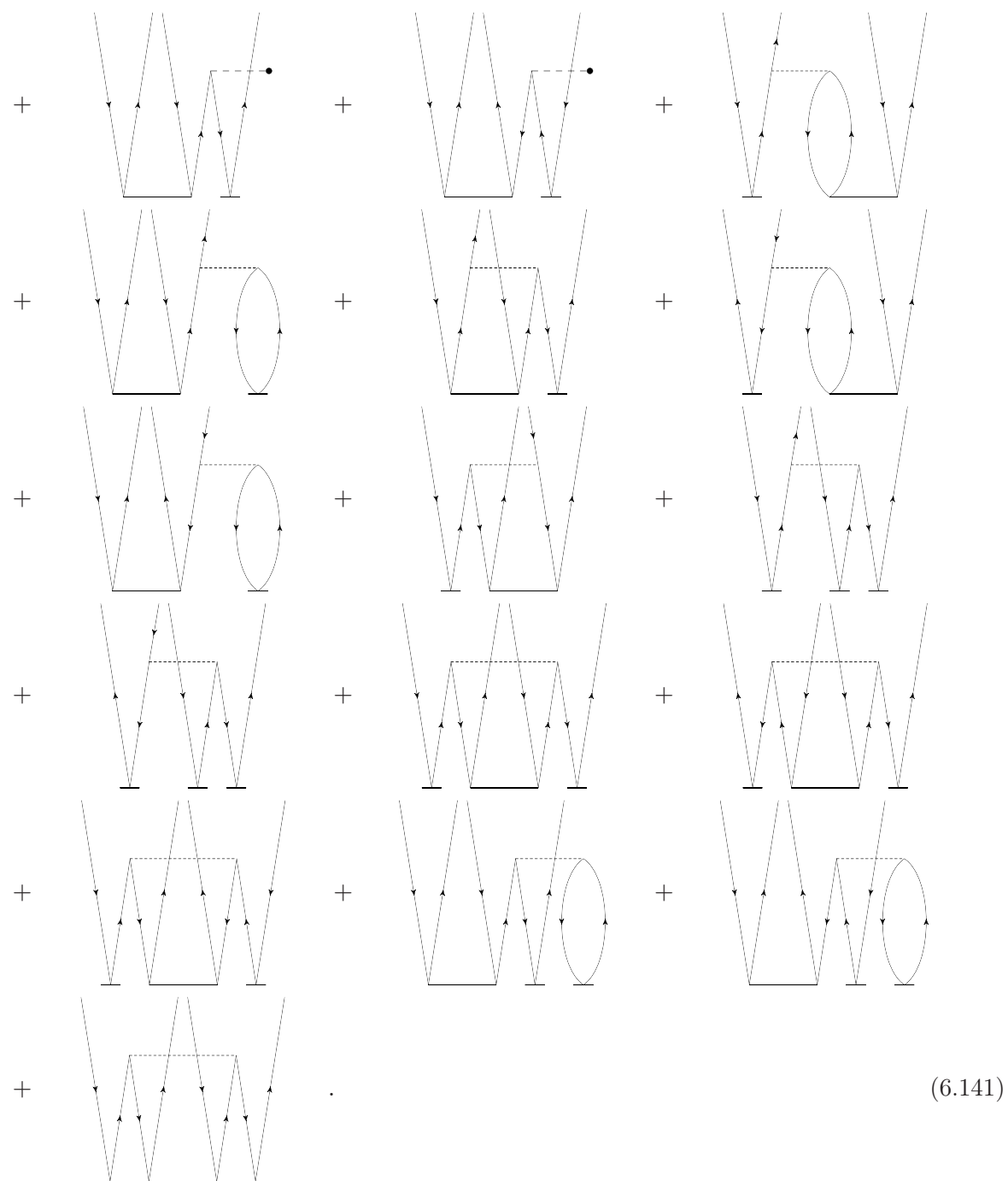


## Diagram Rules

The diagrammatic form of the energy and amplitude equations in (6.133), (6.138) and (6.141) can be transformed into algebraic expressions by so-called diagram rules. In the following, the rules are listed.

1. Label all directed lines with indices  $ijk..$  (hole lines) and  $abc..$  (particle lines).
2. Each operator line contributes with an integral or amplitude.

$$\begin{aligned}\hat{T}_1 &\rightarrow t_i^a \\ \hat{T}_2 &\rightarrow t_{ij}^{ab} \\ \hat{F}_N &\rightarrow f_{\text{in}}^{\text{out}} \\ \hat{V}_N &\rightarrow \langle \text{left-out right-out} | v | \text{left-in right-in} \rangle\end{aligned}$$

3. Summation over all internal indices, viz. all indices that label lines that begin and end at an operator line.
4. A prefactor of  $(-1)^{n_h + n_l}$  is included in the algebraic expression, where  $n_h$  denotes the number of hole lines, and  $n_l$  denotes the number of loops. A loop is defined as either a route of directed lines that returns to its beginning, or a route that begins and ends at an external line.
5. For each pair of equivalent lines, i.e. lines that begin and end at the same operator line, a prefactor of  $\frac{1}{2}$  is included.
6. For each pair of equivalent vertices, i.e. two  $\hat{T}_n$  operator lines that connect to a fragment of  $\hat{H}_N$  in exactly the same manner, a prefactor of  $\frac{1}{2}$  is included.
7. For each pair of unique external hole or particle lines, a permutation function  $P(pq)$  is included.  $P(pq)$  acting on a function  $f(pq)$  yields

$$P(pq)f(p, q) \equiv f(p, q) - f(q, p),$$

The permutation function is included in order to ensure antisymmetry of the final expression.

### 6.4.7 Amplitude Equations on Algebraic Form

We will in this section utilize the diagram rules in order to transform the amplitude equations into algebraic expressions. We will use Einstein's summation convention, viz.

$$f_a^i t_i^a \equiv \sum_{ia} f_a^i t_i^a. \quad (6.142)$$

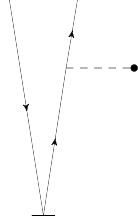
Thus, identical quantum numbers in an expression implies a summation.

## $\hat{T}_1$ Amplitude Equation

We will in the following transform each diagram of Eq. (6.138) into an algebraic expression.

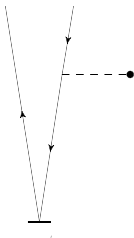


$$= f_i^a$$

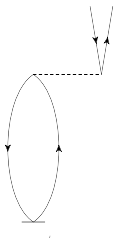


$$= f_a^b t_i^a$$

(6.143)

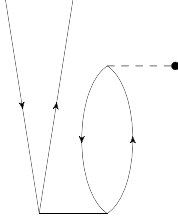


$$= -f_i^j t_j^a$$

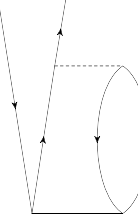


$$= \langle ia|v|bj\rangle t_i^b$$

(6.144)

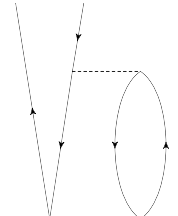


$$= f_a^i t_{ji}^{ba}$$

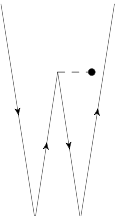


$$= \frac{1}{2} \langle ai|v|bc\rangle t_{ji}^{bc}$$

(6.145)

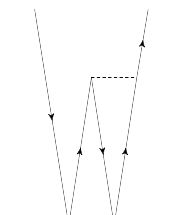


$$= -\frac{1}{2} \langle ij|v|ka\rangle t_{ij}^{ba}$$

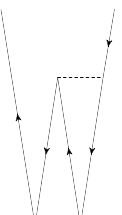


$$= -f_a^i t_j^a t_i^b$$

(6.146)

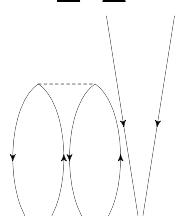


$$= -\langle ia|v|bc\rangle t_j^b t_i^c$$

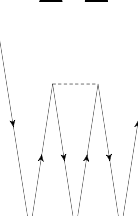


$$= \langle ij|v|ak\rangle t_i^b t_j^a$$

(6.147)

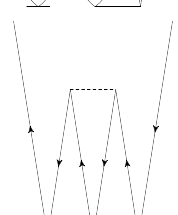


$$= \langle ij|v|ab\rangle t_i^a t_{jk}^{bc}$$

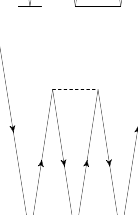


$$= \frac{1}{2} \langle ij|v|ab\rangle t_k^a t_{ij}^{bc}$$

(6.148)



$$= \frac{1}{2} \langle ij|v|ab\rangle t_i^c t_{jk}^{ab}$$



$$= \langle ij|v|ab\rangle t_k^a t_i^b t_j^c$$

(6.149)

The final algebraic expression of the  $\hat{T}_1$  equation reads,

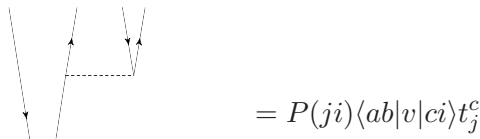
$$0 = f_i^a + f_a^b t_i^a - f_i^j t_j^a + \langle ia|v|bj\rangle t_i^b + f_a^i t_{ji}^{ba} + \frac{1}{2} \langle ai|v|bc\rangle t_{ji}^{bc} - \frac{1}{2} \langle ij|v|ka\rangle t_{ij}^{ba} \\ - f_d^i t_j^a t_i^b - \langle ia|v|bc\rangle t_j^b t_i^c + \langle ij|v|ak\rangle t_i^b t_j^a + \langle ij|v|ab\rangle t_i^a t_{jk}^{bc} + \frac{1}{2} \langle ij|v|ab\rangle t_k^a t_{ij}^{bc} \\ + \frac{1}{2} \langle ij|v|ab\rangle t_i^c t_{jk}^{ab} + \langle ij|v|ab\rangle t_k^a t_i^b t_j^c. \quad (6.150)$$

### $\hat{T}_2$ Amplitude Equation

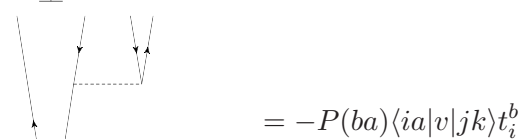
We will in the following transform each diagram of Eq. (6.141) into an algebraic expression.



$$= \langle ij|v|ab\rangle \quad (6.151)$$



$$= P(ji)\langle ab|v|ci\rangle t_j^c \quad (6.152)$$



$$= -P(ba)\langle ia|v|jk\rangle t_i^b \quad (6.153)$$



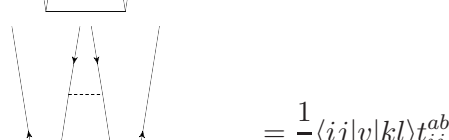
$$= P(cb)f_a^b t_{ij}^{ca} \quad (6.154)$$



$$= -P(ki)f_i^j t_{kj}^{ab} \quad (6.155)$$



$$= \frac{1}{2} \langle ab|v|cd\rangle t_{ij}^{cd} \quad (6.156)$$



$$= \frac{1}{2} \langle ij|v|kl\rangle t_{ij}^{ab} \quad (6.157)$$

$$= P(kj)P(ca)\langle ia|v|bj\rangle t_{ki}^{cb} \quad (6.158)$$

$$= \frac{1}{2}P(ij)\langle ab|v|cd\rangle t_i^c t_j^d \quad (6.159)$$

$$= \frac{1}{2}P(ab)\langle ij|v|kl\rangle t_i^a t_j^b \quad (6.160)$$

$$= P(kj)P(ac)\langle ia|v|bj\rangle t_k^b t_i^c \quad (6.161)$$

$$= \frac{1}{2}P(kl)P(cd)\langle ij|v|ab\rangle t_{ki}^{ca} t_{jl}^{bd} \quad (6.162)$$

$$= \frac{1}{4}\langle ij|v|ab\rangle t_{kl}^{ab} t_{ij}^{cd} \quad (6.163)$$

$$= -\frac{1}{2}P(kl)\langle ij|v|ab\rangle t_{ik}^{ab} t_{jl}^{cd} \quad (6.164)$$

$$= -\frac{1}{2}P(cd)\langle ij|v|ab\rangle t_{kl}^{ca} t_{ij}^{db} \quad (6.165)$$

$$= -P(bc) f_a^i t_{jk}^{ba} t_i^c \quad (6.166)$$

$$= -P(jk) f_a^i t_{ji}^{bc} t_k^a \quad (6.167)$$

$$= P(jk) P(ad) \langle ai | v | bc \rangle t_j^b t_{ik}^{cd} \quad (6.168)$$

$$= P(da) \langle ai | v | bc \rangle t_{jk}^{db} t_i^c \quad (6.169)$$

$$= -\frac{1}{2} P(ad) \langle ai | v | bc \rangle t_{jk}^{bc} t_i^d \quad (6.170)$$

$$= -P(bc) P(kl) \langle ij | v | ka \rangle t_i^b t_{jl}^{ac} \quad (6.171)$$

$$= -P(lk) \langle ij | v | ka \rangle t_{li}^{bc} t_j^a \quad (6.172)$$

$$= \frac{1}{2} P(lk) \langle ij | v | ak \rangle t_l^a t_{ij}^{bc} \quad (6.173)$$

$$= -\frac{1}{2}P(jk)P(ad)\langle ai|v|bc\rangle t_j^b t_k^c t_i^d \quad (6.174)$$

$$= \frac{1}{2}P(bc)P(kl)\langle ij|v|ka\rangle t_i^b t_l^a t_j^c \quad (6.175)$$

$$= P(kl)P(cd)\langle ij|v|ab\rangle t_k^a t_{il}^{cb} t_j^d \quad (6.176)$$

$$= \frac{1}{4}P(cd)\langle ij|v|ab\rangle t_i^c t_{kl}^{ab} t_j^d \quad (6.177)$$

$$= \frac{1}{4}P(kl)\langle ij|v|ab\rangle t_k^a t_{ij}^{cd} t_l^b \quad (6.178)$$

$$= -P(cd)\langle ij|v|ab\rangle t_{kl}^{ca} t_i^d t_j^b \quad (6.179)$$

$$= -P(kl)\langle ij|v|ab\rangle t_{ki}^{cd} t_l^a t_j^b \quad (6.180)$$

$$= \frac{1}{4}P(kl)P(cd)\langle ij|v|ab\rangle t_k^a t_i^c t_l^b t_j^d \quad (6.181)$$

Collecting all terms, we finally obtain the algebraic expression for the  $\widehat{T}_2$  equation,

$$\begin{aligned}
 0 = & \langle ij|v|ab\rangle + P(ji)\langle ab|v|ci\rangle t_j^c - P(ba)\langle ia|v|jk\rangle t_i^b + P(cb)f_a^b t_{ij}^{ca} - P(ki)f_i^j t_{kj}^{ab} \\
 & + \frac{1}{2}\langle ab|v|cd\rangle t_{ij}^{cd} + \frac{1}{2}\langle ij|v|kl\rangle t_{ij}^{ab} + P(kj)P(ca)\langle ia|v|bj\rangle t_{ki}^{cb} + \frac{1}{2}P(ij)\langle ab|v|cd\rangle t_i^c t_j^d \\
 & + \frac{1}{2}P(ab)\langle ij|v|kl\rangle t_i^b t_j^b + P(kj)P(ac)\langle ia|v|bj\rangle t_k^b t_i^c + \frac{1}{2}P(kl)P(cd)\langle ij|v|ab\rangle t_{ki}^{ca} t_{jl}^{bd} \\
 & + \frac{1}{4}\langle ij|v|ab\rangle t_{kl}^{ab} t_{ij}^{cd} - \frac{1}{2}P(kl)\langle ij|v|ab\rangle t_{ik}^{ab} t_{jl}^{cd} - \frac{1}{2}P(cd)\langle ij|v|ab\rangle t_{kl}^{ca} t_{ij}^{db} - P(bc)f_a^i t_{jk}^{ba} t_i^c \\
 & - P(jk)f_a^i t_{ji}^{bc} t_k^a + P(jk)P(ad)\langle ai|v|bc\rangle t_j^b t_{ik}^{cd} + P(da)\langle ai|v|bc\rangle t_{jk}^{db} t_i^c - \frac{1}{2}P(ad)\langle ai|v|bc\rangle t_{jk}^{bc} t_i^d \\
 & - P(bc)P(kl)\langle ij|v|ka\rangle t_i^b t_{jl}^{ac} - P(lk)\langle ij|v|ka\rangle t_{li}^{bc} t_j^a + \frac{1}{2}P(lk)\langle ij|v|ak\rangle t_l^a t_{ij}^{bc} \\
 & - \frac{1}{2}P(jk)P(ad)\langle ai|v|bc\rangle t_j^b t_k^c t_i^d + \frac{1}{2}P(bc)P(kl)\langle ij|v|ka\rangle t_i^b t_l^a t_j^c + P(kl)P(cd)\langle ij|v|ab\rangle t_k^a t_{il}^{cb} t_j^d \\
 & + \frac{1}{4}P(cd)\langle ij|v|ab\rangle t_i^c t_{kl}^{ab} t_j^d + \frac{1}{4}P(kl)\langle ij|v|ab\rangle t_k^a t_{ij}^{cd} t_l^b - P(cd)\langle ij|v|ab\rangle t_{kl}^{ca} t_i^d t_j^b \\
 & - P(kl)\langle ij|v|ab\rangle t_{ki}^{cd} t_l^a t_j^b + \frac{1}{4}P(kl)P(cd)\langle ij|v|ab\rangle t_k^a t_i^c t_l^b t_j^d. \tag{6.182}
 \end{aligned}$$

The amplitude equations are coupled and non-linear in the amplitudes  $t_i^a$  and  $t_{ij}^{ab}$ . Therefore, they must be solved iteratively. At this point we will not go further into how this is done in a computer program. We will in Chapter 7 present the implementation of the equations in detail.



## Part III

# IMPLEMENTATIONS AND RESULTS



# Chapter 7

## Implementation

In this chapter we present the implementation of the Hartree-Fock (HF) method and the Coupled-Cluster Singles and Doubles (CCSD) method. We also present the code-structures and the implementation of classes. The focus will be on the CCSD code and its structure. We will present the implementation of the algorithm, the energy equation and the amplitude equations in detail. Implementation of important analytical expressions will be shown with pseudo-codes. We will also present how to run the codes.

Both programs are object-oriented. When designing numerical software in computational science, it is often common to specialize it to the problem that is examined. It is often timesaving (in the sense that one obtain results for a specific problem) to start programming without considering generalizations, class implementations, and so forth. In many-body methods, such as for example Variational Monte Carlo (see [18]), only small changes are often required when considering other systems. A specialized code scatters the parts which needs modifications around. An object-oriented programming style offers an amazing opportunity to structure the code into parts that are “independent”. Such a programming style also able us to generalize parts of the code that are identical for many systems. Moreover, when the original system changes, the class structure often require modifications at well-defined places.

The middle-level C++ language [65] has been chosen for its efficiency and its opportunity for object-orientation. One of its competitors, Python [66], which is a general-purpose high-level programming language, has a simpler syntax and offers the opportunity of object-orientation. However, it cannot compete with the efficiency of C++. Furthermore, we have used the BLITZ++ library for handling arrays, and LPP/LAPACK libraries providing routines for linear algebra.

### 7.1 Implementation of the Hartree-Fock Method

We will in this section present the implementation of the Restricted Hartree-Fock method (RHF) for a 2-dimensional closed-shell parabolic quantum dot. The program is structured into classes, with base classes and derived classes. By relatively small changes, the code can handle other electronic systems such as atoms. The current version of the program only considers the closed-shell system where the orbitals within a shell are all occupied. An extension of the code would obviously be to handle open-shell systems. This would require a linear combination of Slater determinants in the ansatz.

We have implemented the Hartree-Fock scheme presented in Chapter 5. The Hartree-Fock orbitals in Eq. (5.2) are expanded in single-particle basis functions, and the expansion coefficients are varied in order to minimize the energy expectation value in Eq. (5.4). The minimization is done through solving the Hartree-Fock equations in (5.14) iteratively. The program calculates an approximation of the ground state energy, and computes the Hartree-Fock orbitals (expansion coefficients) that minimize the energy.

### 7.1.1 Overview

The HF scheme presented in Chapter 5 considers the case of a two-body Hamiltonian. The central equations are given in Eqs. (5.2), (5.5) and (5.14). The system under consideration is defined through

1. the single-particle matrix elements  $\langle\alpha|h|\beta\rangle$ , and
2. the two-particle interaction matrix elements  $\langle\alpha\beta|v|\gamma\delta\rangle$ ,

where  $\hat{h}$  is the single-particle Hamiltonian and  $\hat{v}$  is the interaction operator. In the parabolic quantum dot case,  $\hat{h}$  is given in Eq. (4.92), and  $\hat{v}$  is the Coulomb interaction in Eq. (4.93). Moreover, the matrix elements also define the basis set, i.e. the single-particle functions that we expand the HF orbitals in. By small changes in the code, the program can handle other functions as well. In order to run the program, two data-files must be provided:

1. One file containing single-particle matrix elements  $\langle\alpha|h|\beta\rangle$ , with setup

$$\alpha \quad \beta \quad \langle\alpha|h|\beta\rangle$$

2. One file containing interaction elements  $\langle\alpha\beta|v|\gamma\delta\rangle$ , with setup

$$\alpha \quad \beta \quad \gamma \quad \delta \quad \langle\alpha\beta|v|\gamma\delta\rangle$$

The configuration parameters is written in `parameters.inp`. An example is shown in Table 7.1.1.

```
#####
# CONFIGURATION FILE
# System: 2-dimensional Parabolic Quantum Dot
# Method: Hartree-Fock
#####

# --- Model space parameters
N = 2          # number of electrons (closed-shell, i.e. 2,6,12,20,30,...)
R = 10         # number of shells in the basis
dim = 2        # dimensions
Rf = 1         # Fermi-shell

# --- Interaction parameters
omega = 1.0    # oscillator strength

# --- Computational parameters
tol = 1e-10      # self-consistency tolerance
max_iter = 500   # maximum number of iterations
sp_energy_file = spEnergy.dat  # <p|h|q>-file
tp_energy_file = interaction.dat # <pq|v|rs>-file

# --- Storing parameters
int_type      = standard       # type of interaction
```

**Table 7.1:** `parameters.inp`: HF configuration parameters file for a 2-dimensional parabolic quantum dot.

### 7.1.2 Validation of the Code

The Hartree-Fock code should reproduce the solutions of the non-interacting system. For  $N = 2, 6, 12$  and  $20$ , the non-interacting energy is  $2\hbar\omega$ ,  $10\hbar\omega$ ,  $28\hbar\omega$  and  $60\hbar\omega$ , respectively. The code reproduced these results. However, a complete validation requires that we reproduce other HF results for the interacting system. Our program reproduces the HF results of Ref. [67].

### 7.1.3 Code Structure and Class Implementation

The program is structured into classes, with base classes and derived classes. This offers the opportunity to divide parts of the code that are specified by the system, and the parts that are identical for every system, into different fragments. Thus in order to handle other systems, we can modify the code in well-defined parts of the program. This is the beauty of object-oriented computing, see [65] for an introduction. The code is divided into four base classes, viz. `HfAlgo`, `quantumNumber`, `singleParticleElement` and `interactionElement`. These classes include members (i.e. variables and functions) that are universal in the sense that they are common for all system. Each base class has a derived class associated with it. They are named `algo1`, `qdotQuantumNumber`, `sp1` and `coulombElement`, respectively.

The code is tuned to deal with the harmonic oscillator basis (see Eq. 4.64). Since we are dealing with closed-shell systems only, we only include full shells in the basis. Thus the size of the basis is determined by the number of shells. This number defines the orbitals that are included. The objective of `qdotQuantumNumber` is to handle the single-particle orbitals. It establish the mapping

$$|\alpha\rangle \rightarrow |n\ m\ m_s\rangle, \quad (7.1)$$

shown in Table 8.1. It also establish a mapping scheme for each orbital-couple  $|\alpha\beta\rangle$ , i.e.

$$|p\rangle \rightarrow |\alpha\beta\rangle. \quad (7.2)$$

For each couple it calculates the total angular momentum

$$M = m_\alpha + m_\beta, \quad (7.3)$$

and total spin

$$M_s = m_{s_\alpha} + m_{s_\beta}, \quad (7.4)$$

and tabulates couples with equal  $M$  and  $M_s$ . Furthermore, the aim of `singleParticleElement` is to read  $\langle\alpha|h|\beta\rangle$  from file and store the elements. Since we are using the harmonic oscillator functions as basis functions, the single-particle matrix is diagonal, i.e.

$$\langle\alpha\beta|h|\gamma\delta\rangle = \varepsilon_\alpha \delta_{\alpha\beta}, \quad (7.5)$$

where  $\varepsilon_\alpha$  is given in Eq. (8.16). For each  $M$  and  $M_s$ , called a channel, the program declares an object of `interactionElement` which stores all matrix elements

$$\langle p|v|q\rangle \equiv \langle\alpha\beta|v|\gamma\delta\rangle \quad (7.6)$$

in a two-dimensional array. This can be done since

$$\langle MM_s|v|\tilde{M}\tilde{M}_s\rangle = 0, \quad (7.7)$$

when  $M \neq \tilde{M}$  or/and  $M_s \neq \tilde{M}_s$ . Thus we only store nonzero matrix elements, and avoid a four-dimensional array.

The `HfAlgo` class is an abstract base class constructed for the Hartree-Fock algorithm. We have chosen to implement the specific HF scheme (presented in Chapter 5) in the derived class `algo1`. The header file of `HfAlgo` is shown below. All members are defined in `algo1`.

```
class HfAlgo {
protected:
    int N;                                // number of particles
    int nbBasis;                            // number of basis functions
    double energyDiff;                      // energy difference
    double oldEnergy, newEnergy;            // hartree-fock energy for (i-1)'th and i'th iteration
```

```

double** HF_matrix;           // Hartree-Fock matrix
double* eigenvalues;          // eigenvalues
singleParticleElement* spMatrixElement; // sp matrix elements <a/h/b>
interactionElement** tpMatrixElement; // tp matrix elements <ab/v/cd>
quantumNumber* QN;            // quantum number object
double* off_diag;             // to be used in Householder's method
char* spEnergy_file;
char* interaction_file;
public:
    double** eigenvectors;      // eigenvectors
    double hfEnergy;             // hartree-fock energy
    int iter;                   // number of iterations in self-consistency procedure
    int maxIter;                // maximum iteration value
    double tol;                  // self-consistency tolerance
    ofstream file;
/*
 * allocate and set up single-particle matrix element object
 */
virtual void setUp_spMatrixElement() = 0;
/*
 * allocate and calculate two-particle (interaction) matrix elements
 */
virtual void setUp_tpMatrixElement() = 0;
/*
 * virtual run-algo function
 */
virtual void runAlgo() = 0;
/*
 * write HF-coeff to file
 */
virtual void write_hf_coeff_to_file() = 0;
/*
 * generates the hartree-fock matrix
 */
virtual void getHFmatrix() = 0;
/*
 * function that re-arrange the eigenvalues (with corresponding eigenvectors)
 * from the minimum value to the maximum value
 */
virtual void reArrangeEig() = 0;
/*
 * function that returns the hartree-fock energy from given single-particle HF energies
 */
virtual double getHFenergy() = 0;
/*
 *
 */
virtual void eigSolver(double**, double*, int) = 0;
/*
 * virtual destructor
 */
virtual ~HfAlgo(){
    delete[] HF_matrix;
    delete[] eigenvectors;
    delete[] eigenvalues;
    delete spMatrixElement;
    delete[] tpMatrixElement;
    delete[] off_diag;
}
};


```

Consider the Hartree-Fock equations in Eq. (5.14). We define the Hartree-Fock matrix

(HF\_matrix) as

$$h^{\text{HF}} \equiv \begin{pmatrix} \tilde{h}_{11} & \tilde{h}_{12} & \tilde{h}_{13} & \tilde{h}_{14} & \cdots & \tilde{h}_{1n} \\ \tilde{h}_{21} & \tilde{h}_{22} & \tilde{h}_{23} & \tilde{h}_{24} & \cdots & \tilde{h}_{2n} \\ \tilde{h}_{31} & \tilde{h}_{32} & \tilde{h}_{33} & \tilde{h}_{34} & \cdots & \tilde{h}_{3n} \\ \tilde{h}_{41} & \tilde{h}_{42} & \tilde{h}_{43} & \tilde{h}_{44} & \cdots & \tilde{h}_{4n} \\ \vdots & \vdots & \vdots & \vdots & \ddots & \vdots \\ \tilde{h}_{n1} & \tilde{h}_{n2} & \tilde{h}_{n3} & \tilde{h}_{n4} & \cdots & \tilde{h}_{nn} \end{pmatrix}, \quad (7.8)$$

where  $\tilde{h}_{\alpha\beta} \equiv h_{\alpha\beta}^{\text{HF}}$  (see Eq. 5.13), and  $n$  is the number of basis functions. Furthermore, we define the coefficient vector (**eigenvectors**) as

$$\mathbf{C}_k \equiv \begin{pmatrix} C_{k1} \\ C_{k2} \\ C_{k3} \\ C_{k4} \\ \vdots \\ C_{kn} \end{pmatrix}, \quad (7.9)$$

which contains the expansion coefficients of HF orbital  $k$  (see Eq. 5.2). The HF equation for orbital  $k$  can thus be written as the following matrix eigenvalue equation,

$$h^{\text{HF}} \mathbf{C}_k = \vartheta_k \mathbf{C}_k, \quad (7.10)$$

where  $\vartheta_k$  is the eigenvalue of  $\mathbf{C}_k$ . Since the HF matrix depends on all the other coefficient vectors ( $\mathbf{C}_1, \mathbf{C}_2, \dots, \mathbf{C}_n$ ), the equation is non-linear and must be solved iteratively. We end up with the following HF algorithm.

### Hartree-Fock Algorithm

1. Calculate  $\langle \alpha | h | \beta \rangle$  and  $\langle \alpha \beta | v | \gamma \delta \rangle$ .
2. Initialize coefficient vectors  $\mathbf{C}_1, \mathbf{C}_2, \dots, \mathbf{C}_N$ .
3. While not converged:
  - a. Calculate the HF matrix.
  - b. Calculate the eigenvectors and eigenvalues of the HF matrix.
  - c. Determine the eigenvectors with the  $N$  lowest eigenvalues, where  $N$  is the number of particles in the system.
  - d. Calculate new HF energy.
  - e. Calculate the difference between the new HF energy and the energy from the previous iteration.

**Results:** HF energy and expansion coefficients.

The single-particle elements  $\langle \alpha | h | \beta \rangle$  and interaction elements  $\langle \alpha \beta | v | \gamma \delta \rangle$  are read from file in `algo1::setUp_spMatrixElement()` and `algo1::setUp_tpMatrixElement()`, respectively. The **eigenvector** matrix is defined as

$$\mathbf{C} \equiv (\mathbf{C}_1 \quad \mathbf{C}_2 \quad \cdots \quad \mathbf{C}_n), \quad (7.11)$$

where  $n$  is the number of basis functions. It is initialized to

$$\mathbf{C} = \mathbf{I}, \quad (7.12)$$

i.e. the identity matrix, in `algo1::algo1(..)`. The initial HF ansatz is thus equal to the non-interacting ground state. The iteration procedure is implemented in `algo1::runAlgo()`. A pseudo-code is shown below.

```
void algo1::runAlgo(){
    ...
    while(abs(energyDiff)>tol && (iter+1)<maxIter){
        // update iteration variable
        iter += 1;
        // calculate the hartree-fock matrix
        getHFmatrix();
        // calculate new eigenvalues and eigenvectors by Householder's method
        eigSolver(HF_matrix, eigenvalues, nbBasis);
        // determine the smallest energy eigenvalues with corresponding eigenvectors
        reArrangeEig();
        // get new hartree-fock energy
        newEnergy = getHFenergy();
        // difference between new and old hartree-fock energy
        energyDiff = newEnergy - oldEnergy;
        // prepare for next iteration
        oldEnergy = newEnergy;
        ...
    } // end self-consistency loop
    // update hartree-fock energy variable
    hfEnergy = oldEnergy;
    ...
}
```

The HF energy is calculated by the formula [18]

$$E_{\text{HF}} = \frac{1}{2} \sum_{k=1}^N (\vartheta_k + \langle \varphi_k | h | \varphi_k \rangle), \quad (7.13)$$

where

$$\langle \varphi_k | h | \varphi_k \rangle = \sum_{\alpha\beta} C_{k\alpha}^* C_{k\beta} \langle \alpha | h | \beta \rangle \quad (7.14)$$

is the HF orbital in Eq. (5.2). It can be shown that this expression is equal to Eq. (5.5).

## 7.2 Implementation of the Coupled-Cluster Method

In this section we present the implementation of the Coupled-Cluster Singles and Doubles method (CCSD). The program can in principle handle other electronic systems such as the 3-dimensional parabolic quantum dot, quantum dots with other confinement potentials, atoms, molecules, and so forth, *without* modifying the code. One of the main disadvantages of a generalized-code requirement is that the code becomes less numerical efficient. Nevertheless, in the case of a parabolic quantum dot in 2 dimensions, the program is able to handle 20 electron with 110 basis functions (10 shells) in approximately 2 days. In this thesis we have chosen to develop a generalized  $m$ -scheme code that in principle is able to handle all electronic systems. The current version of the program can only handle closed-shell systems. Thus for the parabolic quantum dot in 2 dimensions, CCSD calculations can only be done for 2, 6, 12, 20, 30, 42, etc. electrons. The reason is that in the CC wavefunction, the exponentiated cluster operator  $\hat{T}$  acts on the ground state of the non-interacting system. The non-interacting ground state of an open-shell

system cannot be written as one Slater determinant, but as a linear combination of determinants. Thus in order to handle open-shell systems, a linear combination of Slater determinants must be included in the reference state.

The program calculates an approximation to the ground state energy of the closed-shell. Moreover, it determines the excitation amplitudes  $t_i^a$  and  $t_{ij}^{ab}$  that define the CC wavefunction. We will in this section present our implementation of the CCSD method, and the structure of the computer program. We will also present the validation of the code.

### 7.2.1 Overview

The many-body system under study is specified through

1. the single-particle matrix elements  $\langle \alpha | h | \beta \rangle$ , and
2. the two-particle matrix elements  $\langle \alpha \beta | v | \gamma \delta \rangle_{AS}$ ,

where  $\hat{h}$  is the one-particle Hamiltonian, and  $\hat{v}$  is the two-body interaction. The “AS” subscript denotes that the elements are antisymmetrized, i.e.

$$\langle \alpha \beta | v | \gamma \delta \rangle_{AS} = \langle \alpha \beta | v | \gamma \delta \rangle - \langle \alpha \beta | v | \gamma \delta \rangle.$$

The single-particle basis, and thus the  $N$ -particle model space, is defined through the matrix elements. The matrix elements can sometimes be difficult, or perhaps impossible, to calculate analytically. In these cases, numerical integration is necessary. Two data files must be provided in order to run the CCSD program; one containing the single-particle elements  $\langle \alpha | h | \beta \rangle$  and one containing  $\langle \alpha \beta | v | \gamma \delta \rangle$ . These files must have the following structures:

- |    |          |         |                                      |          |  |
|----|----------|---------|--------------------------------------|----------|--|
| 1. | $\alpha$ | $\beta$ | $\langle \alpha   h   \beta \rangle$ |          |  |
| 2. | $\alpha$ | $\beta$ | $\gamma$                             | $\delta$ | $\langle \alpha \beta   v   \gamma \delta \rangle$ |

Before this can be done, the model space must be determined with a proper mapping of single-particle states. Each basis function must be labeled with an integer between 0 and  $n_b - 1$ , where  $n_b$  is the number of basis functions. Functions that are in the occupied space must be labeled with integers from 0 up to  $n_h - 1$ , where  $n_h$  is the number of hole states (i.e. number of particles in the system). Basis functions that are in the unoccupied space must be labeled with integers from  $n_h$  up to  $n_b - 1$ . When a proper mapping is determined and the matrix elements are calculated and stored in two separate files, the CCSD calculation can in principle start. The main-file, `main.cpp`, requires 6 arguments:

1. `nh`: Number of hole states, i.e. occupied single-particle orbitals
2. `np`: Number of particle states, i.e. unoccupied single-particle orbitals
3. `tol`: Self-consistency tolerance
4. `max_Iter`: Maximum number of iterations
5. `sp_energy_file`:  $\langle \alpha | h | \beta \rangle$ -filename
6. `tp_energy_file`:  $\langle \alpha \beta | v | \gamma \delta \rangle$ -filename

We have written a PYTHON script (`ccsd.py`) for the 2-dimensional parabolic quantum dot. It reads configuration parameters from `parameters.inp` (shown below), starts the CCSD calculation, and organizes the results into folders. If we were to consider another electron system, a new configuration script must be provided. Alternatively, the arguments above can be typed in manually.

```
#####
# CONFIGURATION FILE
# System: 2-dimensional Parabolic Quantum Dot
# Method: Coupled-Cluster Singles and Doubles
#####

# --- Model space parameters
N = 2          # number of electrons (closed-shell, i.e. 2,6,12,20,30,...)
Rb = 2         # number of shells (1,2,3,4,5,...)

# --- Interaction parameters
omega = 1.0    # oscillator strength

# --- Computational parameters
tol = 1e-7      # self-consistency tolerance
max_iter = 500   # maximum number of iterations
sp_energy_file = spEnergy.dat # <p/h/q>-file
tp_energy_file = interaction.dat # <pq/v/rs>-file

# -- Storing parameters
int_type = standard # type of interaction
```

**Table 7.2:** `parameters.inp`: CCSD configuration parameters file for a 2-dimensional parabolic quantum dot.

### 7.2.2 Validation of the Code

When a method has been implemented in a computer program, the code must be checked for errors. The first check is often to run the program for the non-interacting case, where analytical expressions often can be obtained. The program should obviously reproduce these analytical results. However, although the program reproduces the non-interacting energies, the whole code is still not validated. The CCSD code can be validated through exact diagonalization of the Hamiltonian for the 2-particle case. In the literature, exact diagonalization is commonly called Full Configuration Interaction method (FCI). We will now give a very shallow presentation of the basic concepts of FCI. We refer to [30] for a more profound introduction.

We define the Hamiltonian of the  $N$ -electron system as

$$\hat{H} = \hat{H}_0 + \hat{V},$$

where

$$\hat{H}_0 = \sum_{i=1}^N \hat{h}_i \tag{7.15}$$

is the Hamiltonian of the non-interacting system, and

$$\hat{V} = \sum_{i=1 < j}^N \hat{v}_{ij} \tag{7.16}$$

is the interaction. Furthermore, we define

$$\mathcal{B}_1 \equiv \{|\alpha_i\rangle\}_{i=1}^{d_m} \tag{7.17}$$

to be an arbitrary basis set of the model space with dimensionality  $d_m$ . In the matrix formulation of quantum mechanics [24], the time-independent Schrödinger equation reads

$$\mathbf{H}\mathbf{c} = E\mathbf{c}, \tag{7.18}$$

where the Hamiltonian matrix is defined by its elements  $H_{mn} = \langle \Phi_m | \hat{H} | \Phi_n \rangle$ ,  $|\Phi_m\rangle$  is a Slater determinant (build up of orbitals contained in  $\mathcal{B}$ ), and

$$\mathbf{c} = \begin{pmatrix} c_1 \\ c_2 \\ c_3 \\ \vdots \\ c_{N_B} \end{pmatrix}.$$

When  $d_m \rightarrow \infty$ , the energy eigenvalue equation in (7.18) yields exact eigenvalues and eigenvectors. However, the Hilbert space must be truncated, and the solution of Eq. (7.18) within a truncated Hilbert space of dimensionality  $d_m$  gives an approximation to the eigenfunctions and eigenvalues. For a given value of  $d_m$ , the eigenfunctions is given as

$$|\Psi_\lambda\rangle = \sum_{i=1}^{d_m} c_{\lambda i} |\Phi_i\rangle. \quad (7.19)$$

By writing the Hamiltonian in second quantized form, i.e.

$$\hat{H} = \sum_{\alpha\beta} \langle \alpha | h | \beta \rangle a_\alpha^\dagger a_\beta + \frac{1}{4} \sum_{\alpha\beta\gamma\delta} \langle \alpha\beta | v | \gamma\delta \rangle a_\alpha^\dagger a_\beta^\dagger a_\delta a_\gamma,$$

we conclude that, due to Wick's theorem, the matrix element  $H_{mn} = \langle \Phi_m | \hat{H} | \Phi_n \rangle$  can be written in terms of  $\langle \alpha | h | \beta \rangle$  and  $\langle \alpha\beta | v | \gamma\delta \rangle$ .

We now choose the harmonic oscillator functions as basis functions. Analytical expressions can be obtained for  $\langle \alpha\beta | v | \gamma\delta \rangle$  (see [68]). Thus for a given size of the model space, the Hamiltonian matrix can be computed, and approximate eigenvalues and eigenfunctions can be found by diagonalization. Exact diagonalization (FCI) results can be used to validate CCSD results, and in principle all CC schemes (CCSDT, CCSDTQ, and so forth). For a given model space, the CCSDT..N energy ( $N$  is the number of electrons) is equal to the energy obtained by exact diagonalization [30]. We have validated the CCSD by considering the 2-electron parabolic quantum dot in 2 shells, i.e. 6 basis functions. We have used the following mapping:

$$\begin{aligned} |0\rangle &\rightarrow |n=0, m=0, m_s=-1/2\rangle \\ |1\rangle &\rightarrow |n=0, m=0, m_s=+1/2\rangle \\ |2\rangle &\rightarrow |n=0, m=-1, m_s=-1/2\rangle \\ |3\rangle &\rightarrow |n=0, m=-1, m_s=+1/2\rangle \\ |4\rangle &\rightarrow |n=0, m=+1, m_s=-1/2\rangle \\ |5\rangle &\rightarrow |n=0, m=+1, m_s=+1/2\rangle \end{aligned} \quad (7.20)$$

Since the Coulomb interaction is spherically symmetric and does not depend on the spin, the only nonzero interaction elements are

$$\langle M, M_s | v | M, M_s \rangle,$$

where

$$\begin{aligned} M &= m_\alpha + m_\beta = m_\gamma + m_\delta = 0 \\ M_s &= m_{s_\alpha} + m_{s_\beta} = m_{s_\gamma} + m_{s_\delta} = 0. \end{aligned}$$

We observe that  $|01\rangle$ ,  $|25\rangle$  and  $|34\rangle$  have  $M = 0$  and  $M_s = 0$ , and the dimensionality  $\mathbf{H}$  reduces to 3. The Hamiltonian reads

$$\mathbf{H} = \begin{pmatrix} \langle \Phi_{01} | H_0 | \Phi_{01} \rangle + \langle \Phi_{01} | V | \Phi_{01} \rangle & \langle \Phi_{01} | H_0 | \Phi_{25} \rangle + \langle \Phi_{01} | V | \Phi_{25} \rangle & \langle \Phi_{01} | H_0 | \Phi_{34} \rangle + \langle \Phi_{01} | V | \Phi_{34} \rangle \\ \langle \Phi_{25} | H_0 | \Phi_{01} \rangle + \langle \Phi_{25} | V | \Phi_{01} \rangle & \langle \Phi_{25} | H_0 | \Phi_{25} \rangle + \langle \Phi_{25} | V | \Phi_{25} \rangle & \langle \Phi_{25} | H_0 | \Phi_{34} \rangle + \langle \Phi_{25} | V | \Phi_{34} \rangle \\ \langle \Phi_{34} | H_0 | \Phi_{01} \rangle + \langle \Phi_{34} | V | \Phi_{01} \rangle & \langle \Phi_{34} | H_0 | \Phi_{25} \rangle + \langle \Phi_{34} | V | \Phi_{25} \rangle & \langle \Phi_{34} | H_0 | \Phi_{34} \rangle + \langle \Phi_{34} | V | \Phi_{34} \rangle \end{pmatrix},$$

where the Slater determinant is defined as

$$|\Phi_{\alpha\beta}\rangle = \frac{1}{\sqrt{2}}(|\alpha\beta\rangle - |\beta\alpha\rangle). \quad (7.21)$$

We then obtain

$$\begin{aligned} \mathbf{H} &= \begin{pmatrix} 2 + \langle 01|v|01\rangle_{AS} & \langle 01|v|25\rangle_{AS} & \langle 01|v|34\rangle_{AS} \\ \langle 25|v|01\rangle_{AS} & 4 + \langle 25|v|25\rangle_{AS} & \langle 25|v|34\rangle_{AS} \\ \langle 34|v|01\rangle_{AS} & \langle 34|v|25\rangle_{AS} & 4 + \langle 34|v|34\rangle_{AS} \end{pmatrix} \\ &= \begin{pmatrix} 3.2533141373154997 & 0.3133285343288749 & -0.3133285343288749 \\ 0.3133285343288749 & 4.8616534694044069 & -0.2349964007466563 \\ -0.3133285343288749 & -0.2349964007466563 & 4.8616534694044069 \end{pmatrix}, \end{aligned}$$

by using the formula in Eq. (8.16) and the analytical expressions in [68]. MATLAB yields the following diagonalization result,

$$E_0 = 3.15232800710.$$

Our CCSD program reproduces this result.

### 7.2.3 Code Structure and Class Implementation

The code is structured into four *abstract* base classes:

- **CCalgo**: CCSD algorithm class.
- **Amplitudes**: Class for handling the CCSD amplitudes  $t_i^a$  and  $t_{ij}^{ab}$ .
- **Fmatrix**: Class for handling the F-matrix in Eq. (6.67).
- **Interaction**: Class for handling the interaction elements  $\langle\alpha\beta|v|\gamma\delta\rangle$ .

The following derived classes have been constructed:

- **ccsd1**: Implementation of the CCSD algorithm.
- **amp1**: Implementation of the amplitude equations, structuring of amplitudes, and calculations of intermediates.
- **Fmatrix**: Structuring of  $\langle\alpha|h|\beta\rangle$ , calculation and structuring of F-matrix.
- **Interaction**: Structuring of  $\langle\alpha\beta|v|\gamma\delta\rangle$ .

Figure 7.1 shows the class diagrams of our CCSD program. We will in the following sections present each class, its structure and functionality. The focus will be on the implementations of the CCSD algorithm, the energy equation and the amplitude equations.



Figure 7.1: Class diagrams of our CCSD program.

### 7.2.4 Implementation of the CCSD Algorithm

The CCSD algorithm is implemented in `ccsd1`. The derived class inherits all members of `CCalgo` and defines these. The header file `CCalgo.hpp` is shown below.

```
//// CCalgo.hpp /**
class CCalgo {
public:
    // number of hole states
    int nh;
    // number of particle states;
    int np;
    // f-matrix object
    Fmatrix* F;
    // interaction object
    Interaction* V;
    // amplitude object
    Amplitudes* T;
    // reference energy <Phi_0|H|Phi_0>
    double E_ref;
    // new ground state energy
    double E_new;
    // old ground state energy
    double E_old;
    // self-consistency tolerance
    double tol;
    // maximum number of iterations
    int max_iter;
    // iteration variable
    int iter;
    // output file
    ofstream file;
    // <p|h|q>-file
    char* sp_energy_file;
    // <pq|v|rs>-file
    char* tp_energy_file;
/*
 * constructor
 */
CCalgo();
/*
 * destructor
 */
virtual ~CCalgo();
/*
 * start ccsd calculation
 */
virtual void start_calculation() = 0;
/*
 * self-consistent iteration procedure
 */
virtual void start_iteration_procedure() = 0;
/*
 * set up reference energy <Phi_0|H|Phi_0>
 */
virtual void calculate_ref_energy() = 0;
/*
 * calculate coupled-cluster energy
 */
virtual void calculate_energy() = 0;
};
```

The aim of constructing an abstract base class `CCalgo` is that other algorithm schemes can be implemented in derived classes. The members shown in the header file are universal in the sense that they are needed in most schemes. Moreover, additional variables and functions can of course

be included in derived classes. We have in this thesis implemented the following CCSD algorithm in `ccsd1`.

---

### Coupled-Cluster Algorithm

---

1. Set up model space
2. Calculate  $f_p^q$  and  $\langle pq|v|rs \rangle$
3. Set up reference energy  $E_{\text{ref}} = \langle \Phi_0 | \hat{H} | \Phi_0 \rangle$
4. Initialize amplitudes  $t_i^a$  and  $t_{ij}^{ab}$ , and energy variables  $E_{\text{new}}$  and  $E_{\text{old}}$
5. While not converged ( $\text{diff} > \epsilon$ )
  - a. Calculate intermediates
  - b. Calculate new 1p1h excitation amplitudes  $t_i^a$
  - c. Calculate new 2p2h excitation amplitudes  $t_{ij}^{ab}$
  - d. Calculate new energy  $E_{\text{new}}$
  - e. Calculate  $\text{diff} = E_{\text{new}} - E_{\text{old}}$
  - f. Set  $E_{\text{old}} = E_{\text{new}}$

**Results:** Ground state energy  $E_{\text{new}}$ , and excitation amplitudes  $t_i^a$  and  $t_{ij}^{ab}$ .

---

The number of basis functions, i.e. the dimension of the single-particle model space, is given as

$$n_b = n_h + n_p, \quad (7.22)$$

where  $n_h$  and  $n_p$  are given in the arguments of `main.cpp`. However, the basis in itself is determined by the single-particle matrix elements  $\langle \alpha|h|\beta \rangle$  or interaction elements  $\langle \alpha\beta|v|\gamma\delta \rangle$ . Thus the model space is determined by the matrix elements. The  $f_p^q$ -elements are calculated in `f1`. We will present `f1` and `int1` in the next two sections. Items 1-5 are carried out in `ccsd1::start_calculation()`. The code is shown below.

```
void ccsd1::start_calculation(){
    // read interaction energy elements
    V->read_interaction();
    // read <p/h/q>-elements from file
    F->read_sp_energy();
    // set up f-matrix
    F->set_up_fmatrix();
    // set up reference energy E_ref = <phi_0|H|phi_0>
    calculate_ref_energy();
    // initialize t1 amplitudes
    T->init_t1();
    // initialize t2 amplitudes
    T->init_t2();
    ...
    // initialize energy
    E_new = E_ref;
    E_old = 0;
    // start self-consistency procedure
    start_iteration_procedure();
} // end start_calculation
```

Items 5a-f are implemented in `ccsd1::start_iteration_procedure()`. The code is shown below.

```
void ccsd1::start_iteration_procedure(){
    ...
    // self-consistent iteration procedure
    while(abs(diff)>tol && iter<max_iter){
        // update iteration variable
        iter = iter + 1;
        // calculate t1 amplitudes
        T->calc_t1();
        // calculate t2 amplitude
        T->calc_t2();
        // calculate energy
        calculate_energy();
        // energy difference
        diff = E_new - E_old;
        // update amplitudes
        T->t1_old = T->t1;
        T->t2_old = T->t2;
        // update old energy variable
        E_old = E_new;
    }
    // save data
    ...
} // end start_iteration_procedure
```

We start out with initial amplitudes  $t_i^a$  and  $t_{ij}^{ab}$ . These are inserted into the amplitude equations yielding new amplitudes. Then we calculate the new CC energy, and determine whether the energy is converged or not. If not, the procedure starts over again, till convergence is obtained.

In order to calculate the ground state energy, the reference energy is needed (see Eq. 6.79). The expression reads

$$E_{\text{ref}} = \langle \Phi_0 | \hat{H} | \Phi_0 \rangle = \sum_i \langle i | h | i \rangle + \frac{1}{2} \sum_{ij} \langle ij | v | ij \rangle,$$

and is implemented in `void ccsd1::calculate_ref_energy()`.

```
void ccsd1::calculate_ref_energy(){
    ...
    // E_ref = <phi_0|H|phi_0> = SUM_i <i|h_0|i> + 0.5*SUM_ij <i j|v|i j>
    E_ref = 0.0;
    for(i=0; i<nh; i++){
        E_ref += F->s_hh(i,i);
        for(j=0; j<nh; j++){
            E_ref += 0.5*V->hhhh(i,j,i,j);
        }
    }
} // end calculate_ref_energy
```

For each iteration in the self-consistency procedure, the new CC energy is calculated for given values of  $t_i^a$  and  $t_{ij}^{ab}$ . The energy equation

$$E_{\text{CC}} = \sum_{ia} f_a^i t_i^a + \frac{1}{2} \sum_{ijab} \langle ij | v | ab \rangle t_i^a t_j^b + \frac{1}{4} \sum_{ijab} \langle ij | v | ab \rangle t_{ij}^{ab}$$

is implemented in `void ccsd1::calculate_energy()`.

```
void ccsd1::calculate_energy(){
    ...
    // <Phi_0|HT1|Phi_0>
    p1 = 0.0;
    for(i=0; i<nh; i++) {
```

```

        for(a=0; a<np; a++){
            p1 = p1 + F->f_hp(i,a)*T->t1(a,i);
        }
    }
    // <Phi_0|HT1T1|Phi_0>
    p2 = 0.0;
    for(j=0; j<nh; j++){
        for(i=0; i<nh; i++){
            for(b=0; b<np; b++){
                for(a=0; a<np; a++){
                    p2 = p2 + V->pphh(a,b,i,j)*T->t1(a,i)*T->t1(b,j);
                }
            }
        }
    }
    p2 = p2*0.5;
    // <Phi_0|HT2|Phi_0>
    p3 = 0.0;
    for(j=0; j<nh; j++){
        for(i=0; i<nh; i++){
            for(b=0; b<np; b++){
                for(a=0; a<np; a++){
                    p3 = p3 + V->pphh(a,b,i,j)*T->t2(a,b,i,j);
                }
            }
        }
    }
    p3 = p3*0.25;
    // total coupled-cluster energy
    p = p1 + p2 + p3;
    // total ground state energy
    E_new = p + E_ref;
    ...
} // end calculate_energy

```

The rest of the functions in `ccsd1::start_calculation` and `ccsd1::start_iteration_procedure()` will be described soon.

### 7.2.5 F-matrix and Interaction Elements

The F-matrix is defined in Eq. (6.66). We have chosen to construct an abstract `Fmatrix` class, and a derived class `f1` that defines its members. The header file `Fmatrix.hpp` is shown below.

```

/// Fmatrix.hpp /**
class Fmatrix {
public:
    // f-matrices
    Array<double,2> f_hh;
    Array<double,2> f_hp;
    Array<double,2> f_ph;
    Array<double,2> f_pp;
    // sp-energy matrices
    Array<double,2> s_hh;
    Array<double,2> s_hp;
    Array<double,2> s_ph;
    Array<double,2> s_pp;
    // <p/h/q>-file
    char* sp_energy_file;
    // Interaction* object
    Interaction* V;
    /*
     * constructor
     */
    Fmatrix();
}

```

```

/*
 * read single-particle energies from file
 */
virtual void read_sp_energy() = 0;
/*
 * set up f-matrix
 */
virtual void set_up_fmatrix() = 0;
/*
 * destructor
 */
virtual ~Fmatrix();
};

```

The function `f1::read_sp_energy()` reads the single-particle elements  $\langle \alpha|h|\beta \rangle$  from file, and structure the data into four arrays `s_hh`, `s_hp`, `s_ph` and `s_pp`. The `h` denotes a hole state  $i$ , while `p` denotes a particle state  $a$ . The position of `h/p` reflects the position of the states in the matrix elements, viz.

$$\begin{aligned}s_{hh} &= \langle i|h|i \rangle \\ s_{hp} &= \langle i|h|a \rangle \\ s_{ph} &= \langle a|h|i \rangle \\ s_{pp} &= \langle a|h|b \rangle.\end{aligned}$$

Furthermore, the elements of the F-matrix are defined as

$$f_p^q = \langle p|h|q \rangle + \sum_i \langle pi|v|qi \rangle, \quad (7.23)$$

where the interaction elements are antisymmetrized, and  $pqr..$  denote both hole and particle states. The elements are structured into four arrays,

$$\begin{aligned}f_{hh} &= f_i^j \\ f_{hp} &= f_i^a \\ f_{ph} &= f_a^i \\ f_{pp} &= f_a^b.\end{aligned}$$

The function `f1::set_up_fmatrix()` calculates and structures the F-matrix. The code is shown below.

```

void f1::set_up_fmatrix(){
    ...
    // set up f_hh = <i/h_0/j> + SUM_k <i k//j k>
    for(i=0; i<nh; i++){
        for(j=0; j<nh; j++){
            f_hh(i,j) = s_hh(i,j);
            for(k=0; k<nh; k++){
                f_hh(i,j) += V->hhhh(i,k,j,k);
            }
        }
    }
    // set up f_hp = <i/h_0/a> + SUM_k <i k//a k>
    // <h h//p h> = <p h//h h>
    for(i=0; i<nh; i++){
        for(a=0; a<np; a++){
            f_hp(i,a) = s_hp(i,a);
            for(k=0; k<nh; k++){
                f_hp(i,a) += V->phhh(a,k,i,k);
            }
        }
    }
}

```

```

    }
    // set up f_ph = <a|h_0|i> + SUM_k <a k||i k>
    for(a=0; a<np; a++){
        for(i=0; i<nh; i++){
            f_ph(a,i) = s_ph(a,i);
            for(k=0; k<nh; k++){
                f_ph(a,i) += V->phhh(a,k,i,k);
            }
        }
    }
    // set up f_pp = <a|h_0|b> + SUM_k <a k||b k>
    for(a=0; a<np; a++){
        for(b=0; b<np; b++){
            f_pp(a,b) = s_pp(a,b);
            for(k=0; k<nh; k++){
                f_pp(a,b) += V->pphh(a,k,b,k);
            }
        }
    }
} // end set_up_fmatrix

```

The abstract base class `Interaction`, with derived class `int1`, is constructed to handle the interaction elements  $\langle pq|v|rs \rangle$ . The header file `Interaction.hpp` is shown below.

```

/// Interaction.hpp /**
class Interaction {
public:
    // number of hole states
    int nh;
    // number of particle states
    int np;
    // interaction matrices
    Array<double,4> hhhh;      // <hh||hh>
    Array<double,4> phhh;      // <ph||hh>
    Array<double,4> pphh;      // <pp||hh>
    Array<double,4> phph;      // <ph||ph>
    Array<double,4> ppph;      // <pp||ph>
    Array<double,4> pppp;      // <pp||pp>
    // <pq|v|rs>-file
    char* tp_energy_file;
/*
 * constructor
 */
Interaction();
/*
 * read interaction elements <p q||r s> from file
 */
virtual void read_interaction() = 0;
/*
 * destructor
 */
virtual ~Interaction();
};

```

The aim of the class is to read  $\langle pq|v|rs \rangle$  from file, and structure the data into six arrays: `hhhh`, `phhh`, `pphh`, `phph`, `ppph` and `pppp`. The position of `h/p` reflects the position of the corresponding

state in the interaction element, viz.

$$\begin{aligned} \text{hhhh} &= \langle ij|v|kl \rangle \\ \text{phhh} &= \langle aj|v|kl \rangle \\ \text{pphh} &= \langle ab|v|kl \rangle \\ \text{phph} &= \langle aj|v|bl \rangle \\ \text{ppph} &= \langle ab|v|cl \rangle \\ \text{pppp} &= \langle ab|v|cd \rangle, \end{aligned}$$

where  $ijkl..$  denote hole states, and  $abcd..$  denote particle states. If we were to store  $\langle pq|v|rs \rangle$  in a four-dimensional array, we would use unnecessary amount of memory. The matrix would actually increase exponentially with respect to the size of the basis. Furthermore, since  $\langle \alpha\beta|v|\gamma\delta \rangle$  is antisymmetrized, i.e.

$$\langle pq|v|rs \rangle = \langle rs|v|pq \rangle = \langle qp|v|sr \rangle = -\langle pq|v|sr \rangle = -\langle qp|v|rs \rangle,$$

we obtain the following matrix relations,

$$\begin{aligned} \text{phhh} &= -\text{hphh} = \text{hhph} = -\text{hhhp} \\ \text{pphh} &= \text{hhpp} \\ \text{phph} &= \text{hphp} = -\text{hpph} = -\text{phhp} \\ \text{ppph} &= \text{phpp} = -\text{pphp} = -\text{hppp}. \end{aligned}$$

All possible combinations are covered. Thus it is sufficient to only store  $\langle pq|v|rs \rangle$  with  $p, q, r$  and  $s$  matching one of the six arrays. The function `int1::read_interaction()` reads  $\langle pq|v|rs \rangle$  from file and structures the elements. For a given array-name (`hhhh`, `phhh`, and so forth), we know the orbital subspace of each single-particle state in the elements. Thus we number each element from 0 up to number of hole/particle states. For example, assume we have 6 basis functions with the mapping given in Eq. (7.20). We also assume that we have 2 hole states, i.e.  $|0\rangle$  and  $|1\rangle$ . Thus we have 4 particle states:  $|2\rangle$ ,  $|3\rangle$ ,  $|4\rangle$  and  $|5\rangle$ . Let  $nh = 2$  (number of hole states) and  $np = 4$  (number of particle states). The following examples illustrate the convention used to store the interaction elements.

$$\begin{aligned} \text{phph}(1,1,2,0) &= \langle (nh+1)1|v|(nh+2)2 \rangle = \langle 31|v|40 \rangle \\ \text{pphh}(1,3,0,1) &= \langle (nh+1)(nh+3)|v|01 \rangle = \langle 35|v|01 \rangle \\ \text{ppph}(0,1,2,1) &= \langle (nh)(nh+1)|v|(nh+2)1 \rangle = \langle 23|v|41 \rangle \end{aligned}$$

### 7.2.6 Implementation of the Amplitude Equations

We will in this section present our implementation of the CCSD amplitude equations in detail. We have constructed the abstract base class `Amplitudes`, and the derived class `amp1` with the implementation. The objective of the class is to calculate new amplitudes from old (previous iteration) amplitudes. See CCSD algorithm in Sec. 7.2.4. The header file `Amplitudes.hpp` is shown below.

```
class Amplitudes {
public:
    // number of hole states
    int nh;
    // number of particle states
    int np;
    // T1 amplitude arrays
    Array<double,2> t1;
    Array<double,2> t1_old;
    // T2 amplitude array
```

```

Array<double,4> t2;
Array<double,4> t2_old;
// Fmatrix object
Fmatrix* F;
// Interaction object
Interaction* V;
// output files
ofstream file;
ofstream file2;
/*
 * intermediate arrays
 */
Array<double,2> I1;
Array<double,2> I2;
Array<double,2> I3;
Array<double,4> I4;
Array<double,4> I5;
Array<double,4> I6;
Array<double,4> I7;
Array<double,2> I8;
Array<double,4> I9;
Array<double,4> I10;
Array<double,4> I11;
/*
 * intermediates calculation
 */
virtual void calc_I1() = 0;
virtual void calc_I2() = 0;
virtual void calc_I3() = 0;
virtual void calc_I4() = 0;
virtual void calc_I5() = 0;
virtual void calc_I6() = 0;
virtual void calc_I7() = 0;
virtual void calc_I8() = 0;
virtual void calc_I9() = 0;
virtual void calc_I10() = 0;
virtual void calc_I11() = 0;
/*
 * T1 functions
 */
virtual void init_t1() = 0;
virtual void calc_t1() = 0;
virtual void calc_t1_intermediates() = 0;
virtual void calc_t1_term2(Array<double,2>) = 0;
virtual void calc_t1_term3(Array<double,2>) = 0;
virtual void calc_t1_term4(Array<double,2>) = 0;
virtual void calc_t1_term5(Array<double,2>) = 0;
virtual void calc_t1_term6(Array<double,2>) = 0;
virtual void calc_t1_term7(Array<double,2>) = 0;
virtual void calc_t1_d(Array<double,2>) = 0;
/*
 * T2 functions
 */
virtual void init_t2() = 0;
virtual void calc_t2() = 0;
virtual void calc_t2_intermediates() = 0;
virtual void calc_t2_term2(Array<double,4>) = 0;
virtual void calc_t2_term3(Array<double,4>) = 0;
virtual void calc_t2_term4(Array<double,4>) = 0;
virtual void calc_t2_term5(Array<double,4>) = 0;
virtual void calc_t2_term6(Array<double,4>) = 0;
virtual void calc_t2_term7(Array<double,4>) = 0;
virtual void calc_t2_term8(Array<double,4>) = 0;
virtual void calc_t2_d(Array<double,4>) = 0;
/*

```

```

    * constructor
    */
Amplitudes();
/*
 * destructor
 */
~Amplitudes();
/*
 * write converged amplitudes to file
 */
virtual void write_amplitudes_to_file() = 0;
};

```

We now turn to the implementation of the amplitude equations. The formal expressions are given in Eqs. (6.134) and (6.135), and the diagrammatic representations in Eqs. (6.138) and (6.141). The algebraic expressions are given in Eqs. (6.150) and (6.182). Before we turn to the implementation of the amplitude equations, manipulations of the algebraic expressions are needed.

Consider the  $\hat{T}_1$  equation in Eq. (6.150). We first rearrange the equation into

$$\begin{aligned} 0 = f_i^a + \langle ia|v|bj\rangle t_i^b + \frac{1}{2}\langle ai|v|bc\rangle t_{ji}^{bc} + & \left( f_a^b t_i^a - \langle ia|v|bc\rangle t_j^b t_i^c \right) \\ & + \left( -f_i^j t_j^a - f_a^i t_j^a t_i^b + \langle ij|v|ak\rangle t_i^b t_j^a + \langle ij|v|ab\rangle t_k^a t_i^b t_j^c + \frac{1}{2}\langle ij|v|ab\rangle t_i^c t_{jk}^{ab} \right) \\ & + \left( -\frac{1}{2}\langle ij|v|ka\rangle t_{ij}^{ba} + \frac{1}{2}\langle ij|v|ab\rangle t_k^a t_{ij}^{bc} \right) + \left( f_a^i t_{ji}^{ba} + \langle ij|v|ab\rangle t_i^a t_{jk}^{bc} \right), \end{aligned}$$

leading to

$$\begin{aligned} 0 = f_i^a + \langle ia|v|bj\rangle t_i^b + \frac{1}{2}\langle ai|v|bc\rangle t_{ji}^{bc} + & \left( f_a^b t_i^a + \langle ai|v|bc\rangle t_j^b t_i^c \right) \\ & - \left( f_i^j t_j^a + f_a^i t_j^a t_i^b + \langle ij|v|ka\rangle t_i^b t_j^a + \langle ji|v|ab\rangle t_k^a t_i^b t_j^c + \frac{1}{2}\langle ji|v|ab\rangle t_i^c t_{jk}^{ab} \right) \\ & + \frac{1}{2} \left( \langle ij|v|ka\rangle t_{ij}^{ab} + \langle ij|v|ab\rangle t_k^a t_{ij}^{bc} \right) + \left( f_a^i t_{ji}^{ba} + \langle ij|v|ab\rangle t_i^a t_{jk}^{bc} \right). \end{aligned}$$

Relabeling some of the dummy-indices and moving amplitudes outside the parentheses, yields

$$\begin{aligned} 0 = f_i^a + \langle ma|v|ei\rangle t_m^e + \frac{1}{2}\langle am|v|ef\rangle t_{im}^{ef} + & \left( f_e^a + \langle am|v|ef\rangle t_m^f \right) t_i^e \\ & - \left( f_i^m + f_e^m t_i^e + \langle mn|v|ie\rangle t_n^e + \langle mn|v|ef\rangle t_i^e t_n^f + \frac{1}{2}\langle mn|v|ef\rangle t_{in}^{ef} \right) t_m^a \\ & + \frac{1}{2} \left( \langle mn|v|ie\rangle + \langle mn|v|fe\rangle t_i^f \right) t_{mn}^{ea} + \left( f_e^m + \langle mn|v|ef\rangle t_n^f \right) t_{im}^{ae}. \end{aligned}$$

We define the following *intermediates*,

$$\begin{aligned} [I1]_e^a & \equiv f_e^a + \langle am|v|ef\rangle t_m^f \\ & = f_e^a + \langle ef|v|am\rangle t_m^f \end{aligned} \tag{7.24}$$

$$\begin{aligned} [I2]_e^m & \equiv f_e^m + \langle mn|v|ef\rangle t_n^f \\ & = f_e^m + \langle ef|v|mn\rangle t_n^f \end{aligned} \tag{7.25}$$

$$\begin{aligned} [I3]_i^m & \equiv f_i^m + f_e^m t_i^e + \langle mn|v|ie\rangle t_n^e + \langle mn|v|ef\rangle t_i^e t_n^f + \frac{1}{2}\langle mn|v|ef\rangle t_{in}^{ef} \\ & = f_i^m + \langle mn|v|ie\rangle t_n^e + \frac{1}{2}\langle mn|v|ef\rangle t_{in}^{ef} + \left( f_e^m + \langle mn|v|ef\rangle t_n^f \right) t_i^e \\ & = f_i^m - \langle ei|v|mn\rangle t_n^e + \frac{1}{2}\langle ef|v|mn\rangle t_{in}^{ef} + \left( f_e^m + \langle ef|v|mn\rangle t_n^f \right) t_i^e \\ & = f_i^m - \langle ei|v|mn\rangle t_n^e + \frac{1}{2}\langle ef|v|mn\rangle t_{in}^{ef} + [I2]_e^m t_i^e \end{aligned} \tag{7.26}$$

$$\begin{aligned}
 [I4]_{ie}^{mn} &\equiv \langle mn|v|ie\rangle + \langle fe|v|mn\rangle t_i^f \\
 &= -\langle ei|v|mn\rangle + \frac{1}{2}\langle fe|v|mn\rangle t_i^f + \frac{1}{2}\langle fe|v|mn\rangle t_i^f \\
 &= [I5]_{ie}^{mn} + \frac{1}{2}\langle fe|v|mn\rangle t_i^f
 \end{aligned} \tag{7.27}$$

$$[I5]_{ie}^{mn} \equiv -\langle ei|v|mn\rangle + \frac{1}{2}\langle fe|v|mn\rangle t_i^f \tag{7.28}$$

Using these definitions, the  $\hat{T}_1$  amplitude equation reads

$$\begin{aligned}
 0 &= f_i^a + \langle ma|v|ei\rangle t_m^e + \frac{1}{2}\langle am|v|ef\rangle t_{im}^{ef} + [I1]_e^a t_i^e - [I3]_i^m t_m^a \\
 &\quad + \frac{1}{2}[I4]_{ie}^{mn} t_{mn}^{ea} + [I2]_e^m t_{im}^{ae}.
 \end{aligned}$$

We want to obtain an equation for  $t_i^a$ . Rewriting the equation into

$$\begin{aligned}
 0 &= f_i^a + \langle ia|v|ai\rangle t_i^a + (1 - \delta_{ea}\delta_{mi})\langle ma|v|ei\rangle t_m^e + \frac{1}{2}\langle am|v|ef\rangle t_{im}^{ef} \\
 &\quad + [I1]_a^a t_i^a + (1 - \delta_{ea})[I1]_e^a t_i^e - [I3]_i^i t_i^a - (1 - \delta_{mi})[I3]_i^m t_m^a \\
 &\quad + \frac{1}{2}[I4]_{ie}^{mn} t_{mn}^{ea} + [I2]_e^m t_{im}^{ae},
 \end{aligned}$$

and collecting all  $t_i^a$ -terms, yields

$$\begin{aligned}
 0 &= f_i^a + \left( \langle ia|v|ai\rangle + [I1]_a^a - [I3]_i^i \right) t_i^a + \frac{1}{2}\langle am|v|ef\rangle t_{im}^{ef} \\
 &\quad + (1 - \delta_{ea}\delta_{mi})\langle ma|v|ei\rangle t_m^e + (1 - \delta_{ea})[I1]_e^a t_i^e - (1 - \delta_{mi})[I3]_i^m t_m^a \\
 &\quad + \frac{1}{2}[I4]_{ie}^{mn} t_{mn}^{ea} + [I2]_e^m t_{im}^{ae}.
 \end{aligned}$$

We now define

$$d_i^a \equiv -\langle ia|v|ai\rangle - [I1]_a^a + [I3]_i^i, \tag{7.29}$$

leading to the following equation for  $t_i^a$ ,

$$\begin{aligned}
 d_i^a t_i^a &= f_i^a + \frac{1}{2}\langle ef|v|am\rangle t_{im}^{ef} - (1 - \delta_{ea}\delta_{mi})\langle am|v|ei\rangle t_m^e + (1 - \delta_{ea})[I1]_e^a t_i^e \\
 &\quad - (1 - \delta_{mi})[I3]_i^m t_m^a + \frac{1}{2}[I4]_{ie}^{mn} t_{mn}^{ea} + [I2]_e^m t_{im}^{ae}.
 \end{aligned} \tag{7.30}$$

This equation is implemented in `amp1::calc_t1()`. In the following we also show the implementation of each term in Eq. (7.30). The implementation of the intermediates will be shown after the  $\hat{T}_2$  equation is modified.

```

void amp1::calc_t1(){
    ...
    // calculate intermediates I1, I2, I3, I4 and I5
    calc_t1_intermediates();
    ...
    // f_i^a
    t1 = F->f_ph;
    // 0.5<ef|v|am>t_(im)^^(ef)
    calc_t1_term2(temp);
    t1 = t1 + temp;
    // -(1 - \delta_(ea)\delta_(mi))<am|v|ei>t_m^e
    calc_t1_term3(temp);
    t1 = t1 + temp;
    // (1 - \delta_(ea))[I1]_e^at_i^a
    calc_t1_term4(temp);
}

```

```

t1 = t1 + temp;
// -(1 - \delta_{ea} \delta_{mi}) [I3]_i^m t_m^a
calc_t1_term5(temp);
t1 = t1 + temp;
// 0.5 [I4]_e^m (ie)^m (mn) t_(mn)^a (ea)
calc_t1_term6(temp);
t1 = t1 + temp;
// [I2]_e^m t_(im)^a (ae)
calc_t1_term7(temp);
t1 = t1 + temp;
// calculate denominator d_i^a
calc_t1_d(temp);

// calculate final t1 amplitudes
t1 = t1/temp;
...
} //end calc_t1
    
```

$$d_i^a t_i^a \leftarrow \frac{1}{2} \langle ef | v | am \rangle t_{im}^{ef}$$

```

void amp1::calc_t1_term2(Array<double,2> ans){
    ...
    for(i=0; i<nh; i++){
        for(a=0; a<np; a++){
            temp = 0.0;
            for(m=0; m<nh; m++){
                for(f=0; f<np; f++){
                    for(e=0; e<np; e++){
                        temp = temp + V->ppph(e,f,a,m)*t2_old(e,f,i,m);
                    }
                }
            }
            ans(a,i) = ans(a,i) + 0.5*temp;
        }
    }
} // end calc_t1_term2
    
```

$$d_i^a t_i^a \leftarrow -(1 - \delta_{ea} \delta_{mi}) \langle am | v | ei \rangle t_m^e$$

```

void amp1::calc_t1_term3(Array<double,2> ans){
    ...
    for(i=0; i<nh; i++){
        for(a=0; a<np; a++){
            temp = 0.0;
            for(m=0; m<nh; m++){
                for(e=0; e<np; e++){
                    if(m!=i || e!=a){
                        temp = temp + V->phph(a,m,e,i)*t1_old(e,m);
                    }
                }
            }
            ans(a,i) = ans(a,i) - temp;
        }
    }
} // end calc_t1_term3
    
```

$$d_i^a t_i^a \leftarrow (1 - \delta_{ea}) [I1]_e^a t_i^e$$

```

void amp1::calc_t1_term4(Array<double,2> ans){
    ...
    for(i=0; i<nh; i++){
        for(a=0; a<np; a++){
            temp = 0.0;
            for(e=0; e<np; e++){
                if(e!=a){
                    temp = temp + I1(a,e)*t1_old(e,i);
                }
            }
            ans(a,i) = ans(a,i) + temp;
        }
    }
} // end calc_t1_term4
    
```

$$d_i^a t_i^a \leftarrow -(1 - \delta_{mi}) [I3]_i^m t_m^a$$

```

void amp1::calc_t1_term5(Array<double,2> ans){
    ...
    for(i=0; i<nh; i++){
        for(a=0; a<np; a++){
            temp = 0.0;
            for(m=0; m<nh; m++){
                if(m!=i){
                    temp = temp + I3(m,i)*t1_old(a,m);
                }
            }
            ans(a,i) = ans(a,i) - temp;
        }
    }
} // end calc_t1_term5
    
```

$$d_i^a t_i^a \leftarrow \frac{1}{2} [I4]_{ie}^{mn} t_{mn}^{ea}$$

```

void amp1::calc_t1_term6(Array<double,2> ans){
    ...
    for(i=0; i<nh; i++){
        for(a=0; a<np; a++){
            temp = 0.0;
            for(n=0; n<nh; n++){
                for(m=0; m<nh; m++){
                    for(e=0; e<np; e++){
                        temp = temp + I4(m,n,i,e)*t2_old(e,a,m,n);
                    }
                }
            }
            ans(a,i) = ans(a,i) + 0.5*temp;
        }
    }
} // end calc_t1_term6
    
```

$$d_i^a t_i^a \leftarrow [I2]_e^m t_{im}^{ae}$$

```

void amp1::calc_t1_term7(Array<double,2> ans){
    ...
    for(i=0; i<nh; i++){
        for(a=0; a<np; a++){
            temp = 0.0;
            for(m=0; m<nh; m++){
        
```

```

        for(e=0; e<np; e++){
            temp = temp + I2(m,e)*t2_old(a,e,i,m);
        }
        ans(a,i) = ans(a,i) + temp;
    }
}

} // end calc_t1_term7
    
```

$$d_i^a \equiv -\langle ia|v|ai\rangle - [I1]_a^a + [I3]_i^i = \langle ai|v|ai\rangle - [I1]_a^a + [I3]_i^i,$$

```

void amp1::calc_t1_d(Array<double,2> ans){
    ...
    for(i=0; i<nh; i++){
        for(a=0; a<np; a++){
            ans(a,i) = V->phph(a,i,a,i) - I1(a,a) + I3(i,i);
        }
    }
}

} // end calc_t1_d
    
```

Consider the  $\widehat{T}_2$  equation in Eq. (6.182). We first rearrange the equation into

$$\begin{aligned}
 0 &= \langle ij|v|ab\rangle + \frac{1}{2}\langle ab|v|cd\rangle t_{ij}^{cd} \\
 &+ \left( P(ki)f_i^j t_{kj}^{ab} + P(jk)f_a^i t_{ji}^{bc} t_k^a + P(lk)\langle ij|v|ka\rangle t_{li}^{bc} t_j^a + P(kl)\langle ij|v|ab\rangle t_{ki}^{cd} t_l^a t_j^b \right. \\
 &\quad \left. + \frac{1}{2}P(kl)\langle ij|v|ab\rangle t_{ik}^{ab} t_{jl}^{cd} \right) \\
 &+ \frac{1}{2} \left( \langle ij|v|kl\rangle t_{ij}^{ab} + P(lk)\langle ij|v|ak\rangle t_l^a t_{ij}^{bc} + \frac{1}{2}\langle ij|v|ab\rangle t_{kl}^{ab} t_{ij}^{cd} + \frac{1}{4}P(kl)\langle ij|v|ab\rangle t_k^a t_{ij}^{cd} t_l^b \right) \\
 &+ \left( P(cb)f_a^b t_{ij}^{ca} - P(bc)f_a^i t_{jk}^{ba} t_k^c + P(da)\langle ai|v|bc\rangle t_{jk}^{db} t_i^c - P(cd)\langle ij|v|ab\rangle t_{kl}^{ca} t_i^d t_j^b \right. \\
 &\quad \left. - \frac{1}{2}P(cd)\langle ij|v|ab\rangle t_{kl}^{ca} t_{ij}^{db} \right) \\
 &+ \left( P(kj)P(ca)\langle ia|v|bj\rangle t_{ki}^{cb} + P(jk)P(ad)\langle ai|v|bc\rangle t_j^b t_{ik}^{cd} - P(bc)P(kl)\langle ij|v|ka\rangle t_i^b t_{jl}^{ac} \right. \\
 &\quad \left. + P(kl)P(cd)\langle ij|v|ab\rangle t_k^a t_{il}^{cb} t_j^d + \frac{1}{2}P(kl)P(cd)\langle ij|v|ab\rangle t_{ki}^{ca} t_{jl}^{bd} \right) \\
 &+ \left( -P(ba)\langle ia|v|jk\rangle t_i^b - \frac{1}{2}P(ad)\langle ai|v|bc\rangle t_{jk}^{bc} t_i^d + P(kj)P(ac)\langle ia|v|bj\rangle t_k^b t_i^c \right. \\
 &\quad \left. - \frac{1}{2}P(jk)P(ad)\langle ai|v|bc\rangle t_j^b t_k^c t_i^d + \frac{1}{2}P(ab)\langle ij|v|kl\rangle t_i^a t_j^b + \frac{1}{4}P(cd)\langle ij|v|ab\rangle t_i^c t_{kl}^{ab} t_j^d \right. \\
 &\quad \left. + \frac{1}{2}P(bc)P(kl)\langle ij|v|ka\rangle t_i^b t_l^a t_j^c + \frac{1}{4}P(kl)P(cd)\langle ij|v|ab\rangle t_k^a t_i^c t_l^b t_j^d \right) \\
 &+ \left( P(ji)\langle ab|v|ci\rangle t_j^c + \frac{1}{2}P(ij)\langle ab|v|cd\rangle t_i^c t_j^d \right)
 \end{aligned} \tag{7.31}$$

Relabeling some of the dummy-indices, and moving amplitudes and  $P$ -functions outside the parentheses, yields

$$\begin{aligned}
 &= \langle ab|v|ij\rangle + \frac{1}{2}\langle ab|v|ef\rangle t_{ij}^{ef} \\
 &- P(ij) \left( f_j^m + f_e^m t_j^e + \langle mn|v|je\rangle t_n^e + \langle mn|v|ef\rangle t_j^e t_n^f + \frac{1}{2}P(kl)\langle mn|v|ef\rangle t_{jn}^{ef} \right) t_{im}^{ab} \\
 &+ \frac{1}{2} \left( \langle mn|v|ij\rangle + P(ij)\langle mn|v|ie\rangle t_j^e + \frac{1}{2}\langle mn|v|ef\rangle t_{ij}^{ef} + \frac{1}{2}P(ij)\langle mn|v|ef\rangle t_i^e t_j^f \right) t_{mn}^{ab} \\
 &+ P(ab) \left( f_e^b - f_e^m t_m^b + \langle bm|v|ef\rangle t_m^f - \langle mn|v|ef\rangle t_m^b t_n^f - \frac{1}{2}\langle mn|v|ef\rangle t_{mn}^{bf} \right) t_{ij}^{ae} \\
 &+ P(ij)P(ab) \left( \langle mb|v|ej\rangle + \langle bm|v|fe\rangle t_j^f - \langle nm|v|je\rangle t_n^b - \langle nm|v|fe\rangle t_n^b t_j^f + \frac{1}{2}\langle nm|v|fe\rangle t_{jn}^{bf} \right) t_{im}^{ae} \\
 &- P(ab) \left( \langle mb|v|ij\rangle + \frac{1}{2}\langle mb|v|ef\rangle t_{ij}^{ef} + P(jk)\langle mb|v|ej\rangle t_i^e + \frac{1}{2}P(jk)\langle bm|v|fe\rangle t_i^e t_j^f \right. \\
 &\quad \left. - \frac{1}{2}\langle mn|v|ij\rangle t_n^b - \frac{1}{4}\langle mn|v|ef\rangle t_n^b t_{ij}^{ef} - \frac{1}{2}P(jk)\langle mn|v|ie\rangle t_n^b t_j^e - \frac{1}{4}P(jk)\langle mn|v|fe\rangle t_n^b t_j^e t_i^f \right) t_m^a \\
 &+ P(ij) \left( \langle ab|v|ej\rangle + \frac{1}{2}\langle ab|v|ef\rangle t_j^f \right) t_i^e. \tag{7.32}
 \end{aligned}$$

In order to simplify the equation, we first define

$$[I6]_{ej}^{mb} \equiv -\langle bm|v|ej\rangle + \frac{1}{2}\langle fe|v|bm\rangle t_j^f.$$

We now consider each expression in parenthesis in Eq. (7.32). We define the following intermediates:

$$\begin{aligned}
 [I7]_{ij}^{mn} &\equiv \langle mn|v|ij\rangle + P(ij)\langle mn|v|ie\rangle t_j^e + \frac{1}{2}\langle mn|v|ef\rangle t_{ij}^{ef} + \frac{1}{2}P(ij)\langle mn|v|ef\rangle t_i^e t_j^f \\
 &= \langle mn|v|ij\rangle + \frac{1}{2}\langle mn|v|ef\rangle t_{ij}^{ef} + P(ij) \left( \langle mn|v|ie\rangle + \frac{1}{2}\langle mn|v|fe\rangle t_i^f \right) t_j^e \\
 &= \langle mn|v|ij\rangle + \frac{1}{2}\langle ef|v|mn\rangle t_{ij}^{ef} + P(ij) \left( -\langle ei|v|mn\rangle + \frac{1}{2}\langle fe|v|mn\rangle t_i^f \right) t_j^e \\
 &= \langle mn|v|ij\rangle + \frac{1}{2}\langle ef|v|mn\rangle t_{ij}^{ef} + P(ij) [I5]_{ie}^{mn} t_j^e \tag{7.33}
 \end{aligned}$$

$$\begin{aligned}
 [I8]_e^b &\equiv f_e^b - f_e^m t_m^b + \langle bm|v|ef\rangle t_m^f - \langle mn|v|ef\rangle t_m^b t_n^f - \frac{1}{2}\langle mn|v|ef\rangle t_{mn}^{bf} \\
 &= \left( f_e^b + \langle bm|v|ef\rangle t_m^f \right) - \frac{1}{2}\langle mn|v|ef\rangle t_{mn}^{bf} - \left( f_e^m + \langle mn|v|ef\rangle t_n^f \right) t_m^b \\
 &= \left( f_e^b + \langle ef|v|bm\rangle t_m^f \right) - \frac{1}{2}\langle ef|v|mn\rangle t_{mn}^{bf} - \left( f_e^m + \langle ef|v|mn\rangle t_n^f \right) t_m^b \\
 &= [I1]_e^b - \frac{1}{2}\langle mn|v|ef\rangle t_{mn}^{bf} - [I2]_e^m t_m^b \tag{7.34}
 \end{aligned}$$

$$\begin{aligned}
 [I9]_{ej}^{mb} &\equiv \langle mb|v|ej\rangle + \langle bm|v|fe\rangle t_j^f - \langle nm|v|je\rangle t_n^b - \langle nm|v|fe\rangle t_n^b t_j^f + \frac{1}{2} \langle nm|v|fe\rangle t_{jn}^{bf} \\
 &= \left( \langle mb|v|ej\rangle + \frac{1}{2} \langle bm|v|fe\rangle t_j^f \right) + \frac{1}{2} \langle bm|v|fe\rangle t_j^f - \left( \langle nm|v|je\rangle + \langle nm|v|fe\rangle t_j^f \right) t_n^b \\
 &\quad + \frac{1}{2} \langle nm|v|fe\rangle t_{jn}^{bf} \\
 &= \left( -\langle bm|v|ej\rangle + \frac{1}{2} \langle fe|v|bm\rangle t_j^f \right) + \frac{1}{2} \langle fe|v|bm\rangle t_j^f \\
 &\quad - \left( -\langle ej|v|nm\rangle + \frac{1}{2} \langle fe|v|nm\rangle t_j^f + \frac{1}{2} \langle fe|v|nm\rangle t_j^f \right) t_n^b + \frac{1}{2} \langle fe|v|nm\rangle t_{jn}^{bf} \\
 &= [I6]_{ej}^{mb} + \frac{1}{2} \langle fe|v|bm\rangle t_j^f - [I4]_{je}^{nm} t_n^b + \frac{1}{2} \langle fe|v|nm\rangle t_{jn}^{bf} \tag{7.35}
 \end{aligned}$$

$$\begin{aligned}
 [I10]_{ij}^{mb} &\equiv \langle mb|v|ij\rangle + \frac{1}{2} \langle mb|v|ef\rangle t_{ij}^{ef} + P(ij) \langle mb|v|ej\rangle t_i^e + \frac{1}{2} P(ij) \langle bm|v|fe\rangle t_i^e t_j^f \\
 &\quad - \frac{1}{2} \langle mn|v|ij\rangle t_n^b - \frac{1}{4} \langle mn|v|ef\rangle t_n^b t_{ij}^{ef} - \frac{1}{2} P(ij) \langle mn|v|ie\rangle t_n^b t_i^e \\
 &\quad - \frac{1}{4} P(ij) \langle mn|v|fe\rangle t_n^b t_i^e t_j^f \\
 &= \langle mb|v|ij\rangle + \frac{1}{2} \langle mb|v|ef\rangle t_{ij}^{ef} + P(ij) \left( \langle mb|v|ej\rangle + \frac{1}{2} \langle bm|v|fe\rangle t_j^f \right) t_i^e \\
 &\quad - \frac{1}{2} \left( \langle mn|v|ij\rangle + \frac{1}{2} \langle mn|v|ef\rangle t_{ij}^{ef} + P(ij) \left( \langle mn|v|ie\rangle + \frac{1}{2} \langle mn|v|fe\rangle t_i^f \right) t_j^e \right) t_n^b \\
 &= -\langle bm|v|ij\rangle - \frac{1}{2} \langle ef|v|bm\rangle t_{ij}^{ef} + P(ij) \left( -\langle bm|v|ej\rangle + \frac{1}{2} \langle fe|v|bm\rangle t_j^f \right) t_i^e \\
 &\quad - \frac{1}{2} \left( \langle mn|v|ij\rangle + \frac{1}{2} \langle ef|v|mn\rangle t_{ij}^{ef} + P(ij) \left( -\langle ei|v|mn\rangle + \frac{1}{2} \langle fe|v|mn\rangle t_i^f \right) t_j^e \right) t_n^b \\
 &= -\langle bm|v|ij\rangle - \frac{1}{2} \langle ef|v|bm\rangle t_{ij}^{ef} + P(ij) [I6]_{ej}^{mb} t_i^e - \frac{1}{2} [I7]_{ij}^{mn} t_n^b \tag{7.36}
 \end{aligned}$$

$$[I11]_{ej}^{ab} \equiv \langle ab|v|ej\rangle + \frac{1}{2} \langle ab|v|ef\rangle t_j^f \tag{7.37}$$

The  $\widehat{T}_2$  equation can now be written as

$$\begin{aligned}
 0 &= \langle ab|v|ij\rangle + \frac{1}{2} \langle ab|v|ef\rangle t_{ij}^{ef} - P(ij) [I3]_j^m t_{im}^{ab} + \frac{1}{2} [I7]_{ij}^{mn} t_{mn}^{ab} + P(ab) [I8]_e^b t_{ij}^{ae} \\
 &\quad + P(ij)P(ab) [I9]_{ej}^{mb} t_{im}^{ae} - P(ab) [I10]_{ij}^{mb} t_m^a + P(ij) [I11]_{ej}^{ab} t_i^e. \tag{7.38}
 \end{aligned}$$

We want to obtain an equation for  $t_{ij}^{ab}$ . Rewriting the equation into

$$\begin{aligned}
 0 &= \langle ab|v|ij\rangle + \frac{1}{2} \langle ab|v|ab\rangle t_{ij}^{ab} + \frac{1}{2} (1 - \delta_{ea} \delta_{fb}) \langle ab|v|ef\rangle t_{ij}^{ef} - P(ij) [I3]_j^j t_{ij}^{ab} \\
 &\quad - P(ij) (1 - \delta_{mj}) [I3]_j^m t_{im}^{ab} + \frac{1}{2} [I7]_{ij}^{ij} t_{ij}^{ab} + \frac{1}{2} (1 - \delta_{mi} \delta_{nj}) [I7]_{ij}^{mn} t_{mn}^{ab} \\
 &\quad + P(ab) [I8]_b^b t_{ij}^{ab} + P(ab) (1 - \delta_{eb}) [I8]_e^b t_{ij}^{ae} + P(ij)P(ab) [I9]_{ej}^{mb} t_{im}^{ae} \\
 &\quad - P(ab) [I10]_{ij}^{mb} t_m^a + P(ij) [I11]_{ej}^{ab} t_i^e. \tag{7.39}
 \end{aligned}$$

and collecting all  $t_{ij}^{ab}$ -terms, yields

$$\begin{aligned}
 0 = & \langle ab|v|ij\rangle + \left( \frac{1}{2}\langle ab|v|ab\rangle - P(ij)[I3]_j^j + \frac{1}{2}[I7]_{ij}^{ij} + P(ab)[I8]_b^b \right) t_{ij}^{ab} \\
 & + \frac{1}{2}(1 - \delta_{ea}\delta_{fb})\langle ab|v|ef\rangle t_{ij}^{ef} - P(ij)(1 - \delta_{mj})[I3]_j^m t_{im}^{ab} \\
 & + \frac{1}{2}(1 - \delta_{mi}\delta_{nj})[I7]_{ij}^{mn} t_{mn}^{ab} + P(ab)(1 - \delta_{eb})[I8]_e^b t_{ij}^{ae} \\
 & + P(ij)P(ab)[I9]_{ej}^{mb} t_{im}^{ae} - P(ab)[I10]_{ij}^{mb} t_m^a + P(ij)[I11]_{ej}^{ab} t_i^e.
 \end{aligned} \tag{7.40}$$

By defining

$$d_{ij}^{ab} \equiv -\frac{1}{2}\langle ab|v|ab\rangle + P(ij)[I3]_j^j - \frac{1}{2}[I7]_{ij}^{ij} - P(ab)[I8]_b^b, \tag{7.41}$$

we obtain the following  $\widehat{T}_2$  amplitude equation,

$$\begin{aligned}
 d_{ij}^{ab} t_{ij}^{ab} = & \langle ab|v|ij\rangle + \frac{1}{2}(1 - \delta_{ea}\delta_{fb})\langle ab|v|ef\rangle t_{ij}^{ef} - P(ij)(1 - \delta_{mj})[I3]_j^m t_{im}^{ab} \\
 & + \frac{1}{2}(1 - \delta_{mi}\delta_{nj})[I7]_{ij}^{mn} t_{mn}^{ab} + P(ab)(1 - \delta_{eb})[I8]_e^b t_{ij}^{ae} \\
 & + P(ij)P(ab)[I9]_{ej}^{mb} t_{im}^{ae} - P(ab)[I10]_{ij}^{mb} t_m^a + P(ij)[I11]_{ej}^{ab} t_i^e.
 \end{aligned} \tag{7.42}$$

This equation is implemented in `amp1::calc_t2()`, which is shown below. We will in the following also show the implementation of each term in Eq. (7.42).

```

void amp1::calc_t2(){
    ...
    // calculate intermediates I6, I7, I8, I9, I10 and I11
    calc_t2_intermediates();
    ...
    // <ab/v|ij>
    t2 = V->pphh;
    // 0.5(1 - \delta_{ea}\delta_{fb})<ab/v|ef>t_(ij)^^(ef)
    calc_t2_term2(temp);
    t2 = t2 + temp;
    // - P(ij)(1 - \delta_{mj})[I3]_j^m t_(im)^^(ab)
    calc_t2_term3(temp);
    t2 = t2 + temp;
    // 0.5(1 - \delta_{mi}\delta_{nj})[I7]_(ij)^^(mn)t_(mn)^^(ab)
    calc_t2_term4(temp);
    t2 = t2 + temp;
    // P(ab)(1 - \delta_{eb})[I8]_e^bt_(ij)^^(ae)
    calc_t2_term5(temp);
    t2 = t2 + temp;
    // P(ij)P(ab)[I9]_(ej)^^(mb)t_(im)^^(ae)
    calc_t2_term6(temp);
    t2 = t2 + temp;
    // -P(ab)[I10]_(ij)^^(mb)t_m^a
    calc_t2_term7(temp);
    t2 = t2 + temp;
    // P(ij)[I11]_(ej)^^(ab)t_i^e
    calc_t2_term8(temp);
    t2 = t2 + temp;
    // calculating denominator d_(ij)^^(ab)
    calc_t2_d(temp);

    // calculating final t2 amplitudes
    t2 = t2/temp;
    ...
} // end t2_calc

```

$$d_{ij}^{ab} \leftarrow \frac{1}{2}(1 - \delta_{ea}\delta_{fb})\langle ab|v|ef\rangle t_{ij}^{ef}$$

```

void amp1::calc_t2_term2(Array<double,4> ans){
    ...
    for(j=0; j<nh; j++){
        for(i=0; i<nh; i++){
            for(b=0; b<np; b++){
                for(a=0; a<np; a++){
                    temp = 0.0;
                    for(f=0; f<np; f++){
                        for(e=0; e<np; e++){
                            if(a!=e || b!=f){
                                temp = temp + V->pppp(a,b,e,f)*t2_old(e,f,i,j);
                            }
                        }
                    }
                    ans(a,b,i,j) = 0.5*temp;
                }
            }
        }
    }
} // end calc_t2_term2

```

$$d_{ij}^{ab} \leftarrow -P(ij)(1 - \delta_{mj}) [I3]_j^m t_{im}^{ab}$$

```

void amp1::calc_t2_term3(Array<double,4> ans){
    ...
    for(j=0; j<nh; j++){
        for(i=0; i<nh; i++){
            for(b=0; b<np; b++){
                for(a=0; a<np; a++){
                    temp = 0.0;
                    for(m=0; m<nh; m++){
                        temp1 = 0.0;
                        temp2 = 0.0;
                        if(j!=m){
                            temp1 = I3(m,j)*t2_old(a,b,i,m);
                        }
                        if(i!=m){
                            temp2 = I3(m,i)*t2_old(a,b,j,m);
                        }
                        temp = temp + (temp1 - temp2);
                    }
                    ans(a,b,i,j) = -temp;
                }
            }
        }
    }
} // end calc_t2_term3

```

$$d_{ij}^{ab} \leftarrow \frac{1}{2}(1 - \delta_{mi}\delta_{nj}) [I7]_{ij}^{mn} t_{mn}^{ab}$$

```

void amp1::calc_t2_term4(Array<double,4> ans){
    ...
    for(j=0; j<nh; j++){
        for(i=0; i<nh; i++){
            for(b=0; b<np; b++){
                for(a=0; a<np; a++){
                    temp = 0.0;
                    for(n=0; n<nh; n++){
                        for(m=0; m<nh; m++){

```

```

        if(i!=m || j!=n){
            temp = temp + I7(m,n,i,j)*t2_old(a,b,m,n);
        }
    }
}
ans(a,b,i,j) = 0.5*temp;
}
}
}

} // end calc_t2_term4

```

$$d_{ij}^{ab} \leftarrow P(ab)(1 - \delta_{eb}) [I8]_e^b t_{ij}^{ae}$$

```

void amp1::calc_t2_term5(Array<double,4> ans){
    ...
    for(j=0; j<nh; j++){
        for(i=0; i<nh; i++){
            for(b=0; b<np; b++){
                for(a=0; a<np; a++){
                    temp = 0.0;
                    for(e=0; e<np; e++){
                        temp1 = 0.0;
                        temp2 = 0.0;
                        if(b!=e){
                            temp1 = I8(b,e)*t2_old(a,e,i,j);
                        }
                        if(a!=e){
                            temp2 = I8(a,e)*t2_old(b,e,i,j);
                        }
                        temp = temp + (temp1 - temp2);
                    }
                    ans(a,b,i,j) = temp;
                }
            }
        }
    }
} // end calc_t2_term5

```

$$d_{ij}^{ab} \leftarrow P(ij)P(ab) [I9]_{ej}^{mb} t_{im}^{ae}$$

```

void amp1::calc_t2_term6(Array<double,4> ans){
    ...
    for(j=0; j<nh; j++){
        for(i=0; i<nh; i++){
            for(b=0; b<np; b++){
                for(a=0; a<np; a++){
                    temp = 0.0;
                    for(m=0; m<nh; m++){
                        for(e=0; e<np; e++){
                            temp = temp + ((I9(m,b,e,j)*t2_old(a,e,i,m) - I9(m,a,e,j)*t2_old(b,e,i,m)) -
                                (I9(m,b,e,i)*t2_old(a,e,j,m) - I9(m,a,e,i)*t2_old(b,e,j,m)));
                        }
                    }
                    ans(a,b,i,j) = temp;
                }
            }
        }
    }
} // end calc_t2_term6

```

$$d_{ij}^{ab} \leftarrow -P(ab) [I10]_{ij}^{mb} t_m^a$$

```

void amp1::calc_t2_term7(Array<double,4> ans){
    ...
    /*
     * t1 used instead if t1_old for a quicker convergence
     */
    for(j=0; j<nh; j++){
        for(i=0; i<nh; i++){
            for(b=0; b<np; b++){
                for(a=0; a<np; a++){
                    temp = 0.0;
                    for(m=0; m<nh; m++){
                        temp = temp + (I10(m,b,i,j)*t1(a,m) - I10(m,a,i,j)*t1(b,m));
                    }
                    ans(a,b,i,j) = -temp;
                }
            }
        }
    }
} // end calc_t2_term7

```

$$d_{ij}^{ab} \leftarrow P(ij) [I11]_{ej}^{ab} t_i^e$$

```

void amp1::calc_t2_term8(Array<double,4> ans){
    ...
    /*
     * t1 used instead if t1_old for a quicker convergence
     */
    for(j=0; j<nh; j++){
        for(i=0; i<nh; i++){
            for(b=0; b<np; b++){
                for(a=0; a<np; a++){
                    temp = 0.0;
                    for(e=0; e<np; e++){
                        temp = temp + (I11(a,b,e,j)*t1(e,i) - I11(a,b,e,i)*t1(e,j));
                    }
                    ans(a,b,i,j) = temp;
                }
            }
        }
    }
} // end calc_t2_term8

```

$$d_{ij}^{ab} \equiv P(ij) [I3]_j^j - P(ab) [I8]_b^b - \frac{1}{2} [I7]_{ij}^{ij} - \frac{1}{2} \langle ab|v|ab\rangle$$

```

void amp1::calc_t2_d(Array<double,4> ans){
    ...
    for(j=0; j<nh; j++){
        for(i=0; i<nh; i++){
            for(b=0; b<np; b++){
                for(a=0; a<np; a++){
                    ans(a,b,i,j) = I3(i,i) + I3(j,j) - I8(a,a) - I8(b,b) - 0.5*I7(i,j,i,j) -
                        0.5*V->pppp(a,b,a,b);
                }
            }
        }
    }
} // end calc_t2_d

```

We will in the following show the implementation of the intermediates.

$$[I1]_e^a = f_e^a + \langle ef|v|am\rangle t_m^f$$

```
void amp1::calc_I1(){
    ...
    I1 = F->f_pp;
    for(e=0; e<np; e++){
        for(a=0; a<np; a++){
            for(m=0; m<nh; m++){
                for(f=0; f<np; f++){
                    I1(a,e) = I1(a,e) + V->ppph(e,f,a,m)*t1(f,m);
                }
            }
        }
    }
} // end calc_I1
```

$$[I2]_e^m = f_e^m + \langle ef|v|mn\rangle t_n^f$$

```
void amp1::calc_I2(){
    ...
    I2 = F->f_hp;
    for(e=0; e<np; e++){
        for(m=0; m<nh; m++){
            for(n=0; n<nh; n++){
                for(f=0; f<np; f++){
                    I2(m,e) = I2(m,e) + V->pphh(e,f,m,n)*t1(f,n);
                }
            }
        }
    }
} // end calc_I2
```

$$[I3]_i^m = f_i^m - \langle ei|v|mn\rangle t_n^e + \frac{1}{2} \langle ef|v|mn\rangle t_{in}^{ef} + [I2]_e^m t_i^e$$

```
void amp1::calc_I3(){
    ...
    I3 = F->f_hh;
    for(i=0; i<nh; i++){
        for(m=0; m<nh; m++){
            for(n=0; n<nh; n++){
                for(e=0; e<np; e++){
                    I3(m,i) = I3(m,i) - V->phhh(e,i,m,n)*t1(e,n);
                }
            }
        }
        for(i=0; i<nh; i++){
            for(m=0; m<nh; m++){
                for(n=0; n<nh; n++){
                    for(f=0; f<np; f++){
                        for(e=0; e<np; e++){
                            I3(m,i) = I3(m,i) + 0.5*V->pphh(e,f,m,n)*t2(e,f,i,n);
                        }
                    }
                }
            }
        }
    }
}
```

```

        for(e=0; e<np; e++){
            I3(m,i) = I3(m,i) + I2(m,e)*t1(e,i);
        }
    }
}

} // end calc_I3
    
```

$$[I4]_{ie}^{mn} = [I5]_{ie}^{mn} + \frac{1}{2} \langle fe|v|mn\rangle t_i^f$$

```

void amp1::calc_I4(){
    ...
    I4 = I5;
    for(e=0; e<np; e++){
        for(i=0; i<nh; i++){
            for(n=0; n<nh; n++){
                for(m=0; m<nh; m++){
                    for(f=0; f<np; f++){
                        I4(m,n,i,e) = I4(m,n,i,e) + 0.5 * V->pphh(f,e,m,n)*t1(f,i);
                    }
                }
            }
        }
    }
}

} // end calc_I4
    
```

$$[I5]_{ie}^{mn} = -\langle ei|v|mn\rangle + \frac{1}{2} \langle fe|v|mn\rangle t_i^f$$

```

void amp1::calc_I5(){
    ...
    I5 = 0.0;
    for(e=0; e<np; e++){
        for(i=0; i<nh; i++){
            for(n=0; n<nh; n++){
                for(m=0; m<nh; m++){
                    I5(m,n,i,e) = -V->phhh(e, i, m, n);
                    for(f=0; f<np; f++){
                        I5(m,n,i,e) = I5(m,n,i,e) + 0.5 * V->pphh(f,e,m,n)*t1(f,i);
                    }
                }
            }
        }
    }
}

} // end calc_I5
    
```

$$[I6]_{ej}^{mb} = -\langle bm|v|ej\rangle + \frac{1}{2} \langle fe|v|bm\rangle t_j^f$$

```

void amp1::calc_I6(){
    ...
    I6 = 0.0;
    for(j=0; j<nh; j++){
        for(e=0; e<np; e++){
            for(m=0; m<nh; m++){
                for(b=0; b<np; b++){
                    I6(m,b,e,j) = -V->pphh(b,m,e,j);
                }
            }
        }
    }
}

} // end calc_I6
    
```

```

    for(b=0; b<np; b++){
        for(e=0; e<np; e++){
            for(j=0; j<nh; j++){
                for(f=0; f<np; f++){
                    I6(m,b,e,j) = I6(m,b,e,j) + 0.5 * V->ppph(f,e,b,m)*t1(f,j);
                }
            }
        }
    }
} // end calc_I6

```

$$[I7]_{ij}^{mn} = \langle mn|v|ij\rangle + \frac{1}{2}\langle ef|v|mn\rangle t_{ij}^{ef} + P(ij) [I5]_{ie}^{mn} t_j^e$$

```

void amp1::calc_I7(){
    ...
    double temp = 0.0;
    I7 = V->hhhh;
    for(j=0; j<nh; j++){
        for(i=0; i<nh; i++){
            for(n=0; n<nh; n++){
                for(m=0; m<nh; m++){
                    temp = 0.0;
                    for(f=0; f<np; f++){
                        for(e=0; e<np; e++){
                            temp = temp + V->pphh(e,f,m,n)*t2(e,f,i,j);
                        }
                    }
                    I7(m,n,i,j) = I7(m,n,i,j) + 0.5*temp;
                }
            }
        }
    }
    for(j=0; j<nh; j++){
        for(i=0; i<nh; i++){
            for(n=0; n<nh; n++){
                for(m=0; m<nh; m++){
                    temp = 0.0;
                    for(e=0; e<np; e++){
                        temp = temp + (I5(m,n,i,e)*t1(e,j) - I5(m,n,j,e)*t1(e,i));
                    }
                    I7(m,n,i,j) = I7(m,n,i,j) + temp;
                }
            }
        }
    }
} // end calc_I7

```

$$[I8]_e^b = [I1]_e^b - \frac{1}{2}\langle mn|v|ef\rangle t_{mn}^{bf} - [I2]_e^m t_m^b$$

```

void amp1::calc_I8(){
    ...
    I8 = I1;
    for(e=0; e<np; e++){
        for(b=0; b<np; b++){
            for(m=0; m<nh; m++){
                for(n=0; n<nh; n++){
                    for(f=0; f<np; f++){
                        I8(b,e) = I8(b,e) - 0.5*V->pphh(e,f,m,n)*t2(b,f,m,n);
                    }
                }
            }
        }
    }
} // end calc_I8

```

```

        }
    }

    for(e=0; e<np; e++){
        for(b=0; b<np; b++){
            for(m=0; m<nh; m++){
                I8(b,e) = I8(b,e) - I2(m,e) * t1(b,m);
            }
        }
    }
} // end calc_I8

```

$$[I9]_{ej}^{mb} = [I6]_{ej}^{mb} + \frac{1}{2} \langle fe|v|bm\rangle t_j^f - [I4]_{je}^{nm} t_n^b + \frac{1}{2} \langle fe|v|nm\rangle t_{jn}^{bf}$$

```

void amp1::calc_I9(){
    ...
    I9 = I6;
    for(m=0; m<nh; m++){
        for(b=0; b<np; b++){
            for(e=0; e<np; e++){
                for(j=0; j<nh; j++){
                    for(f=0; f<np; f++){
                        I9(m,b,e,j) = I9(m,b,e,j) + 0.5 * V->ppph(f,e,b,m)*t1(f,j);
                    }
                }
            }
        }
    }
    for(m=0; m<nh; m++){
        for(b=0; b<np; b++){
            for(e=0; e<np; e++){
                for(j=0; j<nh; j++){
                    for(n=0; n<nh; n++){
                        I9(m,b,e,j) = I9(m,b,e,j) - I4(n,m,j,e)*t1(b,n);
                    }
                }
            }
        }
    }
    for(m=0; m<nh; m++){
        for(b=0; b<np; b++){
            for(e=0; e<np; e++){
                for(j=0; j<nh; j++){
                    for(n=0; n<nh; n++){
                        for(f=0; f<np; f++){
                            I9(m,b,e,j) = I9(m,b,e,j) + 0.5*V->pphh(f,e,n,m)*t2(b,f,j,n);
                        }
                    }
                }
            }
        }
    }
} // end calc_I9

```

$$[I10]_{ij}^{mb} = -\langle bm|v|ij\rangle - \frac{1}{2} \langle ef|v|bm\rangle t_{ij}^{ef} + P(ij) [I6]_{ej}^{mb} t_i^e - \frac{1}{2} [I7]_{ij}^{mn} t_n^b$$

```

void amp1::calc_I10(){
    ...
    double temp = 0.0;
    I10 = 0.0;
    for(j=0; j<nh; j++){

```

```

    for(i=0; i<nh; i++){
        for(m=0; m<nh; m++){
            for(b=0; b<np; b++){
                I10(m,b,i,j) = -V->phhh(b,m,i,j);
            }
        }
    }

    for(j=0; j<nh; j++){
        for(i=0; i<nh; i++){
            for(b=0; b<np; b++){
                for(m=0; m<nh; m++){
                    temp = 0.0;
                    for(f=0; f<np; f++){
                        for(e=0; e<np; e++){
                            temp = temp - V->ppph(e,f,b,m)*t2(e,f,i,j);
                        }
                    }
                    I10(m,b,i,j) = I10(m,b,i,j) + 0.5*temp;
                }
            }
        }
    }

    for(j=0; j<nh; j++){
        for(i=0; i<nh; i++){
            for(b=0; b<np; b++){
                for(m=0; m<nh; m++){
                    temp = 0.0;
                    for(e=0; e<np; e++){
                        temp = temp + (I6(m,b,e,j)*t1(e,i) - I6(m,b,e,i)*t1(e,j));
                    }
                    I10(m,b,i,j) = I10(m,b,i,j) + temp;
                }
            }
        }
    }

    for(j=0; j<nh; j++){
        for(i=0; i<nh; i++){
            for(b=0; b<np; b++){
                for(m=0; m<nh; m++){
                    temp = 0.0;
                    for(n=0; n<nh; n++){
                        temp = temp + I7(m,n,i,j)*t1(b,n);
                    }
                    I10(m,b,i,j) = I10(m,b,i,j) - 0.5*temp;
                }
            }
        }
    }
}

// end calc_I10

```

$$[I11]_{ej}^{ab} = \langle ab|v|ej\rangle + \frac{1}{2}\langle ab|v|ef\rangle t_j^f.$$

```

void ampi::calc_I11(){
    ...
    double temp = 0.0;
    I11 = V->ppph;
    for(j=0; j<nh; j++){
        for(e=0; e<np; e++){
            for(b=0; b<np; b++){
                for(a=0; a<np; a++){
                    temp = 0.0;
                    for(f=0; f<np; f++){

```

```
    temp = temp + V->pppp(a,b,e,f)*t1(f,j);
}
I11(a,b,e,j) = I11(a,b,e,j) + 0.5*temp;
}
}
}

} // end calc_I11
```

# Chapter 8

## Numerical Results and Analysis

### 8.1 Standard interaction

In this section we present the Hartree-Fock (HF) and Coupled-Cluster Singles and Doubles (CCSD) results for a 2-dimensional parabolic quantum dot. The model Hamiltonian reads

$$\hat{H} = -\frac{\hbar^2}{2m^*} \sum_{i=1}^N \nabla_i^2 + \frac{1}{2} m^* \omega^2 \sum_{i=1}^N r_i^2 + \frac{e^2}{4\pi\epsilon_0\epsilon_r} \sum_{i=1 < j}^N \frac{1}{r_{ij}}, \quad (8.1)$$

see Section 4.4 for a discussion. In Section 4.5 we scaled the Hamiltonian into the following dimensionless form,

$$\hat{H}' = -\frac{\omega'}{2} \sum_{i=1}^N \nabla_i'^2 + \frac{1}{2} \omega' \sum_{i=1}^N r_i'^2 + \sqrt{\omega'} \sum_{i=1 < j}^N \frac{1}{r_{ij}'}, \quad (8.2)$$

where

$$\omega' = \frac{\hbar\kappa^2}{m^*} \omega \quad (8.3)$$

$$\kappa = \frac{4\pi\epsilon_0\epsilon_r\hbar}{e^2} \quad (8.4)$$

$$r_i' = l_0 r_i \quad (8.5)$$

$$r_{ij}' = l_0 r_{ij} \quad (8.6)$$

$$\nabla_i'^2 = \frac{1}{l_0^2} \nabla_i^2 \quad (8.7)$$

$$l_0 = \frac{\hbar\kappa}{m^*}. \quad (8.8)$$

We refer to Section 4.5 for a full derivation. Length is now measured in units of  $l_0$ ,  $\omega'$  in units of  $\omega_k$  and energy in units of effective Hartrees  $E_H^*$ , defined as

$$E_H^* \equiv \frac{m^*}{\kappa^2}. \quad (8.9)$$

We observe from Eq. (8.2) that the frequency constitutes an important parameter in the system. A change in the frequency will influence all parts that contribute to the total energy, and thus change the energy spectrum. Qualitatively, this is what we expect. For example, when  $\omega$  increases, the harmonic oscillator potential pushes the electrons closer together. This would obviously affect the contributions from both the electron-electron repulsion, and the kinetic energy. From an experimental point of view, the frequency is a controllable quantity. It is therefore interesting to analyze numerical calculations for different frequencies in order to

gain important information about the system, such as the correlation energy. In addition, the reliability of numerical methods can be studied by such an analysis.

All numerical calculations have been done with the dimensionless Hamiltonian in Eq. (8.2), and the results are presented in this scaling. Therefore, we will from now on drop the prime-subscript. In this section we present the HF and CCSD results obtained with standard interaction, which we define as the Coulomb interaction. The interaction between two electrons is obviously given by the Coulomb interaction. However, the reason that we define the Coulomb interaction as the standard interaction is that we later introduce an effective interaction in order to improve our results. We will present the basic ideas of effective interaction theory in Section 8.2. We will in this section only consider the results obtained with standard interaction.

Both HF and CCSD require a single-particle basis set, and we have in these calculations chosen the eigenfunctions of

$$\left( -\frac{\omega}{2} \sum_{i=1}^N \nabla_i^2 + \frac{1}{2} \omega \sum_{i=1}^N r_i^2 \right) \psi_\alpha(\mathbf{r}) = \varepsilon_\alpha \psi_\alpha(\mathbf{r}) \quad (8.10)$$

as basis functions, where  $\alpha$  denotes a set of three quantum numbers  $(n, m, m_s)$ . We identify this equation as the time-independent Schrödinger equation for the single-electron parabolic quantum (see Section 4.3), in our dimensionless scaling. Multiplying the Hamiltonian in Eq. (8.10) by  $E_H^*$  yields back the expression in Eq. (4.28). Furthermore, the total wavefunction  $\psi_\alpha(\mathbf{r})$  is given as (see Section 2.2.3)

$$\psi_\alpha(\mathbf{r}) = \phi_{nm}(x, y) \otimes |\chi_{m_s}\rangle, \quad (8.11)$$

where  $\phi_{nm}(x, y)$  is the spatial part, and  $|\chi_{m_s}\rangle$  is the spin part. The quantum number  $m_s$  is associated with the  $z$ -projection of the spin, and is given as

$$m_s = \pm \frac{1}{2}, \quad (8.12)$$

with corresponding eigenvectors

$$\left| \frac{1}{2} \right\rangle \equiv |+\rangle \quad (8.13)$$

$$\left| -\frac{1}{2} \right\rangle \equiv |-\rangle, \quad (8.14)$$

which are often referred to as spin up and spin down, respectively, see Section (2.2.2). The spatial part of the wavefunction satisfies

$$\left( -\frac{\omega}{2} \sum_{i=1}^N \nabla_i^2 + \frac{1}{2} \omega \sum_{i=1}^N r_i^2 \right) \phi_{nm}(x, y) = \varepsilon_{nm} \phi_{nm}(x, y), \quad (8.15)$$

where  $n$  and  $m$  are quantum numbers, and  $\varepsilon_{nm}$  is the energy eigenvalue. Since the Hamiltonian in Eq. (8.15) is “linear” in  $\omega$ , the eigenfunctions do not depend on the frequency. However, the energy eigenvalue  $\varepsilon_{nm}$  depends on  $\omega$ , and is given as (see Eq. 4.65)

$$\varepsilon_{nm} = (1 + 2n + |m|)\omega. \quad (8.16)$$

The eigenfunctions of Eq. (8.15) is given in Eq. (4.57) with  $m^* = \hbar = 1$ . We will refer to the total wavefunctions in Eq. (8.11) as harmonic oscillator functions.

Since  $\hat{h}$  is the single-electron Hamiltonian in Eq. (8.15), our choice of basis leads to a diagonal single-particle matrix,

$$\langle \alpha | h | \beta \rangle = \delta_{\alpha\beta} \varepsilon_\alpha, \quad (8.17)$$

where  $\alpha = (n, m, m_s)$  and  $\varepsilon_\alpha = \varepsilon_{nm}$ . As pointed out in the previous chapter, both the HF and the CCSD program (see Chapter 7) reads  $\langle \alpha | h | \beta \rangle$  and  $\langle \alpha \beta | v | \gamma \delta \rangle$  from file. The required file structure is shown in Sections (7.1) and (7.2). We established the mapping  $\alpha \rightarrow (n, m, m_s)$  shown in Table 8.1. Table 8.2 shows the shell structure in the  $\alpha$ -labelling of harmonic oscillator functions. Furthermore, in order to calculate the antisymmetrized interaction elements

$$\langle \alpha \beta | v | \gamma \delta \rangle, \quad (8.18)$$

where  $v$  is the Coulomb interaction (standard interaction), we have used the analytical expressions derived in [68].

$\alpha$	n	m	s																				
0	0	0	-1	20	0	-4	-1	40	2	1	-1	60	1	-5	-1	80	2	-4	-1	100	2	5	-1
1	0	0	1	21	0	-4	1	41	2	1	1	61	1	-5	1	81	2	-4	1	101	2	5	1
2	0	-1	-1	22	0	4	-1	42	0	-6	-1	62	1	5	-1	82	2	4	-1	102	3	-3	-1
3	0	-1	1	23	0	4	1	43	0	-6	1	63	1	5	1	83	2	4	1	103	3	-3	1
4	0	1	-1	24	1	-2	-1	44	0	6	-1	64	2	-3	-1	84	3	-2	-1	104	3	3	-1
5	0	1	1	25	1	-2	1	45	0	6	1	65	2	-3	1	85	3	-2	1	105	3	3	1
6	0	-2	-1	26	1	2	-1	46	1	-4	-1	66	2	3	-1	86	3	2	-1	106	4	-1	-1
7	0	-2	1	27	1	2	1	47	1	-4	1	67	2	3	1	87	3	2	1	107	4	-1	1
8	0	2	-1	28	2	0	-1	48	1	4	-1	68	3	-1	-1	88	4	0	-1	108	4	1	-1
9	0	2	1	29	2	0	1	49	1	4	1	69	3	-1	1	89	4	0	1	109	4	1	1
10	1	0	-1	30	0	-5	-1	50	2	-2	-1	70	3	1	-1	90	0	-9	-1				
11	1	0	1	31	0	-5	1	51	2	-2	1	71	3	1	1	91	0	-9	1				
12	0	-3	-1	32	0	5	-1	52	2	2	-1	72	0	-8	-1	92	0	9	-1				
13	0	-3	1	33	0	5	1	53	2	2	1	73	0	-8	1	93	0	9	1				
14	0	3	-1	34	1	-3	-1	54	3	0	-1	74	0	8	-1	94	1	-7	-1				
15	0	3	1	35	1	-3	1	55	3	0	1	75	0	8	1	95	1	-7	1				
16	1	-1	-1	36	1	3	-1	56	0	-7	-1	76	1	-6	-1	96	1	7	-1				
17	1	-1	1	37	1	3	1	57	0	-7	1	77	1	-6	1	97	1	7	1				
18	1	1	-1	38	2	-1	-1	58	0	7	-1	78	1	6	-1	98	2	-5	-1				
19	1	1	1	39	2	-1	1	59	0	7	1	79	1	6	1	99	2	-5	1				

**Table 8.1:** Mapping scheme for harmonic oscillator functions. The functions are given by three quantum numbers:  $n$ ,  $m$  and  $m_s$ . The first two quantum numbers,  $n$  and  $m$ , emerge when solving Eq. (8.15). See Section 4.3. The allowed values are  $n = 0, 2, 3, \dots$  and  $m = 0, \pm 1, \pm 2, \pm 3, \dots$  The third quantum number,  $m_s$ , is associated with the  $z$ -projection of the spin, with allowed values  $m_s = \pm 1/2$  (spin up/down). We have in our implementation chosen to represent  $m_s = 1/2$  with 1, and  $m_s = -1/2$  with -1.

$R$	$ \alpha\rangle$
1	0-1
2	2-5
3	6-11
4	12-19
5	20-29
6	30-41
7	42-55
8	56-71
9	72-89
10	90-109

**Table 8.2:** Shell structure of the parabolic quantum dot in 2 dimensions. The shell number is denoted by  $R$ , and the harmonic oscillator functions are denoted by  $|\alpha\rangle$ . The mapping scheme  $\alpha \rightarrow (n, m, s)$  is given in Table 8.1.

### 8.1.1 Tables of Numerical Results

The HF and CCSD results with standard interaction are tabulated in Tables 8.5-8.9. We have done calculations for 2, 6, 12 and 20 electrons, and oscillator frequencies ranging from 0.4 up to 50. Table 8.4 shows for which values of  $N$  (number of electrons) and  $\omega$  (frequency) the CCSD energy converges within the iteration procedure, see Section 7.2.4. All calculations with standard interaction have been done with the direct product (DP) model space

$$\mathcal{P}_{\text{DP}} \subset \mathcal{H}_N^{\text{AS}}, \quad (8.19)$$

$\alpha$	$\varepsilon_\alpha$										
0	1	20	5	40	6	60	8	80	9	100	10
1	1	21	5	41	6	61	8	81	9	101	10
2	2	22	5	42	7	62	8	82	9	102	10
3	2	23	5	43	7	63	8	83	9	103	10
4	2	24	5	44	7	64	8	84	9	104	10
5	2	25	5	45	7	65	8	85	9	105	10
6	3	26	5	46	7	66	8	86	9	106	10
7	3	27	5	47	7	67	8	87	9	107	10
8	3	28	5	48	7	68	8	88	9	108	10
9	3	29	5	49	7	69	8	89	9	109	10
10	3	30	6	50	7	70	8	90	10		
11	3	31	6	51	7	71	8	91	10		
12	4	32	6	52	7	72	9	92	10		
13	4	33	6	53	7	73	9	93	10		
14	4	34	6	54	7	74	9	94	10		
15	4	35	6	55	7	75	9	95	10		
16	4	36	6	56	8	76	9	96	10		
17	4	37	6	57	8	77	9	97	10		
18	4	38	6	58	8	78	9	98	10		
19	4	39	6	59	8	79	9	99	10		

**Table 8.3:** Single-particle energies  $\varepsilon_\alpha/\omega = \varepsilon_{nm}/\omega = (1 + |m| + 2n)$ . The harmonic oscillator functions are defined by  $\alpha$ . The mapping between  $\alpha$  and  $(n, m, s)$  is given in Table 8.1.

$\omega$	$N = 2$	$N = 6$	$N = 12$	$N = 20$
0.2	conv.	not conv.	not conv.	not conv.
0.4	conv.	conv.	not conv.	not conv.
0.5	conv.	conv.	not conv.	not conv.
0.6	conv.	conv.	not conv.	not conv.
0.8	conv.	conv.	not conv.	not conv.
1.0	conv.	conv.	conv.	not conv.
2.0	conv.	conv.	conv.	conv.
3.0	conv.	conv.	conv.	conv.
4.0	conv.	conv.	conv.	conv.
5.0	conv.	conv.	conv.	conv.
10.0	conv.	conv.	conv.	conv.
20.0	conv.	conv.	conv.	conv.
50.0	conv.	conv.	conv.	conv.

**Table 8.4:** The table shows for which values of  $\omega$  the HF (effective interaction) and CCSD energy (standard interaction and effective interaction) converges within the iteration procedure. We have used harmonic oscillator functions as basis functions. When the energy converges, it converges for all values of  $R^b$  from  $R^f$  (Fermi shell) up to 10. When it does not converge, it does not converge for any value of  $R^b$ .

where  $\mathcal{H}_N^{\text{AS}}$  is the  $N$ -electron Hilbert space. The basis of  $\mathcal{P}_{\text{DP}}$  is given as

$$\mathcal{B}_{\text{DP}} = \mathcal{B}_{\text{DP}}(R^b) = \left\{ |\Phi_{\alpha_1 \alpha_2 \dots \alpha_N}\rangle : \max_i \{\varepsilon_i\} \leq R^b \right\}, \quad (8.20)$$

where  $|\Phi_{\alpha_1 \alpha_2 \dots \alpha_N}\rangle$  is a Slater determinant with harmonic oscillator functions as single-particle orbitals, and  $\varepsilon_i$  is the single-particle energy given in Eq. (8.16). The direct product basis means that there are no restrictions on which single-particle states (defined by  $\alpha_{\text{max}}$ ) that can be occupied. When turning to the effective interaction in Section 8.2 we will also consider another model space, called the energy cut (EC) model space. In this space we have restrictions on which single-particle states that can be occupied. See Section 8.2 for details.

Tables 8.5-8.8 show the CCSD energies for different sizes of the model space, denoted by  $R^b$ . The single-particle basis, which is used to construct the  $N$ -particle basis, is given as

$$\mathcal{B}_1 = \left\{ |\alpha\rangle \right\}_{\alpha=0}^{\alpha_{\text{max}}}, \quad (8.21)$$

where  $\alpha_{\text{max}}$  is equal to 1, 5, 11, 19, 29, 41, 55, 71, 89 or 109. We have only used these values of  $\alpha_{\text{max}}$  since we are dealing with closed-shell systems (see Table 8.1). Stated differently, when increasing the single-particle basis by the smallest amount means that we include all orbitals

within the “next” shell. The size of the single-particle basis can therefore be characterized by the number of shells in the basis,  $R^b$ . Moreover,  $R^b$  also defines the size of  $\mathcal{P}_{\text{DP}}$  (see Eq. 8.20).

Tables 8.5–8.8 present the CCSD energy with the standard interaction for  $R^b = R^f$  up to  $R^b = 10$ , where  $R^f$  is the Fermi shell defined as the outermost shell that contains occupied single-particle orbitals. Table 8.9 presents results for  $R^b = 10$ .

$\omega$	$R^b$	$N = 2$		$N = 6$	
		HF energy	CCSD energy	HF energy	CCSD energy
0.4	1	1.592665	1.592665	-	-
	2	1.592665	1.494392	11.728488	11.728488
	3	1.508042	1.392856	11.156151	11.005419
	4	1.508042	1.386722	10.504554	10.208494
	5	1.508024	1.383259	10.467626	10.064250
	6	1.508024	1.381489	10.405715	9.987983
	7	1.508015	1.380338	10.405292	9.977274
	8	1.508015	1.379554	10.405222	9.970650
	9	1.508011	1.378983	10.405195	9.966218
	10	1.508011	1.378551	10.405166	9.963027
0.5	1	1.886227	1.886227	-	-
	2	1.886227	1.786914	13.640713	13.640713
	3	1.799856	1.681633	13.051620	12.895476
	4	1.799856	1.673874	12.357471	12.047565
	5	1.799748	1.669500	12.325128	11.914166
	6	1.799748	1.667259	12.271499	11.841655
	7	1.799745	1.665801	12.271375	11.827869
	8	1.799745	1.664808	12.271361	11.819437
	9	1.799743	1.664085	12.271337	11.813819
	10	1.799743	1.663537	12.271326	11.809788
0.6	1	2.170813	2.170813	-	-
	2	2.170813	2.070856	15.465426	15.465426
	3	2.083158	1.962891	14.864332	14.703670
	4	2.083158	1.953712	14.135156	13.814684
	5	2.082926	1.948533	14.106585	13.690123
	6	2.082926	1.945869	14.059885	13.621142
	7	2.082926	1.944135	14.059867	13.604622
	8	2.082926	1.942953	14.059716	13.594539
	9	2.082924	1.942090	14.059698	13.587834
	10	2.082924	1.941436	14.059697	13.583037
0.8	1	2.720998	2.720998	-	-
	2	2.720998	2.620341	18.929733	18.929733
	3	2.631563	2.508827	18.312821	18.144988
	4	2.631563	2.497304	17.528556	17.193050
	5	2.631058	2.490771	17.505795	17.081893
	6	2.631058	2.487386	17.469841	17.018754
	7	2.631055	2.485175	17.469813	16.997854
	8	2.631055	2.483665	17.469269	16.985003
	9	2.631054	2.482560	17.469263	16.976408
	10	2.631054	2.481724	17.469257	16.970279
1.0	1	3.253314	3.253314	-	-
	2	3.253314	3.152329	22.219813	22.219813
	3	3.162691	3.038605	21.593198	21.419889
	4	3.162691	3.025232	20.766919	20.421325
	5	3.161921	3.017607	20.748402	20.319716
	6	3.161921	3.013627	20.720257	20.260893
	7	3.161909	3.011021	20.720132	20.236760
	8	3.161909	3.009237	20.719248	20.221750
	9	3.161909	3.007931	20.719248	20.211590
	10	3.161909	3.006938	20.719217	20.204345
2.0	1	5.772454	5.772454	-	-
	2	5.772454	5.671234	37.281425	37.281425
	3	5.679048	5.553152	36.637217	36.448558
	4	5.679048	5.534274	35.689555	35.322283
	5	5.677282	5.523274	35.681728	35.242971
	6	5.677282	5.517386	35.672333	35.193258
	7	5.677206	5.513491	35.671851	35.161115
	8	5.677206	5.510801	35.670358	35.140124
	9	5.677204	5.508822	35.670333	35.125055
	10	5.677204	5.507311	35.670144	35.114198

**Table 8.5:** Hartree-Fock and Coupled-Cluster Singles and Doubles results for a parabolic quantum dot with 2 and 6 electrons using standard interaction. We have used the DP space as model space (see Eq. 8.20). The size of the space is denoted by  $R^b$  (shell number), and the oscillator frequency is given by  $\omega$ . Energy is measured in effective Hartrees  $E_H^*$ .

$\omega$	$R^b$	$N = 2$		$N = 6$	
		HF energy	CCSD energy	HF energy	CCSD energy
3.0	1	8.170804	8.170804	-	-
	2	8.170804	8.069761	51.165337	51.165337
	3	8.076274	7.950410	50.517683	50.321752
	4	8.076274	7.928709	49.508478	49.135135
	5	8.073884	7.915891	49.504750	49.062885
	6	8.073884	7.908930	49.501573	49.014446
	7	8.073751	7.904296	49.501011	48.979127
	8	8.073751	7.901081	49.499580	48.955363
	9	8.073744	7.898706	49.499520	48.937698
	10	8.073744	7.896889	49.499237	48.924839
4.0	1	10.506628	10.506628	-	-
	2	10.506628	10.405775	64.439626	64.439626
	3	10.411470	10.285895	63.791597	63.591329
	4	10.411470	10.262419	62.743808	62.368661
	5	10.408646	10.248423	62.742006	62.298906
	6	10.408646	10.240751	62.741163	62.249606
	7	10.408469	10.235621	62.740611	62.212557
	8	10.408469	10.232050	62.739357	62.187127
	9	10.408456	10.229405	62.739276	62.167826
	10	10.408456	10.227378	62.738940	62.153663
5.0	1	12.802496	12.802496	-	-
	2	12.802496	12.701808	77.324332	77.324332
	3	12.706930	12.581669	76.676854	76.473661
	4	12.706930	12.556949	75.602124	75.226743
	5	12.703782	12.542112	75.601300	75.157693
	6	12.703782	12.533923	75.601221	75.106872
	7	12.703567	12.528429	75.600706	75.068703
	8	12.703567	12.524595	75.599630	75.042121
	9	12.703550	12.521751	75.599534	75.021677
	10	12.703550	12.519568	75.599173	75.006580
10.0	1	23.963327	23.963327	-	-
	2	23.963327	23.863173	138.642441	138.642441
	3	23.866830	23.742766	137.999396	137.789201
	4	23.866830	23.714877	136.856842	136.485196
	5	23.862773	23.697829	136.856753	136.413343
	6	23.862773	23.688243	136.854607	136.354504
	7	23.862443	23.681757	136.854284	136.313637
	8	23.862443	23.677199	2136.853782	136.284071
	9	23.862411	23.673802	136.853661	136.260729
	10	23.862411	23.671183	136.853287	136.243183
20.0	1	45.604991	45.604991	-	-
	2	45.604991	45.505319	254.648664	254.648664
	3	45.507912	45.385045	254.011527	253.796720
	4	45.507912	45.354878	252.821683	252.457058
	5	45.503120	45.336174	252.820088	252.378355
	6	45.503120	45.325508	252.811954	252.309241
	7	45.502684	45.318241	252.811811	252.266330
	8	45.502684	45.313105	252.811687	252.234390
	9	45.502636	45.309263	252.811568	252.208972
	10	45.502636	45.306293	252.811247	252.189591
50.0	1	108.862269	108.862269	-	-
	2	108.862269	108.763094	586.407125	586.407125
	3	108.764735	108.643160	585.777168	585.558594
	4	108.764735	108.610971	584.547339	584.192313
	5	108.759222	108.590750	584.542520	584.103507
	6	108.759222	108.579064	584.524974	584.021400
	7	108.758672	108.571049	584.524954	583.976331
	8	108.758672	108.565356	584.524950	583.941913
	9	108.758604	108.561080	584.524852	583.914635
	10	108.758604	108.557765	584.524623	583.893560

**Table 8.6:** Hartree-Fock and Coupled-Cluster Singles and Doubles results for a parabolic quantum dot with 2 and 6 electrons using standard interaction. We have used the DP space as model space (see Eq. 8.20). The size of the space is denoted by  $R^b$  (shell number), and the oscillator frequency is given by  $\omega$ . Energy is measured in effective Hartrees  $E_H^*$ .

$\omega$	$R^b$	$N = 12$		$N = 20$	
		HF energy	CCSD energy	HF energy	CCSD energy
1.0	1	-	-	-	-
	2	-	-	-	-
	3	73.765549	73.765549	-	-
	4	70.673849	70.297531	177.963297	177.963297
	5	67.569930	66.989912	168.426371	x
	6	67.296869	66.452006	161.339721	x
	7	66.934745	65.971686	159.958722	x
	8	66.923094	65.889324	158.400172	x
	9	66.912244	65.838932	158.226030	x
	10	66.912035	65.806539	158.017667	x
2.0	1	-	-	-	-
	2	-	-	-	-
	3	120.722260	120.722260	-	-
	4	117.339642	116.978642	286.825295	286.825295
	5	113.660396	113.020282	276.898196	275.845577
	6	113.484866	112.613571	267.269712	266.325997
	7	113.247601	112.264166	266.213200	264.830000
	8	113.246579	112.189996	264.933622	263.325189
	9	113.246303	112.135551	264.874009	263.089951
	10	113.245854	112.094025	264.809954	262.928937
3.0	1	-	-	-	-
	2	-	-	-	-
	3	163.268256	163.268256	-	-
	4	159.769062	159.414625	384.318425	384.318425
	5	155.762811	155.097118	373.776094	373.229501
	6	155.639179	154.762454	363.162287	362.175933
	7	155.475049	154.487959	362.323215	360.924104
	8	155.475049	154.408521	361.277490	359.652011
	9	155.474144	154.348106	361.254334	359.469820
	10	155.473848	154.302641	361.233837	359.337510
4.0	1	-	-	-	-
	2	-	-	-	-
	3	203.531098	203.531098	-	-
	4	199.971455	199.619694	475.926595	475.926595
	5	195.745462	195.066235	465.021258	464.483436
	6	195.653702	194.776202	453.717528	452.706359
	7	195.535485	194.547735	453.029759	451.624943
	8	195.535177	194.463255	452.163171	450.533964
	9	195.532936	194.398503	452.154007	450.370119
	10	195.532772	194.350424	452.148052	450.245879
5.0	1	-	-	-	-
	2	-	-	-	-
	3	242.334879	242.334879	-	-
	4	238.739591	238.388819	x563.773952	563.773952
	5	234.352741	233.665684	552.630093	552.098704
	6	234.282331	233.405545	540.804720	539.777215
	7	234.194820	233.207198	540.227793	538.821500
	8	234.194059	233.118844	539.499326	537.871223
	9	234.190797	233.051061	539.495941	537.713326
	10	234.190714	233.000991	539.494612	537.589832

**Table 8.7:** Hartree-Fock and Coupled-Cluster Singles and Doubles results for a parabolic quantum dot with 12 and 20 electrons using standard interaction. We have used the DP space as model space (see Eq. 8.20). The size of the space is denoted by  $R^b$  (shell number), and the oscillator frequency is given by  $\omega$ . The CCSD energy does not converge within the iteration procedure (see Section 7.2.4) for certain values of  $R^b$ , denoted by “x”. Energy is measured in effective Hartrees  $E_H^*$ .

$\omega$	$R^b$	$N = 12$		$N = 20$	
		HF energy	CCSD energy	HF energy	CCSD energy
10.0	1	-	-	-	-
	2	-	-	-	-
	3	424.723373	424.723373	-	-
	4	421.066552	420.714412	973.032700	973.032700
	5	416.245656	415.548025	961.371081	960.853435
	6	416.221892	415.352162	948.057077	946.995097
	7	416.198611	415.213229	947.765474	946.367418
	8	416.196677	415.115445	947.410305	945.798531
	9	416.191836	415.040983	947.409440	945.634643
	10	416.191833	414.985087	947.404930	945.499122
20.0	1	-	-	-	-
	2	-	-	-	-
	3	764.669757	764.669757	-	-
	4	760.999568	760.642727	1727.547904	1727.547904
	5	755.851177	755.158770	1715.636447	1715.121677
	6	755.847874	754.988910	1701.112340	1700.040683
	7	755.846430	754.864771	1701.000555	1699.622516
	8	755.844396	754.761753	1700.881357	1699.291198
	9	755.840282	754.683971	1700.876899	1699.113200
	10	755.840196	754.623201	1700.866177	1698.965611
50.0	1	-	-	-	-
	2	-	-	-	-
	3	1723.611301	1723.611301	-	-
	4	1719.954910	1719.591333	3834.126475	3834.126475
	5	1714.516506	1713.842082	3822.122324	3821.601747
	6	1714.514709	1713.670423	3806.466383	3805.411147
	7	1714.502278	1713.526638	3806.454602	3805.108329
	8	1714.500976	1713.420167	3806.448065	3804.882880
	9	1714.498844	1713.340085	3806.442304	3804.694261
	10	1714.498639	1713.274652	3806.431632	3804.541353

**Table 8.8:** Hartree-Fock and Coupled-Cluster Singles and Doubles results for a parabolic quantum dot with 12 and 20 electrons using standard interaction. We have used the DP space as model space (see Eq. 8.20). The size of the space is denoted by  $R^b$  (shell number), and the oscillator frequency is given by  $\omega$ . Energy is measured in effective Hartrees  $E_H^*$ .

$N$	$\omega$	$\langle \Phi_0   \hat{H}_0   \Phi_0 \rangle$	$E_{HF}$	$E_{CCSD}$	$E_{CCSD}-E_{HF}$	$\langle \Phi_0   \hat{H}   \Phi_0 \rangle$	$\langle \Phi_0   \hat{H}_N \hat{T}_1   \Phi_0 \rangle$	$\langle \Phi_0   \hat{H}_N \hat{T}_1^2   \Phi_0 \rangle$	$\langle \Phi_0   \hat{H}_N \hat{T}_2   \Phi_0 \rangle$	$\langle \Phi_0   \hat{H}_N (\hat{T}_1 + \hat{T}_1^2 + \hat{T}_2)   \Phi_0 \rangle$
2	0.4	0.8	1.508011	1.378551	-0.129460	1.592665	-0.086879	0.007582	-0.134818	-0.214114
	0.5	1.0	1.799743	1.663537	-0.136206	1.886227	-0.088901	0.007137	-0.140926	-0.222690
	0.6	1.2	2.082924	1.941436	-0.141488	2.170813	-0.090443	0.006770	-0.145703	-0.229377
	0.8	1.6	2.631054	2.481724	-0.149330	2.720998	-0.092663	0.006190	-0.152801	-0.239274
	1.0	2.0	3.161909	3.006938	-0.154971	3.253314	-0.094206	0.005745	-0.157915	-0.246376
	2.0	4.0	5.677204	5.507311	-0.169893	5.772454	-0.098061	0.004447	-0.171530	-0.265143
	3.0	6.0	8.073744	7.896889	-0.176855	8.170804	-0.099735	0.003774	-0.177955	-0.273915
	4.0	8.0	10.408456	10.227378	-0.181078	10.506628	-0.100707	0.003343	-0.181885	-0.279250
	5.0	10.0	12.703550	12.519568	-0.183982	12.802496	-0.101356	0.003035	-0.184606	-0.282928
	10.0	20.0	23.862411	23.671183	-0.191228	23.963327	-0.102895	0.002223	-0.191471	-0.292144
	20.0	40.0	45.502636	45.306293	-0.196343	45.604991	-0.103907	0.001609	-0.196400	-0.298698
	50.0	100.0	108.758604	108.557765	-0.200839	108.862269	-0.104739	0.001037	-0.200803	-0.304504
6	0.4	4.0	10.405166	9.963027	-0.442139	11.728488	-1.576346	0.257724	-0.446838	-1.765461
	0.5	5.0	12.271326	11.809788	-0.461538	13.640713	-1.609268	0.244324	-0.465980	-1.830924
	0.6	6.0	14.059697	13.583037	-0.476660	15.465426	-1.634956	0.233265	-0.480698	-1.882389
	0.8	8.0	17.469257	16.970279	-0.498978	18.929733	-1.673066	0.215745	-0.502134	-1.959454
	1.0	10.0	20.719217	20.204345	-0.514872	22.219813	-1.700464	0.202215	-0.517218	-2.015468
	2.0	20.0	35.670144	35.114198	-0.555946	37.281425	-1.773149	0.161679	-0.555757	-2.167227
	3.0	30.0	49.499237	48.924839	-0.574398	51.165337	-1.807268	0.139802	-0.573032	-2.240498
	4.0	40.0	62.738940	62.153663	-0.585277	64.439626	-1.828063	0.125380	-0.583281	-2.285963
	5.0	50.0	75.599173	75.006580	-0.592593	77.324332	-1.842415	0.114887	-0.590225	-2.317752
	10.0	100.0	136.853287	136.243183	-0.610104	138.642441	-1.878444	0.086342	-0.607156	-2.399258
	20.0	200.0	252.811247	252.189591	-0.621656	254.648664	-1.904107	0.063785	-0.618751	-2.459073
	50.0	500.0	584.524623	583.893560	-0.631063	586.407125	-1.926850	0.041953	-0.628673	-2.513565
12	1.0	28.0	66.912035	65.806539	-1.105496	73.765549	-8.083917	1.180485	-1.055578	-7.959010
	2.0	56.0	113.245854	112.094025	-1.151829	120.722260	-8.483021	0.966841	-1.112054	-8.628235
	3.0	84.0	155.473848	154.302641	-1.171207	163.268256	-8.675835	0.846680	-1.136461	-8.965615
	4.0	112.0	195.532772	194.350424	-1.182348	203.531098	-8.795704	0.765705	-1.150674	-9.180674
	5.0	140.0	234.190714	233.000991	-1.189723	242.334879	-8.879606	0.705903	-1.160184	-9.333888
	10.0	280.0	416.191833	414.985087	-1.206746	424.723373	-9.094802	0.539378	-1.182862	-9.738286
	20.0	560.0	755.840196	754.623201	-1.216995	764.669757	-9.252451	0.403719	-1.197825	-10.046556
	50.0	1400.0	1714.498639	1713.274652	-1.223987	1723.611301	-9.395486	0.268914	-1.210076	-10.336649
	2.0	120.0	264.809954	262.928937	-1.881017	286.825295	-25.409371	3.303809	-1.790796	-23.896357
	3.0	180.0	361.233837	359.337510	-1.896327	384.318425	-26.104762	2.931583	-1.807734	-24.980915
	4.0	240.0	452.148052	450.245879	-1.902173	475.926595	-26.535690	2.672422	-1.817447	-25.680716
	5.0	300.0	539.494612	537.589832	-1.904780	563.773952	-26.837784	2.477431	-1.823767	-26.184120
	10.0	600.0	947.404930	945.499122	-1.905808	973.032700	-27.616252	1.920436	-1.837762	-27.533578
	20.0	1200.0	1700.866177	1698.965611	-1.900566	1727.547904	-28.189744	1.453073	-1.845622	-28.582293
	50.0	3000.0	3806.431632	3804.541353	-1.890279	3834.126475	-28.712212	0.977796	-1.850706	-29.585122

**Table 8.9:** Energy results for a parabolic quantum dot with 2, 6, 12 and 20 electrons in 2 dimensions. The results are obtained with standard interaction and the DP space as model space (see Eq. 8.20). For each oscillator frequency  $\omega$ , the following are tabulated: Non-interacting ground state energy  $\langle \Phi_0 | \hat{H}_0 | \Phi_0 \rangle$ , Hartree-Fock energy  $E_{HF}$ , Coupled-Cluster Singles and Doubles energy  $E_{CCSD}$ , difference between CCSD and HF energy ( $E_{CCSD}-E_{HF}$ ), reference expectation energy  $\langle \Phi_0 | \hat{H} | \Phi_0 \rangle$ , and the three contributions to the correlation energy  $\langle \Phi_0 | \hat{H}_N (\hat{T}_1 + \hat{T}_1^2 + \hat{T}_2) | \Phi_0 \rangle$  in Eq. (6.115). All calculations are done with  $R^b = 10$ . Energy is measured in effective Hartrees  $E_H^*$ .

### 8.1.2 General Analysis and Discussion

Consider the HF results for the 2-electron quantum dot ( $N = 2$ ) in Tables 8.5 and 8.6. We observe that the HF energy does not change when the size of the basis increases from an odd to an even number by 1 shell. This behavior occurs for all oscillator frequencies. For example, for  $\omega = 1.0$ , the HF energy remains 3.253314 when the basis is increased from  $R^b = 1$  to  $R^b = 2$ . This can be understood by the following argument. The HF ansatz for  $N = 2$  reads

$$\Phi_{\text{HF}}(\mathbf{r}_1, \mathbf{r}_2) = \begin{pmatrix} \varphi_a(\mathbf{r}_1) & \varphi_a(\mathbf{r}_2) \\ \varphi_b(\mathbf{r}_1) & \varphi_b(\mathbf{r}_2) \end{pmatrix}, \quad (8.22)$$

where

$$\varphi_a(\mathbf{r}) = \sum_{i=1}^{\alpha_{\max}} C_{a\alpha} \psi_i(\mathbf{r}) \quad (8.23)$$

is a so-called HF orbital, and  $\{\psi_i(\mathbf{r})\}_{i=1}^{\alpha_{\max}}$  is the single-particle basis of harmonic oscillator functions, see Chapter 5 for a presentation of the HF method. Since each HF orbital is written as a linear combination of harmonic oscillator functions, the HF wavefunction in Eq. (8.22) is a linear combination of  $2 \times 2$  determinants. Since the HF ansatz (see Eq. 5.1) only includes one-particle one-hole (1p1h) excited determinants [56], i.e. determinants where only one particle is excited from a hole state  $i$ , to a particle state  $a$ . Therefore, in the 2-electron case, 2p2h excitations are not included in the HF wavefunction. In the general  $N$ -electron case, all excitations beyond 1p1h are excluded, i.e. 2p2p, 3p3h, and so forth up to  $NpNh$ . Turning back to the 2-electron case, when  $R^b = 1$ , we have that  $R^b = R^f$ . This means that

$$\Phi_{\text{HF}}(\mathbf{r}_1, \mathbf{r}_2) = \Phi_0(\mathbf{r}_1, \mathbf{r}_2), \quad (8.24)$$

where  $\Phi_0(\mathbf{r}_1, \mathbf{r}_2)$  is the non-interacting ground state, and

$$E_{\text{HF}} = E_{\text{ref}} = \langle \Phi_0 | \hat{H} | \Phi_0 \rangle = 3.253314, \quad (8.25)$$

where  $E_{\text{HF}}$  is the HF energy, and  $E_{\text{ref}}$  is the non-interacting ground state energy. When we increase our basis to  $R^b = 2$ , we open for the possibility to include 1p1h excitations in the HF wavefunction. The non-interacting ground state of the 2-electron systems reads

$$\Phi_0(\mathbf{r}_1, \mathbf{r}_2) = \begin{pmatrix} \psi_0(\mathbf{r}_1) & \psi_0(\mathbf{r}_2) \\ \psi_1(\mathbf{r}_1) & \psi_1(\mathbf{r}_2) \end{pmatrix}, \quad (8.26)$$

where the harmonic oscillator functions are given in Table 8.1. In the bra-ket notation, the following two states are occupied (hole states),

$$|0\rangle = |0, 0, -1\rangle \quad (8.27)$$

$$|1\rangle = |0, 0, 1\rangle, \quad (8.28)$$

where  $|\alpha\rangle = |n, m, m_s\rangle$ . When  $R^b = 2$ , we include

$$|2\rangle = |0, -1, -1\rangle \quad (8.29)$$

$$|3\rangle = |0, -1, 1\rangle \quad (8.30)$$

$$|4\rangle = |0, 1, -1\rangle \quad (8.31)$$

$$|5\rangle = |0, 1, 1\rangle, \quad (8.32)$$

in the basis. Since the Coulomb interaction is independent of the angular momentum and the spin, the *total* angular momentum

$$M \equiv m_\alpha + m_\beta, \quad (8.33)$$

and *total* spin

$$M_s \equiv m_{s_\alpha} + m_{s_\beta}, \quad (8.34)$$

must be conserved. For example, assume the electrons are in the non-interacting ground state in Eq. (8.26). The occupied states are given in Eqs. (8.27) and (8.28), with total angular momentum  $M = 0$  and total spin  $S = 0$ . We propose the 1p1h excitation

$$\begin{pmatrix} \psi_0(\mathbf{r}_1) & \psi_0(\mathbf{r}_2) \\ \psi_2(\mathbf{r}_1) & \psi_2(\mathbf{r}_2) \end{pmatrix}, \quad (8.35)$$

i.e. an electron excited into state  $|2\rangle$ , with  $m = -1$  and  $m_s = -1$ . The total angular momentum and spin is  $-1$  and  $-2$ , respectively. Hence this is not an allowed excitation. All 1p1h excitations that do not conserve  $M$  and  $S$ , are not allowed. When  $R^b = 2$ , we cannot construct any 1p1h excited determinant that has  $M = 0$  and  $M_s = 0$ . This is clearly seen in Eqs. (8.29), (8.30), (8.31) and (8.32). No more correlations are therefore included when we increase the basis from  $R^b = 1$  to  $R^b = 2$ , and the energy remains the same. In all the other cases, when  $R^b$  increases from 3 to 4, 5 to 6, and so forth, no “new” 1p1h excitations are allowed, and the energies thus remain constant. For systems containing 6, 12 and 20 electrons, we observe from Tables 8.5-8.6 that the HF energies are different for all  $R^b$ . Thus by increasing  $R^b$  we include “new” allowed 1p1h correlations.

The HF method is variational, i.e. the HF energy overestimates the exact ground state energy. By looking at Tables 8.5-8.8, we conclude that increasing  $R^b$  yields a better energy, viz.

$$E_0 < E_{\text{HF}}(R^b + 1) \leq E_{\text{HF}}(R^b), \quad (8.36)$$

with equality for certain values of  $R^b$  in the 2-electron system. This is what we expect. For the 2-electron system, we observe that the HF energy converges rapidly for all frequencies. We have in Figure 8.1 and 8.2 plotted the HF energy as function of  $R^b$ . The energy changes only by approximately  $10^{-5}$  when  $R^b$  increases from 8 to 10. For systems containing 6, 12 and 20 electrons, the HF energy also converges relatively rapidly. When  $R^b$  increases from 9 to 10, the energy changes approximately  $10^{-3} - 10^{-5}$ . The HF results for  $R^b = 10$  are therefore good estimates of the HF limits, i.e.

$$\lim_{R^b \rightarrow \infty} E_{\text{HF}}(R^b), \quad (8.37)$$

We conclude that the most important 1p1h excitations are included when  $R^b = 10$ . When the system contains 2 electrons, the most important correlations are 1p1h excitations into shell 3. These are included when  $R^b = 3$ . When  $\omega = 0.4$ ,

$$E_{\text{HF}}(R^b = 10) - E_{\text{HF}}(R^b = 3) \approx -3 \cdot 10^{-5}, \quad (8.38)$$

and when  $\omega = 50.0$ ,

$$E_{\text{HF}}(R^b = 10) - E_{\text{HF}}(R^b = 3) \approx -6 \cdot 10^{-3}. \quad (8.39)$$

For systems containing 6, 12 and 20 electrons, 1p1h excitations in higher shells yield considerably contributions. For a system containing  $N$  electrons, we observe that we have relatively good energy estimates when

$$R^b = R^f + 4, \quad (8.40)$$

relative to the HF energies for  $R^b = 10$ , where  $R^f$  is the Fermi shell.

Consider the CCSD results in Tables 8.5-8.8. We observe that

$$E_{\text{CCSD}}(R^b) \leq E_{\text{HF}}(R^b), \quad (8.41)$$

for all frequencies. We obtain equality when  $R^b = R^f$ . The CCSD method is not variational. Thus we cannot, in principle, conclude *with certainty* whether HF or CCSD yields the best energy estimate. By this we mean the energy that is closest to the exact value. In order to decide the best estimate, results from other variational methods, such as Full Configuration Interaction (FCI) [30], Variational Monte Carlo (VMC) [18] or Diffusion Monte Carlo (DMC) [18], are needed. That said, the CCSD energies are *more likely* better estimates. Since CCSD includes more correlations than HF, we should obtain a much better energy. We now choose to anticipate the course of events. For the 2-electron system, the CCSD results with effective interaction yields *exact* energies (see Section 8.2). We observe that the results with standard interaction are always higher than the exact energies, i.e.

$$E_{\text{CCSD}}^{\text{std}}(R^b) > E_0 = E_{\text{CCSD}}^{\text{eff}}(R^b), \quad (8.42)$$

where “std” denotes standard interaction, and “eff” denotes effective interaction. We conclude that with standard interaction, the CCSD energies are better estimates than the HF energies. This is what we expect. For systems containing 6, 12 and 20 electrons, however, the exact ground state energies are unknown. Since CCSD yields better results than HF in the 2-electron case, it is probable that it also yields better estimates for larger systems. We emphasize that, in principle, we cannot say anything with certainty before comparing with other variational methods. Table 8.30 shows results from other many-body methods. We will discuss these results in more detail later. Comparing with the CCSD results, we conclude that for  $\omega = 1.0$  and  $N = 6, 12$  and  $20$ , the CCSD energies are better estimates than the HF energies. This is what we expect since CCSD includes excitations from 1p1h up to  $NpNh$ . Excitations beyond 2p2h are obtained with combinations of  $\hat{T}_1$  and  $\hat{T}_2$ . For example, 3p3h excitations are obtained by

$$\hat{T}_1 \hat{T}_2 |\Phi_0\rangle, \quad (8.43)$$

where  $|\Phi_0\rangle$  is the reference determinant. Therefore, since CCSD includes *much* more correlations than HF, the results should be better. Since CCSD yields better results in the 2-electron case (all frequencies) and for larger systems (6, 12 and 20 electrons) with  $\omega = 1.0$ , it is reasonable to believe that the CCSD energies are better estimates than HF for all frequencies ( $\omega = 0.4 - 50.0$ ) and electron number ( $N = 2, 6, 12$  and  $20$ ).

Consider the 2-electron system. We observe that the energy changes for every value of  $R^b$ , in contrast to the HF energy. This is a direct consequence of 2p2h excitations. As we discussed earlier, when  $R^b = 2$ , 1p1h excitations are not allowed. However, there exist two 2p2h excitations that conserve total angular momentum  $M$  and spin  $M_s$ . We see from Table 8.1 that the determinants

$$\begin{pmatrix} \psi_3(\mathbf{r}_1) & \psi_3(\mathbf{r}_2) \\ \psi_4(\mathbf{r}_1) & \psi_4(\mathbf{r}_2) \end{pmatrix}, \quad (8.44)$$

and

$$\begin{pmatrix} \psi_3(\mathbf{r}_1) & \psi_3(\mathbf{r}_2) \\ \psi_4(\mathbf{r}_1) & \psi_4(\mathbf{r}_2) \end{pmatrix}, \quad (8.45)$$

have  $M = 0$  and  $M_s = 0$ . Since the reference state in Eq. (8.26) has  $M = 0$  and  $M_s = 0$ , these 2p2h excitations are allowed. Thus the energy changes when we increase  $R^b$  from 1 to 2. In general, increasing  $R^b$  will always yield “new” allowed excitations. Furthermore, we observe that CCSD with  $\omega = 0.4 - 5.0$  and  $R^b = 2$  gives a better energy than HF with  $R^b = 10$ . This means that the allowed 2p2h excitations in Eqs. (8.44) and (8.45) are more important than 1p1h excitations in shell 2 – 10. The HF energy is practically converged for all frequencies, meaning that (at least for  $\omega = 0.4 - 1.0$ ) the 2p2h excitations in Eqs. (8.44) and (8.45) describe the correlations in the system better than *all* 1p1h excitations beyond shell 2. For example, when

$\omega = 1.0$  and  $R^b = 2$ , the CCSD energy is 3.152329. The corresponding HF energy is 3.161909. We have that

$$E_{\text{HF}}(R^b = 10) - E_{\text{CCSD}}(R^b = 2) \approx 0.01, \quad (8.46)$$

and

$$E_{\text{HF}}(R^b = 8) - E_{\text{HF}}(R^b = 10) < 10^{-6}, \quad (8.47)$$

supporting the statement above.

Figures 8.1 and 8.2 show the HF energy and CCSD energy as function of the size of the model space ( $R^b$ ) for 2, 6, 12 and 20 electrons. In addition, the relative error

$$\Delta E(R^b) \equiv \frac{E(R^b) - E(R^b = 10)}{E(R^b = 10)} \quad (8.48)$$

is plotted for the CCSD energy. We have chosen frequencies 0.4, 1.0 and 5.0 for the 2- and 6-electron system, 1.0 and 5.0 for the 12-electron system, and 2.0 and 5.0 for the 20-electron system. First, consider the HF energy. For the 2-electron system we observe that the energy is almost constant for  $R^b \geq 3$ . For the 6-electron system, the energy is almost constant for  $R^b \geq 4$  when  $\omega = 5.0$ . Decreasing the frequency to  $\omega = 0.4$  results in significant contributions from shell 5 and 6. Turning to the 12-electron system with  $\omega = 5.0$ , the most important excitations are included when  $R^b = 5 - 6$ . When the frequency is 0.4, we have important contributions from  $R^b = 6$  and  $R^b = 7$ . For the 20-electron system, lowering the frequency from 5.0 to 2.0 makes the contributions from shells 6 and 7 more important. Thus in general, contributions from higher-lying shells tend to be important for low frequencies. Furthermore, consider the CCSD energy in Figure 8.1 and 8.2. For the 2-electron system, we clearly observe that when  $R^b = 3$ , important correlations are included. These correlations are particularly important when  $\omega = 0.4$ . Increasing the frequency leads to important contributions from higher-lying shells. When  $\omega = 1.0$ , contributions from shells 4 and 5 are more important than for  $\omega = 0.4$ . When  $\omega = 5.0$ , we also have important contributions from shells 6 and 7. Turning to the 6-electron system, we observe that the correlations included when  $R^b = 4$  are particularly important. When  $\omega = 0.4$ , important contributions are also present in shells 5 and 6. Increasing the frequency (1.0 and 5.0) leads to a slower convergence. For the 12-electron system, the correlations that are included when  $R^b = 5$ , are important. These correlations are particularly important when  $\omega = 5.0$ . Decreasing the frequency to 1.0 leads to a larger contributions from shells 5 and 6. Finally, for the 20-electron system, the same behavior occurs. Important correlations are included when  $R^b = 6$ . When the frequency is lowered from 5.0 to 2.0, we obtain important contributions from shell 7. In general, when the frequency increases, the CCSD energy exhibits a slower convergence. Particularly important correlations are included when

$$R^b = R^f + 2. \quad (8.49)$$

Also, except for the 2-electron system, contributions from low-lying shells become more important when the frequency decreases.

Consider the relative error plots in Figure 8.1 and 8.2. The relative error can be approximated as

$$\Delta E(R) \approx k_1 R^a, \quad (8.50)$$

where  $R \equiv R^b$ , and  $k_1$  and  $a$  are constants. Both constants depend on the number of electrons and the frequency. We observe that the convergence rate is higher for larger systems, i.e.

$$|a_N| > |a_{N'}| \quad (8.51)$$

when  $N > N'$ .

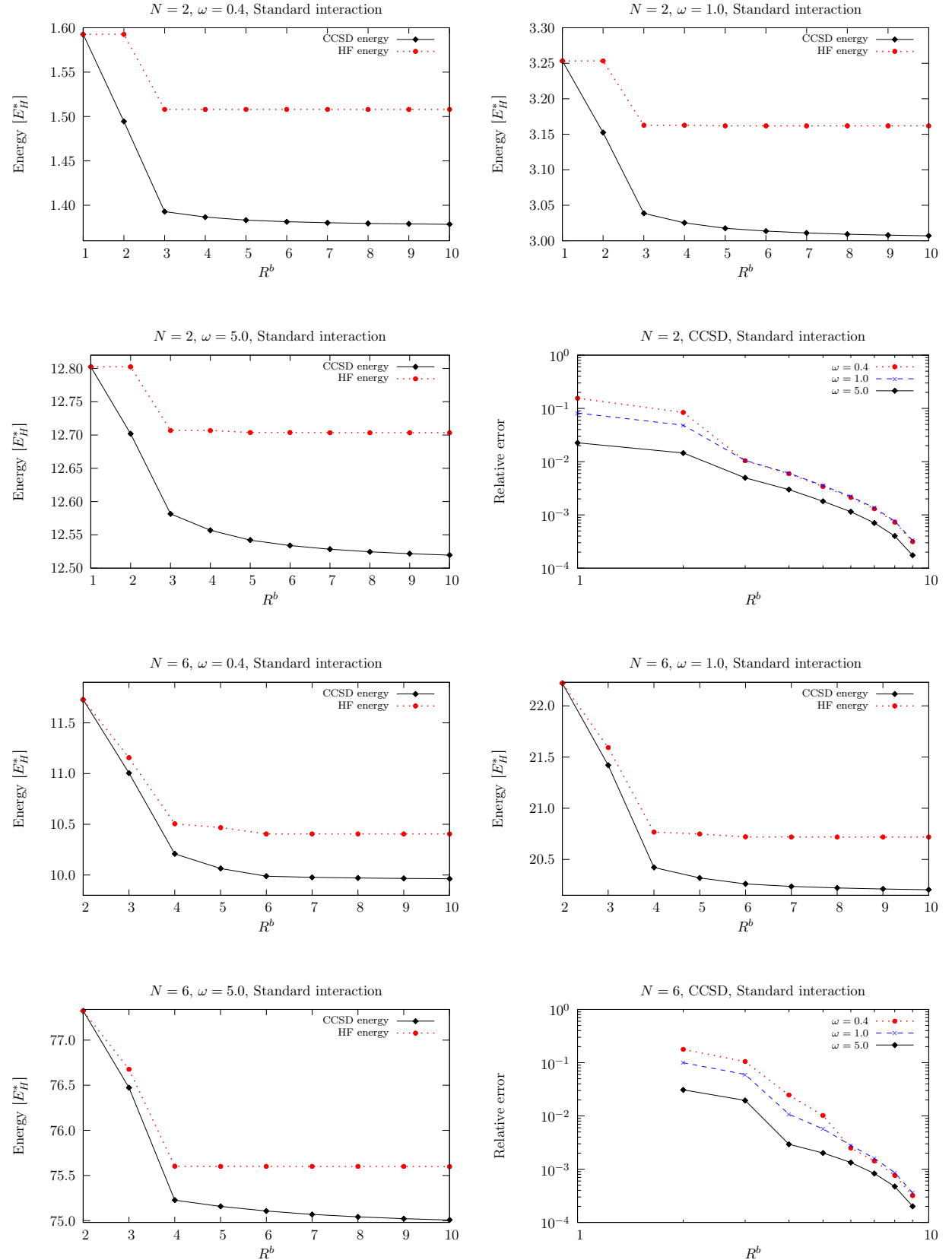


**Figure 8.1:** CCSD and HF energy as function of  $R^b$  for the 2- and 6-electron system with  $\omega = 0.4, 1.0$  and  $5.0$ . For the CCSD energy, the relative error as function of  $R^b$  is also shown. The relative error is given by  $[E(R^b) - E(10)] / E(10)$ . Energy is measured in effective Hartrees ( $E_H^*$ ).

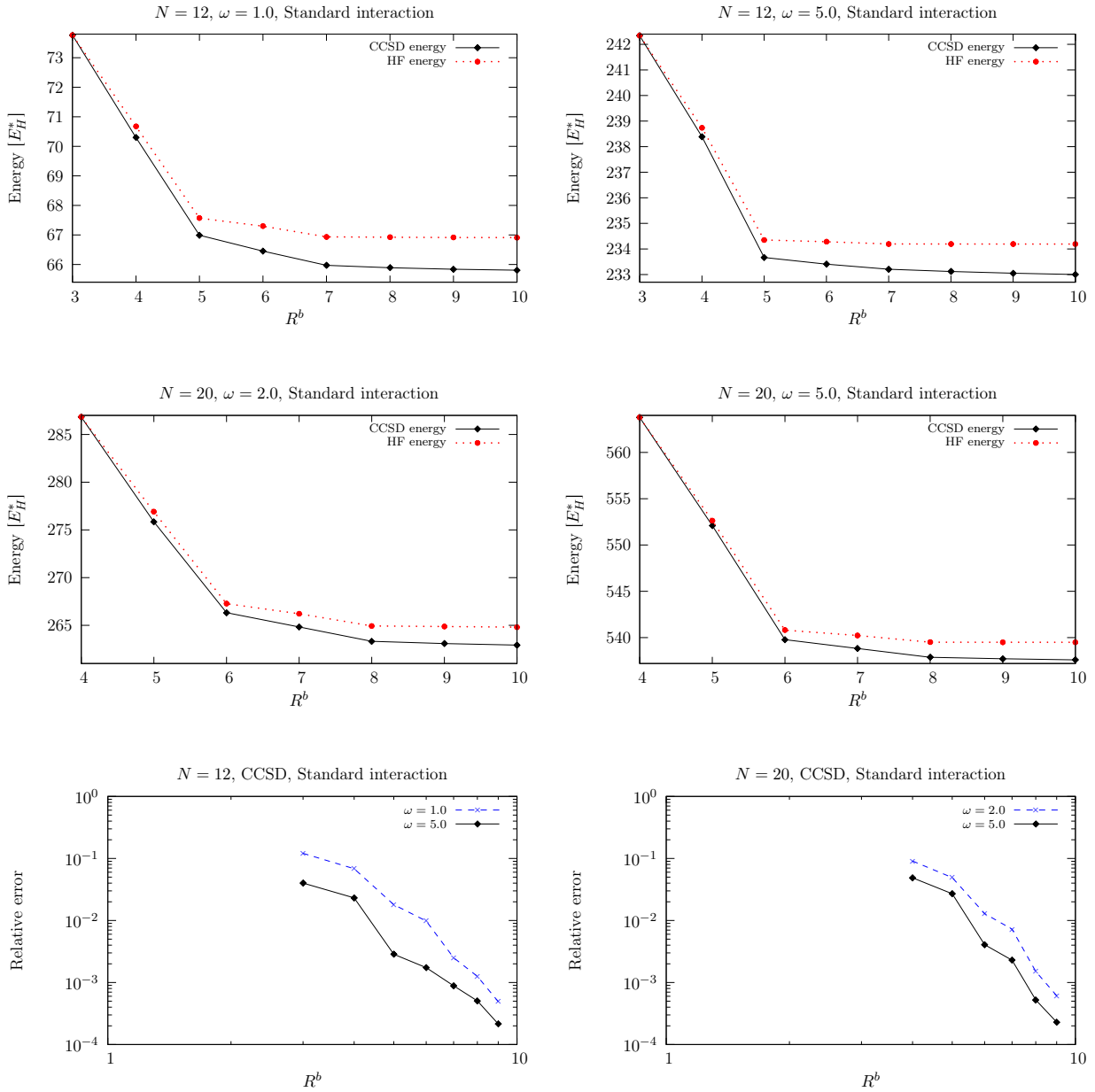


**Figure 8.2:** CCSD and HF energy as function of  $R^b$  for the 12- and 20-electron system. With a harmonic oscillator basis, the CCSD energy does not converge for  $\omega < 1.0$  ( $N = 12$ ), and  $\omega < 2.0$  ( $N = 20$ ). We have therefore chosen  $\omega = 1.0$  and 5.0 for  $N = 12$ , and  $\omega = 2.0$  and 5.0 for  $N = 20$ . The relative error as function of  $R^b$  is also shown for the CCSD energy. The relative error is given by  $[E(R^b) - E(10)] / E(10)$ . Energy is measured in effective Hartrees ( $E_H^*$ ).

The exact results for  $N = 2, 6$  and  $12$  with  $\omega = 1.0$  are given by Taut's analytical result [69] ( $N = 2$ ) and the Diffusion Monte Carlo (DMC) [70] results in Table 8.30. We emphasize that the DMC energy is not the exact energy. However, the exact energy is within the uncertainty of the DMC result [62]. Since the DMC results in Table 8.30 have uncertainties of approximately  $\pm 10^{-4}$ , we refer to these energies as “exact”. For the 2-electron system we see that the difference between the CCSD result for  $R^b = 10$  and the exact result is approximately 0.007. For the 6-electron system, the difference is approximately 0.04. For the 12-electron system, the difference is approximately 0.1.

Table 8.11 shows the CCSD energy for  $N = 6$  and  $\omega = 1.0$  with  $R^b = 12, 14$  and  $16$ . The energies are taken from [70]. We observe that when the size of the basis increases, we obtain

a better energy. We have done a polynomial curve fitting in MATLAB for  $N = 6$  and  $12$ , and extrapolated the CCSD energy to infinity. We have used the results in Table 8.11 in order to obtain a better estimate. The results are shown in Table 8.10. For the 6-electron system we see that the difference between the extrapolated result and the exact result is approximately  $0.02$ . For the 12-electron system, the difference is  $0.08$ . Even though the extrapolated results are closer to the exact energies, we are still not within the uncertainties of the DMC results.

Furthermore, Table 8.12 shows the CCSDT energy for  $N = 6$ ,  $R^b = 10$  and  $\omega = 1.0$  obtained with standard interaction [70]. Comparing with the CCSD result for  $R^b = 10$  in Table 8.10, we see that inclusion of Triples leads to a better energy. This is what we would expect. However, for  $R^b = 16$ , the CCSD energy is better than the CCSDT result for  $R^b = 10$ . This hints that the size of the model space is very important. We will come back to this in Section 8.2.

$R^b$	$N = 6$		$N = 12$	
	CCSD	$ \Delta E $	CCSD	$ \Delta E $
10	20.204345	$\approx 0.04$	65.806539	$\approx 0.1$
$\infty$	20.181	$\approx 0.02$	65.786	$\approx 0.08$

**Table 8.10:** Extrapolated CCSD energies ( $R^b \rightarrow \infty$ ) for  $N = 6$  and  $12$  with  $\omega = 1.0$  and standard interaction (DP model space). We have done a polynomial curve fitting in MATLAB with the results tabulated in Tables 8.5 and 8.7, and extrapolated to infinity. In order to obtain a better fitting for  $N = 6$ , we have included the results for  $R^b = 12, 14$  and  $16$  in Table 8.18. The difference between the CCSD results and the DMC results (see Table 8.30) are given by  $|\Delta E|$ . Energy is measured in effective Hartrees  $E_H^*$ .

$R^b$	CCSD
12	20.19468
14	20.18855
16	20.18431

**Table 8.11:** CCSD results for the 6-electron system with  $\omega = 1.0$  and  $R^b = 12, 14$  and  $16$ , calculated by [70]. The calculations have been done with a standard interaction and the DP space as model space. Energy is measured in effective Hartrees  $E_H^*$ .

$R^b$	CCSDT
10	20.19880

**Table 8.12:** CCSDT result for the 6-electron system with  $\omega = 1.0$  and  $R^b = 10$ , calculated by [70]. The energy is obtained by using the standard interaction and DP model space. Energy is measured in effective Hartrees  $E_H^*$ .

### 8.1.3 Full Correlation Energy

We have in Table 8.9 tabulated energy results for  $R^b = 10$  and different frequencies. For each electron number  $N$  and frequency  $\omega$ , the table shows the non-interacting ground state energy  $\langle \Phi_0 | \hat{H}_0 | \Phi_0 \rangle$ , the HF energy, the CCSD energy, the difference between the CCSD energy and the HF energy, the reference expectation energy  $\langle \Phi_0 | \hat{H} | \Phi_0 \rangle$ , the  $\hat{T}_1$  contribution  $\langle \Phi_0 | \hat{H}_N \hat{T}_1 | \Phi_0 \rangle$ , the  $\hat{T}_1^2$  contribution  $\langle \Phi_0 | \hat{H}_N \hat{T}_1^2 | \Phi_0 \rangle$ , the  $\hat{T}_2$  contribution  $\langle \Phi_0 | \hat{H}_N \hat{T}_2 | \Phi_0 \rangle$ , and the total contribution  $\langle \Phi_0 | \hat{H}_N (\hat{T}_1 + \hat{T}_1^2 + \hat{T}_2) | \Phi_0 \rangle$  to the CCSD energy. First we observe that the non-interacting ground state energy increases when the frequency increases. This is what we expect since the single-particle energies are given by Eq. (8.16). Figure 8.11 shows the non-interacting energy, the CCSD energy, and the HF energy as function of frequency. We see that the energies are approximately linear functions. By taking the electron-electron repulsion into account, the energy increases more when the frequency is changed.

We define the *Full Correlation Energy* (FCE) as the difference between the exact ground state energy of the interacting system, and the non-interacting energy. The FCE is thus the

contribution to the total energy from the electron-electron interaction. Therefore, the difference between the CCSD energy and the non-interacting energy gives us an approximation to the FCE. The Coulomb interaction is repulsive, meaning that the electrons repel each other. The repulsion should obviously give a positive contribution to the energy. We have in Figure 8.3 plotted the FCE as function of frequency. First we observe that the FCE is positive, as expected.

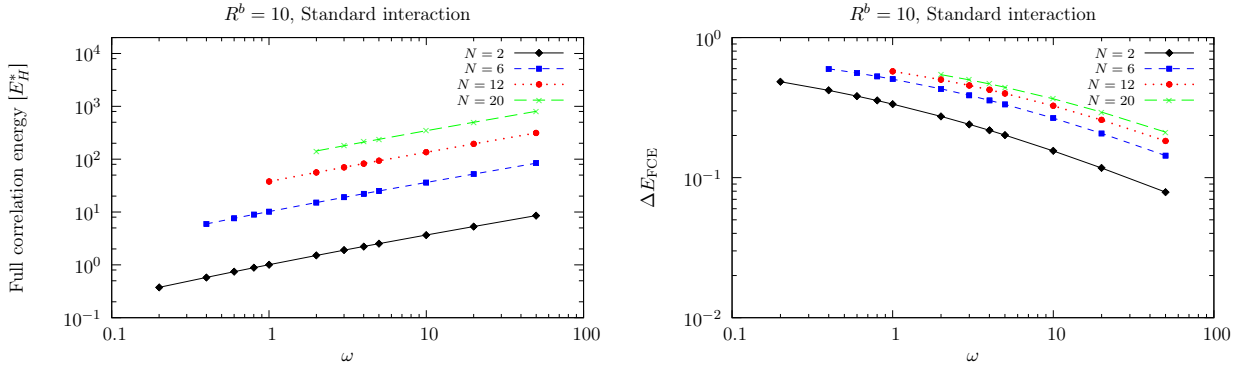


**Figure 8.3:** Full correlation energy (FCE) as function of frequency  $\omega$  (left plot). The FCE is defined as the difference between the CCSD energy and the non-interacting ground state energy. In the right plot, the relative contribution to the CCSD energy  $\Delta E_{\text{FCE}}$  is shown. All calculations have been done with  $R^b = 10$  and standard interaction. Energy is measured in effective Hartrees ( $E_H^*$ ).

Furthermore, the FCE increases when the frequency increases. This can be understood by the following argument: when the frequency increases, the confinement potential

$$u(r) = \frac{1}{2}m^*\omega^2r^2, \quad (8.52)$$

becomes steeper. When the potential well is steeper, the electrons are pushed closer together, yielding a stronger repulsion. Thus the FCE is larger for higher frequencies. However, since the single-particle energy increases when the frequency increases (see Eq. 8.16), this does *not* mean that the contribution from the Coulomb interaction is more important for higher frequencies. We will discuss this in a moment. The FCE can be approximated by

$$f_{\text{FCE}}(\omega) = k_2\omega^b, \quad (8.53)$$

where  $k_2$  and  $b$  are constants. We observe from Figure 8.3 that  $k_2$  depends on the number of electrons in the system, and that  $b$  is approximately independent of the electron number. We have obtained

$$b \approx 0.55. \quad (8.54)$$

Furthermore, for a given frequency, a system containing more electrons than another has a larger contribution from the interaction. This is also what we expect. The more electrons that are present in the system, the larger is the number of interacting particles, obviously. Another important quantity is the relative (full) correlation energy, defined as

$$\Delta E_{\text{FCE}} \equiv \frac{E_{\text{CCSD}} - \langle \Phi_0 | \hat{H}_0 | \Phi_0 \rangle}{E_{\text{CCSD}}}. \quad (8.55)$$

This quantity reveals how important the contribution from the Coulomb interaction is to the total energy, i.e. whether the single-particle field or the Coulomb interaction dominates. The right plot of Figure 8.3 shows  $\Delta E_{\text{FCE}}$  as function of frequency. For a given frequency, the relative contribution is always larger for a system containing more electrons. Secondly, the contribution decreases when the frequency increases. We observe that

$$\Delta E_{\text{FCE}}(\omega) \approx k_3\omega^c, \quad (8.56)$$

where  $k_3$  and  $c$  are constants. This is a rough approximation. We observe that  $k_3$  depends on the number of electrons in the system, and  $c$  is approximately independent of the electron number. We have obtained

$$c \approx -0.3. \quad (8.57)$$

Let us now consider the changes in the relative contribution to the CCSD energy when the frequency increases from the lowest to the highest value. For the 2-electron system, the contribution from FCE is approximately 42% of the CCSD energy when  $\omega = 0.4$ . When  $\omega = 50.0$ , the contribution is 8%. For the 6-electron system, the contribution is approximately 60% when  $\omega = 0.4$ , and 14% when  $\omega = 50.0$ . For the 12-electron system, the contribution is approximately 57% when  $\omega = 1.0$ , and 18% when  $\omega = 50.0$ . For the 20-electron system, the contribution is approximately 54% when  $\omega = 2.0$ , and 21% when  $\omega = 50.0$ . In general, the relative contribution to the energy decreases when the frequency increases. We conclude that the contribution from the electron-electron interaction is more important for low frequencies than for high frequencies. Thus, when the frequency increases, the single-particle field increases more than the electron-electron interaction meaning that the contribution from the Coulomb interaction becomes less and less important.

#### 8.1.4 Correlation Energy

The so-called Correlation Energy (CE) is normally defined as the difference between the HF limit and the exact ground state energy of the interacting system. This definition was introduced in [71]. The CE must not be confused with what we previously defined as the *full* correlation energy (FCE). While the FCE is a measurement of the total contribution from the electron-electron interaction, the CE is a measurement of the contribution from correlations beyond what are included in HF, i.e. 1p1h excitations. In Table 8.9, the difference between the CCSD energy and the HF energy is tabulated. Since the CCSD energy is not exact, and the single-particle basis is truncated in the HF calculation, the difference between the CCSD energy and the HF energy is an approximation to the CE. Figure 8.4 shows the CE (absolute value) as function of frequency. First we observe that the CE does not vary much. Nonetheless, it increases somewhat when the frequency increases, i.e.

$$f_{\text{CE}}(\omega) < f_{\text{CE}}(\omega'), \quad (8.58)$$

for  $\omega > \omega'$ , where  $f_{\text{CE}}$  is the CE. Remember that CE is defined to be negative. For the 2-electron system, the CE changes by approximately  $-0.09$  when the frequency increases from 0.4 to 50.0. For the 6-electron system, it changes by approximately  $-0.19$  when the frequency increases from 0.4 to 50.0. For the 12-electron system, the CE change is approximately  $-0.13$  when the frequency increases from 1.0 to 50.0. Finally, for the 20-electron system, we observe something else. The energy increases from  $\omega = 2.0$  up to  $\omega = 10.0$ , and decreases from  $\omega = 10.0$  up to  $\omega = 50.0$ . We first conclude that a system containing more electrons than another has a larger CE for all frequencies. This is what we expect. Compared to the FCE, however, the differences are relatively small, meaning that 1p1h correlations are important. Anticipate the course of events, this hints to the importance of using a HF basis. We will discuss this in Section 8.1.8. Furthermore, the right plot in Figure 8.4 shows the relative contribution from the CE to the CCSD energy. It is defined as

$$\Delta E_{\text{CE}} = \left| \frac{E_{\text{CCSD}} - E_{\text{HF}}}{E_{\text{CCSD}}} \right|. \quad (8.59)$$

The relative contributions are in accordance with [49]. We observe that  $\Delta E_{\text{CE}}$  can be approximated by a power function function,

$$\Delta E_{\text{CE}}(\omega) \approx k_4 \omega^d, \quad (8.60)$$

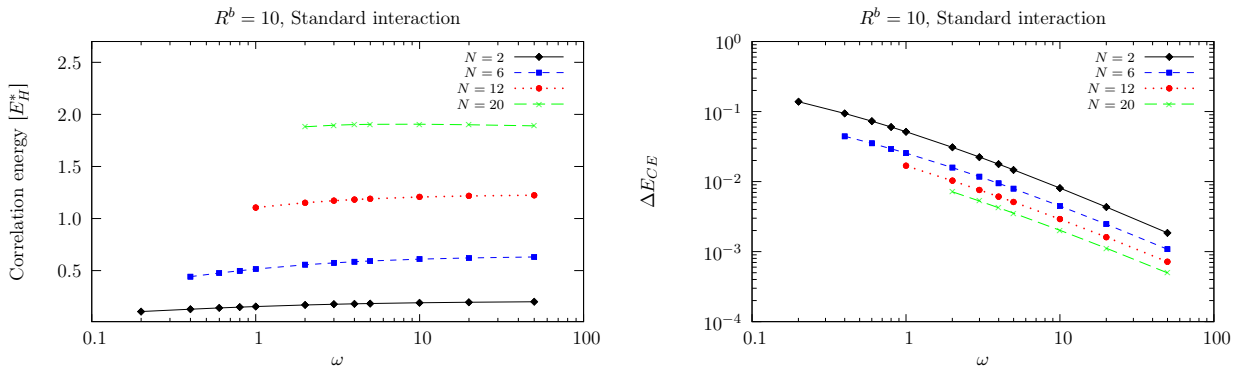


**Figure 8.4:** Correlation energy (absolute value) as function of oscillator frequency  $\omega$  (left plot). The correlation energy is defined as the difference between the CCSD energy and HF energy. In the right plot, the relative contribution from the correlation energy to the CCSD energy (see Eq. 8.55) is shown. All calculations have been done with model space  $R^b = 10$  and standard interaction. Energy is measured in effective Hartrees ( $E_H^*$ ).

where  $k_4$  and  $d$  are constants. We observe that  $k_4$  depends on the number of electrons in the system, and  $d$  is approximately independent of the electron number. We have obtained

$$d \approx -0.78. \quad (8.61)$$

The relative contribution from the CE to the CCSD energy decreases when the frequency increases. Let us for example consider the 2-electron system. When the frequency increases from 0.4 to 50.0, the relative contribution changes from approximately 9% to 0.002%. The CE is therefore much more important for low frequencies. We conclude that when the frequency decreases, the system becomes more correlated. Furthermore, consider the relative contribution from the FCE and the CE in Figures 8.3 and 8.4, respectively. We observe that both contributions decrease when the frequency increases. We have in Eqs. (8.56) and (8.60) approximated the relative correlation energies  $\Delta E_{FCE}$  and  $\Delta E_{CE}$  by power functions, see Eqs. (8.59) and (8.55). We obtained  $c \approx -0.3$  (FCE) and  $d \approx -0.78$  (CE), where  $c$  and  $d$  are the slopes. Thus we have that

$$|c| < |d|. \quad (8.62)$$

Since the FCE is a measurement of the contribution from 1p1h, 2p2h, and so forth up to  $NpNh$  (however, remember  $\hat{T} = \hat{T}_1 + \hat{T}_2$ ), and the CE is a measurement of the contribution from correlations *beyond* 1p1h, we conclude that when the frequency increases, the relative contribution from 1p1h decreases less than the relative contribution from correlations beyond 1p1h. Moreover, when the frequency decreases, the relative contribution from correlations beyond 1p1h increases more than 1p1h correlations, meaning that many-body correlations are important for low frequencies. This does *not* necessarily mean that many-body correlations are more important than 1p1h. We see from Figures 8.3 and 8.4 that the relative FCE is much larger than the relative CE (absolute value), meaning that 1p1h excitations are very important. This has important consequences for the choice of basis for small frequencies. We will discuss this in Section 8.1.8.

Another clear difference between CE and FCE is that their relative contributions depend differently on  $N$ . When the number of electrons in the system increases, the relative contribution from FCE increases while the contribution from CE decreases. As pointed out before, CE is a measurement of the contribution from correlations beyond 1p1h. Increasing the size of the system lowers the relative contribution from 2p2h, 3p3h, up to  $NpNh$  excitations. Thus the correlations beyond the HF approximation is less important when the size of the system increases, i.e. 1p1h excitations are important. This is what we expect.

### 8.1.5 CCSD Correlation Energy

The CCSD energy can be written as (see Section 6.4.3)

$$E_{\text{CCSD}} = \langle \Phi_0 | \hat{H} | \Phi_0 \rangle + \langle \Phi_0 | \hat{H}_N \hat{T}_1 | \Phi_0 \rangle + \langle \Phi_0 | \hat{H}_N \hat{T}_1^2 | \Phi_0 \rangle + \langle \Phi_0 | \hat{H}_N \hat{T}_2 | \Phi_0 \rangle. \quad (8.63)$$

We define the CCSD correlation energy (CCSD-CE) as

$$\begin{aligned} f_{\text{CCSD-CE}} &\equiv E_{\text{CCSD}} - \langle \Phi_0 | \hat{H} | \Phi_0 \rangle \\ &= \langle \Phi_0 | \hat{H}_N \hat{T}_1 | \Phi_0 \rangle + \langle \Phi_0 | \hat{H}_N \hat{T}_1^2 | \Phi_0 \rangle + \langle \Phi_0 | \hat{H}_N \hat{T}_2 | \Phi_0 \rangle. \end{aligned} \quad (8.64)$$

We have in Table 8.9 tabulated  $\langle \Phi_0 | \hat{H} | \Phi_0 \rangle$ ,  $\langle \Phi_0 | \hat{H}_N \hat{T}_1 | \Phi_0 \rangle$ ,  $\langle \Phi_0 | \hat{H}_N \hat{T}_1^2 | \Phi_0 \rangle$ ,  $\langle \Phi_0 | \hat{H}_N \hat{T}_2 | \Phi_0 \rangle$  and  $f_{\text{CCSD-CE}}$ . Figure 8.5 shows the contribution from  $\hat{T}_1$ ,  $\hat{T}_1^2$  and  $\hat{T}_2$  to the CCSD-EC as function of frequency, for 2, 6, 12 and 20 electrons. First we observe that

$$\langle \Phi_0 | \hat{H}_N \hat{T}_1 | \Phi_0 \rangle < 0 \quad (8.65)$$

$$\langle \Phi_0 | \hat{H}_N \hat{T}_1^2 | \Phi_0 \rangle > 0 \quad (8.66)$$

$$\langle \Phi_0 | \hat{H}_N \hat{T}_2 | \Phi_0 \rangle < 0. \quad (8.67)$$

For the 2-electron system, the contribution from  $\hat{T}_2$  is always larger than the contribution from  $\hat{T}_1$  and  $\hat{T}_1^2$ . This means that 2p2h excitations are important. It also explains why the HF energy is not a very good approximation to the exact energy in the 2-electron case. For example, when  $\omega = 1.0$ , the exact energy is 3 [69], the CCSD energy is 3.006938, and the HF energy is 3.161909. Since the CCSD result is close to the exact value, the difference between the HF energy and the exact result is mainly because 2p2h correlations are not included. Furthermore, for larger systems (6, 12 and 20 electrons), we observe that

$$\left| \langle \Phi_0 | \hat{H}_N \hat{T}_1 | \Phi_0 \rangle \right| > \left| \langle \Phi_0 | \hat{H}_N \hat{T}_1^2 | \Phi_0 \rangle \right| \quad (8.68)$$

$$\left| \langle \Phi_0 | \hat{H}_N \hat{T}_1 | \Phi_0 \rangle \right| > \left| \langle \Phi_0 | \hat{H}_N \hat{T}_2 | \Phi_0 \rangle \right|, \quad (8.69)$$

i.e. the contribution from  $\hat{T}_1$  is larger than both the contribution from  $\hat{T}_1^2$ , and from  $\hat{T}_2$ . When the size of the system increases from 6 to 12 electrons, the contribution from  $\hat{T}_1$  increases by approximately a factor of 8, while the contribution from  $\hat{T}_1^2$  and  $\hat{T}_2$  roughly remain the same. When the size of the system increases from 12 to 20 electrons, the contribution from  $\hat{T}_1$  and  $\hat{T}_2$  still remains roughly the same. However, the contribution from  $\hat{T}_1$  increases by roughly a factor of 3. We conclude that the single-particle field is stronger for a system containing more electrons. Furthermore, the contribution from  $\hat{T}_1$  and  $\hat{T}_2$  increase (absolute value) when the frequency increases. However, the contribution from  $\hat{T}_1^2$  decreases. We also see that the contribution from  $\hat{T}_2$  is less sensitive to changes in the frequency for larger systems. For the 20-electron system, the change is approximately 0.05 when the frequency increases from 2.0 to 50.0. For the 2-electron system, the change is approximately 0.07 when the frequency increases from 0.4 to 50.0.

We have in Figure 8.6 plotted the CCSD-CE (left plot) defined in Eq. (8.64), i.e. the total contributions from  $\hat{T}_1$ ,  $\hat{T}_1^2$  and  $\hat{T}_2$ , and the relative contribution to the CCSD energy (right plot). The relative contribution is defined as

$$\Delta E_{\text{CCSD-CE}} \equiv \left| \frac{f_{\text{CCSD-CE}}}{E_{\text{CCSD}}} \right|. \quad (8.70)$$

First we observe that the CCSD-EC increases (absolute value) when the size of the system increases. This is what we would expect. Moreover, when the frequency increases, the CCSD-EC also increases. However, the CCSD-EC is much more sensitive to changes in the frequency for larger systems. We observe that for the 2-electron system, the curve is flat compared to the 20-electron system. We conclude that when the frequency increases, the CCSD-EC (absolute

value) increases more for a system containing more electrons than another. Furthermore, for a given frequency, the relative contribution from the CCSD-EC increases when the size of the system increases. This is the same behavior as the Full Correlation Energy (FCE). Even though the definitions of FCE and CCSD-EC are different, both quantities give information about the correlations in the system. We observe that when the frequency decreases, the relative contribution from CCSD-EC increases. Thus the system is more correlated for low frequencies.

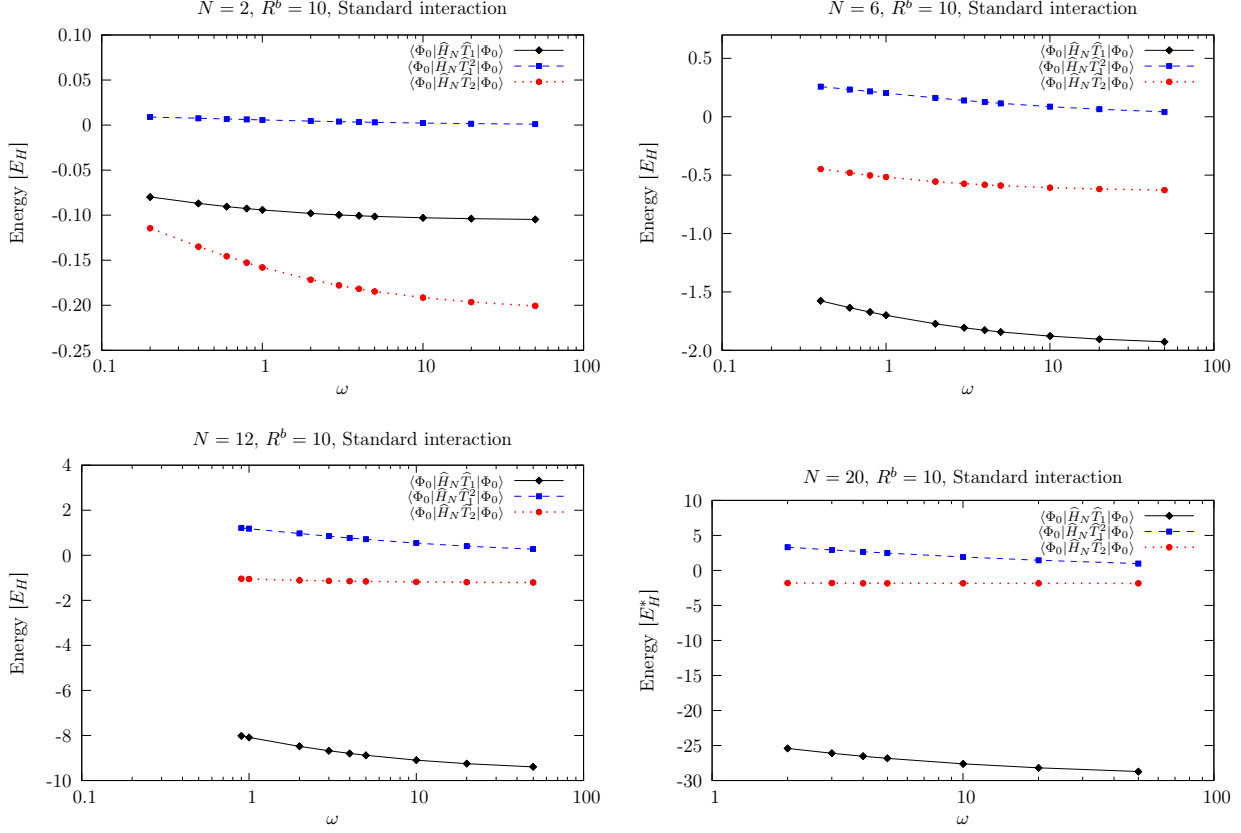


**Figure 8.5:** Contributions to the CCSD correlation energy (defined in Eq. 8.64) as function of frequency  $\omega$ , for 2, 6, 12 and 20 electrons. The CCSD calculations have been done with model space  $R^b = 10$ , and standard interaction. Energy is measured in effective Hartrees  $E_H^*$ .

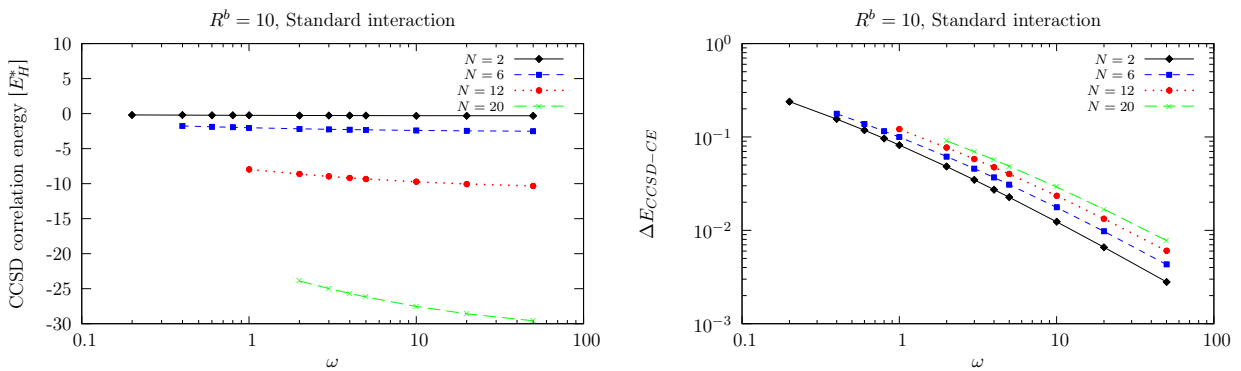


**Figure 8.6:** CCSD correlation energy as function of frequency for 2, 6, 12 and 20 electrons (left plot). The CCSD correlation energy is defined in Eq. (8.64). The right plots shows the relative contribution to the CCSD energy as function of frequency, defined in Eq. (8.70). The CCSD calculations have been done with  $R^b = 10$  and standard interaction. Energy is measured in effective Hartrees  $E_H^*$ .

### 8.1.6 Analysis of the Amplitudes

We will in this section analyze the  $\widehat{T}_1$  and  $\widehat{T}_2$  amplitudes. We want to find out if it is possible to extract general tendencies for different system sizes and oscillator frequencies. We first define the total  $\widehat{T}_1$  contribution as

$$t_1(R) \equiv \sum_{i \leq i_f} \sum_{a \in R} |t_i^a|^2, \quad (8.71)$$

where  $i_f$  is the Fermi state, and  $a \in R$  means all orbitals within shell  $R$  (see Table 8.2). Remember that  $i$  denotes a hole state and  $a$  denotes a particle state. We see from the definition that  $t_1(R)$  is the sum of all  $\widehat{T}_1$  amplitudes (squared) having contribution from shell  $R$ . This is an interesting quantity since it may reveal the shells that are most important. Figure 8.7 shows the plot of  $t_1(R)$ . We observe that for the 2-electron system,

$$t_1(R) \approx \mathcal{C} e^{\eta R}, \quad (8.72)$$

where  $\mathcal{C}$  is a constant determined by the frequency, and  $\eta$  is a constant that is approximately independent of the frequency. We observe that

$$\eta \approx -1.2. \quad (8.73)$$

The  $\widehat{T}_1$  amplitudes are nonzero for odd shells. Stated differently, when we increase the basis from an even number to an odd number by one, we do not get additional 1p1h excitations. This is exactly what we observed for the HF energy in Table 8.5. This reflects that HF includes 1p1h excitations only.

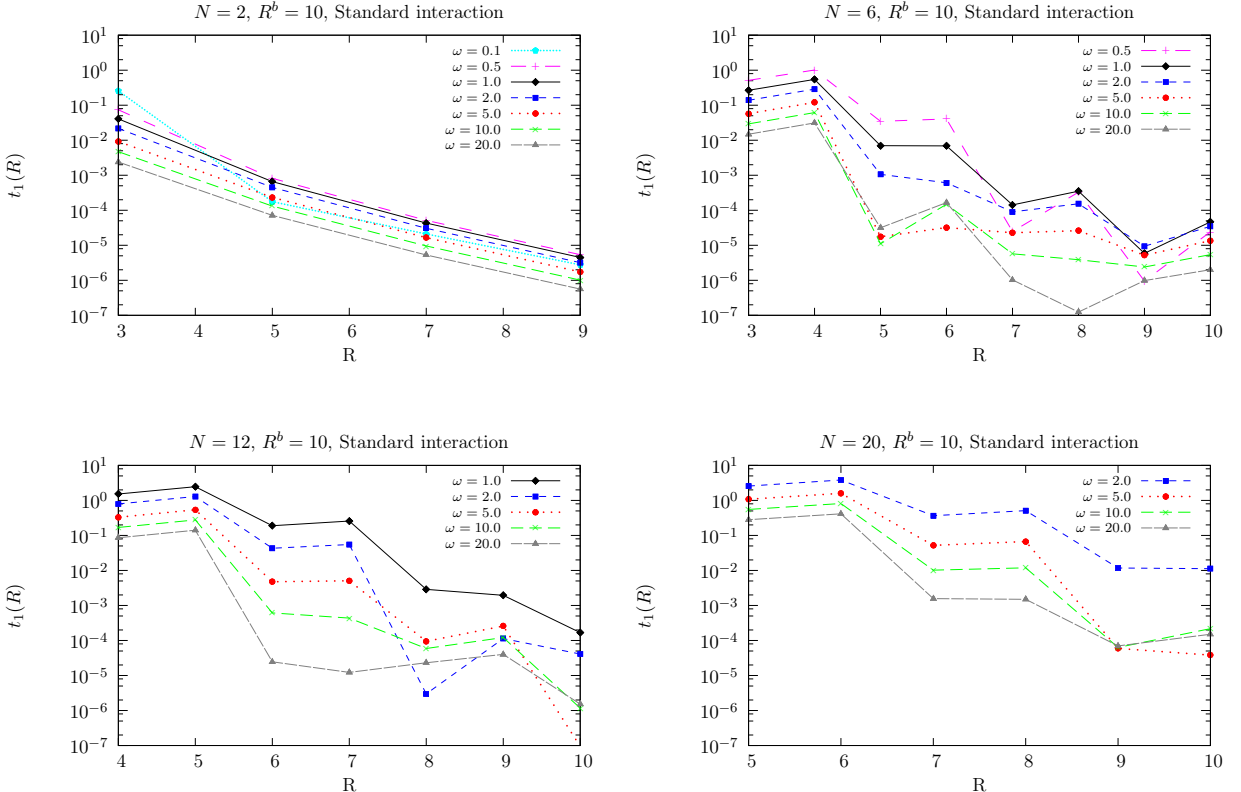


**Figure 8.7:** Total  $\widehat{T}_1$  contribution  $t_1(R)$  (defined in Eq. 8.71) for systems with 2, 6, 12 and 20 electrons. The CCSD calculations have been done with model space  $R^b = 10$  and for different frequencies  $\omega$ . Note that the excitation amplitudes are not normalized.

Turning to systems containing 6, 12 and 20 electrons we see that  $t_1(R)$  changes radically. Although it tends to decrease for higher shells,  $t_1(R)$  can increase from one shell to another. For example, the contribution from shell 4 tend to be more important than the contribution from shell 3. For  $\omega = 1.0$  we observe that  $t_1(R_{\text{odd}})$  and  $t_1(R_{\text{even}})$  are approximately exponential functions (straight lines in the plot) for systems containing 6 and 12 electrons. However, this is not true for other frequencies. It is important to note that the excitation amplitudes are *not* normalized. This follows from Eq. (6.48). Thus we cannot directly compare the quantitative values of  $t_1(R)$  for different frequencies. Figure 8.7 can only be used to gain insight into how  $t_1(R)$  depends on  $R$  for a given frequency. It is difficult to observe general tendencies in the figure. The “staggering-effect” is the reason for this.

We define the total  $\hat{T}_2$  contribution as

$$t_2(R_1, R_2) \equiv \frac{1}{2} \sum_{ij \leq i_f} \sum_{a \in R_1} \sum_{b \in R_2} |t_{ij}^{ab}|^2, \quad (8.74)$$

where  $a \in R_1$  means all orbitals within shell  $R_1$ , and  $b \in R_2$  means all orbitals within shell  $R_2$ . We see from the definition that  $t_2(R_1, R_2)$  is the sum of all  $\hat{T}_2$  amplitudes (squared) having contributions from shell  $R_1$  and  $R_2$ . It gives an indication of which shells that are most important. Thus it is an interesting quantity to analyze. Figures 8.8 and 8.9 show the plot of

$$t_2^{R_1}(R_2) \equiv t_2(R_1, R_2), \quad (8.75)$$

for different values of  $R_1$ . Note that the excitation amplitudes are not normalized. Consider the 2-electron system. We observe that

$$t_{ij}^{ab} = t_{ij}^{ba} = 0 \quad (8.76)$$

when

$$a \in R_{\text{odd}} \quad (8.77)$$

$$b \in R_{\text{even}}, \quad (8.78)$$

where  $R_{\text{odd}}$  is an odd shell, and  $R_{\text{even}}$  is an even shell. This is due to the fact that there are none 2p2h excitations that conserve total angular momentum and total spin. As we discussed previously for the 2-electron system, states that have

$$M = 0 \quad (8.79)$$

$$S = 0 \quad (8.80)$$

are allowed. Consider for example shell 3 and 4 with corresponding single-particle states in Table 8.2. The mapping scheme is given in Table 8.1. We see that orbitals within shell 3 have  $m = -2, 0$  and  $2$ , and orbitals within shell 4 have  $m = -3, -1, 1$  and  $3$ . Thus we cannot excite one electron into shell 3, and another electron into shell 4. This is what we observe in Figure 8.8. Furthermore, we observe that  $t_2(R)$  decreases in an exponential way. This indicates that low-lying shells are most important.

Turning to the system consisting of 6 electrons we observe that  $t_2(R)$  changes radically. The “staggering-effect” makes it difficult to observe any general tendencies besides that  $t_2(R)$  tend to decrease. When the system is larger (12 or 20 electrons) we observe that the “staggering-effect” is less present. Still we cannot draw any general conclusions.

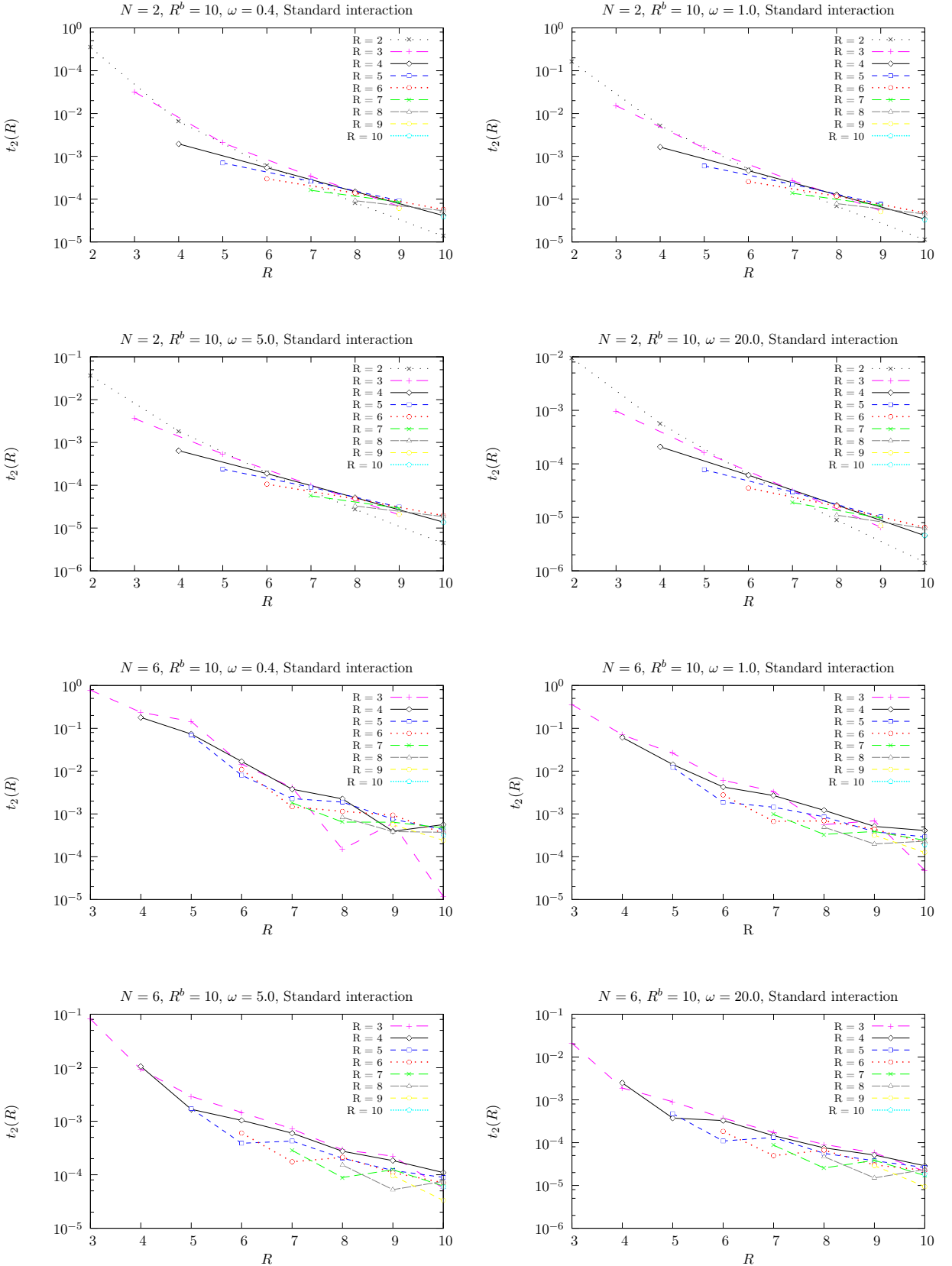


**Figure 8.8:** Total  $\widehat{T}_2$  contribution  $t_2(R)$  (defined in Eqs. 8.74 and 8.75) for systems containing 2 and 6 electrons. The CCSD calculations have been done with model space  $R^b = 10$  and for different frequencies  $\omega$ . Note that the excitation amplitudes are not normalized.

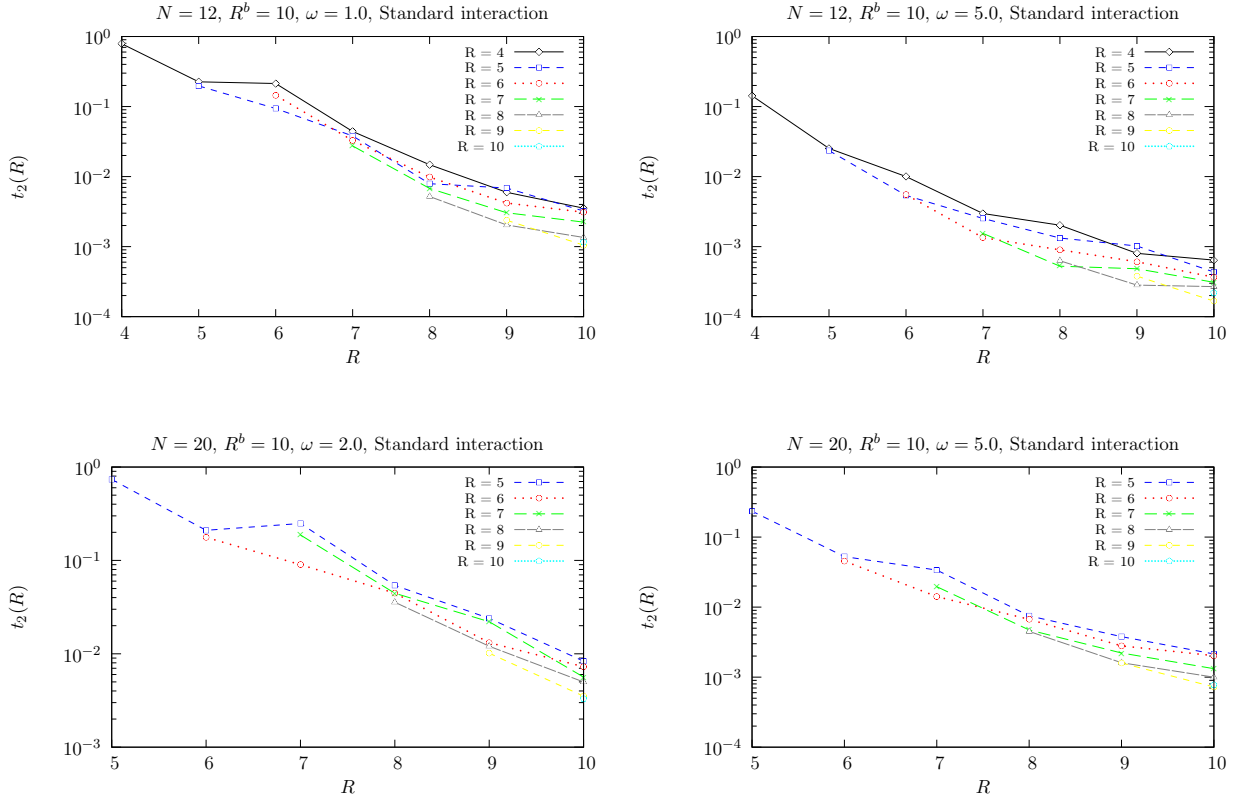


**Figure 8.9:** Total  $\hat{T}_2$  contribution  $t_2(R)$  (defined in Eqs. 8.74 and 8.75) for systems containing 12 and 20 electrons. The CCSD calculations have been done with model space  $R^b = 10$  and for different frequencies  $\omega$ . Note that the excitation amplitudes are not normalized.

### 8.1.7 Analysis of Basis Size

The accuracy of the CCSD results are obviously dependent on the size of the model space. Normally we obtain a better accuracy when the size of the model space increases. Thus we often like to run our calculations with a model space as large as possible. In wavefunction-based methods, such as Coupled-Cluster and Configuration Interaction [30], we quickly reach the maximum size of the model space due to computational limitations. It is therefore interesting to gain insight into how sensitive our results are on the size of the model space for different frequencies. In order to analyze this, we have in Figure 8.10 plotted

$$g_6(\omega) \equiv E_{R^b=6}(\omega) - E_{R^b=10}(\omega) \quad (8.81)$$

$$g_9(\omega) \equiv E_{R^b=9}(\omega) - E_{R^b=10}(\omega), \quad (8.82)$$

where  $E_{R^b}$  is the CCSD energy with model space  $R^b$ . The relative errors, defined as

$$\Delta E_6(\omega) \equiv \frac{g_6(\omega)}{E_{R^b=10}(\omega)} \quad (8.83)$$

$$\Delta E_9(\omega) \equiv \frac{g_9(\omega)}{E_{R^b=10}(\omega)}, \quad (8.84)$$

are also shown. First we observe that for a given frequency, both  $g_6(\omega)$  and  $g_9(\omega)$  increases when the size of the system increases, i.e.

$$g_6^N(\omega) > g_6^{N'}(\omega) \quad (8.85)$$

$$g_9^N(\omega) > g_9^{N'}(\omega), \quad (8.86)$$

when  $N > N'$ . This is an important similarity. Furthermore, we observe that  $g_6(\omega)$  and  $g_9(\omega)$  vary much more in the low-frequency region than in the high-frequency region. In the 2-electron case,  $g_6(\omega)$  and  $g_9(\omega)$  are roughly independent of the frequency. The curve is almost flat. Turning to the 6-electron system, both  $g_6(\omega)$  and  $g_9(\omega)$  increase somewhat in the low-frequency region, and then flatten out. In the case of 12 and 20 electrons,  $g_6(\omega)$  and  $g_9(\omega)$  depend quite differently on the frequency. We see that  $g_6(\omega)$  decreases exponentially for systems containing 12 and 20 electrons. However, for the 12-electron system,  $g_9(\omega)$  increases when the frequency increases. For the 20-electron system,  $g_9(\omega)$  decreases when the frequency increases from 2.0 to 5.0, and then increases from 5.0 to 50.0. Both  $g_6(\omega)$  and  $g_9(\omega)$  tend to stabilize (converge) in the high-frequency region.

Consider the relative error plots in the second column of Figure 8.10. We see that the plots of  $\Delta E_6(\omega)$  and  $\Delta E_9(\omega)$  are relatively equal. For systems containing 2 and 6 electrons,

$$\frac{d}{d\omega} \Delta E_6(\omega) = \frac{d}{d\omega} \Delta E_9(\omega) = 0, \quad (8.87)$$

when  $\omega \approx 0.8$ . The errors increase up to  $\omega \approx 0.8$ , and then decrease for higher frequencies. For systems containing 12 and 20 electrons, the relative errors are given by

$$\Delta E_6(\omega) \approx k_6 \omega^{\lambda_6} \quad (8.88)$$

$$\Delta E_9(\omega) \approx k_9 \omega^{\lambda_9}, \quad (8.89)$$

where  $k_6 = k_6(N)$ ,  $k_9 = k_9(N)$ ,  $\lambda_6$  and  $\lambda_9$  are constants. We see that  $\lambda_6 < 0$  and  $\lambda_9 < 0$ . For low frequencies, both  $\Delta E_6(\omega)$  and  $\Delta E_9(\omega)$  depend strongly on the number of electrons. However, the relative errors converge in the high-frequency region. Moreover, here they are approximately independent of the electron number. We observe that  $\Delta E_6(\omega)$  is approximately equal for 2, 6 and 12 electrons, and  $\omega \geq 10$ . When  $20 \leq \omega \leq 50$ ,

$$\Delta E_6(20 \leq \omega \leq 50) \approx 5 \cdot 10^{-4}, \quad (8.90)$$

for 2, 6, 12 and 20 electrons. Since  $\Delta E_9(\omega)$  is about a factor 1/10 lower than  $\Delta E_6(\omega)$ , it seems to converge somewhat slower. When  $\omega \geq 20$ ,  $\Delta E_9(\omega)$  is approximately equal for systems containing 2, 6, 12 and 20 electrons. When  $\omega = 50$ ,

$$\Delta E_9(\omega = 50) \approx 5 \cdot 10^{-5}. \quad (8.91)$$

We conclude that in general, the size of the model space is more important for low frequencies than for high frequencies, except for  $\omega \leq 0.8$  and  $N = 2$  and 6. We also conclude that when the number of electrons in the system increases, the size of basis is more important. Thus in the low frequency region ( $\omega \leq 10$ ), in order to obtain an accuracy for a system containing  $N$  electrons that is equal to the accuracy of a system containing  $N'$  electrons, where  $N > N'$ , the model space must be larger.

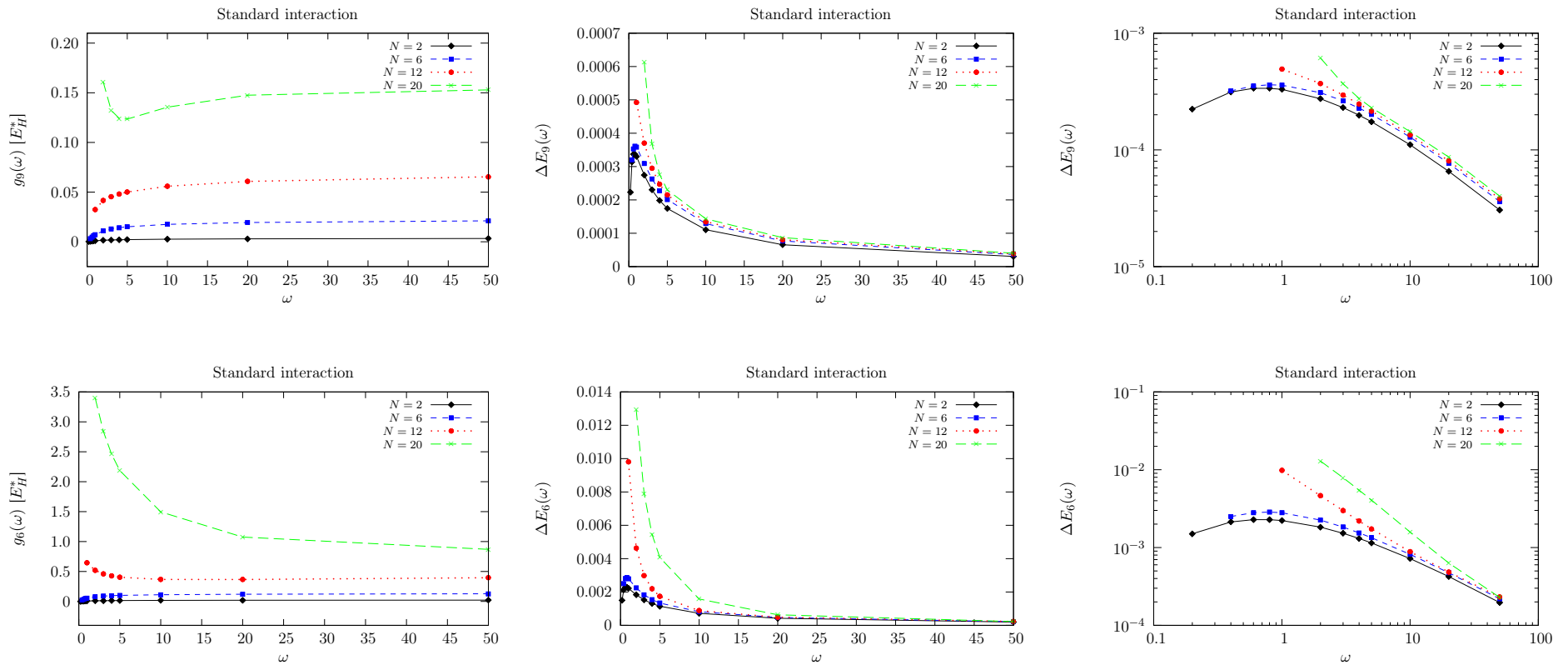


**Figure 8.10:** The first column shows the difference between the CCSD energy for  $R^b = 10$  and  $R^b = 6/R^b = 9$  as function of oscillator frequency  $\omega$ . See definitions of  $g_6(\omega)$  and  $g_9(\omega)$  in Eqs. (8.81) and (8.82). Energy is measured in effective Hartrees ( $E_H^*$ ). The relative errors,  $\Delta E_6(\omega)$  and  $\Delta E_9(\omega)$  (see Eqs. 8.83 and 8.84), are shown in the second column, with corresponding loglog-plots in the third column.

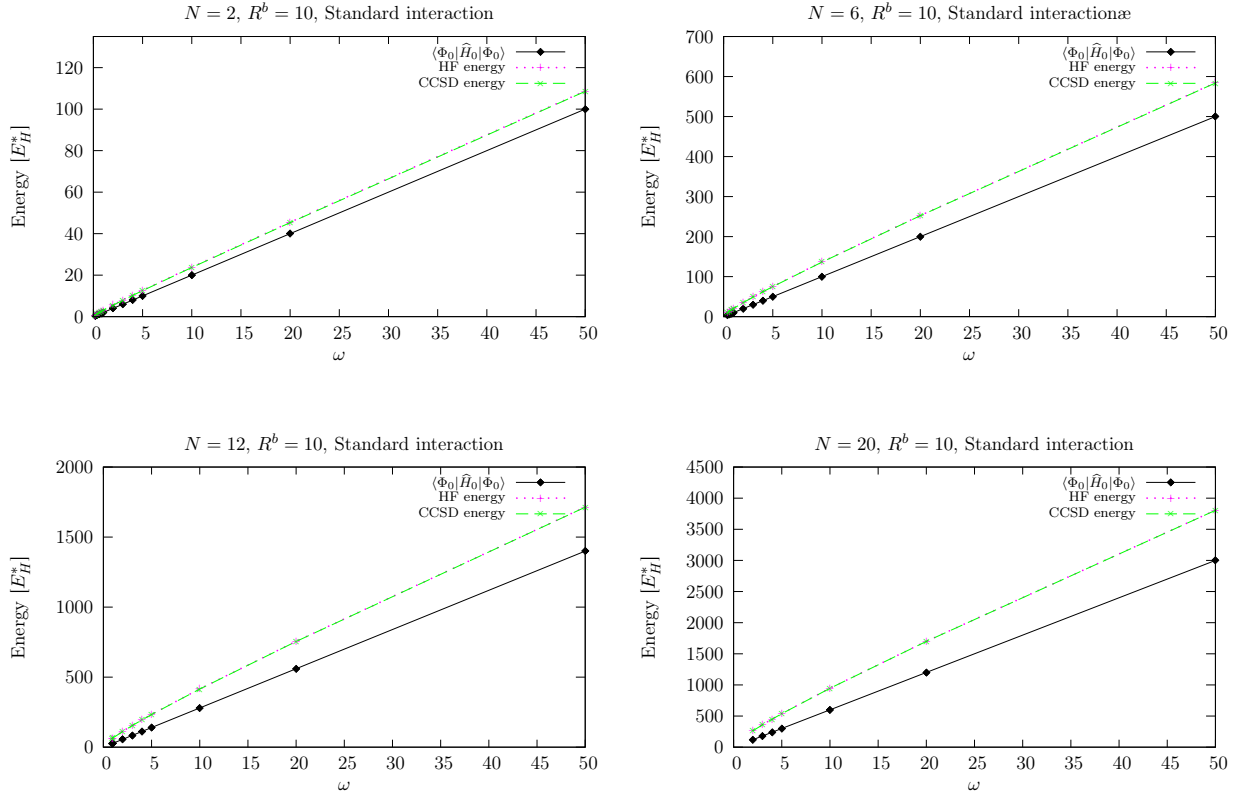


**Figure 8.11:** Non-interacting energy  $\langle \Phi_0 | \hat{H}_0 | \Phi_0 \rangle$ , HF energy, and CCSD energy as function of frequency. All calculations have been done with  $R^b = 10$  and standard interaction. Energy is measured in effective Hartrees  $E_H^*$ .

### 8.1.8 Hartree-Fock Basis

The results presented till now have been calculated with harmonic oscillator functions as basis functions. We have seen that the CCSD energy does not converge for certain (low) values of  $\omega$  (see Table 8.4). Moreover, when size of the system increases, the limit (frequency) where the energy converges and where it does not converge seems to increase. This is an unsatisfactory situation. We would like to calculate the ground state energy for low values of the frequency as well. In addition, low frequencies often represent the most interesting cases. We have in the previous sections seen (in the analysis of FCE, CE and CCSD-CE) that the relative contribution from the electron-electron interaction is larger for low frequencies. We would obviously like to investigate the accuracy of the CCSD method for these cases as well.

The question is: “what can we do in order to obtain convergence for low values of the frequency?” In CC calculations of the atomic nucleus, one must use a Hartree-Fock basis in order to obtain convergence, see for example [72]. We therefore propose to generate a HF basis for the parabolic quantum dot and run the CCSD calculation with these basis functions. The HF basis is the set of orthonormal HF orbitals obtained by a HF calculation. See Chapter 5 for details. The HF basis is given as

$$\mathcal{B}_{\text{HF}} = \left\{ \varphi_a(\mathbf{r}) \right\}_{a=1}^{d_b}, \quad (8.92)$$

where  $d_b$  is the dimension of the single-particle model space. The HF orbitals reads

$$\varphi_a(\mathbf{r}) = \sum_{\alpha=1}^{d_b} C_{a\alpha} \psi_{\alpha}(\mathbf{r}), \quad (8.93)$$

where

$$\mathcal{B}_1 = \left\{ \psi_\alpha(\mathbf{r}) \right\}_{\alpha=1}^{d_b} \quad (8.94)$$

is the set of harmonic oscillator functions. Note that  $\mathcal{B}_{HF}$  and  $\mathcal{B}_1$  span the same single-particle model space. Using  $\mathcal{B}_{HF}$  as single-particle basis we obtain that

$$\langle a|h|b \rangle = \sum_{\alpha\beta}^{d_b} C_{a\alpha}^* C_{b\beta} \langle \alpha|h|\beta \rangle, \quad (8.95)$$

and

$$\langle ab|v|cd \rangle = \sum_{\alpha\beta\gamma\delta}^{d_b} C_{a\alpha}^* C_{b\beta}^* C_{c\gamma} C_{d\delta} \langle \alpha\beta|v|\gamma\delta \rangle, \quad (8.96)$$

where the expansion coefficients are determined by the HF calculation.

In order to check the CCSD machinery with a HF basis, we have in Table 8.13 tabulated the results for  $N = 2$  and  $\omega = 1.0$  using a HF basis. We observe that we reproduce the results obtained with harmonic oscillator functions as basis functions, see Table 8.5.

We have chosen to calculate the CCSD energy for  $\omega = 0.2$  ( $N = 6$ ),  $\omega = 0.8$  ( $N = 12$ ) and  $\omega = 1.0$  ( $N = 20$ ) with a HF basis. The results are tabulated in Tables 8.14, 8.15 and 8.16, respectively. We observe that the CCSD energies converge. Thus by including some of the correlations, viz. 1p1h correlations, in the basis, we obtain convergence.

$R^b$	$N = 2$
2	3.152329
4	3.025232
6	3.013627
8	3.009237
10	3.006938

**Table 8.13:** CCSD results for the 2-electron system with  $\omega = 1.0$  obtained by using a HF basis (see Eq. 8.92). We have used standard interaction and DP model space. We see that the energies are equal the results obtained with harmonic oscillator functions in Table 8.5. Energy is measured in effective Hartrees  $E_H^*$ .

$R^b$	$N = 6$
2	7.464866
4	6.192991
6	5.963611
8	5.953721
10	5.950087

**Table 8.14:** CCSD results for the 6-electron system with  $\omega = 0.2$  obtained by using a HF basis (see Eq. 8.92). We have used standard interaction and DP model space. Energy is measured in effective Hartrees  $E_H^*$ .

$R^b$	$N = 12$
4	60.007157
6	56.386937
8	55.792561
10	55.709855

**Table 8.15:** CCSD results for the 12-electron system with  $\omega = 0.8$  obtained using a HF basis (see Eq. 8.92). We have used standard interaction and DP model space. Energy is measured in effective Hartrees  $E_H^*$ .

$R^b$	$N = 20$
4	177.963297
6	160.592549
8	157.035291
10	156.365862

**Table 8.16:** CCSD results for the 20-electron system with  $\omega = 1.0$  obtained using a HF basis (see Eq. 8.92). We have used standard interaction and DP model space. Energy is measured in effective Hartrees  $E_H^*$ .

## 8.2 Effective Interaction

The CCSD results with standard interaction converge slowly as function  $R^b$ . Moreover, the energies for 6 and 12 electrons with  $\omega = 1.0$  are not within the uncertainty of the DMC results in Table 8.30. The differences is tabulated in Table 8.10. In order to improve our results we must increase the size of the model space.

The number of Slater determinants increases exponentially with respect to the size of the single-particle basis. It is given by the binomial factor

$$n_S = \binom{n}{N}, \quad (8.97)$$

where  $n$  is the number of single-particle states, and  $N$  is the number of electrons. For example, when  $N = 6$  and  $n = 110$  (10 shells) we have  $2 \times 10^{10}$  available Slater determinants. This set spans the  $DP(R^b)$  model space. Since the number increases exponentially we quickly reach the computational limit. A common way to circumvent the dimensionality problem is to introduce a renormalized Coulomb interaction, called effective interaction, that is defined in the model space. Effective Hamiltonians and interactions are commonly used in nuclear shell-model calculations [21, 22]. We will not give a profound presentation of the nuclear effective interaction theory. We refer to [22, 73, 74] for further reading. Put simply, an effective Hamiltonian is a Hamiltonian that reproduces exact eigenvalues of the full problem within a finite-dimensional model space [75]. We will in the following give a brief overview of the basic ideas.

### 8.2.1 Basic Ideas

Assume that the  $N$ -electron Hilbert space is finite-dimensional, i.e.  $n = \dim(\mathcal{H}_N)$ . The spectral decomposition of the Hamiltonian reads

$$\hat{H} = \sum_{k=1}^n E_k |\Psi_k\rangle\langle\Psi_k|, \quad (8.98)$$

where  $\{|\Psi_k\rangle\}_{k=1}^n$  is the orthonormal set of energy eigenfunctions satisfying

$$\hat{H}|\Psi_k\rangle = E_k |\Psi_k\rangle, \quad (8.99)$$

where  $E_k$  is the energy eigenvalue that corresponds to  $|\Psi_k\rangle$ . We define the model space  $\mathcal{P} \subset \mathcal{H}$  as

$$\mathcal{P} \equiv \text{span}\{|e_k\rangle : k = 1, 2, \dots, m\}, \quad (8.100)$$

where  $\{|e_k\rangle\}_{k=1}^m$  is an orthonormal basis, and  $m = \dim(\mathcal{P})$ . Furthermore, we define the operator  $\hat{P}$  as the orthogonal projector of  $\mathcal{P}$ . Its spectral decomposition reads

$$\hat{P} = \sum_{i=1}^m |e_i\rangle\langle e_i|. \quad (8.101)$$

The orthogonal complement of  $\mathcal{P}$  is  $\mathcal{Q} \subset \mathcal{H}_N$ , which is often called the excluded space. Its orthogonal projector reads

$$\widehat{Q} = 1 - \sum_{i=1}^m |e_i\rangle\langle e_i| \quad (8.102)$$

$$= \sum_{i=(m+1)}^n |e_i\rangle\langle e_i|, \quad (8.103)$$

The dimension of  $\mathcal{Q}$  is  $l = \dim(\mathcal{Q}) = n - m$ . We have now divided  $\mathcal{H}_N$  into  $\mathcal{P}$  and  $\mathcal{Q}$ . This division transfers to operators in  $\mathcal{H}_N$ . An arbitrary operator  $\widehat{A}$  splits up in four parts, viz.

$$\widehat{A} = (\widehat{P} + \widehat{Q}) \widehat{A} (\widehat{P} + \widehat{Q}) = \widehat{P}\widehat{A}\widehat{P} + \widehat{P}\widehat{A}\widehat{Q} + \widehat{Q}\widehat{A}\widehat{P} + \widehat{Q}\widehat{A}\widehat{Q}, \quad (8.104)$$

since

$$\widehat{P} + \widehat{Q} = 1. \quad (8.105)$$

We see that  $\widehat{P}\widehat{A}\widehat{P}$  maps  $\mathcal{P}$  into itself,  $\widehat{P}\widehat{A}\widehat{Q}$  maps  $\mathcal{Q}$  into  $\mathcal{P}$ , and so forth. It is convenient to picture this in the following block (matrix) form:

$$\widehat{A} = \begin{pmatrix} \widehat{P}\widehat{A}\widehat{P} & \widehat{P}\widehat{A}\widehat{Q} \\ \widehat{Q}\widehat{A}\widehat{P} & \widehat{Q}\widehat{A}\widehat{Q} \end{pmatrix} \quad (8.106)$$

We define the similarity transformed Hamiltonian as

$$\widehat{H}' \equiv e^{-\widehat{S}} \widehat{H} e^{\widehat{S}}, \quad (8.107)$$

where  $\widehat{H}$  is the Hamiltonian of the system, and  $\widehat{S}$  is chosen such that

$$\widehat{Q}\widehat{H}'\widehat{P} = \widehat{P}\widehat{H}'\widehat{Q} = 0. \quad (8.108)$$

This is called the de-coupling equation. The effective Hamiltonian is defined as

$$\widehat{H}_{\text{eff}} \equiv \widehat{P}\widehat{H}'\widehat{P}. \quad (8.109)$$

Since similarity transformations preserve eigenvalues, the  $m$  eigenvalues of  $\widehat{H}_{\text{eff}}$  are identical to some of the  $n$  eigenvalues of  $\widehat{H}$ . We assume that the eigenvalues of  $E_k$  in Eq. (8.98) are arranged so that  $E_k$  ( $k = 1, \dots, m$ ) are reproduced by  $\widehat{H}_{\text{eff}}$ . Furthermore, we define the effective interaction as

$$\widehat{V}_{\text{eff}} \equiv \widehat{H}_{\text{eff}} - \widehat{P}\widehat{H}_0\widehat{P}, \quad (8.110)$$

where  $\widehat{H}_0$  is the Hamiltonian of the non-interacting system. Here we assume that

$$[\widehat{H}_0, \widehat{P}] = 0, \quad (8.111)$$

which is satisfied when the model space is spanned by the eigenvectors (Slater determinants) of  $\widehat{H}_0$ .

We have calculated a 2-particle effective interaction for the parabolic quantum dot using the algorithm exposed in [76]. Calculating the effective interaction for the  $N$ -electron system in a large basis means solving the exact problem, which we cannot do. The diagonalization problem is therefore solved for a sub-cluster Hamiltonian consisting of 2 electrons, leading to missing many-body correlations for  $N > 2$ . The diagonalization is done by first defining the relative coordinates as

$$\mathbf{r} \equiv \mathbf{r}_1 - \mathbf{r}_2, \quad (8.112)$$

and the center-of-mass coordinates as

$$\mathbf{R} \equiv \frac{1}{2}(\mathbf{r}_1 + \mathbf{r}_2), \quad (8.113)$$

where  $\mathbf{r}_1$  and  $\mathbf{r}_2$  are the position vector of electron 1 and 2, respectively. The time-independent Schrödinger equation

$$\left[ -\frac{\hbar^2}{2m^*} \nabla_1^2 - \frac{\hbar^2}{2m^*} \nabla_2^2 + \frac{1}{2} m^* \omega^2 r_1^2 + \frac{1}{2} m^* \omega^2 r_2^2 + \frac{e^2}{4\pi\epsilon_0\epsilon_r} \frac{1}{r_{12}} \right] \Psi(\mathbf{r}_1, \mathbf{r}_2) = E \Psi(\mathbf{r}_1, \mathbf{r}_2) \quad (8.114)$$

is separable in  $\mathbf{r}$  and  $\mathbf{R}$ . Inserting

$$\Psi(\mathbf{R}, \mathbf{r}) \equiv f_1(\mathbf{R}) f_2(\mathbf{r}) \quad (8.115)$$

into the equation yields

$$\left[ \frac{\hbar^2}{4m^*} \nabla_{\mathbf{R}}^2 + m^* \omega^2 \mathbf{R}^2 \right] f_1(\mathbf{R}) = E_1 f_1(\mathbf{R}) \quad (8.116)$$

$$\left[ \frac{\hbar^2}{m^*} \nabla_{\mathbf{r}}^2 + \frac{1}{4} \omega^2 r^2 + \frac{e^2}{4\pi\epsilon_0\epsilon_r} \frac{1}{r} \right] f_2(\mathbf{r}) = E_2 f_2(\mathbf{r}). \quad (8.117)$$

The center-of-mass problem is trivial. The relative coordinate problem is solved by using the so-called generalized half-range Hermite functions (see [76]). The  $m$  eigenvalues of  $\hat{H}'$  will therefore be equal to some of the  $n$  eigenvalues of  $\hat{H}$  for the 2-electron system.

### 8.2.2 Energy Cut Model Space

Using an effective interaction in a CCSD calculation means that the standard interaction  $v$  is replaced by the effective interaction  $v_{\text{eff}}$ , viz.

$$\langle \alpha\beta | v | \gamma\delta \rangle \rightarrow \langle \alpha\beta | v_{\text{eff}} | \gamma\delta \rangle. \quad (8.118)$$

We must generate the effective interaction in the energy cut model space (EC) in order to obtain a well-defined interaction. This is because the EC space contains all the symmetries of the interaction. By generating the interaction in the DP space we would break essential symmetries such as conservation of center-of-mass momentum. The basis of the EC space is defined as

$$\mathcal{B}_{\text{EC}} = \mathcal{B}_{\text{EC}}(R^b) \equiv \left\{ |\Phi_{\alpha_1\alpha_2..\alpha_N}\rangle : \sum_{i=1}^N \varepsilon_i \leq F(R^b) \right\}, \quad (8.119)$$

where  $F(R^b)$  is the cut-off, see [75, 76]. The HF and CCSD results with effective interaction are tabulated in Tables 8.20-8.23. The calculations have been done with  $\text{EC}(R^b)$  as model space. We have tabulated HF and CCSD energies for systems containing 2, 6, 12 and 20 electrons, and frequencies ranging from 0.4 up to 50.0. We have included the results obtained with standard interaction from Tables 8.5-8.8 in order to more easily compare the results. Table 8.4 shows for which values of  $N$  and  $\omega$  the CCSD (and HF) energy converges within the iteration procedure. Additionally, for some values of  $\omega$  we obtain convergence for only certain  $R^b$ .

Consider the HF results with effective interaction in Tables 8.20-8.23. For the 2-electron system we observe the same behavior with respect to  $R^b$  as the HF energy with standard interaction. This is what we would expect. See Section 8.1.2 for details. An important difference ( $N = 2, 6, 12$  and 20) is that

$$E_{\text{HF-V}_{\text{eff}}}(R^b + 1) \geq E_{\text{HF-V}_{\text{eff}}}(R^b), \quad (8.120)$$

while

$$E_{\text{HF-V}}(R^b + 1) \leq E_{\text{HF-V}}(R^b), \quad (8.121)$$

with equality for odd values of  $R^b$  in the 2-electron system. Thus, for a given size of the model space, the HF energy with effective interaction is lower than with the standard interaction, viz.

$$E_{\text{HF-V}_{\text{eff}}}(R^b) < E_{\text{HF-V}}(R^b). \quad (8.122)$$

Since the effective interaction is computed by considering the 2-electron system, the CCSD calculation should in principle yield exact results for the 2-electron system. We have compared the CCSD energies for  $\omega = 1/6$  and 1.0 with Tauts analytical (exact) solutions [69], and the energy for  $\omega = 0.28$  with the DMC result in [77]. Our results for  $\omega = 1/6$  and 1.0 are exact with precision close to numerical accuracy. For  $\omega = 0.28$  the DMC energy is 1.02162(7), and the CCSD energy is 1.021644. The energy is thus within the uncertainty of the DMC result, and it is therefore very probable that this is the exact energy. We have now (numerically) validated the CCSD calculation with an effective interaction. All the energies for the 2-electron system should therefore be exact. Moreover, the energy should be exact for every value of  $R^b$ , i.e. the energy is independent of  $R^b$ . This is observed in Tables 8.20 and 8.21.

Turning to the 6-electron system we first observe that the CCSD energy does not converge for  $3 \leq R^b \leq 5$  when  $\omega = 0.4$  and 0.5. Increasing the frequency leads to convergence for more and more values of  $R^b$ . We note that the energy tends to have problems with the convergence for low frequencies and low values of  $R^b$ . Just like the HF energy we see that ( $N = 6, 12$  and 20)

$$E_{\text{CCSD-V}_{\text{eff}}}(R^b + 1) > E_{\text{CCSD-V}_{\text{eff}}}(R^b), \quad (8.123)$$

whenever we have convergence. Thus in our case the effective interaction (in the EC model space) underestimates the exact ground state energy, while the standard interaction overestimates the exact energy. Furthermore we observe that the differences between the energies for  $R^b = 10$  and  $R^b = 9$  are relatively small ( $10^{-3} - 10^{-4}$ ) for  $0.4 \leq \omega \leq 50.0$ . However, for  $\omega = 1.0$  we are still not within the uncertainty of the DMC result, see Table 8.30. We see that we are definitely closer to the exact value than the standard interaction, see the results tabulated in Table 8.10. This is what we would expect with an effective interaction. The difference between the exact energy and our result is with certainty between 0.002 and 0.003.

For systems containing 12 and 20 electrons we have more problems with convergence. The CCSD energy does not converge for low frequencies and low values of  $R^b$ . The differences between the energies for  $R^b = 10$  and  $R^b = 9$  are relatively large, except for  $N = 12$  with  $1.0 \leq \omega \leq 5.0$ . Furthermore we see that for  $\omega = 1.0$  and  $N = 12$  we are still not within the DMC result in Table 8.30. However, we are closer than with standard interaction as expected, see Table 8.10. The difference between the exact energy and our result is between 0.065 and 0.070.

Table 8.18 shows the CCSD results for the 6-electron system with  $R^b = 12, 14$  and 16, calculated by [70]. We have done a polynomial curve fitting in MATLAB for  $N = 6$  and  $\omega = 1.0$  with the results tabulated in Tables 8.20 and 8.18, and extrapolated to infinity. This is not possible for  $N = 12$  and  $\omega = 1.0$  since the energy does not converge for  $R^b < 9$ . Table 8.17 shows the results for  $N = 6$  and 12 with  $\omega = 1.0$  using an effective interaction and the EC space as model space. We observe that the extrapolated result for  $N = 6$  and  $\omega = 1.0$  is within the DMC uncertainty.

The effective interaction yields an energy that is closer to the exact result than the standard interaction. For  $R^b = 10$  and  $\omega = 1.0$ , the CCSD results ( $N = 6$  and 12) are not within the uncertainties of the DMC results. This means that

1. the model space is too small, and/or
2. we are missing important many-body correlations, such as Triples.

We have seen that by performing calculations with  $R^b = 12, 14$  and 16 for the 6-electron system, the extrapolated value is within the uncertainty of the DMC result, see Table 8.17. This means

$R^b$	$N = 6$		$N = 12$	
	CCSD	$ \Delta E $	CCSD	$ \Delta E $
10	20.157541	0.002-0.003 w.unc.	65.634530	0.065-0.070
$\infty$	20.160		o	o

**Table 8.17:** CCSD energies for  $N = 6$  and 12 with  $\omega = 1.0$  and effective interaction (EC model space). We have done a polynomial curve fitting in MATLAB for  $N = 6$  with the results tabulated in Tables 8.18 and 8.20, and extrapolated to infinity. The approximate difference to the DMC result in Table 8.30 is given by  $|\Delta E|$ . We observe that the result for  $N = 6$  is within the uncertainty of the DMC result, denoted by “w.unc.” We have not been able to extrapolate the energy for  $N = 12$  and  $\omega = 1.0$  since it does not converge for  $R^b < 9$ , denoted by “o” in the table. Energy is measured in effective Hartrees  $E_H^*$ .

$R^b$	CCSD
12	20.15851
14	20.15912
16	20.15958

**Table 8.18:** CCSD results for the 6-electron system with  $\omega = 1.0$  and  $R^b = 12, 14$  and 16 calculated by [70]. The calculations have been done with an effective interaction and the EC space as model space. Energy is measured in effective Hartrees  $E_H^*$ .

that the difference between the DMC energy and the CCSD energy for  $R^b = 10$  is mainly due to the size of the mode space; it is too small. Table 8.19 shows the CCSDT energy for  $R^b = 10$  obtained with an effective interaction [70]. We see that the inclusion of Triples lowers the energy. This means that for  $R^b = 10$ , the CCSD energy is closer to the exact energy than the CCSDT energy. This hints, at least for the 6-electron system, that the size of the model space is more important than Triples corrections.

$R^b$	CCSDT
10	20.15533

**Table 8.19:** CCSDT result for the 6-electron system with  $\omega = 1.0$  and  $R^b = 10$ , calculated by [70]. The energy is obtained by using an effective interaction and EC model space. Energy is measured in effective Hartrees  $E_H^*$ .

We would also like to obtain an extrapolated energy for the 12-electron system. However, for  $N = 12$  and  $\omega = 1.0$ , the energy does not converge for  $R^b < 9$ . This means that we cannot extrapolate. We have seen that this is a trend for low frequencies and small model spaces. Since the energy converges by using the standard interaction, the problems with convergence might be a consequence of the EC model space. In order to check this we propose to generate an effective interaction in the  $EC(2R^b)$  space and then run CCSD calculations with the  $DP(R^b)$  space as model space. Figure 8.12 shows an illustration of  $EC(R^b)$ ,  $DP(R^b)$  and  $EC(2R^b)$ . We clearly see that

$$EC(R^b) \subset DP(R^b) \subset EC(2R^b). \quad (8.124)$$

By generating the effective interaction in the  $EC(2R^b)$  space and then run the calculations in  $DP(R^b)$  space means that we only use those interaction elements that corresponds to the  $DP$  space.

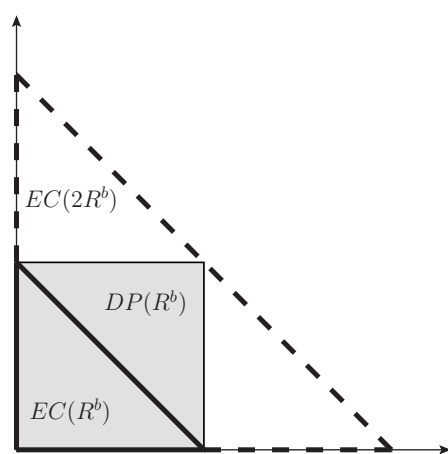


**Figure 8.12:** Illustration of  $EC(R^b)$ ,  $DP(R^b)$  and  $EC(2R^b)$ .

$\omega$	$R^b$	$N = 2$				$N = 6$			
		Standard interaction		Effective interaction		Standard interaction		Effective interaction	
		HF	CCSD	HF	CCSD	HF	CCSD	HF	CCSD
0.4	1	1.592665	1.592665	1.375594	1.375594	-	-	-	-
	2	1.592665	1.494392	1.375594	1.375594	11.728488	11.728488	7.931966	7.931966
	3	1.508042	1.392856	1.427126	1.375594	11.156151	11.005419	x	x
	4	1.508042	1.386722	1.427126	1.375594	10.504554	10.208494	x	x
	5	1.508024	1.383259	1.453967	1.375594	10.467626	10.064250	x	x
	6	1.508024	1.381489	1.453967	1.375594	10.405715	9.987983	10.045408	9.890108
	7	1.508015	1.380338	1.467257	1.375594	10.405292	9.977274	10.173956	9.944735
	8	1.508015	1.379554	1.467257	1.375594	10.405222	9.970650	10.196753	9.942164
	9	1.508011	1.378983	1.475288	1.375594	10.405195	9.966218	10.227403	9.939521
	10	1.508011	1.378551	1.475288	1.375594	10.405166	9.963027	10.245645	9.940905
0.5	1	1.886227	1.886227	1.659772	1.659772	-	-	-	-
	2	1.886227	1.786914	1.659772	1.659772	13.640713	13.640713	9.914958	9.914958
	3	1.799856	1.681633	1.783908	1.659772	13.051620	12.895476	x	x
	4	1.799856	1.673874	1.783908	1.659772	12.357471	12.047565	x	x
	5	1.799748	1.669500	1.817459	1.659772	12.325128	11.914166	x	x
	6	1.799748	1.667259	1.817459	1.659772	12.271499	11.841655	12.556760	11.736520
	7	1.799745	1.665801	1.834071	1.659772	12.271375	11.827869	12.717445	11.787516
	8	1.799745	1.664808	1.834071	1.659772	12.271361	11.819437	12.745941	11.784081
	9	1.799743	1.664085	1.844110	1.659772	12.271337	11.813819	12.784254	11.781074
	10	1.799743	1.663537	1.844110	1.659772	12.271326	11.809788	12.807056	11.782354
0.6	1	2.170813	2.170813	1.936931	1.936931	-	-	-	-
	2	2.170813	2.070856	1.936931	1.936931	15.465426	15.465426	10.946441	10.946441
	3	2.083158	1.962891	1.994233	1.936931	14.864332	14.703670	x	x
	4	2.083158	1.953712	1.994233	1.936931	14.135156	13.814684	x	x
	5	2.082926	1.948533	2.024000	1.936931	14.106585	13.690123	x	13.432229
	6	2.082926	1.945869	2.024000	1.936931	14.059885	13.621142	13.683596	13.505043
	7	2.082926	1.944135	2.038722	1.936931	14.059867	13.604622	13.811551	13.556509
	8	2.082926	1.942953	2.038722	1.936931	14.059716	13.594539	13.836037	13.552735
	9	2.082924	1.942090	2.047546	1.936931	14.059698	13.587834	13.868257	13.549756
	10	2.082924	1.941436	2.047546	1.936931	14.059697	13.583037	13.887058	13.550906
0.8	1	2.720998	2.720998	2.475905	2.475905	-	-	-	-
	2	2.720998	2.620341	2.475905	2.475905	18.929733	18.929733	13.811468	13.811468
	3	2.631563	2.508827	2.537139	2.475905	18.312821	18.144988	x	x
	4	2.631563	2.497304	2.537139	2.475905	17.528556	17.193050	x	x
	5	2.631058	2.490771	2.568856	2.475905	17.505795	17.081893	16.933000	16.809860
	6	2.631058	2.487386	2.568856	2.475905	17.469841	17.018754	17.075290	16.880900
	7	2.631055	2.485175	2.584547	2.475905	17.469813	16.997854	17.207361	16.935520
	8	2.631055	2.483665	2.584547	2.475905	17.469269	16.985003	17.233916	16.931715
	9	2.631054	2.482560	2.593908	2.475905	17.469263	16.976408	17.268048	16.929259
	10	2.631054	2.481724	2.593908	2.475905	17.469257	16.970279	17.287339	16.930135
1.0	1	3.253314	3.253314	3.000000	3.000000	-	-	-	-
	2	3.253314	3.152329	3.000000	3.000000	22.219813	22.219813	16.578993	16.578993
	3	3.162691	3.038605	3.064154	3.000000	21.593198	21.419889	x	x
	4	3.162691	3.025232	3.064154	3.000000	20.766919	20.421325	x	x
	5	3.161921	3.017607	3.097299	3.000000	20.748402	20.319716	20.166941	20.033306
	6	3.161921	3.013627	3.097299	3.000000	20.720257	20.260893	20.310117	20.104242
	7	3.161909	3.011021	3.113707	3.000000	20.720132	20.236760	20.446045	20.162126
	8	3.161909	3.009237	3.113707	3.000000	20.719248	20.221750	20.474497	20.158637
	9	3.161909	3.007931	3.123465	3.000000	20.719248	20.211590	20.510432	20.156905
	10	3.161909	3.006938	3.123465	3.000000	20.719217	20.204345	20.530161	20.157541
2.0	1	5.772454	5.772454	5.496523	5.496523	-	-	-	-
	2	5.772454	5.671234	5.496523	5.496523	37.281425	37.281425	29.621623	29.621623
	3	5.679048	5.553152	5.568856	5.496523	36.637217	36.448558	x	x
	4	5.679048	5.534274	5.568856	5.496523	35.689555	35.322283	34.940481	34.895937
	5	5.677282	5.523274	5.605893	5.496523	35.681728	35.242971	35.067346	34.904897
	6	5.677282	5.517386	5.605893	5.496523	35.672333	35.193258	35.213499	34.977420
	7	5.677206	5.513491	5.624295	5.496523	35.671851	35.161115	35.360563	35.044569
	8	5.677206	5.510801	5.624295	5.496523	35.670358	35.140124	35.395567	35.043402
	9	5.677204	5.508822	5.635166	5.496523	35.670333	35.125055	35.438093	35.045024
	10	5.677204	5.507311	5.635166	5.496523	35.670144	35.114198	35.459520	35.045026

**Table 8.20:** Hartree-Fock and Coupled-Cluster Singles and Doubles results for a parabolic quantum dot with 2 and 6 electrons using both standard interaction and effective interaction. We have used the DP space as model space (see Eq. 8.20) for calculations with standard interaction, and the EC space as model space for calculations with effective interaction (see Eq. 8.119). The size of the space is denoted by  $R^b$  (shell number), and the oscillator frequency is given by  $\omega$ . The CCSD energy does not converge within the iteration procedure (see Section 7.2.4) for certain values of  $R^b$ , denoted by “x”. Energy is measured in effective Hartrees  $E_H^*$ .

$\omega$	$R^b$	$N = 2$				$N = 6$			
		Standard interaction		Effective interaction		Standard interaction		Effective interaction	
		HF	CCSD	HF	CCSD	HF	CCSD	HF	CCSD
3.0	1	8.170804	8.170804	7.883753	7.883753	-	-	-	-
	2	8.170804	8.069761	7.883753	7.883753	51.165337	51.165337	41.976374	41.976374
	3	8.076274	7.950410	7.960167	7.883753	50.517683	50.321752	x	x
	4	8.076274	7.928709	7.960167	7.883753	49.508478	49.135135	48.911412	48.888397
	5	8.073884	7.915891	7.999091	7.883753	49.504750	49.062885	48.870529	48.694263
	6	8.073884	7.908930	7.999091	7.883753	49.501573	49.014446	49.017179	48.767717
	7	8.073751	7.904296	8.018485	7.883753	49.501011	48.979127	49.168672	48.837661
	8	8.073751	7.901081	8.018485	7.883753	49.499580	48.955363	49.207459	48.838404
	9	8.073744	7.898706	8.029916	7.883753	49.499520	48.937698	49.254040	48.842291
	10	8.073744	7.896889	8.029916	7.883753	49.499237	48.924839	49.276642	48.842136
4.0	1	10.506628	10.506628	10.212604	10.212604	-	-	-	-
	2	10.506628	10.405775	10.212604	10.212604	64.439626	64.439626	53.969200	53.969200
	3	10.411470	10.285895	10.291594	10.212604	63.791597	63.591329	x	x
	4	10.411470	10.262419	10.291594	10.212604	62.743808	62.368661	62.222799	62.207046
	5	10.408646	10.248423	10.331687	10.212604	62.742006	62.298906	62.094434	61.909899
	6	10.408646	10.240751	10.331687	10.212604	62.741163	62.249606	62.240659	61.983603
	7	10.408469	10.235621	10.351708	10.212604	62.740611	62.212557	62.394121	62.054033
	8	10.408469	10.232050	10.351708	10.212604	62.739357	62.187127	62.435414	62.056216
	9	10.408456	10.229405	10.363494	10.212604	62.739276	62.167826	62.484777	62.061658
	10	10.408456	10.227378	10.363494	10.212604	62.738940	62.153663	62.508252	62.061505
5.0	1	12.802496	12.802496	12.503561	12.503561	-	-	-	-
	2	12.802496	12.701808	12.503561	12.503561	77.324332	77.324332	65.728844	65.728844
	3	12.706930	12.581669	12.584369	12.503561	76.676854	76.473661	x	x
	4	12.706930	12.556949	12.584369	12.503561	75.602124	75.226743	75.125654	75.113312
	5	12.703782	12.542112	12.625280	12.503561	75.601300	75.157693	74.943996	74.753920
	6	12.703782	12.533923	12.625280	12.503561	75.601221	75.106872	75.089461	74.827516
	7	12.703567	12.528429	12.645744	12.503561	75.600706	75.068703	75.243799	74.979503
	8	12.703567	12.524595	12.645744	12.503561	75.599630	75.042121	75.286899	74.900811
	9	12.703550	12.521751	12.657783	12.503561	75.599534	75.021677	75.338318	74.907377
	10	12.703550	12.519568	12.657783	12.503561	75.599173	75.006580	75.362476	74.907284
10.0	1	23.963327	23.963327	23.651663	23.651663	-	-	-	-
	2	23.963327	23.863173	23.651663	23.651663	138.642441	138.642441	122.653567	122.653567
	3	23.866830	23.742766	23.737201	23.651663	137.999396	137.789201	136.821655	136.817756
	4	23.866830	23.714877	23.737201	23.651663	136.856842	136.485196	136.468182	136.461845
	5	23.862773	23.697829	23.780202	23.651663	136.856753	136.413343	136.173391	135.970427
	6	23.862773	23.688243	23.780202	23.651663	136.854607	136.354504	136.314578	136.042076
	7	23.862443	23.681757	23.801822	23.651663	136.854284	136.313637	136.468590	136.107197
	8	23.862443	23.677199	23.801822	23.651663	136.853782	136.284071	136.516429	136.113676
	9	23.862411	23.673802	23.814526	23.651663	136.853661	136.260729	136.573456	136.123096
	10	23.862411	23.671183	23.814526	23.651663	136.853287	136.243183	136.599654	136.123432
20.0	1	45.604991	45.604991	45.283850	45.283850	-	-	-	-
	2	45.604991	45.505319	45.283850	45.283850	254.648664	254.648664	232.473626	232.473626
	3	45.507912	45.385045	45.372916	45.283850	254.011527	253.796720	252.813945	252.812952
	4	45.507912	45.354878	45.372916	45.283850	252.821683	252.457058	252.479052	252.475760
	5	45.503120	45.336174	45.417442	45.283850	252.820088	252.378355	252.117095	251.906240
	6	45.503120	45.325508	45.417442	45.283850	252.811954	252.309241	252.252367	251.974297
	7	45.502684	45.318241	45.439931	45.283850	252.811811	252.266330	252.402979	252.031493
	8	45.502684	45.313105	45.439931	45.283850	252.811687	252.234390	252.454257	252.040496
	9	45.502636	45.309263	45.453140	45.283850	252.811568	252.208972	252.515579	252.051740
	10	45.502636	45.306293	45.453140	45.283850	252.811247	252.189591	252.543550	252.052681
50.0	1	108.862269	108.862269	108.532386	108.532386	-	-	-	-
	2	108.862269	108.763094	108.532386	108.532386	586.407125	586.407125	551.989727	551.989727
	3	108.764735	108.643160	108.624706	108.532386	585.777168	585.558594	584.550992	584.550743
	4	108.764735	108.610971	108.624706	108.532386	584.547339	584.192313	584.236057	584.234700
	5	108.759222	108.590750	108.670612	108.532386	584.542520	584.103507	583.821763	583.605066
	6	108.759222	108.579064	108.670612	108.532386	584.524974	584.021400	583.949063	583.667717
	7	108.758672	108.571049	108.693908	108.532386	584.524954	583.976331	584.093494	583.713833
	8	108.758672	108.565356	108.693908	108.532386	584.524950	583.941913	584.147709	583.725123
	9	108.758604	108.561080	108.707593	108.532386	584.524852	583.914635	584.212909	583.737561
	10	108.758604	108.557765	108.707593	108.532386	584.524623	583.893560	584.242692	583.739292

**Table 8.21:** Hartree-Fock and Coupled-Cluster Singles and Doubles results for a parabolic quantum dot with 2 and 6 electrons using both standard interaction and effective interaction. We have used the DP space as model space (see Eq. 8.20) for calculations with standard interaction, and the EC space as model space for calculations with effective interaction (see Eq. 8.119). The size of the space is denoted by  $R^b$  (shell number), and the oscillator frequency is given by  $\omega$ . The CCSD energy does not converge within the iteration procedure (see Section 7.2.4) for certain values of  $R^b$ , denoted by “x”. Energy is measured in effective Hartrees  $E_H^*$ .

$\omega$	$R^b$	$N = 12$				$N = 20$			
		Standard interaction		Effective interaction		Standard interaction		Effective interaction	
		HF	CCSD	HF	CCSD	HF	CCSD	HF	CCSD
1.0	1	-	-	-	-	-	-	-	-
	2	-	-	-	-	-	-	-	-
	3	73.765549	73.765549	46.502552	46.502552	177.963297	177.963297	102.282541	102.282541
	4	70.673849	70.297531	42.000000	61.027715	71.238897	x	x	x
	5	67.569930	66.989912	x	x	168.426371	x	x	x
	6	67.296869	66.452006	x	x	161.339721	x	x	x
	7	66.934745	65.971686	x	x	159.958722	x	x	x
	8	66.923094	65.889324	x	x	158.400172	x	x	x
	9	66.912244	65.838932	66.175736	65.618539	158.226030	x	x	x
	10	66.912035	65.806539	66.258111	65.634530	158.017667	x	x	x
2.0	1	-	-	-	-	-	-	-	-
	2	-	-	-	-	-	-	-	-
	3	120.722260	120.722260	82.919042	82.919042	-	-	-	-
	4	117.339642	116.978642	x	103.906310	286.825295	286.825295	181.235783	181.235783
	5	113.660396	113.020282	x	x	276.898196	275.845577	x	220.636627
	6	113.484866	112.613571	x	x	267.269712	266.325997	x	259.240388
	7	113.247601	112.264166	111.434211	111.152591	266.213200	264.830000	x	286.808535
	8	113.246579	112.189996	112.058791	111.603983	264.933622	263.325189	x	x
	9	113.246303	112.135551	112.495988	111.872020	264.874009	263.089951	x	x
	10	113.245854	112.094025	112.562079	111.861880	264.809954	262.928937	260.714153	x
3.0	1	-	-	-	-	-	-	-	-
	2	-	-	-	-	-	-	-	-
	3	163.268256	163.268256	117.419306	117.419306	-	-	-	-
	4	159.769062	159.414625	x	143.421667	384.318425	384.318425	255.851700	255.851700
	5	155.762811	155.097118	x	x	373.776094	373.229501	255.473175	304.640563
	6	155.639179	154.762454	151.298879	x	363.162287	362.175933	x	352.421157
	7	155.475049	154.487959	153.647870	153.334781	362.323215	360.924104	x	x
	8	155.475049	154.408521	154.257210	153.773520	361.277490	359.652011	x	x
	9	155.474144	154.348106	154.686893	154.032341	361.254334	359.469820	x	x
	10	155.473848	154.302641	154.759873	154.025320	361.233837	359.337510	358.202983	357.441187
4.0	1	-	-	-	-	-	-	-	-
	2	-	-	-	-	-	-	-	-
	3	203.531098	203.531098	150.915215	150.915215	-	-	-	-
	4	199.971455	199.619694	x	x	475.926595	475.926595	328.200763	328.200763
	5	195.745462	195.066235	x	x	465.021258	464.483436	x	385.065642
	6	195.653702	194.776202	191.896341	x	453.717528	452.706359	x	440.816169
	7	195.535485	194.547735	193.671035	193.343218	453.029759	451.624943	x	x
	8	195.535177	194.463255	194.278540	193.778488	452.163171	450.533964	x	x
	9	195.532936	194.398503	194.713851	194.042575	452.154007	450.370119	447.620204	x
	10	195.532772	194.350424	194.794571	194.040504	452.148052	450.245879	449.401371	448.600616
5.0	1	-	-	-	-	-	-	-	-
	2	-	-	-	-	-	-	-	-
	3	242.334879	242.334879	183.765318	183.765318	-	-	-	-
	4	238.739591	238.388819	x	x	563.773952	563.773952	399.094328	399.094328
	5	234.352741	233.665684	x	x	552.630093	552.098704	x	463.433094
	6	234.282331	233.405545	230.999630	230.911117	540.804720	539.777215	x	526.882127
	7	234.194820	233.207198	232.298553	231.961480	540.227793	538.821500	x	x
	8	234.194059	233.118844	232.903979	232.393330	539.499326	537.871223	527.599736	x
	9	234.190797	233.051061	233.345264	232.663493	539.495941	537.713326	535.233890	534.738382
	10	234.190714	233.000991	233.432765	232.666033	539.494612	537.589832	536.834713	536.015305

**Table 8.22:** Hartree-Fock and Coupled-Cluster Singles and Doubles results for a parabolic quantum dot with 12 and 20 electrons using both standard interaction and effective interaction. We have used the DP space as model space (see Eq. 8.20) for calculations with standard interaction, and the EC space as model space for calculations with effective interaction (see Eq. 8.119). The size of the space is denoted by  $R^b$  (shell number), and the oscillator frequency is given by  $\omega$ . The CCSD energy does not converge within the iteration procedure (see Section 7.2.4) for certain values of  $R^b$ , denoted by “x”. Energy is measured in effective Hartrees  $E_H^*$ .

$\omega$	$R^b$	$N = 12$				$N = 20$			
		Standard interaction		Effective interaction		Standard interaction		Effective interaction	
		HF	CCSD	HF	CCSD	HF	CCSD	HF	CCSD
10.0	1	-	-	-	-	-	-	-	-
	2	-	-	-	-	-	-	-	-
	3	424.723373	424.723373	342.837272	342.837272	-	-	-	-
	4	421.066552	420.714412	387.852166	x	973.032700	973.032700	741.907454	741.907454
	5	416.245656	415.548025	x	x	961.371081	960.853435	x	x
	6	416.221892	415.352162	414.259253	414.204471	948.057077	946.995097	x	x
	7	416.198611	415.213229	414.221231	413.862491	947.765474	946.367418	x	x
	8	416.196677	415.115445	414.807209	414.274282	947.410305	945.798531	938.828011	938.708830
	9	416.191836	415.040983	415.261980	414.558155	947.409440	945.634643	943.208098	942.653517
	10	416.191833	414.985087	415.371069	414.576142	947.404930	945.499122	944.709187	943.856608
20.0	1	-	-	-	-	-	-	-	-
	2	-	-	-	-	-	-	-	-
	3	764.669757	764.669757	649.864219	649.864219	-	-	-	-
	4	760.999568	760.642727	717.086454	717.085698	1727.547904	1727.547904	1402.547504	1402.547504
	5	755.851177	755.158770	757.317038	757.286320	1715.636447	1715.121677	1528.572359	1528.568611
	6	755.847874	754.988910	754.752961	754.727375	1701.112340	1700.040683	1636.066502	1636.248392
	7	755.846430	754.864771	753.834848	753.463003	1701.000555	1699.622516	1695.229330	1695.426720
	8	755.844396	754.761753	754.381289	753.839129	1700.881357	1699.291198	1695.620663	1695.516615
	9	755.840282	754.683971	754.833236	754.118115	1700.876899	1699.113200	1696.546369	1695.980919
	10	755.840196	754.623201	754.960572	754.149732	1700.866177	1698.965611	1698.009292	1697.143442
50.0	1	-	-	-	-	-	-	-	-
	2	-	-	-	-	-	-	-	-
	3	1723.611301	1723.611301	1543.553745	1543.553745	-	-	-	-
	4	1719.954910	1719.591333	1651.443071	1651.443062	3834.126475	3834.126475	3322.973815	3322.973815
	5	1714.516506	1713.842082	1717.046895	1717.041097	3822.122324	3821.601747	3524.659120	3524.659055
	6	1714.514709	1713.670423	1714.072815	1714.062550	3806.466383	3805.411147	3709.512572	3709.510304
	7	1714.502278	1713.526638	1712.503731	1712.124312	3806.454602	3805.108329	3810.774973	3810.736980
	8	1714.500976	1713.420167	1712.983144	1712.440387	3806.448065	3804.882880	3804.309792	3804.269253
	9	1714.498844	1713.340085	1713.411514	1712.690503	3806.442304	3804.694261	3802.079664	3801.509670
	10	1714.498639	1713.274652	1713.555168	1712.734499	3806.431632	3804.541353	3803.408939	3802.545757

**Table 8.23:** Hartree-Fock and Coupled-Cluster Singles and Doubles results for a parabolic quantum dot with 12 and 20 electrons using both standard interaction and effective interaction. We have used the DP space as model space (see Eq. 8.20) for calculations with standard interaction, and the EC space as model space for calculations with effective interaction (see Eq. 8.119). The size of the space is denoted by  $R^b$  (shell number), and the oscillator frequency is given by  $\omega$ . The CCSD energy does not converge within the iteration procedure (see Section 7.2.4) for certain values of  $R^b$ , denoted by “x”. Energy is measured in effective Hartrees  $E_H^*$ .

### 8.2.3 Direct Product Model Space

Table 8.24 shows the CCSD results obtained with an effective interaction using the  $\text{DP}(R^b)$  space as model space. The effective interaction is generated in the  $\text{EC}(2R^b)$  space. The energy

$\omega$	$R^b$	$N = 6$	$N = 12$	$N = 20$
0.5	1	-	-	-
	2	12.354365	-	-
	3	12.370527	x	-
	4	11.869773	x	x
	5	11.829131	x	x
	6	11.791420	x	x
	7	11.789686	x	x
	8	11.788671	x	x
	9	11.788102	x	x
	10	11.787723	x	x
1.0	1	-	-	-
	2	20.812210	-	-
	3	20.861973	70.313660	-
	4	20.213101	68.801111	x
	5	20.196498	66.272632	x
	6	20.176509	66.045184	x
	7	20.171717	65.725357	x
	8	20.168871	65.704352	x
	9	20.167111	65.690913	x
	10	20.165981	65.683076	x
2.0	1	-	-	-
	2	35.773760	-	-
	3	35.855162	117.074044	-
	4	35.075759	115.443302	280.041849
	5	35.079981	112.271487	272.331986
	6	35.073529	112.140503	264.609591
	7	35.067101	111.936896	263.757069
	8	35.062850	111.930685	262.611398
	9	35.059595	111.921831	262.539444
	10	35.057440	111.912895	262.481615
5.0	1	-	-	-
	2	75.716532	-	-
	3	75.834921	238.494746	-
	4	74.924903	236.782140	556.697251
	5	74.945590	232.844442	548.909506
	6	74.945253	232.835033	538.029207
	7	74.939229	232.775676	537.627077
	8	74.934352	232.769156	536.989443
	9	74.929588	232.758150	536.994956
	10	74.926225	232.749369	536.985127

**Table 8.24:** CCSD energies with effective interaction using the  $\text{DP}(R^b)$  space as model space. We present results for systems containing 6, 12 and 20 electrons. The effective interaction is generated in the  $\text{EC}(2R^b)$  space. The frequency is denoted by  $\omega$  and the number of shells in the basis is denoted by  $R^b$ . Note that “x” means that the energy does not converge. Energy is measured in effective Hartrees  $E_H^*$ .

converges for all values listed in Table 8.4. We see that the energies for systems containing 12 and 20 electrons are much more “well-behaved” than the energies obtained with the EC model space, see Tables 8.22 and 8.23. Furthermore, the energy converges in the same way as for standard interaction, viz.

$$E_{\text{CCSD-V}_{\text{eff}}}(R^b + 1) < E_{\text{CCSD-V}_{\text{eff}}}(R^b). \quad (8.125)$$

This type of convergence therefore seems to be a consequence of the DP space. The CCSD energy with effective interaction and  $\text{DP}(R^b)$  as model space, i.e. an interaction generated in  $\text{EC}(2R^b)$ , is thus always larger than the corresponding energy with  $\text{EC}(R^b)$  as model space.

By comparing the energies for  $\omega = 1.0$  with the DMC results in Table 8.30 we see that our results are still not within the DMC uncertainty. For the 6-electron system, the difference between the exact result and the CCSD energy is between 0.0057 and 0.0061. We obtained a better energy with the  $\text{EC}(R^b)$  model space. Turning to the 12-electron system we see that the difference with the exact result is between 0.018 and 0.021. Thus we are closer to the DMC

energy than the result obtained with the  $\text{EC}(R^b)$  model space. We have done a polynomial curve fitting in MATLAB for  $N = 6$  and 12 with  $\omega = 1.0$  using the results tabulated in Table 8.24, and extrapolated the energies to infinity. Table 8.25 shows the results. We see that the extrapolated energy for  $N = 6$  is closer to the exact energy than the result for  $R^b = 10$ . However, we are not within the uncertainty of the DMC result. Turning to the 12-electron system we observe that the energy obtained with  $R^b = 10$  is closer to the exact energy than the extrapolated result. This hints that we are missing important many-body correlations and/or we are missing important information due to the DP model space. Still, the extrapolated energy is better than the result obtained with  $R^b = 10$  using the EC space as model space, see Table 8.17.

$R^b$	$N = 6$		$N = 12$	
	CCSD	$ \Delta E $	CCSD	$ \Delta E $
10	20.165981	0.0057-0.0061	65.683076	0.018-0.021
$\infty$	20.165	0.0047-0.0051	65.679	0.023-0.025

**Table 8.25:** CCSD energies for  $N = 6$  and 12 with  $\omega = 1.0$  and effective interaction (DP model space). We have done a polynomial curve fitting in MATLAB for  $N = 6$  and 12 with the results tabulated in Table 8.24, and extrapolated to infinity. The approximate difference to the DMC result in Table 8.30 is given by  $|\Delta E|$ . We observe that the energy for  $N = 12$  and  $R^b = 10$  is closer to the exact energy than the extrapolated result. For  $N = 6$  we see that the extrapolated energy is the best result. Energy is measured in effective Hartrees  $E_H^*$ .

Table 8.24 shows that the energy does not converge for the parameters listed in Table 8.4. This was the case for standard interaction as well, see Section 8.1. In the next section we deal with this problem.

### 8.2.4 Hartree-Fock Basis

It is unsatisfactory that the CCSD energy does not converge for certain (low) values of  $\omega$ . In Section 8.1.8 we saw that the energy with the standard interaction converges when we use a HF basis. Thus, we propose the same solution for the effective interaction. We use the  $\text{DP}(R^b)$  space, i.e. an effective interaction generated in  $\text{EC}(2R^b)$ , since this model space yields the most “well-behaved” results with standard interaction. Moreover, the HF energy with effective interaction in  $\text{EC}(R^b)$  model space only converges for the values listed in Table 8.4. Thus in order to generate a HF basis for a frequency where the CCSD energy does not converge, we have no choice: we *must* use the  $\text{DP}(R^b)$  space.

Tables 8.26, 8.27 and 8.28 show the CCSD results obtained with a HF basis for  $\omega = 0.2$  ( $N = 6$ ),  $\omega = 0.8$  ( $N = 12$ ) and  $\omega = 1.0$  ( $N = 20$ ), respectively. We observe that the CCSD energies converge. Thus by including some of the correlations, viz. 1p1h correlations, in the basis, we obtain convergence.

$R^b$	$N = 6$
2	6.364656
4	6.034881
6	5.937662
8	5.938335
10	5.939177

**Table 8.26:** CCSD results for the 6-electron system with  $\omega = 0.2$  obtained by using a HF basis (see Eq. 8.92). We have used an effective interaction and DP model space. The effective interaction is generated in the  $\text{EC}(2R^b)$  space. Energy is measured in effective Hartrees  $E_H^*$ .

## 8.3 Comparison with other CCSD Calculations

Electronic structure calculations of quantum dots with the CC method have to our knowledge not been done to a very large extent. However, T. M. Henderson *et al.* [48] and I. Heidari *et al.*

$R^b$	$N = 12$
4	58.838127
6	55.981295
8	55.614801
10	55.593058

**Table 8.27:** CCSD results for the 12-electron system with  $\omega = 0.8$  obtained by using a HF basis (see Eq. 8.92). We have used an effective interaction and DP model space. The effective interaction is generated in the EC( $2R^b$ ) space. Energy is measured in effective Hartrees  $E_H^*$ .

$R^b$	$N = 20$
4	171.485601
6	158.843069
8	156.377199
10	156.012761

**Table 8.28:** CCSD results for the 20-electron system with  $\omega = 1.0$  obtained by using a HF basis (see Eq. 8.92). We have used an effective interaction and DP model space. The effective interaction is generated in the EC( $2R^b$ ) space. Energy is measured in effective Hartrees  $E_H^*$ .

[49] have calculated ground state energies of parabolic quantum dots in two dimensions using the CCSD method. Their results are presented in Table 8.29. From Table 8.5 we see that our

$N$	$\omega$	CCSD energy [48]	CCSD energy [49]
2	0.4	1.377	1.366
	0.6	1.939	1.932
	0.8	2.479	2.475
	1.0	3.003	3.001
6	1.0	-	20.229
12	1.0	-	65.982
20	1.0	-	107.670

**Table 8.29:** CCSD results for a parabolic quantum dot in two dimensions. The results are taken from [48, 49]. Energy is measured in effective Hartrees  $E_H^*$ .

results for the 2-electron system are somewhat higher than the energies in Table 8.29. However, our results obtained with an effective interaction are lower, see Table 8.20. This is what we would expect since CCSD calculations with an effective interaction yield exact results for the 2-electron system. Turning to the 6-electron system we see from Table 8.7 that our CCSD energy for  $\omega = 1.0$  obtained with the standard interaction is closer to the exact energy (see DMC result in Table 8.30) than the result obtained by [49]. Our results with an effective interaction (both EC and DP space) are even better, see Tables 8.20 and 8.24. Furthermore, for the 12-electron system, our result with standard interaction is also closer to the DMC result in Table 8.30, see Table 8.7. The results obtained with the effective interaction (EC and DP space) in Tables 8.22 and 8.24 are even closer. Finally, turning to the 20-electron system, we observe that the result obtained by [49] is completely different from our results in Tables 8.16 and 8.28. The difference is approximately 50. We see from Table 8.7 that the HF energy is in agreement with our CCSD results. Moreover, we have reproduced the HF result obtained by [67] with  $N = 20$  and  $\omega = 1$ . The result given in [49] is therefore most probably a misprint.

## 8.4 Comparison with other Many-Body Methods

Table 8.30 shows the ground state energies for parabolic quantum dots in two dimensions using other many-body methods. We have already compared our results with the DMC results [70]. As pointed out previously, the *exact* energy is within the uncertainty of the DMC result [62], and we will therefore refer to these results as the “exact” results.

Consider the 2-electron system. The FCI result [76], which is calculated with  $R^b = 8$ , is equal to our CCSD energy in Table 8.5 for  $R^b = 8$ , as expected. Remember that for a given

$R^b$ , FCI and CCSD should yield the same result in the 2-particle case [30]. Furthermore, the VMC result is somewhat lower than our result for the 2-electron system obtained by using the standard interaction. However, with an effective interaction, the CCSD energy is exact with a precision close to numerical accuracy, i.e. we reproduce Taut's analytical result [69]. The DFT energy is calculated by using the so-called local density approximation (LDA) [50]. We see that our CCSD energy with standard interaction is closer to the exact result for  $R^b \geq 3$ , meaning that the LDA is not a very good approximation for the 2-electron system.

Turning to the 6-electron system we see that our CCSD energies obtained by both the standard and effective interaction are closer to the DMC result, i.e. the exact result, than the FCI energy. The energy obtained with standard interaction is actually better than the FCI energy for  $R^b \geq 6$ . Comparing our result for  $R^b = 10$  (standard interaction) with the VMC result, we see that the VMC energy is somewhat closer to the exact energy, see Table 8.5. Table 8.12 shows the CCSDT energy with standard interaction in 10 shells. We see that the VMC result is still closer to the exact energy. This indicates that the model space is too small. Increasing the size of the basis to  $R^b = 14$ , the CCSD energy with standard interaction is closer to the DMC result, i.e. the exact energy, see Table 8.11. When the size of the model space increases to  $R^b = 16$  (see Table 8.11) we obtain an even better energy, as expected. Furthermore, our CCSD energies with effective interaction in EC and DP model space ( $R^b = 10$ ) are closer to the DMC result than the VMC result. The result obtained with  $R^b = 16$  is even better, see Table 8.18.

For the 12-electron system we observe that the difference between the FCI energy and the DMC energy is approximately 4.6. Our CCSD calculation with standard interaction yields a better energy for  $R^b \geq 3$ . Thus, by including excitations into shell 3, the CCSD yields an energy that is closer to the exact result. For  $R^b = 10$ , the difference between the FCI and CCSD result is approximately 4.5, see Table 8.7. The CCSD calculation with an effective interaction yields a even better energy, as expected. Furthermore, we observe that the VMC result is somewhat closer to the exact result than the CCSD energy with standard interaction for  $R^b = 10$ . However, by using an effective interaction, the CCSD energy is closer to the exact energy.

$N$	Method	$\omega$	Energy	Ref.
2	Analytic	1.0	3	[69]
	FCI	1.0	3.009236	[76]
	VMC	1.0	3.0025(1.2)	[67]
	DFT (LDA)	1.0	3.066	[50]
6	VMC	1.0	20.1910(3.5)	[78]
	DMC	1.0	20.16010(16)	[70]
	FCI	1.0	20.316754	[67]
12	VMC	1.0	65.790(1.9)	[67]
	DMC	1.0	65.70281(78)	[70]
	FCI	1.0	70.312502	[67]

**Table 8.30:** Ground state energies for parabolic quantum dots in two dimensions obtained with other many-body methods. The table shows results obtained by Full Configuration Interaction (FCI), Diffusion Monte Carlo (DMC), Variational Monte Carlo (VMC), and Density Functional Theory (DFT) with local density approximation (LDA). The analytic result for the 2-electron system with  $\omega = 1.0$  is also tabulated. Energy is measured in units of effective Hartrees  $E_H^*$ .

# Chapter 9

## Conclusions

We have in this thesis studied numerically systems consisting of several interacting electrons in two dimensions, confined to small regions between layers of semiconductors. These systems are dubbed quantum dots in the literature. We have considered a specific model called the parabolic (or circular) quantum dot. In this approximation the confinement potential is given by the harmonic oscillator potential, and the electron-electron interaction is given by the standard Coulomb interaction. The main aim of the thesis was to study the reliability of the Coupled-Cluster Singles and Doubles (CCSD) method for calculating the ground state energies of parabolic quantum dots in two dimensions. Another objective was to study the accuracy of the method for different sizes of the model space, and for different strengths of the confinement potential. In order to investigate the method we have developed a CCSD program in the  $m$ -scheme. The program can in principle handle other electronic systems such as atoms, molecules and other quantum dot models. We have also created a Restricted Hartree-Fock (RHF) program in order to investigate the CCSD machinery with another basis and to study (in combination with CCSD) the correlations in the system.

Our studies have been limited to closed-shell systems. We have considered quantum dots containing 2, 6, 12 and 20 electrons. The reason that we have not done calculations for systems with more electrons is primarily due to the fact that CCSD calculations with 20 particles take roughly 3 days. Moreover, there have to our knowledge not been published numbers obtained with *ab initio* methods for systems containing more than 20 electrons. We have calculated the HF and CCSD energy for frequencies ranging from 0.4 up to 50.0 with standard Coulomb interaction. In this thesis, we have not investigated when the closed-shell model breaks, i.e. for which strengths of the applied magnetic field the model fails.

We have found that the CCSD results obtained by using the standard Coulomb interaction are better than the Full Configuration Interaction (FCI) results in the literature. This is what we expect since the accuracy of the FCI method is very limited for  $N \geq 4$ , see [70]. Compared with the Variational Monte Carlo (VMC) results, the CCSD energies obtained with the standard interaction are somewhat higher. However, by increasing the size of the model space to  $R^b = 14$  and 16, our result for the 6-electron system is closer to the Diffusion Monte Carlo (DMC) energy. This reflects the importance of a large model space in order to obtain a better accuracy. We have therefore employed an effective interaction in our calculations. The CCSD calculations with an effective interaction reproduce the analytical results for the 2-electron system [69]. Moreover, the accuracy of the results obtained for larger systems are considerably improved, where we are very close to the DMC results for 6 and 12 electrons. Increasing the size of the model space to 16 shells for the 6-electron ( $\omega = 1.0$ ) system leads to an even better energy. The extrapolated energy is within the uncertainty of the DMC result for 6 electrons. We conclude that an effective interaction is necessary in order to improve the accuracy of the CCSD calculations. Moreover, the size of the model space is still important when employing an effective interaction.

We have seen that the inclusion of Triples brings us closer to the DMC energy for the 6-electron system with a standard interaction and  $\omega = 1.0$ . However, when using an effective

interaction, CCSD yields a better energy than CCSDT for  $R^b = 10$ . Since the extrapolated CCSD energy is within the uncertainty of the DMC result, this hints that Triples excitations are not that important in this case. In order to extrapolate the CCSD energy for the 12-electron system, we are forced to use the direct product model space. The extrapolated energy is very close to the DMC result. However, we are still not within the uncertainty. We have four sources of errors:

1. The size of the model space.
2. The effective interaction is generated by considering the 2-particle system, leading to missing many-body correlations.
3. We have limited our CC calculation to Singles and Doubles. Thus we are missing Triples (and in principle all order excitations up to  $N$ ) corrections in our calculations.
4. We are only including certain interaction elements when using the DP model space.

It is clear that our model space is too small for  $N \geq 6$ . How important the many-body correlations that are lost when we generate an effective interaction by considering the 2-electron system, is in general unknown. For  $N = 6$  and  $\omega = 1.0$ , it seems that they are not that important. However, we cannot draw any general conclusions without comparing with more DMC results. Furthermore, the importance of Triples corrections is not clear either. We expect that for sufficient low frequencies and large systems, many-body correlations become more important. In order to investigate the importance of Triples and to extract general tendencies, more CCSDT calculations are needed for different strengths of the confinement potential. Moreover, these results must be compared with DMC results.

In the analysis of the correlations energies (FCE, CE and CCSD-EC) we found that, for a given number of electrons, the system becomes more correlated when the frequency decreases. The CCSD energy does not converge when the relative contribution from the interaction is approximately 50-60% of the total energy. We obtain relative contributions over 50% for sufficiently low frequencies. Moreover, for a given frequency, when the number of electrons increases, the system becomes more correlated. This explains why we have more problems with convergence for large systems. We conclude that the CCSD energy does not converge when the system is sufficiently correlated. This feature applies to CCSD calculations with both a standard interaction and an effective interaction. In order to obtain convergence, we need a Hartree-Fock basis.

In the analysis of the size of the model space we found that the accuracy of our CCSD calculations are worse for low frequencies and large systems. Stated differently, the accuracy of our calculations are worse for more correlated systems. In order to obtain an improved accuracy, we need a larger model space in combination with an effective interaction, and possibly Triples corrections.

## Future Work and Perspectives

CC theory offers a many-body formalism which allows for systematic expansions and error estimates in terms of truncations in the single-particle basis, see [79]. Our calculations can in principle always be improved by increasing the size of the model space and include higher order excitations. Our CCSD code is neither optimized, nor parallelized. By realizing this, we expect to be able to study quantum dots containing more than 50 electrons with a larger basis, probably 16-20 shells. Furthermore, an implementation of CCSDT (alternatively CCSD(T), see [56]), with subsequent optimization, is necessary in order to accommodate for important Triples corrections. When this is done, it would be interesting to move over to more realistic systems such as coupled quantum dots. Since the code is developed in the  $m$ -scheme, it is able to handle systems without spherically symmetric potentials. Furthermore, an implementation of Equation-of-Motion Coupled-Cluster (EOM-CC) [56] with particle attached/removed would

---

be interesting. We could then study the addition spectra of quantum dots and compare with experimental results.

Another interesting field is the link between *ab initio* methods and Density Functional Theory (DFT). The main idea is that an *ab initio* method, such as the CC method, can be used to construct a density functional for a specific system by using the so-called adiabatic-connection method, see [19]. One can then compare with standard functionals (which are approximations) that are frequently used in DFT calculations [54], and investigate differences and general tendencies.

This formalism opens up perspectives for interesting applications and studies of current physics. One can extract spectroscopic factors [80], study the role and effects of spin-orbit interactions [81, 82], and so forth, and compare with experimental results. Furthermore, the coupling between CC and DFT may lead to more accurate DFT calculations of systems containing a large number of quantum dots [19]. One can then for example study and predict the properties of solar cells doped with a large number of quantum dots with an (possibly) improved accuracy.



## Appendix A

# Solution of the Single-Electron Schrödinger Equation

We will now derive the solution of

$$-\frac{\hbar^2}{2m^*} \left( \frac{d^2}{dr^2} + \frac{1}{r} \frac{d}{dr} - \frac{m^2}{r^2} + \frac{emB_0}{\hbar} \right) R(r) + \left( \frac{1}{2} m^* \omega^2 r^2 - \varepsilon_r \right) R(r) = 0, \quad (\text{A.1})$$

where  $R(r)$  is the radial part of the energy eigenfunction, and  $\varepsilon_r$  is the energy eigenvalue (spatial contribution). See Sec. 4.3). This is the radial Schrödinger equation for a single-electron parabolic quantum dot subjected to a constant magnetic field in the z-direction. The idea is to build up an ansatz by considering the limits  $r \rightarrow 0$  and  $r \rightarrow \infty$ . When  $r \rightarrow 0$ ,  $m^2/r^2$  dominates completely, and Eq. (A.1) reduces to

$$r^2 \frac{d^2 R(r)}{dr^2} + r \frac{dR(r)}{dr} - m^2 R(r) = 0. \quad (\text{A.2})$$

We make the ansatz

$$R(r) = r^s, \quad (\text{A.3})$$

and insert this expression into Eq. (A.2), yielding

$$s(s-1)r^s + sr^s - m^2r^s = 0.$$

We thus obtain that

$$s = |m|, \quad (\text{A.4})$$

leading to

$$\lim_{r \rightarrow 0} R(r) = r^{absm}, \quad (\text{A.5})$$

where  $R(r)$  is the solution of Eq.( A.1). Furthermore, in the limit  $r \rightarrow \infty$ ,  $\frac{1}{2}m^*\omega^2r^2$  dominates, and Eq. (A.1) reduces to

$$\frac{d^2 R(r)}{dr^2} + \frac{1}{r} \frac{dR(r)}{dr} - \frac{m^{*2}\omega^2r^2}{\hbar^2} R(r) = 0. \quad (\text{A.6})$$

We make the ansatz

$$R(r) = e^{tr^2}, \quad (\text{A.7})$$

where  $t$  is a constant, and insert this expression into Eq. (A.6), yielding

$$4t^2r^2 + 4t - \frac{m^{*2}\omega^2r^2}{\hbar^2} = 0. \quad (\text{A.8})$$

We obtain

$$t = \pm \frac{m^* \omega}{2\hbar}. \quad (\text{A.9})$$

Mathematics allow both negative and positive values of  $t$ . However, a positive value leads to a wavefunction that cannot be normalized. Thus we choose the negative value. We obtain that

$$\lim_{r \rightarrow \infty} R(r) = e^{-\frac{m^* \omega}{2\hbar} r^2}. \quad (\text{A.10})$$

We now make the following ansatz to the solution of Eq. (A.6),

$$R(r) = r^{|m|} e^{-\frac{m^* \omega}{2\hbar} r^2} g(r), \quad (\text{A.11})$$

where  $g(r)$  is a function that must satisfy

$$\lim_{r \rightarrow 0} g(r) = 1 \quad (\text{A.12})$$

$$\lim_{r \rightarrow \infty} g(r) = \frac{1}{r^{|m|}}. \quad (\text{A.13})$$

Inserting the ansatz into Eq. (A.1) yields

$$\begin{aligned} -\frac{\hbar^2}{2m^*} \left[ \frac{d^2 g(r)}{dr^2} + \left( 1 + 2|m| - \frac{2m^* \omega}{\hbar} r^2 \right) \frac{1}{r} \frac{dg(r)}{dr} - \frac{2m^* \omega}{\hbar} (1 + |m|) g(r) + \frac{m^{*2} \omega^2}{\hbar^2} r^2 g(r) \right] \\ + \left( \frac{1}{2} m^* \omega^2 r^2 - \varepsilon_r - \frac{em\hbar B_0}{2m^*} \right) g(r) = 0. \end{aligned} \quad (\text{A.14})$$

We define

$$\Lambda \equiv \frac{2m^* \varepsilon_r}{\hbar^2} + \frac{emB_0}{\hbar}, \quad (\text{A.15})$$

and

$$\beta \equiv \frac{m^* \omega}{\hbar}. \quad (\text{A.16})$$

By using the definitions above we obtain

$$\frac{d^2 g(r)}{dr^2} + (1 + 2|m| - 2\beta r^2) \frac{1}{r} \frac{dg(r)}{dr} - 2\beta (1 + |m|) g(r) + \Lambda g(r) = 0. \quad (\text{A.17})$$

Furthermore, we define

$$x = \beta r^2 \quad (\text{A.18})$$

$$\lambda = \frac{1}{2} \left( \frac{\Lambda}{2\beta} - |m| - 1 \right), \quad (\text{A.19})$$

leading to

$$x \frac{d^2 g(x)}{dx^2} + (1 + |m| - x) \frac{dg(x)}{dx} + \lambda g(x) = 0. \quad (\text{A.20})$$

This equation is called the associated Laguerre differential equation, and the solutions are the Laguerre polynomials. We assume  $g(x)$  is analytic in the region  $0 < x < \infty$ . The Laurent series is given as [29]

$$g(x) = \sum_{n=0}^{\infty} a_n x^{n+s}, \quad (\text{A.21})$$

---

where  $s$  is real number and  $a_0 \neq 0$ . Inserting Eq. (A.21) into Eq. (A.20), yields

$$\begin{aligned} & x \sum_{n=0}^{\infty} a_n (n+s)(n+s-1) x^{n+s-2} \\ & g + (1+|m|-x) \sum_{n=0}^{\infty} a_n (n+s) x^{n+s-1} \\ & + \lambda \sum_{n=0}^{\infty} a_n x^{n+s} = 0. \end{aligned} \quad (\text{A.22})$$

After changing some dummy indices we obtain

$$\begin{aligned} & \sum_{n=0}^{\infty} a_n (n+s)(n+s-1) x^{n+s-1} \\ & + (1+|m|) \sum_{n=0}^{\infty} a_n (n+s) x^{n+s-1} \\ & - \sum_{n=1}^{\infty} a_{n-1} (n+s-1) x^{n+s-1} \\ & + \lambda \sum_{n=1}^{\infty} a_{n-1} x^{n+s-1} = 0. \end{aligned} \quad (\text{A.23})$$

For  $n = 0$  we obtain

$$a_0 s(s-1) + a_0 s(1+|m|) = 0$$

leading to

$$s(s+|m|) = 0. \quad (\text{A.24})$$

Thus we have two possibilities:  $s = 0$  and  $s = -|m|$ . However, when  $s = -|m|$ , the eigenvectors diverge at  $x = 0$ . We must therefore choose  $s = 0$ . The equation reduces to

$$\begin{aligned} & \sum_{n=0}^{\infty} a_n n(n-1) x^{n-1} \\ & + (1+|m|) \sum_{n=0}^{\infty} a_n n x^{n-1} \\ & - \sum_{n=1}^{\infty} a_{n-1} (n-1) x^{n-1} \\ & + \lambda \sum_{n=1}^{\infty} a_{n-1} x^{n-1} = 0. \end{aligned} \quad (\text{A.25})$$

For  $n \geq 1$  we obtain the following recurrence relation

$$a_{n+1} = \frac{n-\lambda}{(n+1)(1+|m|+n)} a_n. \quad (\text{A.26})$$

Given a boundary condition, the constant  $a_0$  can be determined, yielding  $a_n$  for  $n \geq 1$ . Thus, we have found the solution of Eq. (A.1). It is given by Eqs. (A.11) and (A.21), with  $s = 0$  and  $a_n$  determined by Eq. (A.21). We obtain the following expression for  $g(x)$ ,

$$g(x) = \left[ 1 - \frac{\lambda}{1+|m|} x - \frac{(1-\lambda)\lambda}{2(1+|m|)(2+|m|)} x^2 + \dots \right] a_0. \quad (\text{A.27})$$

We observe that the series converges when  $\lambda \geq 0$ . The normalization condition requires that the series terminate after a certain  $n$ . This is obtained when

$$n = \lambda. \quad (\text{A.28})$$

We end up with the following allowed values for  $n$  (and  $\lambda$ ),

$$n = 0, 1, 2, 3, 4, \dots \quad (\text{A.29})$$

Since Eq. (A.20) can be written as

$$\hat{D}g(x) = 0, \quad (\text{A.30})$$

where

$$\hat{D} = x \frac{d^2}{dx^2} + (1 + |m| - x) + \lambda, \quad (\text{A.31})$$

we can remove  $a_0$  from Eq. (A.27). The solutions of Eq. (A.20) are the associated Laguerre polynomials  $L_n^{|m|}$ . The Rodrigues representation is given as

$$L_n^{|m|}(x) = \frac{e^x x^{-|m|}}{n!} \frac{d^2}{dx^2} \left( e^{-x} x^{n+|m|} \right). \quad (\text{A.32})$$

The polynomials can also be written as a finite series,

$$\sum_{k=0}^n (-1)^k \frac{(n+|m|)!}{(n-k)!(|m|+k)!k!} x^k. \quad (\text{A.33})$$

We finally obtain the solutions of Eq. (A.1),

$n$	$L_n^{ m }(x)$
0	1
1	$1 +  m  - x$
2	$\frac{1}{2} (1 +  m ) (2 +  m ) - 2 (2 +  m ) x + x^2$

**Table A.1:** Lowest order associated Laguerre polynomials.

$$R(r)_{nm} = \mathcal{K}_{nm} r^{|m|} e^{-\frac{1}{2}\beta r^2} L_n^{|m|}(\beta r^2), \quad (\text{A.34})$$

where  $\mathcal{K}_{nm}$  is the normalization constant determined by

$$1 = \mathcal{K}^2 \int_0^\infty \left| r^{|m|} e^{-\frac{1}{2}\beta r^2} L_n^{|m|}(\beta r^2) \right|^2 r dr. \quad (\text{A.35})$$

The spatial part of the eigenfunctions reads (see Section 4.3)

$$\phi_{nm}(r) = \sqrt{\frac{n!}{\pi(n+|m|)!}} \beta^{\frac{1}{2}(1+|m|)} r^{|m|} e^{-\frac{1}{2}\beta r^2} L_n^{|m|}(\beta r^2) e^{im\phi}, \quad (\text{A.36})$$

where

$$n = 0, 1, 2, 3, \dots \quad (\text{A.37})$$

$$m = 0, \pm 1, \pm 2, \pm 3, \dots \quad (\text{A.38})$$

The energy eigenvalue  $\varepsilon_r$  is determined by combining Eqs. (A.28) and (A.19) into

$$\Lambda_{nm} = 2\beta (1 + |m| + 2n). \quad (\text{A.39})$$

Inserting the in Eq. (A.15) finally yields

$$\varepsilon_{r,nm} = (1 + |m| + 2n) \hbar\omega + m\hbar\omega_B, \quad (\text{A.40})$$

where  $\omega_B$  is defined in (4.46).

# Bibliography

- [1] M. Reed, Scientific American **268**, 118 (1993).
- [2] S. M. Reimann and M. Manninen, Rev. Mod. Phys. **74**, 1283 (2002).
- [3] S. Tarucha, D. G. Austing, T. Honda, R. J. van der Hage, and L. P. Kouwenhoven, Phys. Rev. Lett. **77**, 3613 (1996).
- [4] S. Weiss, M. Thorwart, and R. Egger, Eur. Phys. Lett. **76** (2006).
- [5] C. Livermore, C. H. Crouch, R. M. Westervelt, K. L. Campman, and A. C. Gossard, Science **274**, 1332 (1996).
- [6] W. Lu, Z. Ji, L. Pfeiffer, K. W. West, and A. J. Rimberg, Nature **423**, 422 (2003).
- [7] G. Burkard, D. Loss, and D. P. DiVincenzo, Phys. Rev. B **59**, 2070 (1999).
- [8] P. Hawrylak, L. Jacak, and A. Wojs, *Quantum Dots* (Springer Verlag, 1998).
- [9] J. G. Pagan, *Quantum dot light emitting diode* (Ph.D. thesis, University of North Carolina, 2006).
- [10] D. L. Huffaker, G. Park, Z. Zou, O. B. Shchekin, and D. G. Deppe, App. Phys. Lett. **73**, 2564 (1998).
- [11] R. J. Haug, M. Dilger, T. Schmidt, R. H. Blick, K. v. Klitzing, and K. Eberl, Physica B **227**, 82 (1996).
- [12] V. G. Mokerov, F. Y. V., L. E. Velikovski, and M. Y. Scherbakova, IOPP **12**, 552 (2001).
- [13] D. Loss and D. P. DiVincenzo, Phys. Rev. A **57**, 120 (1998).
- [14] T. Jamieson, R. Bakhshi, D. Petrova, R. Pocock, M. Imani, and M. Seifalian, Science Direct **28**, 4717 (2007).
- [15] X. Gao, Y. Cui, L. W. Chung, and S. Nie, Nat. Biotech. **22**, 969 (2004).
- [16] S. Jenks and R. Gilmore, J. Ren. Sust. Energy Rev. **2**, 013111 (2010).
- [17] J. C. Slater, J. Chem. Phys. **41**, 3199 (1964).
- [18] J. M. Thijssen, *Computational Physics* (Cambridge University Press, 2007).
- [19] A. M. Teale, S. Coriani, and T. Helgaker, J. Chem. Phys **130**, 104111 (2009).
- [20] T. D. Crawford and H. F. Schaefer, Rev. Comp. Chem. **14**, 33 (2007).
- [21] P. Navrátil, J. P. Vary, and B. R. Barrett, Phys. Rev. C **62**, 054311 (2000).
- [22] D. J. Dean, T. Engeland, M. Hjorth-Jensen, M. P. Kartamyshev, and E. Osnes, Prog. Part. Nucl. Phys. **53** (2004).

- [23] J. J. Brehm and W. J. Mullin, *Introduction to the Structure of Matter* (Wiley, 1989).
- [24] P. C. Hemmer, *Kvantemekanikk* (Tapir Akademisk Forlag, 2005).
- [25] D. J. Griffiths, *Introduction to Quantum Mechanics* (Pearson, 2005).
- [26] R. Shankar, *Principles of Quantum Mechanics* (Plenum Press, 1994).
- [27] D. C. Lay, *Linear Algebra* (Pearson, 2006).
- [28] E. Merzbacher, *Quantum Mechanics* (Wiley, 1970).
- [29] M. L. Boas, *Mathematical Methods in the Physical Sciences* (Wiley, 2006).
- [30] F. E. Harris, H. J. Monkhorst, and D. L. Freeman, *Algebraic and diagrammatic methods in many-fermion theory* (Oxford University Press, 1992).
- [31] W. H. Dickhoff and D. V. Neck, *Many-Body Theory Exposed!* (World Scientific, 2008).
- [32] R. M. Dreizler and E. K. U. Gross, *Density Functional Theory - An Approach to the Quantum Many-Body Problem* (Springer, 1990).
- [33] A. Kumar, S. E. Laux, and F. Stern, Phys. Rev. B **42**, 5166 (1990).
- [34] M. Macucci, K. Hess, and G. J. Iafrate, Phys. Rev. B **48**, 17354 (1993).
- [35] M. Macucci, K. Hess, and G. J. Iafrate, Phys. Rev. B **55**, 4879 (1997).
- [36] M. Stopa, Phys. Rev. B **54**, 13767 (1996).
- [37] D. Heitmann and J. P. Kotthaus, Physics Today **46**, 56 (1993).
- [38] D. Heitmann, Physica B: Condensed Matter **212**, 201 (1995).
- [39] W. Kohn, Phys. Rev. **123**, 1242 (1961).
- [40] C. Kittel, *Introduction to Solid State Physics* (Wiley, 2005).
- [41] L. Brey, N. F. Johnson, and B. I. Halperin, Phys. Rev. B **40**, 10647 (1989).
- [42] F. M. Peeters, Phys. Rev. B **42**, 1486 (1990).
- [43] C. Sikorski and U. Merkt, Phys. Rev. Lett. **62**, 2164 (1989).
- [44] J. M. Leinaas (2008), lecture Notes FYS3120, University of Oslo.
- [45] L. P. Kouwenhoven, D. G. Austing, and S. Tarucha, Rep. Prog. Phys. **64**, 701 (2001).
- [46] S. Nomura, L. Samuelson, C. Pryor, M.-E. Pistol, M. Stopa, K. Uchida, N. Miura, T. Sugano, and Y. Aoyagi, Phys. Rev. B **58**, 6744 (1998).
- [47] M. B. Tavernier, E. Anisimovas, F. M. Peeters, B. Szafran, J. Adamowski, and S. Bednarek, Phys. Rev. B **68**, 205305 (2003).
- [48] T. M. Henderson, K. Runge, and R. J. Bartlett, Phys. Rev. B **67**, 045320 (2003).
- [49] I. Heidari, S. Pal, B. S. Pujari, and D. G. Kanhere, J. Chem. Phys. **127**, 114708 (2007).
- [50] E. Rasanen, S. Pittalis, J. G. Vilhena, and M. A. L. Marques, ArXiv e-prints: arXiv:1001.3660v1 (2010).
- [51] E. Schrödinger, Phys. Rev. **28**, 1049 (1926).

- [52] J. C. Slater, Phys. Rev. **34**, 1293 (1929).
- [53] E. K. U. Gross, L. N. Oliveira, and W. Kohn, Phys. Rev. A **37**, 2805 (1988).
- [54] R. v. Leeuwen, Adv. Quantum Chem. **43**, 25 (2003).
- [55] E. Clementi and C. Roetti, Atom. Dat. Nucl. Dat. Tab. **14**, 177 (1974).
- [56] I. Shavitt and R. J. Bartlett, *Many-Body Methods in Chemistry and Physics* (Cambridge University Press, 2009).
- [57] J. Čížek, J. Chem. Phys. **45**, 4256 (1966).
- [58] J. Čížek, Adv. Chem. Phys. **14**, 35 (1969).
- [59] A. C. Hurley, *Electron correlation in small molecules* (Academic Press, 1976).
- [60] H. J. Monkhorst, Int. J. Quantum Chem. Symp. **11** (1977).
- [61] G. D. P. III and R. J. Bartlett, J. Chem. Phys. **76**, 1910 (1982).
- [62] B. L. Hammond, W. A. Lester, and P. Reynolds, *Monte Carlo Methods in ab Initio Quantum Chemistry* (World Scientific, 1994).
- [63] S. Raimes, *Many-Electron Theory* (North-Holland Publishing Company, 1972).
- [64] S. A. Kucharski and R. J. Bartlett, Adv. Quantum Chem. **18**, 281 (1986).
- [65] D. Yang, *C++ and Object-Oriented Numeric Computing* (Springer, 2001).
- [66] H. P. Langtangen, *Python Scripting for Computational Science* (Springer, 2008).
- [67] P. Merlot, *Many-Body Approaches to Quantum Dots* (Master thesis, University of Oslo, 2009).
- [68] M. Rontani, Ph.D. thesis, Universita degli Studi di Modena e Reggio Emilia (1999).
- [69] M. Taut, Phys. A: Math. Gen. **27**, 1045 (1994).
- [70] M. P. Lohne, G. Hagen, M. Hjorth-Jensen, S. Kvaal, and F. Pederiva, Unpublished (2010).
- [71] P.-O. Löwdin, Phys. Rev. **97**, 1509 (1955).
- [72] G. Hagen, T. Papenbrock, and M. Hjorth-Jensen, Phys. Rev. Lett. **104**, 182501 (2010).
- [73] P. J. Ellis and E. Osnes, Rev. Mod. Phys. **49**, 777 (1977).
- [74] M. Hjorth-Jensen, T. T. S. Kuo, and E. Osnes, Phys. Rep. **261**, 125 (1995).
- [75] S. Kvaal, *Analysis of many-body methods for quantum dots* (Ph.D. thesis, University of Oslo, 2009).
- [76] S. Kvaal, ArXiv e-prints: arXiv:0810.2644v1 (2008).
- [77] F. Pederiva, C. J. Umrigar, and E. Lipparini, Phys. Rev. B **62**, 8120 (2000).
- [78] R. Albrightsen, *Computational Environment For Many Electron Systems* (Master thesis, University of Oslo, 2009).
- [79] R. Schneider, Numer. Math. **113**, 433 (2009).
- [80] Ø. Jensen, G. Hagen, T. Papenbrock, D. J. Dean, and J. S. Vaagen, ArXiv e-prints: arXiv:1004.2611v1 (2010).

## BIBLIOGRAPHY

---

- [81] C. Fasth, A. Fuhrer, L. Samuelson, V. N. Golovach, and D. Loss, Phys. Rev. Lett. **98**, 266801 (2007).
- [82] A. Ambrosetti, J. M. Escartin, E. Lipparini, and F. Pederiva, ArXiv e-prints: arXiv:1003.2433v1 (2010).